Water Technology and Sciences

Included in Thomson Reuters Science Citation Index® (ISI) • Expanded Thomson Reuters Research Alert® (ISI) • EBSCO • ProQuest • Elsevier • Redalyc

Vol. VI, No. 5, September-October, 2015

Water Technology and Sciences

Edit Board

Editorial coordination and careful editing: Helena Rivas- López • **Editorial assistance and editorial layout:** Luisa Guadalupe Ramírez-Martínez • **Figures design:** Luisa Guadalupe Ramírez-Martínez and Rosario Castro-Rivera • **Coordination arbitration:** Elizabeth Peña and Bibiana Bahena • **Proofreading English:** Ellen Weiss • **Logo design and cover:** Oscar Alonso-Barrón • **Design format:** Gema Alín Martínez-Ocampo • **Marketing:** Marco Antonio Bonilla-Rincón.

Editorial Committee

©***Water Technology and Sciences.*** Vol. VI, No. 5, September-October, 2015, is a bimonthly publication edited by the Instituto Mexicano de Tecnología del Agua, Paseo Cuauhnáhuac 8532, Colonia Progreso, Jiutepec, Morelos, C.P. 62550, telephone +52 (777) 3 29 36 00, extension 474, www.imta.gob.mx/tyca, fsalinas@tlaloc.imta.mx. Responsible editor, Nahún Hamed García Villanueva; Copyright No. 04-2013-121014514100-203, granted by the Instituto Nacional de Derechos de Autor. ISSN pending. Responsible for the latest update of this issue: Sub-Department of Dissemination and Circulation, Francisco José Salinas Estrada, Paseo Cuauhnáhuac 8532, Colonia Progreso, Jiutepec, Morelos, C.P. 62550.

Water Technology and Sciences is the traslation of *Tecnología y Ciencias del Agua*, which is the continuation of the following journals: *Irrigación en México* (1930-1946); *Ingeniería hidráulica en México* (1947-1971); *Recursos hidráulicos* (1972-1978), and *Ingeniería hidráulica en México*, second period (1985-2009).

Coordination for editorial comments,
click here give

For subscriptions, click here

Water Technology and Sciences

Vol. VI, No. 5, September-October, 2015

Cover: Sunrise over the Aguilereño tank in the Aguanaval River, Viesca, Coahuila, Mexico.

Water has become a scarce resource and is crucial to food production. Therefore, the generation of new methods to manage and conserve the vital resource is increasingly needed. In the article Monitoring Soil Moisture using a Wireless Sensor Network" by María Flores-Medina, Francisco Flores-García, Víctor Velasco-Martínez and Guillermo González-Cervantes, a system is presented which helps with the continuous monitoring of soil moisture using a new communications technology—Wireless Sensor Networks (WSN), an emergent technology which has been used in agriculture over recent years (pp.75-88).

Photo: Francisco Valdés Perezgasga (2015 National Award for Nature Conservation).

Tulum, Quintana Roo, Mexico.

Photo: Luisa Guadalupe Ramírez Martínez.

Contents

Contenido

Technical articles

Artículos técnicos

Technical notes

Notas técnicas

k-ε flujo modelado de ósmosis

• Cristiana Laranjeira • Luís Sanches-Fernandes • Amadeu Borges •
• Nuno Cristelo* •
University of Trás-os-Montes e Alto Douro, Portugal
*Autor de correspondencia

Resumen

Laranjeira, C., Sanches-Fernandes, L., Borges, A., & Cristelo, N. k-ε flujo modelado de ósmosis (septiembre-octubre, 2015). Tecnología y Ciencias del Agua, 6(5), 5-16.

Con el fin de satisfacer las necesidades de agua de consumo a escala global se han tomado varias medidas. La desalinización ha demostrado ser una solución viable, y por lo tanto es una de las utilizadas cada vez más en las dos últimas décadas. Este trabajo de investigación pretende ser una contribución que emplea la modelización numérica para predecir el comportamiento de flujo laminar de un fluido incompresible (agua de mar) en los sistemas de desalinización. Dos escenarios diferentes se consideran: con y sin una membrana impulsada por presión. La última ha permitido estudiar los efectos de la gravedad. La descripción teórica del flujo se basa en las ecuaciones de conservación de masa, momento y energía. Se utilizaron técnicas de dinámica de fluidos computacional para simular el flujo en diferentes escenarios, utilizando el software ANSYS 12.1. Los resultados mostraron que la membrana tiene una influencia muy importante en el proceso de flujo, con un impacto importante de la sección x = 0.240 m, cuando se empieza a desarrollar hacia la zona inferior de la sección transversal.

Palabras clave: desalinización, membrana, modelado CFD, ANSYS 12.1.

Abstract

Laranjeira, C., Sanches-Fernandes, L., Borges, A., & Cristelo, N. k-ε Flow Modeling of Osmosis (September-October, 2015). Water Technology and Sciences (in Spanish), 6(5), 5-16.

Several measures have been taken to satisfy global water consumption needs. Desalination has been proven to be a viable solution and has therefore been increasingly used over the past two decades. This research is aimed at making a contribution through the use of numerical modeling to predict the behavior of laminar flow in desalination systems with an incompressible fluid (sea water). The study considered two scenarios— with and without a pressure-driven membrane, the latter enabling the study of the effects of gravity. The theoretical description of flow is based on mass, momentum and energy conservation equations. Computational fluid dynamics techniques were used to simulate flow according to different scenarios using ANSYS 12.1 software. The results show that the membrane significantly influences the flow process, with a significant impact in section x = 0.240 m when beginning to develop in the lower part of the cross-section.

Keywords: *Desalination; Membrane; CFD modeling; ANSYS 12.1.*

Recibido: 17/10/2011
Aceptado: 01/05/2015

Introducción

La desalinización es un proceso utilizado para remover la sal y otros minerales y/o químicos del agua de mar y salobre, convirtiéndola en agua potable lista para el consumo humano (Marcovecchio, Mussati, Aguirre y Scena, 2005; Akgul, Cakmakci, Kayaalp, y Koyuncu, 2008; Charcosset, 2009; Ettouney y El-Dessouky, 2001; Greenlee, Lawler, Freeman, Marrot, y Moulin, 2009; Khawaji, Kutubkanah, y Wie, 2008). Karagiannis y Soldatos (2008) han clasificado los métodos de desalinización en dos grupos mayores: métodos térmicos (procesos de cambio de fase) y métodos de membrana (sin cambio de fase). Fletcher y Wiley (2004) trabajaron hacia el desarrollo de un modelo de dinámica de fluidos computacional (DFC) con el fin de caracterizar con exactitud la tasa de flujo en los canales de alimentación y permeables en los procesos de presión inducida en la membrana. Los autores referidos establecen que la tasa de flujo en ambos

canales está gobernada por la masa, momento y la masa de las ecuaciones de fracciones de soluto. Estas ecuaciones se presentan en un sistema de coordenadas cartesianas, considerando que la densidad, viscosidad y difusividad son una función de la fracción de soluto, y son similares a las utilizadas en trabajos previos (Wiley y Fletcher, 2002, 2003; Alexiades, Bao, Fletcher, Wiley, Clements, 2006), con las siguientes modificaciones: para caracterizar la viscosidad se incluyó un conjunto de constantes relacionadas; también se incluyen las fuerzas gravitacionales, la masa se usa en lugar de la concentración, como en la formulación del flujo compresible, lo cual garantiza la conservación de la masa del soluto. Para las condiciones de flujo consideradas, la densidad es solo una función de la fracción de masa de soluto, puesto que el flujo se considera isotérmico y la dependencia de la presión y densidad es en extremo pequeña, y de tal modo ignorable. En este caso, los efectos de la densidad se incluyen en cada término de las ecuaciones de conservación, y por ello el modelo es más general, asegurando una conservación de masa estricta para todos los modelos válidos constitutivos (Fletcher y Wiley, 2004; Alexiadis *et al*., 2006; Wiley y Fletcher, 2002; Pa, Mohammadi, Hosseinalipour, y Allahdini, 2008). En este trabajo, el proceso de filtrado se implementó aplicando una diferencia de presión entre los canales permeable y de alimentación. La diferencia de presión se usa para determinar el flujo a través de la membrana, pero el hecho de que la presión es decenas de bars mayor en el canal de alimentación no tiene efecto en la hidrodinámica. Por lo tanto, la presión de referencia en la salida de los dos canales es cero ($\rho = 0$) para fines computacionales (solo los gradientes de presión se muestran en las ecuaciones). Este es un patrón computacional para evitar la pérdida de precisión por errores de redondeo. Wardeh y Morvan (2008), utilizando las mismas ecuaciones y geometría de canal, realizaron simulaciones de DFC del flujo y la polarización de la concentración en canales llenos de separadores para la desalinización del agua. Para modelar la transferencia selectiva de la alimentación al canal permeable a través de la superficie de membrana se utilizó el código de elemento finito ANSYS-CFX, y se pudo demostrar que un canal de alimentación con filamento de separadores reduce la polarización de la concentración sobre la superficie de la membrana y por lo tanto el ensuciamiento.

Modelo matemático

Las ecuaciones que gobiernan el flujo de fluidos (ecuaciones de masa, momento y energía) pueden alterarse por factores como la condición del fluido (compresible o incompresible), flujo 2D o 3D, y otros.

Ecuaciones de flujo

Las siguientes son las ecuaciones de continuidad en dos dimensiones (1), momento (2) y de flujo bidimensional, laminar e incompresible sobre un canal de sección transversal regular con una membrana que separa los canales de alimentación y permeable (3). La ecuación (4) representa la variación de la masa de sal sobre el flujo. Advierta que el glosario de símbolos se encuentra al final del artículo:

$$\frac{\partial \rho u}{\partial x} + \frac{\partial \rho v}{\partial y} = 0 \tag{1}$$

$$\frac{\partial \rho u^2}{\partial x} + \frac{\partial \rho uv}{\partial y} = -\frac{\partial p}{\partial x} + 2\frac{\partial}{\partial x}\left(\mu \frac{\partial u}{\partial x}\right) + \frac{\partial}{\partial x}\left[\mu\left(\frac{\partial u}{\partial y} + \frac{\partial v}{\partial x}\right)\right] - \frac{2}{3}\frac{\partial}{\partial x}\left[\mu\left(\frac{\partial u}{\partial x} + \frac{\partial v}{\partial y}\right)\right] - \rho g_x \tag{2}$$

$$\frac{\partial \rho uv}{\partial x} + \frac{\partial \rho v^2}{\partial y} = -\frac{\partial p}{\partial y} + 2\frac{\partial}{\partial y}\left(\mu \frac{\partial v}{\partial y}\right) + \frac{\partial}{\partial y}\left[\mu\left(\frac{\partial u}{\partial y} + \frac{\partial v}{\partial x}\right)\right] - \frac{2}{3}\frac{\partial}{\partial y}\left[\mu\left(\frac{\partial u}{\partial x} + \frac{\partial v}{\partial y}\right)\right] - \rho g_y \tag{3}$$

$$\frac{\partial \rho u m_A}{\partial x} + \frac{\partial \rho v m_A}{\partial y} = \frac{\partial}{\partial x}\left[\rho D_{AB}\left(\frac{\partial m_A}{\partial x}\right)\right] + \frac{\partial}{\partial y}\left[\rho D_{AB}\left(\frac{\partial m_A}{\partial y}\right)\right] \quad (4)$$

En las ecuaciones (1), (2), (3) y (4) x e y son coordenadas espaciales horizontales y verticales, respectivamente; ρ es la densidad, μ es viscosidad dinámica; g es la aceleración gravitacional; D es la difusividad y m_A es el porcentaje de masa de sal.

Condiciones de frontera

Las condiciones de frontera se aplican a las paredes, membrana y sección transversal inicial y final de los canales. La velocidad a través de la membrana se define utilizando la ecuación de continuidad (5):

$$Q_w = Q_p$$
$$A_w \times u_w = A_p \times u_p \quad (5)$$

La tasa de flujo en el sistema se divide en el flujo que permanece en el canal de alimentación (*Qw*) y el flujo que alcanza el canal permeable a través de la membrana (*Qp*). Por lo tanto, la velocidad de infiltración por la membrana (*vw*) se obtuvo considerando que el flujo permeable es igual al flujo que va a través del área de la membrana (*Awm*) (6):

$$v_w = \frac{A_p \times u_p}{A_{wm}} \quad (6)$$

La presión existente en el canal de alimentación se define como la misma que en el caso de la no existencia de la membrana (7):

$$p = 0 \quad (7)$$

En consecuencia, la presión existente sobre el canal permeable, cuando se considera la existencia de la membrana, es igual a la diferencia entre la presión de los canales de alimentación y permeable, obtenido utilizando la ecuación de Bernoulli (8), la cual relaciona la presión con la velocidad u y la caída H en cualquier punto de la línea de flujo considerada:

$$H = \frac{p}{\gamma} + \frac{u^2}{2g} + z \quad (8)$$

La condición de frontera en el inicio del canal define por completo el perfil de velocidad y el porcentaje de masa de sal en el agua (9):

$$u = 6\bar{u}\frac{y}{h}\left(1 - \frac{y}{h}\right)$$
$$v = 0$$
$$m_A = m_{A0} \quad (9)$$

Para las paredes se aplican las condiciones de flujo:

$$u = 0$$
$$v = 0$$
$$\frac{\partial m_A}{\partial y} = 0 \quad (10)$$

En la membrana, sobre el lado del canal de alimentación, la velocidad tangente se define como cero (se considera sin flujo) y se especifica la velocidad de infiltración (11):

$$u = 0$$
$$v = v_w \quad (11)$$

Sobre el canal permeable, se corrige la velocidad de infiltración en la membrana para tomar en cuenta el cambio en la densidad, manteniendo por lo tanto constante la tasa de flujo a través de la membrana (12):

$$u = 0$$
$$v = v_p = v_w \frac{\rho_w}{\rho_p} \quad (12)$$

Estudio experimental

Una sección rectangular (figura 1) se considera para el canal con una geometría similar utilizada

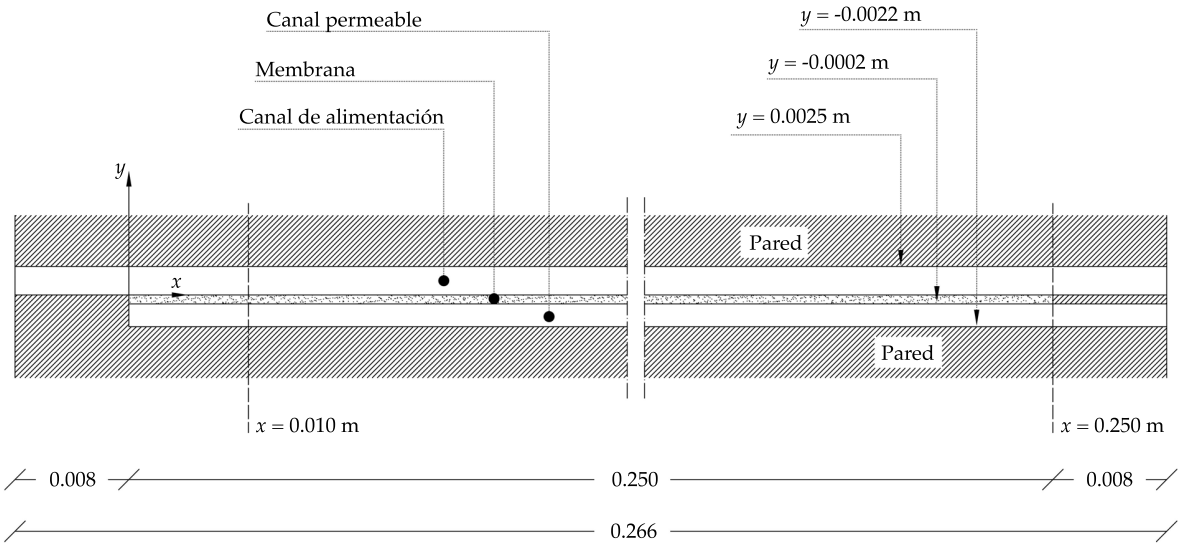

Figura 1. Geometría considerada del canal.

previamente por Fletcher y Wiley (2004), y Wardeh y Morvan (2008), con dimensiones de canal similares a las usadas por Alexiadis *et al.*, (2007), con longitud de 0.266 m y alturas de 0.0025 m y 0.0020 m para los canales de alimentación y permeable, respectivamente. La tasa de flujo se impone sobre el canal de flujo y se define sobre el canal permeable como el valor infiltrado a través de la membrana, la cual tiene 0.250 m de longitud y 0.0002 m de espesor. Con el fin de garantizar un comportamiento aceptable del flujo, se incluyeron dos regiones con longitud de 0.008 m en la entrada y la salida, para los cuales se aplicaron las condiciones de frontera descritas previamente para las secciones de entrada y salida.

La solución considerada en las simulaciones estuvo compuesta por agua con masa de sal de 0.002 kg/kg. Las propiedades físicas del fluido variaron con el porcentaje de masa de sal y se definieron mediante las ecuaciones (13) y (14):

$$\mu = 0.89 \times 10^{-3} \left(1.0 + 1.63 m_A\right) \qquad (13)$$

$$\rho = 997.1 \times \left(1.0 + 0.696 m_A\right) \qquad (14)$$

En estas ecuaciones m_A es el porcentaje de masa de sal (kg por kg de solución); μ es la viscosidad dinámica (N/m^2s) y ϱ es la densidad (kg/m^3).

Considerando el canal mencionado, se ejecutaron cuatro simulaciones con las condiciones descritas en la tabla 1.

El software ANSYS CFD 12.1 (2010) se utilizó para efectuar la simulación de flujo de fluido durante este trabajo de investigación. Es un software de dinámica de fluidos computacional el que combina el pre y el post procesamiento con una capacidad de solución poderosa.

Resultados y discusión

Simulación sin membrana

Perfil de velocidad longitudinal

La figura 2 describe el desarrollo del perfil de la velocidad longitudinal para g = 9 (SIM 1). Es claro que el flujo evoluciona después de $x = 0.010$ m, cuando aumenta la sección del canal. Esta etapa en el canal provoca que el fluido vuelva a fluir o se detenga, lo cual a su vez desarrolla

Tabla 1. Condiciones de las simulaciones efectuadas.

Simulaciones	Condiciones				
	u(m/s)	v(m/s)	p(N/m²)	g(m/s²)	Membrana
SIM 1	0.1	0	0	0	No
SIM 2	0.1	0	0	-9.8	No
SIM 3	0.1	0	0	+9.8	No
SIM 4	0.1	0	0	-9.8	Yes

Las simulaciones 1, 2 y 3 se incluyeron con el objetivo de estudiar la influencia de la aceleración gravitacional sobre el flujo del fluido y, como tal, no se consideró ninguna membrana. La SIM 4 incluyó la membrana y por lo tanto solo se consideró el caso más realista de g = - 9.8 m/s².

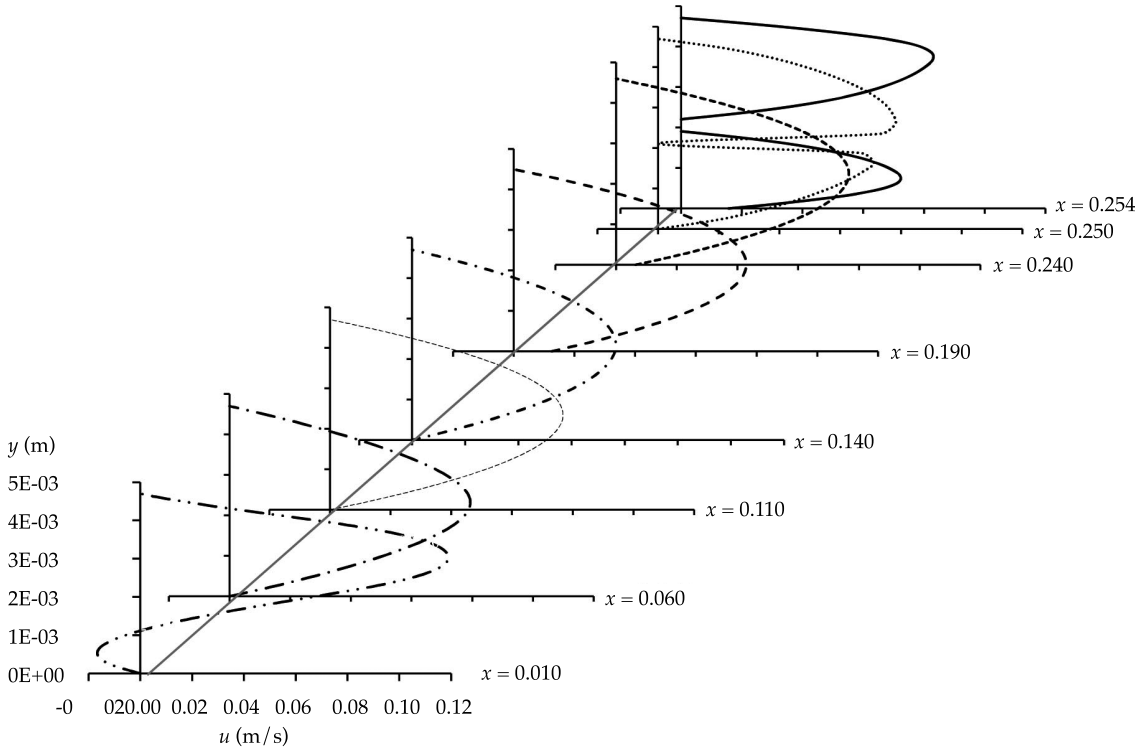

Figura 2. Perfil de velocidad longitudinal para g = 0.

las velocidades negativa y positiva en la misma sección. Para esta sección la velocidad máxima se alcanza aproximadamente a media altura. El flujo es constante en la sección intermedia del canal, el cual es por lo común de un flujo entre dos secciones paralelas, mientras que la velocidad máxima se alcanza a media altura. En la sección x = 0.250 m el flujo cambia debido a las modificaciones en la geometría del canal, lo que resulta en la división horizontal del flujo en dos.

La figura 3 describe el desarrollo del perfil de la velocidad longitudinal para g = -9.8 m/s² (SIM 2). Puede verse que entre las secciones x = 0.010 m y x = 0.240 m el flujo es constante, típico de un flujo laminar, sin ningún cambio significativo en la velocidad. La velocidad máxima se registró casi para la sección transversal completa, disminuyendo solo cerca de la parte superior y la parte inferior. Para esta simulación, como en el caso de las simulaciones

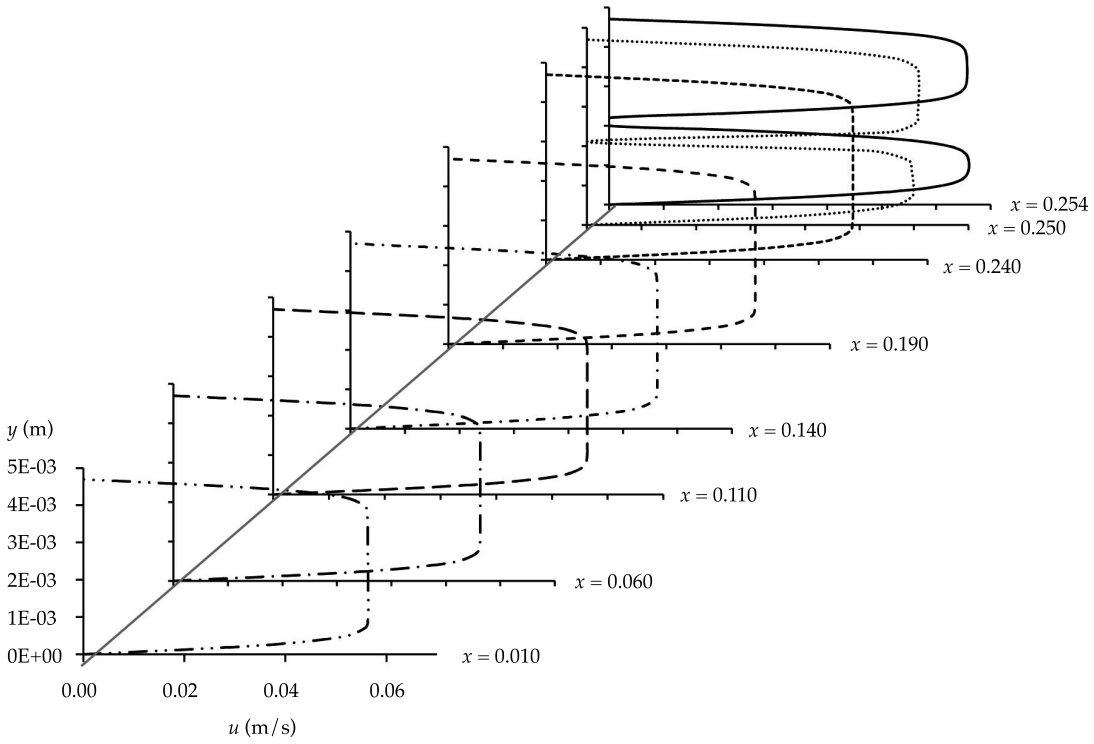

Figura 3. Perfil de velocidad longitudinal para g = -9.8 m/s^2.

restantes, la presencia de la pared horizontal en la sección x = 0.250 m divide el flujo en dos. Hay un ligero aumento en la velocidad en esta sección y en la sección x = 0.254 m (6.5 y 14.0%, respectivamente), en relación con la velocidad en las secciones intermedias. En la sección x = 0.254 m y contrario a lo que sucede en la sección x = 0.250 m (aunque la diferencia no es significativa), el flujo es más intenso por la pared sólida inferior del canal.

El desarrollo del perfil de la velocidad longitudinal para g = -9.8 m/s^2 (SIM 3) fue muy similar al de SIM 1 y por lo tanto la figura 2 se usa para analizar SIM 3. La velocidad máxima y el reflujo/paro del fluido ocurrieron en la sección x = 0.010 m, flujo laminar típico en las secciones intermedias del canal y división en dos flujos en la sección x = 0.250 m debido a la pared horizontal.

En resumen, para SIM 1 y SIM 3, la velocidad es máxima en la sección x = 0.010 m, en tanto que para SIM 2 la velocidad más alta se alcanza en la última sección analizada (x = 0.254 m).

Perfil de velocidad normal

La figura 4 describe el desarrollo del perfil de la velocidad normal a la pared del canal para g = 0 (SIM 1). Como puede verse, en la sección x = 0.010 m el flujo muestra de manera simultánea velocidad normal positiva y negativa, consecuencia del reflujo/paro que se muestra en la figura 2.

Los resultados de las secciones intermedias no se presentan puesto que son aproximadamente cero, con solo un pequeño desarrollo de flujo en la sección x = 0.060 m. Sin embargo, en la sección x = 0.250 m, donde el canal se divide, existe un desarrollo de flujo significativo que resulta en valores de velocidad máximos (tanto positivos como negativos) cerca de las paredes de separación del canal. La siguiente

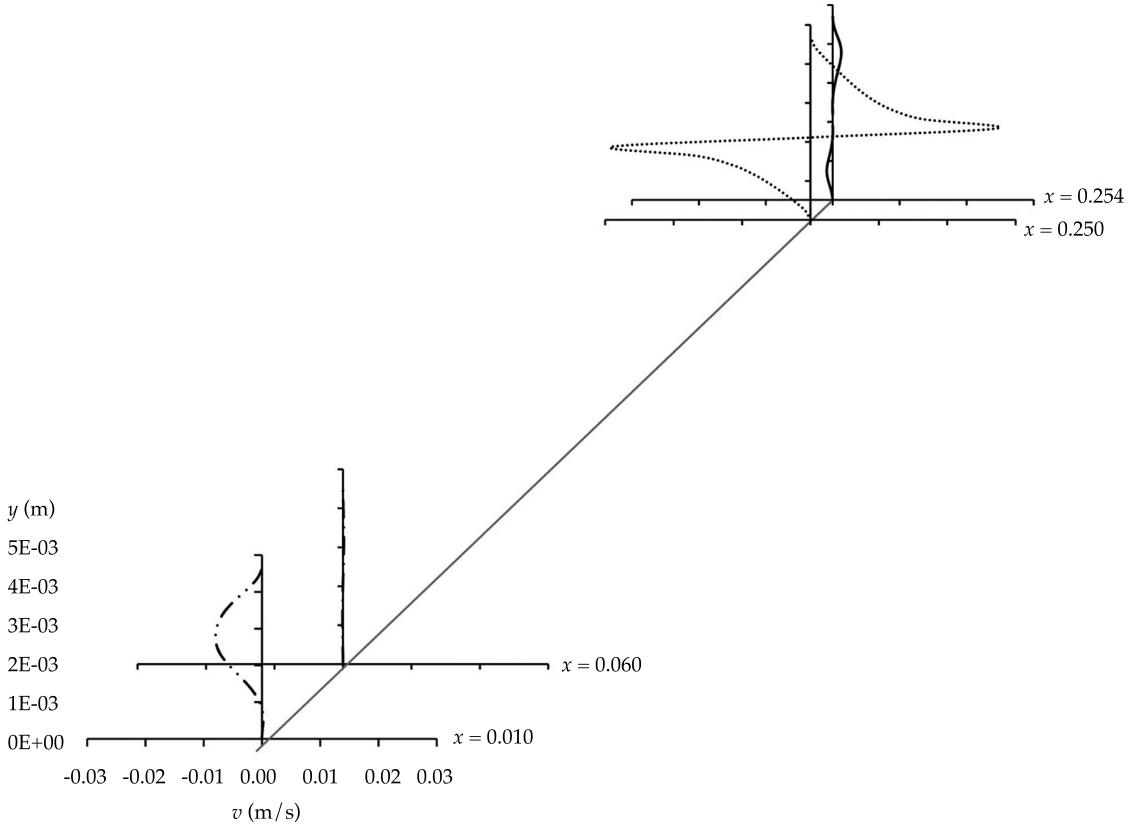

Figura 4. Perfil de velocidad normal para $g = 0$.

sección muestra un flujo menos desarrollado, con reducciones en las velocidades máximas, en relación con la sección previa, de 93 y 60% para valores positivos y negativos, respectivamente.

La SIM 2 reveló un flujo prácticamente horizontal a lo largo de la longitud completa del canal, con la excepción en la sección $x = 0.250$ m. Esto se debe al hecho de que el componente normal de la velocidad, derecho en la primera sección ($x = 0.010$ m) y más allá, es prácticamente cero. Por esta razón no se presentan los resultados para estas secciones. La excepción es la sección $x = 0.250$ m, donde el canal se divide y el flujo muestra un desarrollo muy intenso, con valores de velocidad positivos y negativos iguales.

La SIM 3 mostró la influencia mayor sobre la velocidad normal. En la sección $x = 0.010$ m del desarrollo del flujo (figura 4) la velocidad normal tiene valores positivos y negativos, consecuencia del reflujo/paro del fluido. Una vez más, en la sección $x = 0.250$ m, se crean dos flujos diferentes, con velocidad normal positiva cerca del lado superior de la pared de separación horizontal y velocidad normal negativa cerca del lado inferior de la pared de separación. Las velocidades máximas positiva y negativa se alcanzan en esta misma sección. Es posible concluir que el flujo se desarrolla más cerca de la pared superior del canal, posiblemente debido al hecho de que g tiene orientación hacia arriba. La sección inmediata muestra un flujo menos desarrollado, con velocidades positivas y negativas 77% y 82% menores, con relación a la sección previa.

Como puede verse de las SIM 1, 2 y 3, los perfiles de velocidad normal solo muestran variaciones en las secciones de los extremos,

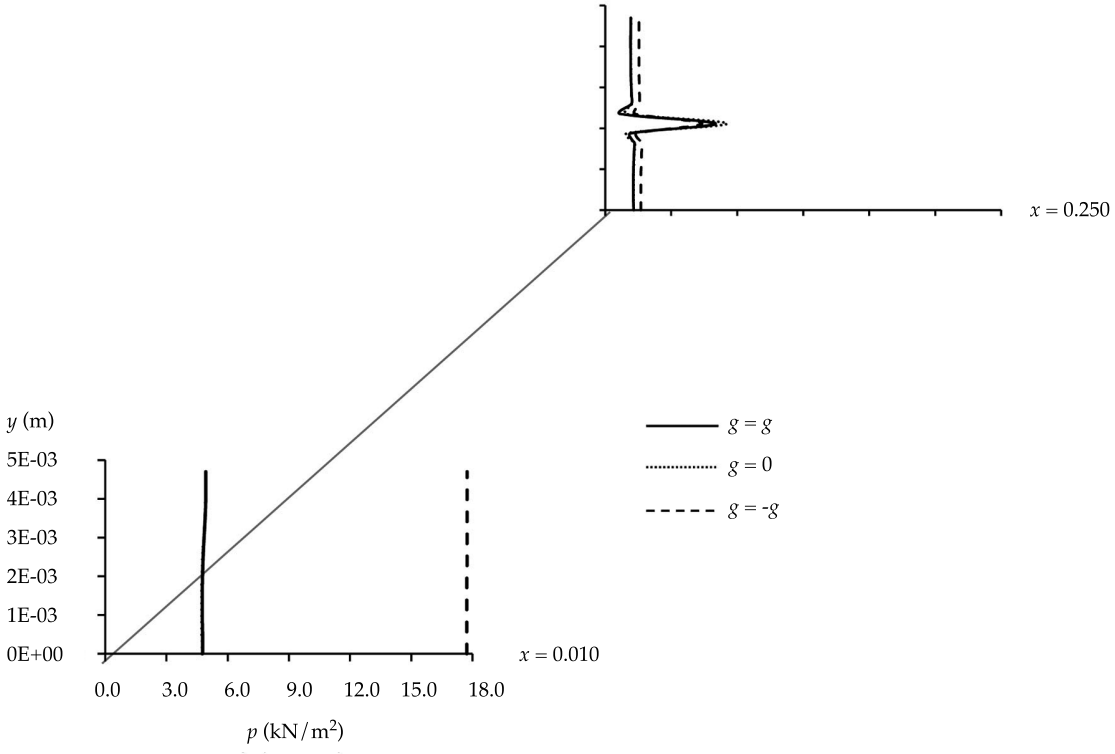

Figura 5. Perfil de presión para $g = 0$, $g = -9.8$ m/s^2 y $g = +9.8$ m/s^2.

siendo aproximadamente constantes para el resto del canal, lo que indica una superficie de flujo casi horizontal. En la sección $x = 0.254$ m, donde la velocidad normal alcanza picos de valores positivos y negativos, el flujo muestra una configuración similar en las tres simulaciones. Sin embargo para la SIM 1 el desarrollo del flujo es más pronunciado cerca del lado del fondo de la pared de separación, para la SIM 2 no se detectó diferencia en el flujo entre los lados superior e inferior, y para la SIM 3 el desarrollo del flujo es más pronunciado cerca del lado superior.

Perfil de presión a lo largo del canal

La figura 5 presenta un perfil comparativo de la presión a lo largo del canal para las tres simulaciones sin membrana$g = 0$, $g = -g$ y $g = +g$. El flujo es laminar y por ello tiene un número de Reynolds bajo, lo que lleva a una diferencia aproximadamente cero en la presión ($D_Q \approx 0$). Por lo tanto, solo se analizaron las secciones donde las variaciones de presión fueron más significativas. La primera de estas secciones ($x = 0.010$ m) muestra un perfil de presión similar para las SIM 1 y SIM 3 con prácticamente los mismos valores. La presión en estas simulaciones es 73% menor que en la SIM 2. En la sección $x = 0.250$ m, donde el punto de presión máxima ocurre a la altura media (la velocidad longitudinal del fluido de altura media fue detenida por la pared horizontal empezando en la sección $x = 0.250$ m), la variación en la presión es muy importante. El valor de la presión en este punto es 7% más alto en la SIM 2 que en la SIM 3.

Simulación con membrana

Perfil de velocidad longitudinal

La figura 6 muestra el desarrollo del perfil de velocidad longitudinal en el canal con membrana (SIM 4). Este desarrollo es particularmente

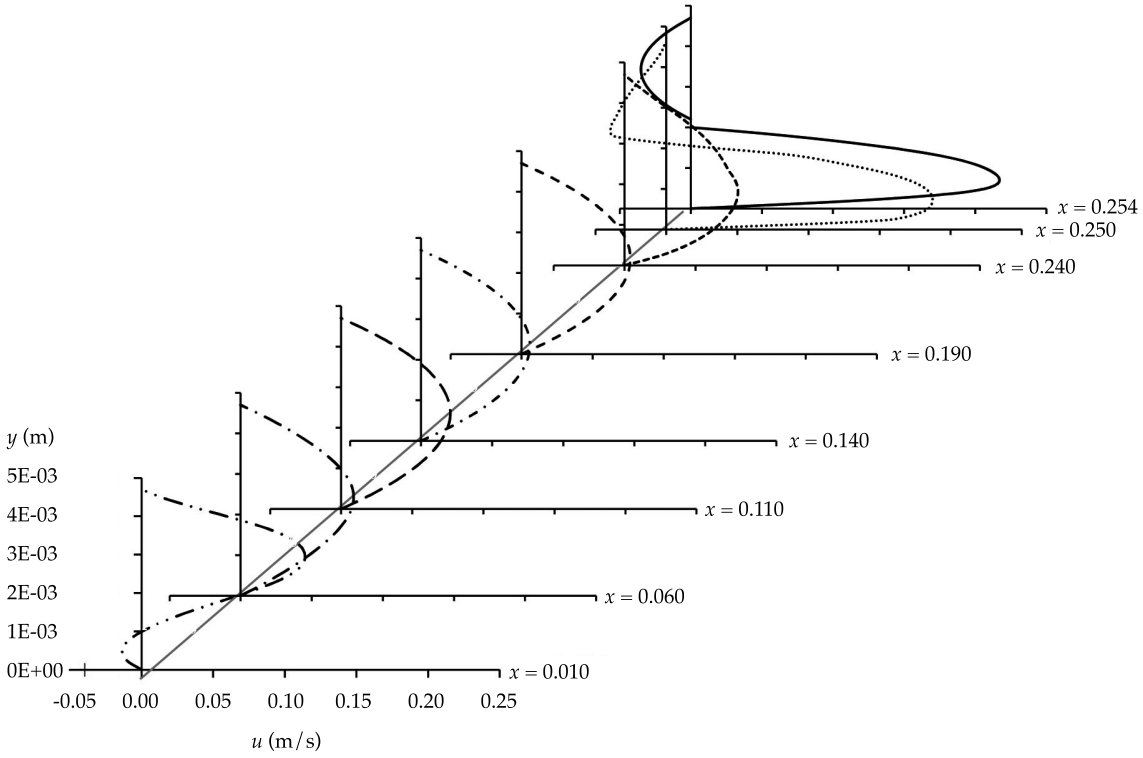

Figura 6. Perfil de velocidad longitudinal considerando la membrana.

notable en la sección $x = 0.010$ m, en una situación similar a la ocurrida con las simulaciones 1 y 3 sin membrana. De nuevo, en esta sección el fluido refluye o se separa, aumentando las velocidades positivas y negativas al mismo tiempo. Las velocidades también presentan valores muy similares a los obtenidos de SIM 1 y 3, alcanzando su valor máximo en la sección media.

En la sección $x = 0.240$ m el flujo empieza a adoptar un comportamiento diferente, y en la sección $x = 0.250$ m, donde el canal se divide horizontalmente y se forman los dos flujos netos, la velocidad longitudinal toma valores positivos cerca del lado del fondo de la pared de separación y valores negativos cerca del lado superior. En este punto el flujo ocurre preferiblemente cerca del fondo del canal, alcanzando su valor máximo en la última sección. En la SIM 4 es claro el desarrollo del flujo en la sección $x = 0.010$ m, inmediatamente después del aumento en la sección transversal del canal, lo cual es contrario a lo que se encontró durante la SIM 2, en la cual el flujo se considera constante y la velocidad es máxima a casi la altura total del canal.

Perfil de velocidad normal

La figura 7 describe el desarrollo del perfil de la velocidad normal a la pared del canal considerando la membrana (SIM 4). Como puede verse, en la sección $x = 0.010$ m el desarrollo del flujo presenta solo velocidad normal negativa, con un pequeño porcentaje de la sección transversal del canal mostrando velocidad cero como consecuencia del reflujo/paro del fluido observado en la figura 6. Las secciones medias del canal no se presentan puesto que los valores de la velocidad son aproximadamente cero, mostrando solo un pequeño desarrollo de flujo en las secciones $x = 0.060$ m y $x = 0.190$ m. En la sección $x = 0.240$ m

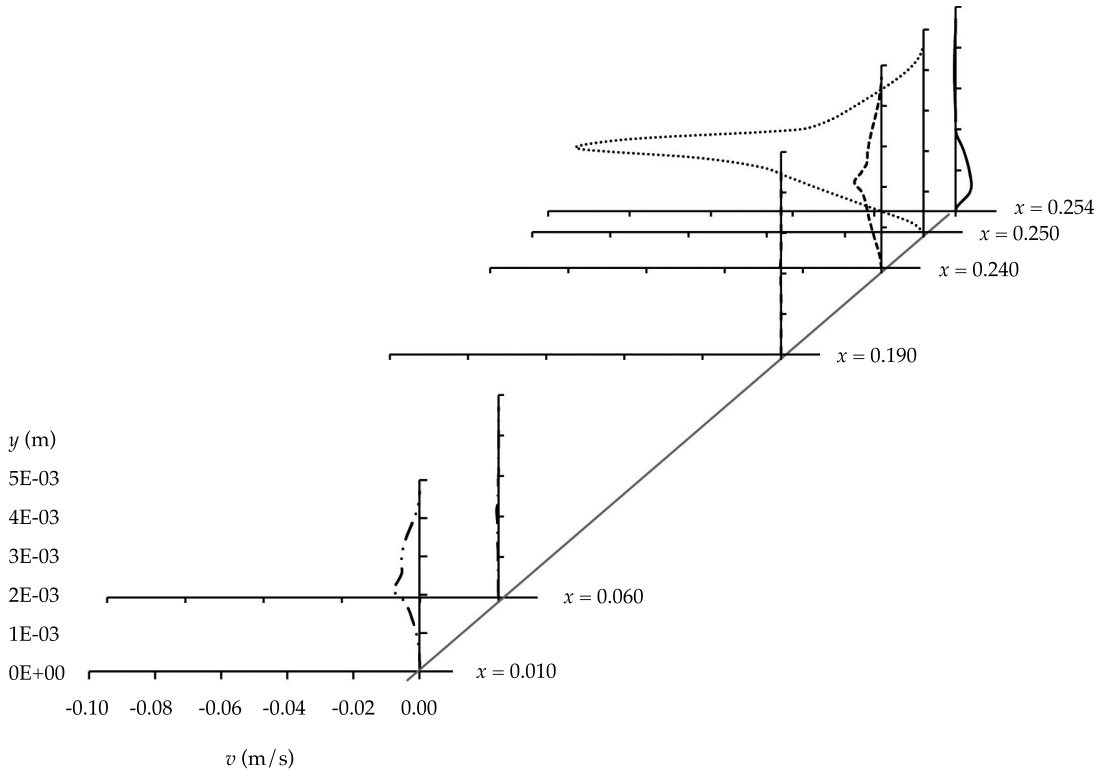

Figura 7. Perfil de velocidad normal considerando la membrana.

y más allá de ella es claro que la existencia de la membrana cambia por completo el comportamiento del flujo. En el caso de la SIM 1, 2 y 3 (figura 4), el flujo alcanza velocidades máximas positiva y negativa en la sección $x = 0.250$ m, en la proximidad de los lados superior e inferior de la pared de separación horizontal del canal, respectivamente. En este caso (SIM 4) no hay simetría de velocidad positiva/negativa; existe en vez de eso una velocidad positiva máxima a la altura de la pared de separación. La sección siguiente inmediata muestra un flujo menos desarrollado, solo visible cerca del fondo del canal, con una velocidad normal positiva.

En general, los perfiles muestran valores negativos. Sin embargo, hay un valor inusualmente alto en $x = 0.250$ m, lo cual solo puede explicarse por la presencia cercana del extremo de la membrana, donde la pared ya no es permeable y, como consecuencia, empiezan a desarrollarse dos flujos separados, como se ilustra en la figura 1. Debe también tomarse en cuenta la simetría cercana del perfil alrededor del punto de separación de los dos flujos. Después de este punto, el flujo superior tiene casi velocidad vertical cero, manteniendo la característica negativa, pero el comportamiento de flujo menor es ahora positivo, debido a la tasa de flujo menor. Advierta que ambos flujos, después del extremo de la membrana, mantienen la condición de simetría a la altura media de cada uno de los semicanales.

La SIM 2 mostró una velocidad máxima a la altura casi completa del canal, la cual se incrementó al inicio, cuando se dividió al canal, y se mantuvo hasta el extremo. Durante la SIM 4 la velocidad máxima sucedió a la altura media. En ambos casos la velocidad máxima se registró en la sección última, con la SIM 4 mostrando un valor mayor que la SIM 2.

Conclusiones

El objetivo de estudiar el comportamiento del flujo de agua de mar en un canal con y sin membrana se alcanzó comparando los dos escenarios y concluyendo respecto a la influencia de la membrana. Como se enunció previamente, el uso del software para estudiar el comportamiento de un fluido en un canal probó ser muy útil, como se esperaba. Esto fue en particular cierto con el software ANSYS, usado para ejecutar las simulaciones de DFC, las cuales produjeron resultados precisos que permitieron un análisis detallado del flujo. Para las simulaciones en las cuales no se consideró la membrana, se obtuvieron diferentes perfiles de velocidad longitudinal y normal. Esta diferencia resultó de los valores de aceleración gravitacional (g) considerados. Los perfiles para $g = 0$ y $g = +g$ tienen un alto parecido y contribuyen al lado derecho de la ecuación de continuidad. Para las secciones medias en la SIM 1 y la SIM 3 la velocidad máxima se alcanza a la altura media y, por lo tanto, los perfiles resultantes son similares a los obtenidos en el flujo laminar. Sin embargo, existe un reflujo/paro del fluido en la sección $x = 0.010$ m, el cual es típico de un flujo sin ningún escalón. En la sección $x = 0.250$ m, donde ocurre la separación del canal, el flujo se divide en dos. En esta sección el flujo se detiene momentáneamente (lo cual se verifica por medio del hecho de que la velocidad longitudinal es cero en toda simulación), y por lo tanto la presión máxima se alcanza. Considerando las simulaciones sin membrana, SIM 2 ($g = -g$) es la más cercana a la realidad puesto que la fuerza gravitacional se considera hacia abajo. El flujo es laminar y por lo tanto muestra un bajo número de Reynolds, lo cual resulta en una diferencia en la presión aproximadamente cero ($\Delta_p \approx 0$). En general, puede concluirse que la membrana tiene una influencia significativa sobre el desarrollo del flujo. Esta influencia es especialmente notable en la sección $x = 0.240$ m y más allá, donde el flujo empieza a desarrollarse más hacia al área del fondo de la sección transversal. En la sección $x = 0.250$ m, y de acuerdo con los valores de la velocidad longitudinal, el flujo corre casi por completo cerca del fondo del canal. Además, con base en la velocidad normal, el flujo se desarrolla en un patrón simétrico, con una velocidad máxima en la pared de la separación horizontal del canal.

Símbolos

A_w – Área del canal de alimentación (m^2/m).
A_p – Área del canal permeable (m^2/m).
$\overline{u}$ – AVelocidad inicial promedio sobre el canal de alimentación (m/s).
V – Velocidad promedio a lo largo del canal (m/s).
D – Difusividad (m^2/s).
μ – Viscosidad dinámica (N/m^2s).
h – Altura del canal de alimentación (m).
v_w – Velocidad de filtración (m/s).
Q_w – Tasa de flujo del canal de alimentación (m^3/s).
Q_p – Tasa de flujo del canal permeable (m^3/s).
g – Aceleración gravitacional (m/s).
x – Dirección longitudinal.
u – Velocidad longitudinal (a lo largo del canal) (m/s).
A_{wm} – Área de la membrana (m^2/m).
y – Dirección normal.
v – Velocidad normal (normal a la membrana) (m/s).
p – Presión (N/m^2).
ΔP – Diferencia de presión a través de la membrana.
m_A – Porcentaje de la masa de sal (kg/kg).
ρ – Densidad del agua de mar (kg/m^3).
ρ_w – Densidad del agua de mar sobre el canal de alimentación(kg/m^3).
ρ_p – Densidad del agua de mar sobre el canal permeable (kg/m^3).
u_w – Velocidad del canal de alimentación (m/s).
u_p – Velocidad del canal permeable(m/s).
γ – Densidad del agua (kg/m^3).

Reconocimientos

Este trabajo fue apoyado por fondos nacionales de la Fundación Portuguesa FCT para la Ciencia y la Tecnología, bajo el proyecto UID/AGR/04033/2013.

Referencias

Akgul, D., Çakmakci, M., Kayaalp, N., & Koyuncu, I. (2008). Cost Analysis of Seawater Desalination with Reverse Osmosis in Turkey. *Desalination*, *220*, 123-131.

Alexiadis, A., Bao, J., Fletcher, D. F., Wiley, D. E., & Clements, D.J. (2006). Dynamic Response of a High-Pressure Reverse Osmosis Membrane Simulation of Time Dependent Disturbances. *Desalination*, *191*, 397-403.

Alexiadis, A., Wiley, D. E., Vishnoi, A., Lee, R. H. K., Fletcher, D. F., & Bao, J. (2007). CFD Modeling of Reverse Osmosis Membrane Flow and Validation with Experimental Results. *Desalination*, *217*, 242-250.

ANSYS 12.1, ANSYS Tutorials, 2010.

Charcosset, C. (2009). A Review of Membrane Processes and Renewable Energies for Desalination. *Desalination*, *245*, 214-231.

Ettouney, H., & El-Dessouky, H. (2001). Teaching Desalination. *Desalination*, *141*, 109-127.

Fletcher, D. F., & Wiley, D.E. (2004). A Computational Fluids Dynamics Study of Buoyancy Effects in Reverse Osmosis. *Journal of Membrane Science*, *245*, 175-181.

Greenlee, L. F, Lawler, D. F., Freeman, B. D., Marrot, B., & Moulin, P. (2009). Reverse Osmosis Desalination: Water Sources, Technology, and Today's Challenges. *Water Research*, *43*, 2317-2348.

Karagiannis, I. C., & Soldatos, P. G. (2008). Water Desalination Cost Literature: Review and Assessment. *Desalination*, *223*, 448-456.

Khawaji, A. D., Kutubkanah, I. K., & Wie, J. M. (2008). Advances in Seawater Desalination Technologies. *Desalination*, *221*, 47-69.

Marcovecchio, M. G., Mussati, S. F., Aguirre, P. A., & Scena, N. J. (2005). Optimization of Hybrid Desalination Processes Including Multi Stage Flash and Reverse Osmosis Systems. *Desalination*, *182*, 111-122.

Pak, A., Mohammadi, T., Hosseinalipour, S. M., & Allahdini, V. (2008). CFD Modeling of Porous Membranes. *Desalination*, *222*, 482-488.

Wardeh, S., & Morvan, H.P. (2008). CFD Simulations of Flow and Concentration Polarization in Spacer-Filled Channels for Application to Water Desalination. *Chemical Engineering Research and Design*, *86*, 1107-1116.

Wiley, D. E., & Fletcher, D.F. (2003). Techniques for Computational Fluid Dynamics Modeling of Flow in Membrane Channels. *Journal of Membrane Science*, *211*, 127-137.

Wiley, D. E., & Fletcher, D.F. (2002). Computational Fluid Dynamics Modeling of Flow and Permeation of Pressure-Driven Membrane Processes. *Desalination*, *145*, 183-186.

Dirección institucional de los autores

MSc. Cristiana Laranjeira
PhD. Luís Fernandes
PhD. Amadeu Borges
PhD. Nuno Cristelo

University of Trás-os-Montes e Alto Douro (UTAD)
Quinta de Prados, Engenharias I, 5000-801 Vila Real,
Portugal
Phone: +35 (125) 9350 356
Fax: +35 (125) 9350 356
cris.pfl@gmail. com
lfilipe@utad.pt
amadeub@utad.pt
ncristel@utad.pt

Modelación hidrológica del río Tampaón en el contexto del cambio climático

• Juan Alberto Velázquez* •
El Colegio de San Luis A.C., México
Autor de correspondencia

• Magali Troin •
Université du Québec à Montréal, Canadá

• Daniel Caya •
Consortium Ouranos, Québec, Canadá

Resumen

Velázquez, J. A., Troin, M., & Caya, D. (septiembre-octubre, 2015). Modelación hidrológica del río Tampaón en el contexto del cambio climático. *Tecnología y Ciencias del Agua*, *6*(5), 17-30.

Este trabajo presenta, en un primer paso, un estudio de comparación de la modelación hidrológica de la cuenca del río Tampaón (localizada en el centro-este de México) con los modelos hidrológicos SWAT y GR4J, y en un segundo paso, la evaluación del impacto del cambio climático en el balance hídrico de la cuenca. La calibración y validación de los modelos (en periodos de 14 años) mostró un desempeño satisfactorio de ambos en la simulación de caudales diarios. Los resultados mostraron que SWAT reproduce de manera más precisa el caudal medio mensual observado, mientras que GR4J lo sobrestima en la temporada seca y lo subestima en la húmeda. El análisis del impacto del cambio climático se realizó a partir de simulaciones provenientes del Modelo Climático Mundial Canadiense (CGCM3) regionalizado con el Modelo Regional Canadiense (CRCM). Las simulaciones climáticas (una vez corregido el sesgo) se usaron como datos de entrada a los modelos hidrológicos para dos periodos: uno referente (1971-2000) y otro futuro (2041-2070). Los resultados estiman una disminución importante del caudal medio mensual en la cuenca del río Tampaón para el periodo futuro (entre -36% y -55%). Además, se valora una disminución del caudal máximo mensual (entre -34% y -60%) y mínimo mensual (entre -36% y -49%). Los resultados de este estudio aportan una visión general del potencial impacto del cambio climático en la respuesta hidrológica de la cuenca del río Tampaón.

Palabras clave: modelo climático regional canadiense, SWAT, GR4J, impacto del cambio climático.

Abstract

Velázquez, J. A., Troin, M., & Caya, D. (September-October, 2015). Hydrological Modeling of the Tampaon River in the Context of Climate Change. Water Technology and Sciences *(in Spanish), 6(5), 17-30.*

This work compares the hydrological modeling of the Tampaon River Basin (in east-central Mexico) with two hydrological models (SWAT and GR4J) and then evaluates the impact of climate change on the water balance of the basin. The calibration and validation of the models (over 14-year periods) show that both performed satisfactorily when simulating daily flows. The results indicate that SWAT more precisely reproduces observed mean monthly streamflow while GR4J overestimates it during the dry season and underestimates it during the rainy season. The analysis of the impact of climate change was performed by using climate ensemble simulations derived from the Canadian Global Climate Model (CGCM3) downscaled by the Canadian Regional Climate Model (CRCM). The climate simulations (after bias correction) were used as input data for both hydrological models for two periods: a reference period (1971 – 2000) and a future period (2041-2070). The results indicate a significant decrease in mean monthly streamflow in the Tampaon River Basin for the future period (-36 to -55%), as well as a decrease in maximum monthly streamflow (-34 to -60%) and minimum monthly streamflow (-36 to -49%). The results from this study provide an overall perspective of the potential impact of climate change on the hydrological response of the Tampaon River Basin.

Keywords: *Canadian Regional Climate Model, SWAT, GR4J, climate change impacts.*

Received:
Accepted:

Introducción

Evaluar los impactos del cambio climático en los recursos hídricos es uno de los principales desafíos del siglo XXI. Los cambios esperados en la temperatura y en la precipitación tendrán un impacto sobre el ciclo hidrológico y, por lo tanto, sobre la disponibilidad del agua para los usos humanos y las actividades económicas. México es particularmente vulnerable al cambio climático, ya que muchas regiones mexicanas son sensibles a los eventos climáticos extremos (Arreguín-Cortés y López-Pérez, 2013). Además, la demanda de agua para los sectores agrícolas, urbano e industrial en México han crecido mucho más rápidamente debido a la rápida expansión de estos sectores en las décadas recientes (Mundo y Martínez-Austria, 1993), y el cambio climático hará más difícil la respuesta a esta demanda creciente de agua (Magaña y Conde, 2000).

Las proyecciones del cambio climático para América Central (incluido México) sugieren aumentos en la temperatura, e incrementos o decrementos en la precipitación que tendrán un impacto futuro en el caudal y la disponibilidad del agua en la región (IPCC, 2014). El cambio proyectado de la temperatura depende del escenario de emisiones considerado y de la ubicación geográfica. Por ejemplo, Martínez-Austria (2007) presentó un análisis de la temperatura proyectada en México con base en las salidas GCM: en el escenario A2 (alto), el incremento de temperatura proyectada se espera que esté entre 4°C y 6°C, mientras que en el escenario B2 (medio) se encontrará entre 2°C y 4°C. Martínez-Austria (2207) también analizó los resultados obtenidos por Morales, Magaña, Barrera y Pérez (2001); este último estudio identificó regiones con el incremento más alto y más bajo proyectado de la temperatura de verano (es decir, el noreste de México y la zona de Chiapas-Tabasco, y la península de Yucatán, respectivamente).

A pesar de la vulnerabilidad de México a los impactos potenciales del cambio climático, pocos estudios han evaluado el impacto del cambio climático sobre los recursos hídricos del país. Por ejemplo, Mendoza, Villanueva y Adem (1977) dividieron el territorio mexicano en doce regiones hidrológicas para evaluar la vulnerabilidad de las regiones hidrológicas a los cambios climáticos futuros. Los escenarios del cambio climático se obtuvieron de dos Modelos de Circulación Global (MCG) y un modelo hidrológico se aplicó para determinar los escurrimientos superficiales anuales, el volumen y almacenamiento de agua bajo condiciones climáticas futuras (año 2050). Estos mostraron que el cambio climático esperado puede tener impactos drásticos sobre el patrón y la magnitud de escurrimientos, sobre la humedad del suelo y la evaporación, y sobre el nivel de aridez de algunas zonas hidrológicas de México. Maderey, Jiménez y Carrillo (2013) estimaron la cantidad de agua disponible a lo largo de tres grandes cuencas en México (esto es, la cuenca Lerma-Chapala, la cuenca del río Balsas y la cuenca del río Pánuco). Los datos climáticos se obtuvieron de dos MCG y un modelo climático termodinámico, y se estimó el cambio en la disponibilidad del agua con un modelo de balance de agua para el periodo 2025-2050. Sus resultados mostraron que los tres modelos climáticos predicen una disminución en los volúmenes de agua disponibles para todas las cuencas.

Rivas-Acosta, Güitrón-De-Los-Reyes y Ballinas-González (2010) evaluaron el impacto del cambio climático sobre el escurrimiento para tres captadores mexicanos con condiciones climáticas contrastadas: la cuenca del río Conchos (norte de México), la cuenca del río Lerma-Chapala (México central) y la cuenca del río Grijalva (sur de México). Rivas-Acosta *et al*. (2010) consideraron salidas desde 23 MCG ponderados bajo dos escenarios de emisiones IPCC (A1B y A2). Los escurrimientos se estimaron con un modelo de balance de agua y se calculó un índice de vulnerabilidad. Los resultados muestran que el escurrimiento anual medio futuro (2030-2050, 2100) se espera que disminuya a lo largo de los tres captadores. Tapia, Minjares y Espinoza (2014) evaluaron los impactos del cambio climático sobre el balance de agua de la cuenca del río Yaqui utilizando datos climáticos de un MCG bajo dos escenarios IPCC (A1B y A2)

para el periodo 2010-2099. Se obtuvieron varios comportamientos de escurrimiento, indicando la posibilidad de sequías frecuentes, alternando con años de escurrimiento sustancialmente alto.

Los estudios anteriores se basan en una resolución espacial baja de los modelos climáticos (es decir, MCG) y las evaluaciones del impacto del cambio climático sobre la hidrología del captador se estimaron utilizando solo un modelo de balance de agua. Los modelos de precipitación-escurrimiento también se han utilizado en la evaluación del impacto del cambio climático sobre los recursos hídricos en los captadores mexicanos. Por ejemplo, Robles-Morua, Che, Mayer y Vivoni (2015) utilizaron un modelo hidrológico semidistribuido y un algoritmo de optimación de embalses para evaluar el impacto hidrológico del cambio climático en la cuenca semiárida del río Sonora (noroeste de México) bajo un escenario de emisión IPPC A2. Los resultados mostraron una precipitación significativamente mayor en el periodo futuro (2031-2040) relativa al periodo histórico (1990-2000) que causaría un incremento en las entradas de los embalses.

En el presente el estudio se explora el cambio proyectado en el caudal basado en los escenarios derivados de los modelos hidrológicos de precipitación-escurrimiento para una captación mexicana central. Este enfoque de modelación, en el cual un modelo de captación hidrológica se alimenta con escenarios de clima regionalizados a partir de MCG, es particularmente útil para una amplia gama de estudios de impactos, incluyendo la planeación de recursos hídricos, desarrollo y manejo, predicción de inundaciones, sequías, calidad del agua e hidro-ecología.

Los modelos hidrológicos tienen diferentes grados de complejidad y conceptualización de procesos físicos. Estos pueden clasificarse considerando su distribución espacial, como modelos agrupados o distribuidos. En un modelo agrupado, la captación se considera como una unidad. Las variables y parámetros representan de tal modo valores promedios para la captación total. Por otra parte, un modelo distribuido toma variaciones espaciales en cuenta (por ejemplo, topografía, vegetación y suelo) en todas las variables y parámetros. Como se mencionó previamente, los modelos hidrológicos difieren también en su representación de procesos físicos: un modelo de base física describe el sistema natural utilizando formulaciones matemáticas de procesos físicos, en tanto que un modelo conceptual se construye con base en procesos físicos, en los cuales las ecuaciones de base física se usan junto con ecuaciones semiempíricas (Refsgaard, 1996). La investigación reciente en el modelado hidrológico trata de tomar un enfoque con base física para entender el comportamiento de los sistemas hidrológicos con el fin de hacer mejores predicciones futuras de caudales y enfrentar mayores desafíos en la administración de recursos hídricos.

Este estudio pretende evaluar el impacto del cambio climático en la hidrología de la cuenca del río Tampaón en México. En la primera etapa, se implementaron dos modelos hidrológicos sobre la cuenca, y se compararon sus desempeños en la simulación del caudal. Los modelos hidrológicos seleccionados tienen diferentes enfoques estructurales: SWAT es un modelo semidistribuido de base física (Arnold, Srini-vasan, Muttiah y Williams, 1998) y GR4J es un modelo agrupado conceptual (Perrin, 2000). Luego, las evaluaciones del impacto del cambio climático en la hidrología de la captación se evalúan utilizando la cadena de modelos hidroclimáticos ilustrados en la figura 1. Esta cadena de modelos consiste en salidas MCG regionalizadas dinámicamente mediante un modelo de clima regional (MCR) para alimentar a ambos modelos hidrológicos. Puesto que las salidas del MCR presentan usualmente sesgos considerables en las variables climáticas, descartando su uso directo en los modelos hidrológicos (Ho Stephenson, Collins, Ferro y Brown, 2012), se hace un ajuste de la precipitación y temperatura simuladas del MCR utilizando un procedimiento de corrección del sesgo; esto permite que las proyecciones de clima se trasladen de manera significativa a la escala hidrológica (Troin, Velázquez, Caya y Brissette, 2015). Las simulaciones hidrológicas se evalúan bajo climas presentes (1971-2000) y futuros (2041-2070) analizando indicadores hidrológicos para flujos medio, alto y bajo.

Figura 1. Ilustración de la cadena del modelo hidroclimático utilizado en este estudio.

El manuscrito está organizado del modo siguiente: primero, se presenta el diseño experimental, incluyendo el área de estudio y las simulaciones del modelo climático utilizadas en este estudio. Segundo, se da una descripción del procedimiento de corrección del sesgo y de los modelos hidrológicos. Tercero, se analizan y discuten los resultados relevantes del modelado hidrológico a escala de captación, así como una evaluación del impacto del cambio climático hidrológico en la cuenca del río Tampaón. Finalmente, las conclusiones cierran el manuscrito.

Diseño experimental

Captación del estudio

La cuenca del río Tampaón se ubica en la región este-central de México, yaciendo principalmente en el estado de San Luis Potosí (23,373 Km^2;

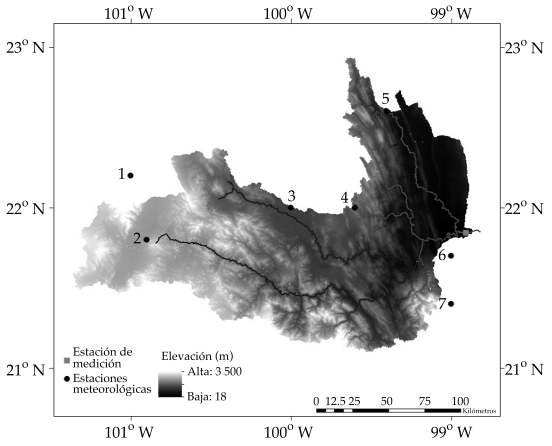

Figura 2. Ubicación de las estaciones de medición meteorológicas y de descargaa lo largo de la cuenca del Río Tampaón.

IMTA, 2014). También cubre el área del norte de los estados de Guanajuato y Querétaro, y una región del sur del estado de Tamaulipas. La cuenca del río Tampaón es una subcaptación de la cuenca del río Pánuco (zona hidrológica 26; Sedue, 1986) la cual fluye hacia el golfo de México. Su relieve topográfico tiene elevaciones que varían de 18 m a 3500 m con una elevación máxima sobre las fronteras montañosas occidentales (figura 2).

La cabecera más alejada de la cuenca del río Tampaón es el río Santa María, el cual se origina en el estado de Guanajuato, fluyendo de oeste a este a través de la cadena montañosa de la Sierra Madre Oriental. La unión del río Santa María con el río Verde forma el inicio del río Tampaón. A partir de aquí, el río Tampaón fluye hacia el noreste para juntarse con el río Gallinas y el río Valles. Este último proporciona el volumen más grande del caudal hacia el río Tampaón. Hay tres regiones climáticas en la cuenca del río Tampaón como resultado de la variación topográfica en la cadena montañosa de la Sierra Madre Oriental (Sedue, 1986): el clima es caliente y húmedo en el este, semicaliente y semihúmedo en la zona central y seco y templado en el oeste.

Tabla 1. Estaciones meteorológicas utilizadas en este estudio.

Estación	Nombre
1	San Luis Potosí
2	Villa de Reyes
3	Rioverde
4	Cárdenas
5	El Salto
6	Ballesmi
7	Xilitla

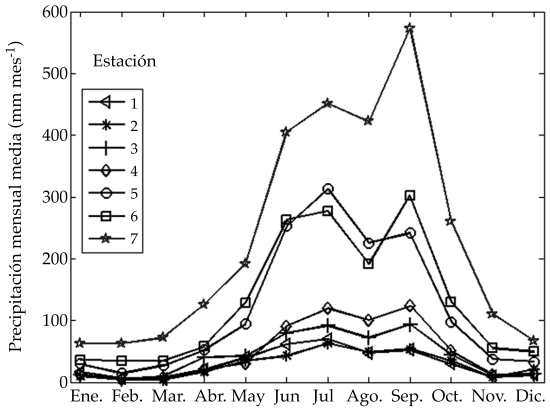

Figura 3. Precipitación mensual media observada para la cuenca del Río Tampaón a lo largo del periodo 1971-2000.

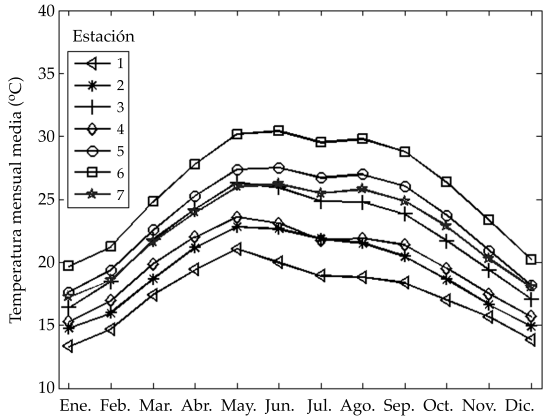

Figura 4. Temperatura mensual media observada para la cuenca del Río Tampaón a lo largo del periodo 1971-2000.

Conjunto de datos observacionales

Las series de tiempo diarias de precipitación (*P*) y las temperaturas mínima y máxima (*T*mín y *T*máx) se tomaron de la base de datos climatológica *CLICOM* 2014, construida por el SMN (Servicio Meteorológico Nacional de México). Estos datos vienen de siete estaciones a lo largo del periodo de 1971-2000 (figura 2, tabla 1). La temporada de lluvia se extiende de mayo a octubre y la temporada seca de noviembre a abril (figura 3). La lluvia anual media del área de captación es alrededor de 1080 mm. La temperatura diaria promedio anual varía de 13 a 30°C con una media anual de 21.5°C (figura 4). Los meses más fríos y más calientes son enero y mayo, respectivamente. Las tres regiones climáticas descritas previamente de la cuenca del río Tampaón son bien descritas por el grupo de datos observacionales.

Los datos de descarga provienen de la estación medidora El Pujal (ubicada aguas abajo del río Valles) para el periodo 1971-2000; estos datos se obtuvieron de la Base de Datos Nacional de Agua Superficial (es decir, Bandas, 2014). La figura 5 muestra las descargas mensuales medias observadas en la estación de medición. Dos flujos pico ocurren en julio y septiembre. La descarga disminuida en agosto se debe a la

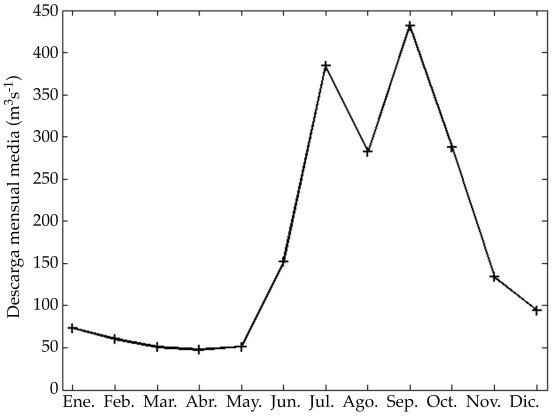

Figura 5. Descargas mensuales medias observadas para la cuenca del Río Tampaón a lo largo del periodo 1971-2000.

sequía a mitad del verano. Los valores bajos de flujo ocurren de enero a mayo.

Las simulaciones del modelo climático

Las simulaciones del ensamble MCG utilizadas en este trabajo son los cinco miembros del Modelo Climático Global Canadiense (CGCM3, Scinocca, Mcfarlane, Lazare, Li y Plummer, 2008) bajo el escenario de emisión de gases de efecto invernadero del SRES-A2 del IPCC. Cada miembro del ensamble se ha estimado repitiendo un experimento de cambio climático utilizando el MCG varias veces cuando las condiciones iniciales solo se cambiaron por pequeñas perturbaciones (Braun, Caya, Frigon y Slivitzky, 2012). Aunque los MCG son la fuente primaria de proyecciones del clima futuro, la resolución espacial de estas salidas del modelo es aún demasiado burda para usarse directamente en los estudios de impacto hidrológico. Por lo tanto, el modelo CGCM3 se regionalizó dinámicamente mediante el Modelo de Clima Regional Canadiense, versión 4.2.3 (CRCM; De Elía y Côté, 2010). La precipitación diaria, así como las series de temperatura máxima y mínima, se dedujeron de las simulaciones del CRCM para los periodos de referencia (1971-2000) y futuro (2041-2070).

El componente atmosférico del CGCM3 se caracteriza por un modelo espectral con resolución horizontal T47 (3.75° x 3.75°) y 31 capas verticales (Scinocca *et al.*, 2008). El modelo Climático Regional Canadiense derivado como una evolución de sus versiones previas (Caya y Laprise, 1999; Laprise, Caya, Frigon y Paquin, 2003; Plummer *et al.*, 2006), el cual cubre el gran dominio norteamericano (AMNO; 200 x 192 puntos de malla) con un espaciamiento del punto de malla de 45 km (verdadero a 60° N). El CRCM se ha usado largamente para evaluar el impacto del cambio climático en las captaciones de Norteamérica (por ejemplo, Muerth *et al.*, 2013; Velázquez *et al.*, 2013; Troin *et al.*, 2015) y esta es la primera vez que el CRCM se ha utilizado para un estudio de impacto en la captación mexicana.

Métodos

Procedimiento de corrección del sesgo

Las simulaciones del modelo climático resultan afectadas por los sesgos (esto es, diferencias entre las simulaciones y observaciones del modelo climático) que, si no se corrigen, pueden llevar a cierta reproducción irreal del caudal. Por lo tanto, es necesario efectuar la corrección del sesgo sobre las salidas de las simulaciones del modelo climático antes de usarlas en modelos hidrológicos para la evaluación de impactos (Teutschbein, Wetterhall y Seibert, 2011).

El método de corrección del sesgo utilizado para ajustar y regionalizar la precipitación y la temperatura simuladas del CRCM a la escala de la estación en la captación es el Método de Traslación Diaria (TD) (Mpelasoka y Chew, 2009). En la TD, se aplican diferentes factores de corrección (diferencias en percentiles entre los datos observados y simulados del modelo climático durante el periodo de referencia) a la distribución de frecuencia de los datos del modelo climático proyectado para el periodo futuro. El método TD se aplica sobre una base mensual, y se calculan cincuenta percentiles para cada mes. La temperatura y la precipitación corregidas en el periodo de referencia (ref) se calculan utilizando las ecuaciones siguientes:

$$T\left(corr\right)_{d}^{ref} = T_{sim(d)}^{ref} + \left(T_{obs(m,q)}^{ref} - T_{sim(m,q)}^{ref}\right) \qquad (1)$$

$$P\left(corr\right)_{d}^{ref} = P_{d}^{ref}\left(\frac{P_{obs(m,q)}^{ref}}{P_{sim(m,q)}^{ref}}\right) \qquad (2)$$

donde T (corr) y P (corr) son las variables corregidas del sesgo, y los subíndices corresponden a los percentiles (q), y las etapas de tiempo diaria (d) y mensual (m), a las simulaciones burdas de clima (sim) y a las observaciones (obs). Para el periodo futuro (fut), la precipitación y las temperaturas corregidas se obtienen utilizando:

$$T\left(corr\right)_{d}^{fut} = T_{sim(d)}^{fut} + \left(T_{obs(m,q)}^{ref} - T_{sim(m,q)}^{ref}\right) \qquad (3)$$

$$P\left(corr\right)_d^{fut} = P_d^{fut}\left(\frac{P_{obs(m,q)}^{ref}}{P_{sim(m,q)}^{ref}}\right) \quad (4)$$

Descripción de los modelos hidrológicos

Se eligieron dos modelos hidrológicos para este estudio: SWAT y GR4J. Los dos modelos difieren en términos del número de parámetros, estructura y significado físico en sus simulaciones de procesos de precipitación-escurrimiento. Aunque este estudio proporciona una oportunidad para la comparación de modelos en la captación mexicana, ambos modelos se aplican también a la cuenca del río Tampaón para evaluar la incertidumbre del modelo hidrológico en los estudios del impacto del cambio climático.

El Modelo de Herramientas de Evaluación de Agua en Suelos (SWAT) fue desarrollado en el Departamento de Agricultura de los Estados Unidos (USDA) por Arnold *et al*. (1998). El SWAT es un modelo semidistribuido de base física que opera la etapa de tiempo diaria (Neitsch, Arnold, Kiniry, Williams y King, 2002). El SWAT toma en cuenta la variabilidad espacial de la topografía, el uso de la tierra y el tipo de suelo con el fin de representar la captación en unidades de respuesta hidrológica (URH) múltiples. Las variables de entrada requeridas para ejecutar el SWAT son la precipitación diaria y las temperaturas del aire diarias máximas y mínimas. La hidrología del parteaguas en el SWAT se simula en dos etapas. La primera es la fase terrestre el ciclo hidrológico, la cual calcula el balance hídrico de cada URH para proporcionar la cantidad de agua disponible para cada canal principal de la subcuenca en una etapa de tiempo dada. La segunda etapa es la ruta del canal, la cual determina el progreso hídrico a través de la red del río hacia la salida de la cuenca (Neitsch et al., 2002). Una descripción detallada de los componentes del modelo se presenta en Neitsch, Arnold, Kiniry y Williams (2005).

El modelo GR4J (el cual representa el *modèle du Gènie Rural à 4 paramètres Journalier*) es un modelo de precipitación-escurrimiento de cuatro parámetros agrupado diariamente desarrollado por Perrin (2000). Las variables de entrada son la precipitación diaria y la evapotranspiración potencial (EP). Para este estudio, la EP se calculó utilizando la formulación (radiación extraterrestre explosiva y temperatura diaria media) propuesta por Oudin *et al*., (2005), la cual se ha demostrado que es tan efectiva para los objetivos de modelado de precipitación-escurrimientos como las formulaciones de evapotranspiración más complejas. En el GR4J la hidrología se simula del modo siguiente: primero, el modelo sustrae la EP de la precipitación para calcular la lluvia neta. Luego, a través de la intercepción, una porción de la precipitación entra en el almacén de producción, donde la evaporación real se calcula y ocurre la percolación. Otra porción de la precipitación va directamente a la ruta del flujo. La parte de la ruta de la estructura consiste en dos componentes de flujo que siguen una ruta por medio de dos hidrográficas unitarias y un almacenamiento no lineal. Una descripción detallada de la estructura del modelo se presenta en Perrin, Michel y Andreassian (2003).

El desempeño de los modelos hidrológicos se evalúa utilizando el coeficiente de Nash-Sutcliffe (NS) (Nash y Sutcliffe, 1970):

$$NS = \frac{\sum_{i=1}^{N}\left(Q_{sim,i} - Q_{obs,i}\right)^2}{\sum_{i=1}^{N}\left(Q_{obs,i} - \bar{Q}_{obs}\right)^2} \quad (5)$$

donde $Q_{obs,i}$ y $Q_{sim,i}$ son las cuencas observadas y simuladas en la etapa de tiempo i, y N es el número total de observaciones. Una eficiencia de 1 ($NS = 1$) corresponde a una correspondencia perfecta de la descarga modelada con los datos observados.

El segundo criterio de desempeño es el error cuadrado medio (ECM), el cual se calcula como:

$$ECM = \frac{\sum_{i=1}^{N}\left(Q_{sim,i} - Q_{obs,i}\right)^2}{N} \quad (6)$$

Un valor del ECM de cero corresponde a una correspondencia perfecta entre la descarga modelada y los datos observados. El ECM se calcula elevando al cuadrado los errores pronosticados,

Tabla 2. Coeficiente de Nash-Sutcliffe (NS) y Error cuadrático medio (ECM) para los periodos de calibración (1971-1985) y validación (1986-2000).

Modelos hidrológicos	NS		MSE	
	Calibración	Validación	Calibración	Validación
SWAT	0.91	0.85	0.10	0.14
GR4J	0.87	0.75	0.14	0.23

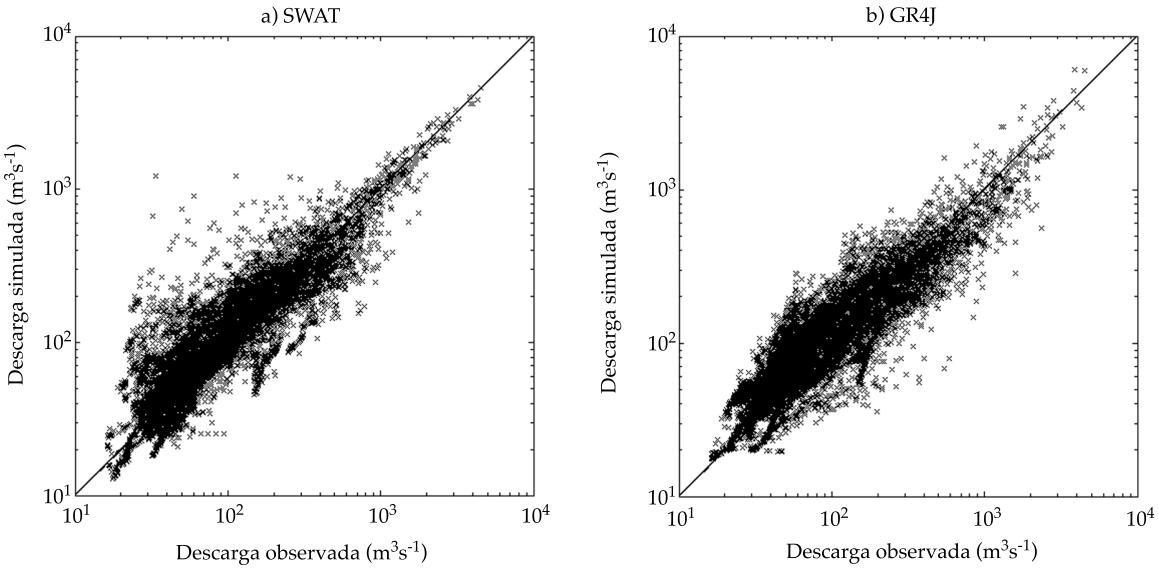

Figura 6. Descargas diarias conforme se simularon mediante a) SWAT y b) GR4J para el periodo 1971-2000.

por lo que es muy sensible a grandes errores y valores atípicos (por ejemplo, Wilks, 2006).

Resultados y discusión

Desempeño de modelos hidrológicos

La tabla 2 muestra el coeficiente de Nash-Sutcliffe (*NS*) para los periodos de calibración (1971-1985) y de validación (1986-2000) para los dos modelos hidrológicos. Ambos modelos presentan altos valores de NS que varían de 0.87 a 0.91 en el periodo de calibración y de 0.75 a 0.85 en el periodo de validación. El SWAT se desempeña ligeramente mejor que el GR4J sobre los periodos de calibración y validación.

La figura 6 muestra los diagramas de dispersión de las descargas observadas contra las

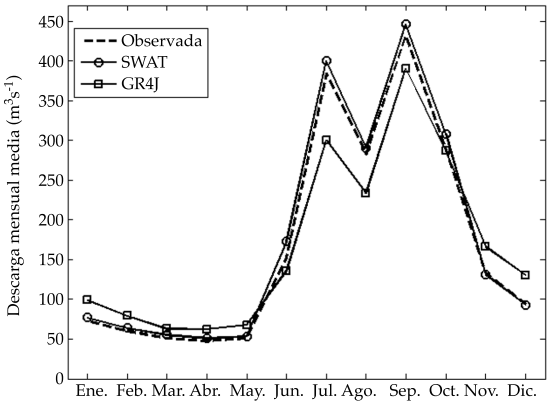

Figura 7. Descargas mensuales medias para la cuenca del Río Tampaón, simuladas mediante ambos modelos (SWAT y GR4J) utilizando datos meteorológicos observados para el periodo 1971-2000.

simuladas para el SWAT y el GR4J a lo largo de los periodos de calibración y validación. En el diagrama de dispersión, cuanto más concuerdan los dos conjuntos de datos, tanto más las dispersiones tienden a concentrarse en la vecindad de la línea 1:1. De la figura 6 puede verse que el GR4J simula mejor los flujos bajos diarios, mientras que los flujos altos diarios se predicen mejor mediante el SWAT. Cuando estos criterios de desempeño penalizan los errores en las cuencas más altas, el SWAT presenta los valores más bajos del ECM (0.10 y 0.14) mientras que el GR4J presenta los valores más altos del ECM (0.14 y 0.23, vea el cuadro 2). La figura 6 muestra también que el SWAT tiende a sobrestimar ligeramente el caudal diario mientras que el GR4J subestima ligeramente el caudal diario.

La figura 7 muestra la descarga mensual media cuando se simula por medio de ambos modelos hidrológicos accionados por los datos meteorológicos observados a lo largo del periodo 1971-2000. La simulación más precisa de las descargas mensuales medias se obtiene utilizando el SWAT. El GR4J sobrestima las descargas mensuales medias de noviembre a mayo y subestima la descarga mensual media de junio a septiembre. Sin embargo, ambos modelos capturan con éxito los flujos pico en julio y septiembre, y durante la sequía a medio verano medio.

El análisis de desempeño muestra que modelos con diferentes esquemas de conceptualización tienen diferentes resistencias en la simulación del caudal de la captación. La simulación de flujos bajos es desafiante puesto que el intercambio de agua ocurre a través del lecho del río y este puede ser alimentado mediante agua subterránea o puede filtrarse para alimentar el acuífero durante el periodo de flujo bajo (Pushpalatha, Perrin, Le Moine, Mathevet y Andréassian, 2011). Por otro lado, la simulación precisa de los flujos elevados proporciona una confianza adicional en la estimación de los eventos hidrológicos extremos, lo cual es crítico para la evaluación del riesgo en los estudios de impacto.

Cambios futuros de precipitación y temperatura

Esta sección presenta un análisis de cambios climáticos proyectados sobre la cuenca del

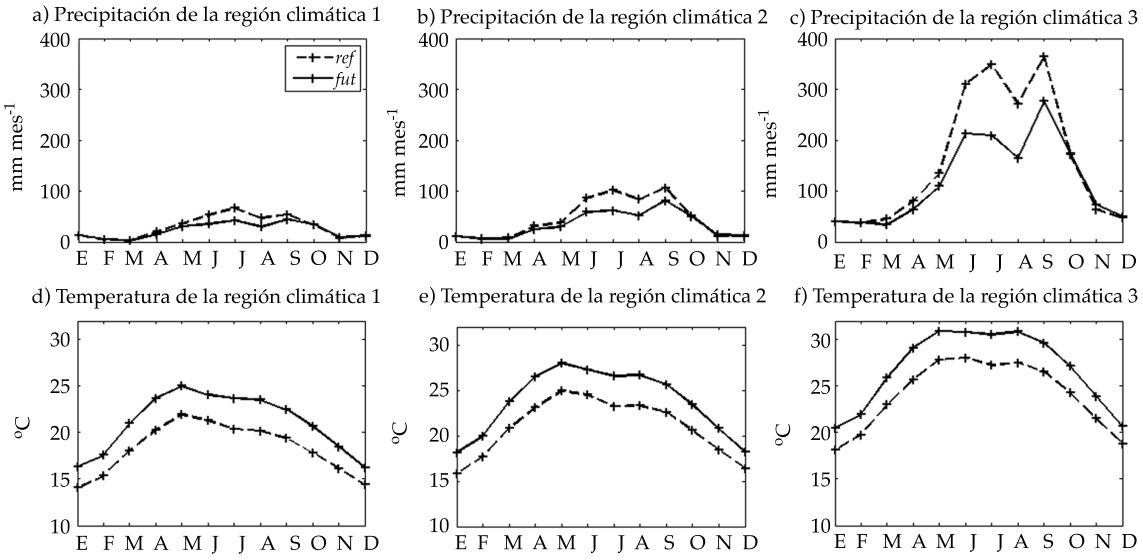

Figura 8. Precipitación y temperatura mensuales medias en los periodos de referencia y futuro a partir de las simulaciones CRCM con corrección de sesgo para tres regiones climáticas.

río Tampaón. Los cambios predichos en la precipitación y la temperatura en el clima futuro se determinan mediante el análisis de las diferencias entre los climas futuro (2040-2071) y de referencia (1971-2000) derivados de las simulaciones CRCM con corrección de sesgo.

La figura 8 muestra el clima mensual medio con corrección de sesgo para el periodo de referencia y proyecciones para el periodo futuro en las tres regiones climáticas a lo largo de la captación. Con base en el escenario de emisiones elegido, los cambios más grandes en la precipitación mensual media se estimaron durante la temporada húmeda (junio a septiembre). Por ejemplo, en la zona templada seca de la cuenca (por ejemplo, la región climática 1), la precipitación mensual media durante la temporada húmeda variará de 55 mm mes^{-1} a 37 mm mes^{-1} (figura 8a). Para el mismo periodo, en la zona semihúmeda, semicaliente de la cuenca (por ejemplo, región climática 2), es probable que la precipitación disminuya de 94 mm mes^{-1} a 63 mm mes^{-1} (figura 8b). El cambio más importante en la precipitación mensual media se estimó en la zona caliente y húmeda de la cuenca (por ejemplo, región climática 3) con una disminución en la precipitación mensual media de 323 mm mes^{-1} a 215 mm mes^{-1} durante la temporada húmeda (figura 8c). Los cambios proyectados

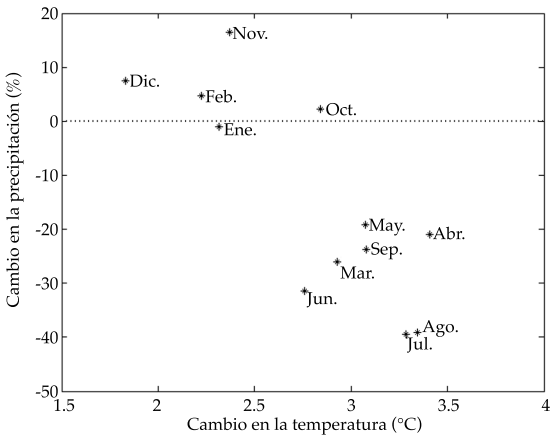

Figura 9. Señales de cambio climático medias a lo largo de la cuenca del Río Tampaón para el horizonte 2070.

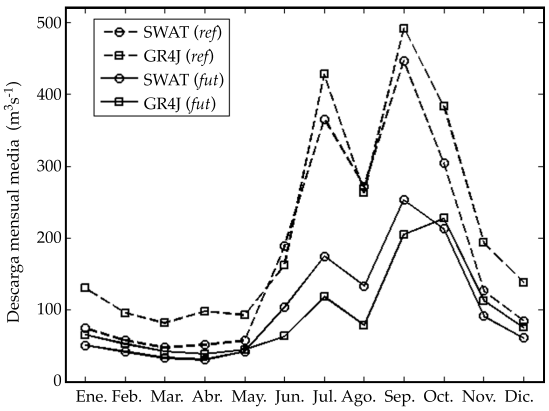

Figura 10. Descargas mensuales medias para la cuenca del Río Tampaón según se simulan mediante SWAT y GR4J a lo largo de los periodos de referencia (1971-2000) y futuro (2041-2070).

en la temperatura mensual media se estimaron muy similares a las tres regiones climáticas, con un incremento en la temperatura media anual de 2.8°C (figura 8d a 8f). Sin embargo, el cambio entre los periodos de referencia y futuros es mayor para la temperatura máxima (2°C; no mostrada) que para la temperatura mínima (2°C; no mostrada) en todas las regiones climáticas.

Las señales de cambio climático proyectado a partir de las simulaciones CRCM con corrección del sesgo sobre la cuenca completa del río Tampaón se resumen en la figura 9. Se estimó que las temperaturas mensuales medias futuras diferirán significativamente de los valores del tiempo presente, con un incremento en la temperatura media entre 1.8 y 3.3°C. El aumento de temperatura más bajo se encontró en el verano (DJF) y el incremento de temperatura mayor se estimó que ocurría en el verano (JJA). Los resultados muestran también que en el futuro la precipitación climática es muy probable que se incremente de octubre a febrero y que disminuya el resto del año.

Impactos del cambio climático sobre el caudal

Los impactos potenciales del cambio climático proyectados sobre la hidrología se exploraron para la cuenca del río Tampaón. Los cambios

del caudal inducidos por el clima se infieren mediante el análisis de las diferencias producidas por el SWAT y el GR4J cuando se accionan por los climas futuro (2041-2070) y de referencia (1971-2000) derivados de las simulaciones CRCM con corrección de sesgo (figura 10). Con base en el escenario de emisiones consideradas, una disminución significativa en el caudal mensual medio se estima sobre la cuenca del río Tampaón como resultado tanto del aumento en la temperatura (lo cual conduce a un aumento en la evapotranspiración potencial) y la disminución en la precipitación. Ambos modelos predicen el caudal pico reducido en julio y septiembre, pero los modelos predicen magnitudes diferentes. Una disminución de 309 (286) $m^3 s^{-1}$ se simula mediante el GR4J en julio (septiembre) y de 191 (194) $m^3 s^{-1}$ por el SWAT para el mismo periodo. En general, el GR4J predice cambios de caudal mayores que el SWAT alrededor de todo el año.

El impacto del cambio climático hidrológico se evalúa de manera adicional utilizando tres indicadores hidrológicos.

- Caudal mensual medio (*Qm*): la media de los valores diarios sobre un mes dado.
- El flujo alto mensual medio (HF): la media de los valores de caudal máximo para un mes dado.
- Flujo bajo mensual medio (LF): la media de los valores de caudal mínimo para un mes dado.

El impacto del cambio climático sobre indicadores hidrológicos (ΔI_{sim}) se expresa como la diferencia entre indicadores hidrológicos simulados a partir del periodo de referencia (I_{sim}^{fut}) al periodo futuro (I_{sim}^{fut}).

$$\Delta I_{sim} = \frac{I_{sim}^{fut} - I_{sim}^{ref}}{I_{sim}^{ref}} \qquad (7)$$

La figura 11 presenta las diferencias relativas (ΔI) en los indicadores investigados (*Qm*, *HF* y *LF*) sobre la cuenca del río Tampaón. El GR4J predice una disminución mayor que el SWAT en todos los indicadores. Por ejemplo, el cambio relativo en los intervalos *Qm* de alrededor de -30% a -52% durante la temporada seca (es decir, diciembre a mayo) y varía de alrededor de -48% a -65% durante la temporada húmeda (es decir, junio a septiembre) para el SWAT y el GR4J, respectivamente (figura 11a). Similarmente, el

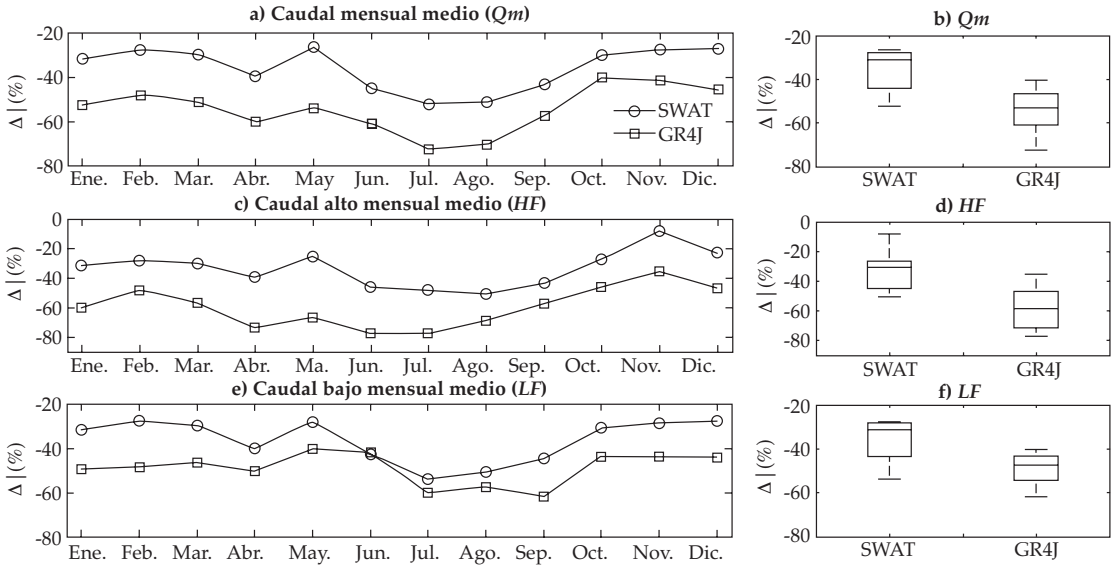

Figura 11. Cambio relativo (%) de los indicadores investigados (*Qm*, *HF* and *LF*) para los flujos mensuales medios a lo largo de la cuenca del Río Tampaón.

cambio relativo en los intervalos HF varía de alrededor de -29% a -58% durante la temporada seca y de alrededor de -47% a -70% durante la temporada húmeda para el SWAT y el GR4J, respectivamente (figura 11c). Finalmente, el cambio relativo en los intervalos LF varía de alrededor de -31% a -46% durante la temporada seca y de alrededor de -48% a -55% durante la temporada húmeda para el SWAT y el GR4J, respectivamente (figura 11e). En general, las diferencias relativas de mediana en los indicadores varían de -36% a -55% para *Qm* (figura 11b), de -34% a -60% para HF (figura 11d) y de -36% a -49% para *LF* (figura 11f). Estos resultados concuerdan con los de Mendoza *et al*. (1997), los cuales afirman que la cuenca del río Pánuco está en riesgo de convertirse en una zona seca en el futuro.

La disminución proyectada en el caudal sobre la cuenca del río Tampaón debido a cambios tanto en la temperatura como en la precipitación podría tener un impacto significativo en la disponibilidad de agua para las actividades económicas y el consumo humano. Entre las actividades económicas en la captación que podrían afectarse por el estrés hídrico debido al cambio climático, se encuentran la producción de azúcar, la producción de cítricos, la ganadería, la manufactura industrial y el turismo (Sedue, 1986). Además, la reducción en la disponibilidad de agua podría comprometer el suministro de agua de muchas ciudades en las regiones. Por ejemplo, San Luis Potosí, San Miguel de Allende y Celaya extraerán agua del río Santa María (Peña, 2013; Conagua, 2012) y se espera que Monterrey reciba el suministro a partir de la transferencia intercuenca de la cuenca del río Pánuco (SADM, 2012).

Conclusiones

Un análisis del cambio hidrológico proyectado se presenta para la cuenca del río Tampaón en el centro-este de México. Los modelos hidrológicos seleccionados son conceptualmente diferentes: SWAT es un modelo semidistribuido con base física y GR4J es un modelo agrupado conceptual. La primera etapa del estudio fue implementar los modelos hidrológicos a lo largo de la captación del estudio. Los resultados muestran que el SWAT produce la simulación más precisa de la descarga mensual observada. El GR4J sobrestima la descarga mensual media de noviembre a mayo y subestima la descarga mensual media de junio a septiembre.

El objetivo de la segunda etapa del estudio fue evaluar el impacto del cambio climático sobre el caudal de la cuenca del río Tampaón. Ambos modelos hidrológicos estiman una reducción importante en el caudal mensual medio, así como en los valores de flujo alto y bajo para el periodo de 2041-2070 comparado con el periodo de línea base 1971-2000. En general, el GR4J estima cambios del caudal mayores que el SWAT. Este resultado subraya la necesidad de considerar la incertidumbre asociada con los modelos hidrológicos en los estudios del impacto del cambio de clima hidrológico. Este tipo de incertidumbre se relaciona con el cálculo interno de procesos hidrológicos, tales como la estimación de la evapotranspiración, la formulación hidrodinámica del suelo y el modelo de nieve.

Como el SWAT se ha calibrado y validado con éxito a lo largo de la captación, la implementación del modelo puede extenderse de forma adicional a otras regiones para proporcionar un análisis regional del impacto potencial del cambio climático sobre los recursos hídricos en México.

La evaluación de los impactos del cambio climático sobre el caudal por lo general se hace a través de una cadena de modelos que incluyen las salidas del MCG para un escenario de emisiones dado, a menudo regionalizado dinámicamente por medio de un MCR y con corrección de sesgo con un método estadístico antes de usarlos para un modelo hidrológico. Cada etapa de la cadena de modelos contribuye a la incertidumbre total en la estimación de los caudales futuros. El estudio de Graham, Hagemann, Jaun y Beniston (2007) encontró que la fuente más importante de incertidumbre proviene del forzamiento MCG, el cual tiene un impacto mayor sobre los cambios hidrológicos proyectados que otras fuentes de incertidumbre. Blöshl y Montanari (2010) señalan que se puede tener una confianza razonable al predecir los

cambios hidrológicos que son activados por la temperatura del aire, tal como la nieve, que aquellos promovidos por la precipitación, tales como las inundaciones. Además, Blöshl y Montanari (2010) argumentan que las condiciones climáticas cambiantes tienen diferentes efectos tanto sobre el clima como sobre la hidrología, dependiendo de las características locales como la topografía, geomorfología y suelos de la captación. Por lo tanto, el trabajo futuro debe incluir fuentes adicionales de incertidumbre, tales como las diferentes salidas del MCG, emisión y escenarios de uso de tierra, con el fin de expandir el análisis de la incertidumbre en los estudios de impacto hidrológico (por ejemplo, Velázquez y Troin, 2015).

Reconocimientos

Este trabajo fue financiado por el Natural Sciences and Engineering Research Council of Canada (NSERC) a través de asociaciones con BC Hydro, Hydro-Québec, Rio Tinto Alcan, the Pacific Climate Impacts Consortium (PCIC), and the Ouranos Consortium. Las simulaciones del MCRC se generaron y fueron proporcionadas por Ouranos.

Referencias

Arnold, J. G., Srinivasan, R., Muttiah, R. S., & Williams, J. R. (1998). Large Area Hydrologic Modelling and Assessment-Part I: Model Development. *Journal of the American Water Resources Association*, *34*, 73-89.

Arreguín-Cortés, F. I., & López-Pérez, M. (2013). Impacts of Climate Change on the Hydrological Cycle in Mexico. *International Journal of Water Resources Development*, *29*(2), 172-183.

Bandas (2014). *Banco Nacional de Datos de Aguas Superficiales* [en línea]. Jiutepec, México: Instituto Mexicano de Tecnología del Agua [citado el 5 de septiembre de 2014]. Recuperado de https://www.imta.gob.mx/bandas.

Blöschl, G., & Montanari, A. (2010). Climate Change Impacts – Throwing the Dice? *Hydrological Processes*, *24*, 374-381.

Braun, M., Caya, D., Frigon, A., & Slivitzky, M. (2012). Internal Variability of Canadian RCM's Hydrological Variables at the Basin Scale in Quebec and Labrador. *Journal of Hydrometeorology*, *13*, 443-462.

Caya, D., & Laprise, R. (1999). A Semi-Implicit Semi-Lagrangian Regional Climate Model: The Canadian RCM. *Monthly Weather Review*, *127*, 341-362.

CLICOM (2014). *Base de Datos Climatológica Nacional* [en línea]. Ensenada, México: Centro de Investigación Científica y de Educación Superior de Ensenada [citado el 25 de junio de 2014]. Recuperado de http://clicom-mex.cicese.mx.

Conagua (2012). *Libro Blanco CONAGUA-08 Diseño, desarrollo de ingeniería y construcción de la presa de almacenamiento El Realito (*123 pp.). México, DF: Comisión Nacional del Agua.

De Elía, R., & Côté, H. (2010). Climate and Climate Change Sensitivity to Model Configuration in the Canadian RCM over North America. *Meteorologische Zeitschrift*, *19*(4), 325-339.

Graham, L. P., Hagemann, S., Jaun, S., & Beniston, M. (2007). On Interpreting Hydrological Change from Regional Climate Models. *Climatic Change*, *81*, 97-122.

Ho, C. K., Stephenson, D. B., Collins, M., Ferro, C. A. T., & Brown, S. J. (2012). Calibration Strategies: A Source of Additional Uncertainty in Climate Change Projections. *Bulletin of the American Meteorological Society*, *93*(1), 21-26.

IPCC (2014). *Climate Change 2014: Impact, Adaptation and Vulnerability. Working Group II Contribution to the IPCC 5th Assessment Report. Final Draft Accepted 30 March 2014* [en línea]. Yokohama, Japan: Intergovernmental Panel on Climate Change [citado el 15 de octubre 2014]. Recuperado de http://ipcc-wg2.gov/AR5/.

Laprise, R., Caya, D., Frigon, A., & Paquin, D. (2003). Current and Perturbed Climate as Simulated by the Second-Generation Canadian Regional Climate Model (CRCM-II) over Northwestern North America. *Climate Dynamics*, *21*, 405-21.

Maderey, L. E, Jiménez, A., & Carrillo, J. J. (2013). Global Climate Change and its Effect on Hydrological Resources of Mexico's Central Region. *Scientific Annals of Alexandru Ioan Cuza, University of Iasi*, *59*(1), 59-78.

Magaña, V. O., & Conde, C. (2000). Climate and Freshwater Resources in Northern Mexico: Sonora, a Case Study. *Environmental Monitoring and Assessment*, *61*(1), 167-185.

Martínez-Austria, P. F. (2007). Effects of Climate Change *on Mexico's Water Ressources* (76 pp.). Jiutepec, México: Instituto Mexicano de Tecnología del Agua.

Mendoza, V. M., Villanueva, E. E., & Adem, J. (1997). Vulnerability of Basins and Watersheds in Mexico to Global Change. *Climate Research*, *9*, 139-145.

Morales, P. R., Magaña, V., Barrera, C. M., & Pérez, J. L. (2001). *Efectos del calentamiento global en la disponibilidad de los recursos hidráulicos de México* (151 pp.) México, DF: IMTA-CNA Proyecto HC 0112.

Mpelasoka, F. S., & Chiew, F. H. S. (2009). Influence of rainfall Scenario Construction Methods on Runoff Projections. *Journal of Hydrometeorology*, *10*, 1168-1183.

Muerth, M. J., Gauvin-St-Denis, B., Ricard, S., Velázquez, J. A., Schmid, J., Minville, M., Caya, D., Chaumont, D., Ludwig, R., & Turcotte, R. (2013). On the Need for Bias Correction in Regional Climate Scenarios to Assess Climate Change Impacts on River Runoff. *Hydrology and Earth System Sciences*, *17*, 1189-1204.

Mundo, M. D., & Martínez-Austria, P. (enero-abril, 1993). Cambio climático: posibles consecuencias y algunas sugerencias para disminuir su efecto en México. *Ingeniería Hidráulica en M*éxico, *8*(1), 14-28.

Nash, J. E., & Sutcliffe, J. V. (1970). River Flow Forecasting through Conceptual Models, Part 1 –A Discussion of Principles. *Journal of Hydrology*, *10*(3), 282-290.

Neitsch, S. L., Arnold, J. G., Kiniry, J. R., & Williams, J. R. (2005). *Soil and Water Assessment Tool, Theoretical Documentation* (476 pp.). Texas: Blackland Research Center.

Neitsch, S. L., Arnold, J. G., Kiniry, J. R., Williams, J. R., & King, K. W. (2002). *Soil and Water Assessment Tool Theoretical Documentation Version 2000* (458 pp.). Texas: Texas Water Resources Institutes.

Oudin, L., Hervieu, F., Michel, C., Perrin, C., Andreassian, V., Anctil, F., & Loumagne, C. (2005). Which Potential Evapotranspiration Input for a Lumped Rainfall-Runoff Model? Part 2 – Towards a Simple and Efficient Potential Evapotranspiration Model for Rainfall Runoff Modelling. *Journal of Hydrology*, *303*(1), 290-306.

Peña, F. (2013). *La sed urbana. La ciudad como construcción hidráulica* (172 pp.). San Luis Potosí, México: El Colegio de San Luis, A.C.

Perrin, C. (2000). *Vers une amélioration d'un modèle global pluie-débit au travers d'une approche comparative* (530 pp.). PhD Thesis. Antony/Grenoble, France: Cemagref.

Perrin, C., Michel, C., & Andréassian, V. (2003). Improvement of a Parsimonious Model for Streamflow Simulation. *Journal of Hydrology*, *279*(1-4), 275-289.

Plummer, D. A., Caya, D., Frigon, A., Côté, H., Giguère, M., Paquin, D., Biner, S., Harvey, R., & De Elía, R. (2006). Climate and Climate Change over North America as Simulated by the Canadian RCM. *Journal of Climate*, *19*(13), 3112-3132.

Pushpalatha, R., Perrin, C., Le Moine, N., Mathevet, T., & Andréassian, V. (2011). A Downward Structural Sensitivity Analysis of Hydrological Models to Improve Low-Flow Simulation. *Journal of Hydrology*, *411*(1-2), 66-76.

Refsgaard, J. C. (1996). Terminology, Modelling Protocol and Classification of Hydrological Model Code (chapter 2) (pp. 17-39). In M. B. Abbott & J. C. Refsgaard (Eds). *Distributed Hydrological Modelling*. Dordrecht, The Netherlands: Water Science and Technology Library, 22, Kluwer Academic Publishers.

Rivas-Acosta, I., Güitrón-De-Los-Reyes, A., & Ballinas-González, H. A. (2010). Vulnerabilidad hídrica global: aguas superficiales (capítulo 4) (pp. 81-113). In P. F. Martínez-Austria, & C. Patiño-Gómez (Eds.). *Atlas de vulnerabilidad hídrica: efectos del cambio climático en los recursos hídricos de México*. Jiutepec, México: Instituto Mexicano de Tecnología del Agua.

Robles-Morua, A., Che, D., Mayer, A. S., & Vivoni, E. R. (2015). Hydrological Assessment of Proposed Reservoirs in the Sonora River Basin, Mexico, under Historical and Future Climate Scenarios. *Hydrological Sciences Journal*, *60*(1), 50-66.

SADM (2012). *Manifestación de impacto ambiental modalidad regional para el proyecto Monterrey VI* [en línea]. Monterrey, México: Servicio de Agua y Drenaje de Monterrey, I.P.D. Citado el 15 de julio de 2014. Recuperado de http://sinat.semarnat.gob.mx/dgiraDocs/documentos/nl/estudios/2012/19NL2012H0018.pdf.

Scinocca, J. F., Mcfarlane, N. A., Lazare, M., Li, J., & Plummer, D. (2008). The CCCma third generation AGCM and its extension into the middle atmosphere. *Atmospheric Chemistry and Physics*, *8*, 7055-7074.

Sedue (1986). *Estudio de calidad y clasificación del río Tampaón, San Luis Potosí y Querétaro* (223 pp.). México, DF: Secretaría de Desarrollo Urbano y Ecología.

Tapia, E. M., Minjarez, I., & Espinoza, I. (2014). Use of Stella Software for the Modelling of Climate Change Impacts on Water Balance for the Yaqui Basin River, Sonora, Mexico. *European Scientific Journal Edition*, *10*, 1857- 7431.

Teutschbein, C., Wetterhall, F., & Seibert, J. (2011). Evaluation of Different Downscaling Techniques for Hydrological Climate-Change Impact Studies at the Catchment Scale. *Climate Dynamics*, *37*(9-10), 2087-2105.

Troin, M., Velázquez, J. A., Caya, D., & Brissette, F. (2015). Comparing Statistical Post-Processing of Regional and Global Climate Scenarios for Hydrological Impacts Assessment: A Case Study of Two Canadian Catchments. *Journal of Hydrology*, *520*, 268-288.

Velázquez, J. A., Schmid, J., Ricard, S., Muerth, M. J., Gauvin St-Denis, B., Minville, M., Chaumont, D., Caya, D., Ludwig, R., & Turcotte, R. (2013). An Ensemble Approach to Assess Hydrological Models' Contribution to Uncertainties in the Analysis of Climate Change Impact on Water Resources. *Hydrology and Earth System Sciences*, *17*, 565-578.

Velázquez, J. A., & Troin, M. (2015, in preparation). Evaluating the uncertainty of the impacts of climate change on the hydrology of two Mexican catchments.

Wilks, D. S. (2006). *Statistical Methods in the Atmospheric Sciences* (627 pp.) (2nd edición). Burlington, USA: Academic Press.

Dirección institutional de los autores

Juan Alberto Velázquez Ph.D.

Catedrático Conacyt- El Colegio de San Luis A.C.
Parque de Macul 155
78299 San Luis Potosí, México
Tel.: (444) 8110101 x 5301
jvelazquez@colsan.edu.mx

Magali Troin Ph.D.

Université du Québec à Montréal
Centre ESCER
CP 8888, Succ. «Centre-Ville»
Montréal (Québec) Canada H3C 3P8
Tel: (514) 2826 464 x 347
troin.magali@ouranos.ca

Daniel Caya Ph.D.

Consortium Ouranos
550 Sherbrooke West, West Tower, 19th floor
Montréal (Québec), Canada H3A 1B9
Tel: (514) 2826 464 x340
caya.daniel@ouranos.ca

Effects of Estrogens, as Emerging Pollutants, on Health and the Environment

• Irwing M. Ramírez-Sánchez* • Polioptro Martínez-Austria •
• Marco A. Quiroz-Alfaro • Erick R. Bandala •
Universidad de las Américas Puebla, México
*Corresponding Author

Abstract

Ramírez-Sánchez, I. M., Martínez-Austria, P., Quiroz-Alfaro, M. A., & Bandala, E. R. (September-October, 2015). Effects of Estrogens, as Emerging Pollutants, on Health and the Environment. *Water Technology and Sciences* (in Spanish), 6(5), 31-42.

Emerging pollutants are substances that have the potential to be harmful to humans, flora and fauna and are not regulated by legislation. Estrogens are included in this definition of emerging pollutants, and are harmful when concentrations in humans or in the environment increase. Humans are exposed to high concentrations of estrogens because of their use in hormone replacement therapy and as contraceptives. Flora and fauna are exposed to estrogens that enter the environment through the discharge of municipal wastewater, treatment plant effluents and runoff containing waste from livestock and other farming activities. This work presents a review of the current knowledge about the effects of estrogens on humans and wildlife. It also identifies anthropogenic origins and the characteristics of estrogens in the environment. Lastly, particular treatment processes to reduce or eliminate estrogens in water are discussed.

Keywords: Estrogens, environment, cancer, human, vitellogenin, wildlife, treatment.

Resumen

Ramírez-Sánchez, I. M., Martínez-Austria, P., Quiroz-Alfaro, M. A., & Bandala, E. R. (septiembre-octubre, 2015). Efectos de los estrógenos como contaminantes emergentes en la salud y el ambiente. Tecnología y Ciencias del Agua, *6(5), 31-42.*

Los contaminantes emergentes son sustancias que tienen el potencial de dañar al ser humano, flora y fauna, y no están regulados por la legislación. Los estrógenos son parte de esta definición, es decir, contaminantes emergentes, que cuando incrementan su concentración en el ser humano o el ambiente causan daño. Los seres humanos están expuestos a concentraciones altas de estrógenos debido a su uso como parte de terapias de reemplazo hormonal o métodos anticonceptivos. Flora y fauna están expuestas a los estrógenos cuando se incorporan al ambiente por descargas de agua residual municipal, efluentes de plantas de tratamiento o por escurrimientos con desechos de la ganadería y otras actividades pecuarias. En este trabajo se presenta una revisión del estado del conocimiento sobre los efectos de los estrógenos en los seres humanos y la vida silvestre. Asimismo, se identifican el origen antropogénico, presencia y características de los estrógenos en el ambiente. Por último, se señalan algunos procesos de tratamiento para reducir o eliminar los estrógenos del agua.

Palabras clave: *estrógenos, ambiente, cáncer, humanos, vitelogenina, vida silvestre, tratamiento.*

Received: 10/09/2014
Accepted: 05/06/2015

Introduction

A total of 88.3 million organic and inorganic chemicals were registered as of June 2014 (American Chemical Society, 2014), not including protein and nucleotide sequences. Nevertheless, only 0.03% of these substances is regulated by an international agency. Even though many unregulated substances can enter the environment, their presence is not measured regularly and their effects on humans and wildlife are not well known (Pica, 2012).

Emerging pollutants is the name given to substances in the environment that are not regulated but have the potential of harming health or the environment, even in very low concentrations. Although an inventory of emerging pollutants in the environment has

Table 1. Emerging pollutants for Mexico, according to Muñoz (2012).

Group	Compound
Steroids and hormones	1. Estradoil 2. Testosterone 3. Estrone 4. α-ethinylestradiol 5. β-ethinylestradiol
Personal care products	6. Galaxolide 7. Tonalide and other PCPs 8. Triclosan (mouthwash) 9. Oxybenzone 10. DEET (insect repellent)
Industrial products	11. Pentachlorophenol (PCP) 12. Nonylphenols 13. Bisphenol A 14. Organotin compounds 15. butylbenzylphthalate
Pharmaceuticals	17. Mefenamic acid 18. Sulfasalazine 19. Ibuprofen 20. Diclofenac 21. Nimesulide 22. Ketoprofen 23. Methyl salicylic acid 24. Gemfibrozil 25. Clofibric acid and metabolites 26. Bezafibrate 27. Carbamazepine 28. Salvarsan 29. Methylprednisolone 30. Tadalafil 31. Dexamethasone 32. Chlorpheniramine 33. Astemizole 34. Amlodipine 35. Ditiazem 36. Pentoxifylline 37. Avilamycin 38. Metoprol 39. Sildenafil citrate
Antibiotics	40. Sulfamethoxazole 41. Trimethoprim 42. Ciprofloxacin 43. Roxithromycin 44. Norfloxacin 45. Sulfadiazine 46. Chloramphenicol 47. Conazole 48. Imidazoles and triazoles 49. Sulfachloropyridazine

not been performed, Muñoz (2012) proposed a list of 49 (Table 1) that are potentially significant in Mexico in terms of the quantities used, relevance to public health, toxicological action and scientific importance due to their action mechanism.

Some of the substances previously reported have been classified as endocrine disruptors. According to the EPA (2013), these agents interfere with the production, release, transport, metabolism, bridging, action or elimination of natural hormones in the body. Endocrine disruptors can be classified according to their origins as natural (estrogens and androgens), synthetic (contraceptives) or synthetic (xenoestrogens).

Xenoestrogens, such as DDT, have been associated with endocrine disruptor effects since the 1970s (Hileman, 1994; Dimogerontas & Liapi, 2014), and many of their effects on humans and the environment are known today. Nevertheless, interest in the effects of natural and semi-synthetic estrogens has recently increased due to cases of cancer among women who used hormone replacement therapy or contraceptives, and cases of feminization of fish in rivers.

Natural and Synthetic Estrogens

Estrogens are hormones whose molecule is based on the phenantrene structure. They are produced in the ovaries of females in response to signals from the brain and other organs, and are present in vertebrates and invertebrates.

In all vertebrates, including humans, the main estrogens are estrone, estradiol and estriol. Estradiol is the strongest of these since it has the most affinity with estrogen receptors (Houtman, Legler, & Thomas, 2011). Semi-synthetic estrogens such as 17 α- ethinylestradiol and mestranol are a matter of importance to humans and the environment. The chemical structure of natural and semi-synthetic estrogens is shown in Figure 1.

In the case of invertebrates, most of their hormones are ecdysteroids, which have a structure similar to estrogen in vertebrates. Oetken, Bachmann, Schulte-Oehlmann and

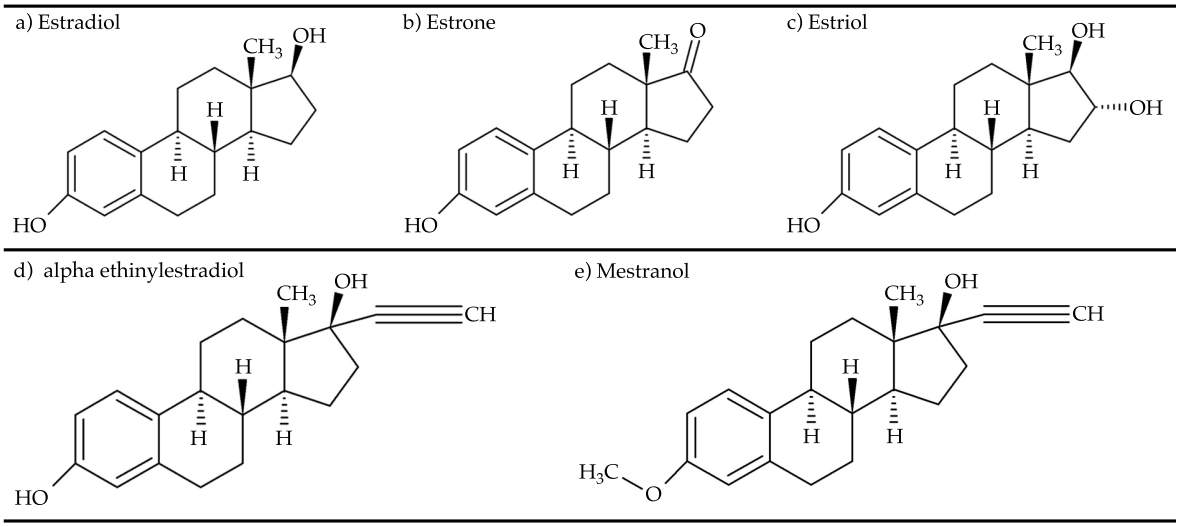

Figure 1. Chemical structure of estrogens: a, b and c are natural estrogens; d and e are semi-synthetic estrogens.

Oehlmann (2004) reported that some invertebrate taxons have estrogens, such as estradiol in mollusks and crustaceans, and estradiol and estrone in echinoderms.

Although estrogens are naturally present in vertebrates and invertebrates, adverse affects on the endocrine system are produced when humans and wildlife are exposed to concentrations greater than those produced naturally by the organism. A possible source of human exposure to high concentrations of estrogens is the use of pharmaceuticals for hormone replacement treatment, to regulate the menstrual cycle and as contraceptives. The Mexico Pharmaceutical Specialties Dictionary (PML, 2013) reports the products shown in Table 2 as containing natural and semi-synthetic estrogens.

Estrogens are also used as hormone therapies for livestock and domestic animals. The Veterinary Specialties Manual (PEV, 2014) reports the use of estrogens for therapeutic purposes, including estradiol for induction and synchronization of the estrus cycle in cows (estradiol benzoate, Bioestrogen, Estrogenic, Forestro) and estriol for treating urinary incontinence in dogs (Incurin).

Endocrine System and Estrogens

Estrogens (estradiol, estrone and estriol) are naturally produced mainly by developing

Table 2. Pharmaceutical products in Mexico that contain estrogens.

Estrogens	Combined	Commercial brand
Estradiol		Essventia, Estreva, Evorel, Oestrogel, Primogyn, Sandrena
Estradiol	Algestone	Patector, Patector N.F., Perlutal
	Ciproterone	Climene
	Dienogest	Qlaira
	Drospirenone	Angeliq
	Gestodene	Avaden
	Hydroxyprogesterone	Gravidinona
	Medroxyprogesterone	Cyclofémina, Femydrol
	Norethisterone	Meslart, Cliane, Mesigyna
	Norgestrel	Progyluton
	Prasterone	Binodian Depot
	Progesterone	Gestrygen, Proger F.
	Testosterone	Despamen
	Trimegestone	Totelle
Estriol		Ovestin (crema, óvulos, tabletas)
Estriol	Progesterone	Florgynal
Ethinylestradiol	Cyproterone	Diane
	Chlormadinone	Belara 20, Belara
	Desogestrel	Mercilon, Novial, Marvelon
	Drospirenone	Ilimit, Radiance 20, Radiance, Yasmin 24/4, Yasmin
	Etonogestrel	Nuvaring
	Gestodene	Gynovin, Minesse
	Levonorgestrel	Microgynon, Neogynon, Nordet, Triquilar
	Norelgestromine	Evra
Mestranol	Chlormadinone	Lutoral E, Secuentex 21
	Norethisterone	Norinyl 1, Norinyl 28

ovarian follicles in the corpus luteum of the placenta, adrenal cortex, brain, testicles, liver and adipose tissue (Dimogerontas & Liapi, 2014). Estrogens are produced by men and women, but in greater quantities in women ((Hileman, 1994). Their biosynthesis includes the aromatization of testosterone by the aromatase enzyme (Dimogerontas & Liapi, 2014), as shown in Figure 2. Aromatase is present in many tissues, including the adipose and the brain.

Hammond (1995) indicated that estrogens are transported through the blood and have access to the cell by bonding with SHBG proteins. After the bonded estrogens reach the cellular membrane they disassociate and the hormone can enter the cell as a result of diffusion through the cellular membrane. Once inside the cell, the estrogens can bond with estrogen receptors (ER), called ERα and ERβ (Hileman, 1994), after which a complex is formed to enter the nucleus, where a DNA bond is produced to regulate estrogen-responsive genes.

The main function of estrogens in the body is to regulate the development, maintenance and functioning of the reproductive system in both sexes. Dimogerontas and Liapi (2014) proposed that an imbalance in the amount of transported estrogens can affect the development and evolution of diseases such as breast and colon cancer, osteoporosis, cardiovascular and neurodegenerative diseases and endometriosis and obesity.

Presence of Estrogens in the Environment

Estrogens present in the environment come from natural and anthropogenic origins. A natural source is the daily human excretion of estradiol, estrone and estriol in men (1.6, 3.9, 1.5 µg, respectively) and women (3.5, 8, 4.8 µg, respectively). Pregnant women can excrete as much as 6 000 µg of estriol daily (Petrovic, *et al*., 2008).

As an anthropogenic source, the concentration of estrogens in the environment can be associated with the total amount manufactured, prescribed or acquired for hormone therapies used in humans as well as livestock and domestic animals. Williams and Brooks (2012) proposed a conceptual model of the lifecycle of these substances, which is shown in Figure 3. For example, Petrovic *et al*. (2008) reported that women who use ethinylestradiol-based contraceptives excrete 35 µg of this synthetic estrogen daily.

Estrogens represent an environmental risk due to their high potential for remaining in ecosystems and their accumulation and toxicity in wildlife (Silva, Otero, & Esteves,

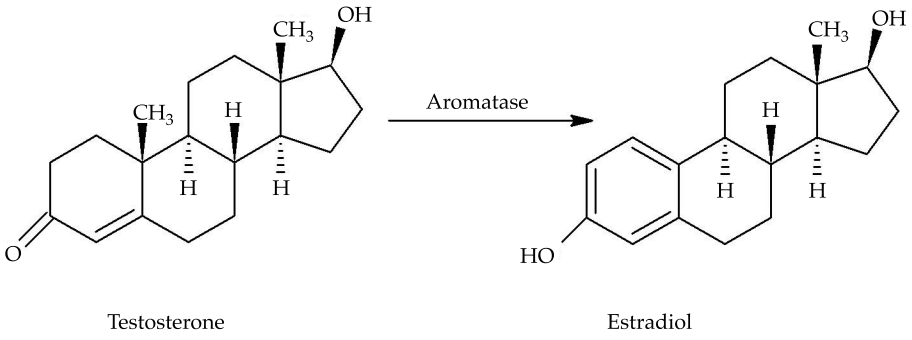

Figure 2. Estradiol biomass resulting from testosterone.

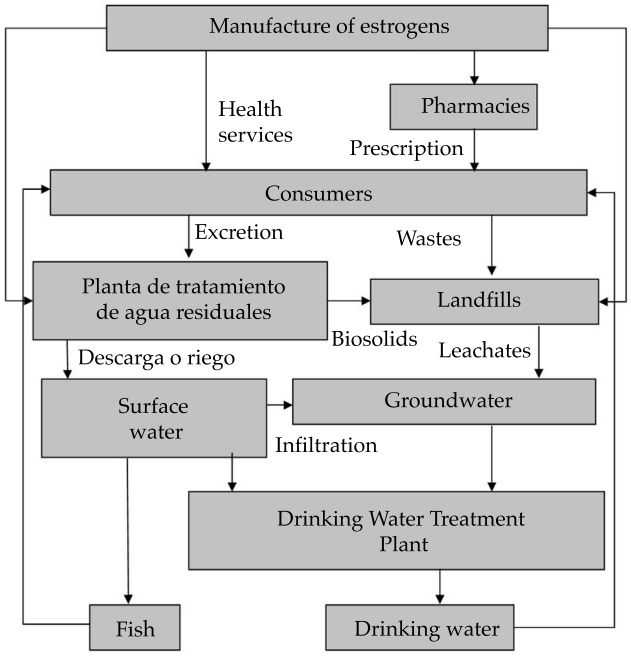

Figure 3. Means of exposure to estrogens (adapted from Williams & Brooks, 2012).

2012; Díaz-Torres, Gibson, González-Farías, Zarco-Arista, & Mazari-Hiriart, 2013). The concentration of these pollutants in water bodies is expected to vary according to the season, which can be difficult to monitor during rainy and dry seasons (Williams & Brooks, 2012; Díaz-Torres *et al*., 2013).

Estrogens have been found in treated and surface water. According to Jarošová, Bláha, Giesy and Hilscherová (2014), municipal wastewater is one of the primary sources of estrogen in the environment and produces estrogenic activity in receptor bodies. Desbrow, Routledge, Brighty, Sumpter and Waldock (1998) found maximum concentrations of 50, 80 and 7 ng/l of estradiol, estrone and ethinylestradiol, respectively, in wastewater discharged into rivers by seven water treatment plants in England. In Mexico, Díaz-Torres *et al*. (2013) found estradiol and estrone (among other endocrine disruptors) in the Xochimilco canals in Mexico City. The maximum concentrations reported by these authors were 1.68 ng/μL of estradiol and 10.38 ng/μL of estrone. They indicate that these concentrations do not represent a risk to the ecosystem but could increase stress in endemic species such as *A. mexicanum* and *C. montezumae*.

Some initiatives to regulate estrogens have been developed because of their presence in the environment and their potential risk to health and wildlife. Because of evidence of their potential as endocrine disruptors, the EPA (2012) included estradiol, estriol, estrone and ethinylestradiol on their list for the evaluation of new pollutants. Gilbert (2012) reported that the European Commission proposed to its member states the establishment of an average annual concentration limit for ethinylestradiol of 0.035 ng/l. Nevertheless, this author mentions that this regulation faces strong opposition from pharmaceutical industries which claim that there is little evidence of harm to fish populations.

Effects of Estrogens and Endocrine Disruptors

Effects at the cellular level

In humans, the non-physiological concentration of estrogens increase the risk of breast, uterine and testicular cancer (Cavalieri, Frenkel, Liehr, Rogan, & Roy, 2000; Dimogerontas & Liapi, 2014). Biological effects are produced when a hormone receptor, joined with an estrogen or endocrine disruptor, bonds to specific DNA regions in the nucleus of the cell (Hileman, 1994) or during the metabolizing of estrogens.

Cavalieri *et al*. (2000) found that estradiol, estrone and diethylbestrol induce chromosomal errors and gene mutation in animals, *in vitro* and *in vivo* , due to the generation of reactive oxygen during the metabolization of estrogens. Specifically, they report that intermediate quinones from the oxidation of 4-hydroxiestradoil or 4-hydroxiestrone can react with purines (adenine and guanine) in DNA and form mutagenic sites.

In 2002, the United States National Toxicology Program (2011) confirmed that the estrogens 17-β-estradiol, estrone, 17α-etinylestradoil and mestranol are potentially carcinogenic. The report states that epidemiological studies of humans have shown that the use of estrogens by women in post-menopause and as a contraceptive is associated with an increased risk of breast cancer.

Prenatal and Postnatal Effects

In prenatal and postnatal development of males and females, a particular ratio of estrogen and androgens (male hormones) is needed for the differentiation and formation of reproductive organs. Hileman (1994) mentions that these organs may not completely develop if this ratio is altered.

Effects in Women

The function of estrogens in women is to prepare the uterus to accept the fertilized egg and aid in pregnancy and lactation. Hileman (1994) proposed that estrogens decrease the risk of heart attack and osteoporosis but increase the risk of breast and uterine cancer.

The first study about the association between cancer and estrogenic compounds was documented in a case that occurred between 1948 and 1971, in which 2 to 6 million women in the United States and Europe took synthetic estrogen called diethylbestrol (DES) to prevent miscarriages (Hileman, 1994; Dimogerontas & Liapi, 2014). The study found that a small percentage (0.1%) of the daughters of women who took diethylbestrol developed a type of cancer called vaginal adenocarcinoma (which begins in the glandular cells) during their first 20 years of life and had high rates of infertility.

In another case, Li *et al.* (2003) found that 975 women between the ages of 65 and 79 years old diagnosed with invasive breast cancer had been taking combined hormone replacement therapy (CHRT) with estrogens and progestins.

Effects in Men

The function of estrogens in the male reproductive system is to regulate spermatogenesis (Dimogerontas & Liapi, 2014). Nevertheless, it has been documented that a high concentration of estrogens in men can inhibit sperm production (Hileman, 1994). In the study mentioned above of women treated with diethylbestrol, their children were found to have an increased incidence of abnormalities of the scrotum, non-descending testicle, malformation of the urethra, low sperm count, risk of testicular cancer and prostate problems (Hileman, 1994).

Diabetes Mellitus

Diabetes mellitus is one of the most serious health problems worldwide, with over 177 million people affected, and is one of the main causes of death globally (Dimogerontas & Liapi, 2014). Estradiol has recently been reported as a factor in the development of mellitus diabetes. Nadal, Alonso-Magdalena, Soriano, Quesada and Ropero (2009) found that 17β-estradiol serves an important function in the balance of energy, metabolism of lipids and the homeostasis of glucose. These researchers have proposed that the activation of the estrogen receptors (ERα) by 17β-estradiol promotes an increase in the biosynthesis of insulin. Nevertheless, an overstimulation of the biosynthesis of insulin by the action of environmental estrogens contributes to the development of type II diabetes.

Effects on Vertebrates

It has been confirmed that estrogens are responsible for endocrine disorders in aquatic environments (Petrovic *et al*. 2008). Some of these disorders are hermaphroditism in fish, development of deformed reproductive organs in reptiles (lizards and turtles), abnormal annidation, thin shells and immune and reproductive system dysfunctions in grey seals (Dimogerontas & Liapi, 2014).

Hileman (1994) conducted one of the first studies about the effects of estrogen on wildlife. The study consisted of painting some of the eggs from lizards with estradiol and others with the DDT byproduct. Incubation temperature was controlled which determines the sex of the individuals. They found that all of those incubated in a clean environment were male, 80% of the eggs painted with estradiol were females, and those painted with the DDT byproduct resulted in 40% intersexuals, 20% females and 40% males.

In fish eggs, exposure to estrogen during critical stages of development has been associated with a predisposition to the genetic expression of one phenotype (Houtman *et al*., 2011). In adult fish, the sex is generally determined. Nevertheless, exposing males to the hormones can cause typically female characteristics to develop.

The measurement of vitellogenin (biomarker) has been used to determine the exposure of fish to estrogens. Vitellogenin is normally found in female fish and eggs. Nevertheless, when male fish are exposed to estrogens they produce large amounts of vitellogenin (Gilbert, 2012).

Hileman (1994) reported on an experiment in which rainbow trout were confined for several weeks near a wastewater discharge in England, finding that concentrations of vitellogenin in fish were over 500 times normal. Later studies by Desbrow *et al*. (1998) suggested that estradiol, estrone and ethinylestradiol estrogens could be responsible for the synthesis of vitellogenin in male fish located downstream of wastewater discharges. Gilbert (2012) recently reported that a sampling of 51 sites in England showed that 86% of male fish had intersexual characteristics, which was primarily attributed to ethinylestradiol discharged in municipal wastewater effluents.

In another experiment, rainbow trout (*Oncorhynchus mykiss*) and roach fish (*Rutilus rutilus*) were exposed to concentrations of 1 to 10 ng/l of estradiol and estrone for 21 days. Routledge *et al*. (1998) found that these concentrations were sufficient for increasing the synthesis of vitellogenin protein in the levels observed in the fish in the Desbrow *et al*. (1998) experiment.

The European Commission has reported on the effects of estrogens on the fish population with respect to ranges of exposure to ethinylestradiol. It found smaller effects on fish for values between 0.1 and 0.2 ng/l, the expression of vitellogenin in fish for 1 ng/l, intersexual characteristics and reduced

fertility for 4 ng/l, and the collapse of the fish population for the 5 to 6 ng/l range (Gilbert, 2012).

Effect on Invertebrates

Oetken *et al*. (2004) and Matozzo, Gagne, Marin, Ricciardi and Blaise (2008) indicated that the effects of endocrine disruptors (xenoestrogens) on invertebrates have not received enough attention, considering that they represent 95% of species and play an important role in ecosystems, particularly aquatic environments. Kopec in 1917, and Wigglesworth, Fukuda and Williams in 1934 and 1940 (Riddiford & Truman, 1978) described the earliest evidence of the use of hormones for growth processes in invertebrates.

In a review by Oetken *et al*. (2004) and Matozzo *et al*. (2008) about the effects of endocrine disruptors (including estrogens) in invertebrates, they found strong evidence of effects on development, fertility and production. Given their biological importance, Prat, Rieradevall,

Barata y Munné (2013), and Souza, Hallgren, Balseiro and Hansson (2013) recently investigated the use of invertebrates as biomarkers of estrogens in water bodies, with the measurement of oxidative stress as a biomarker, in addition to vitellogenin in fish.

Effect on Vegetable Species

In a study about the genotoxic effect of estrone, estriol and estradiol, Gaitán (2006) found that estriol has a cytotoxic effect on the roots of fava beans. The effect detected was an inhibition of cellular division. This author explained that this effect can occur because estrogens are a strong inhibitor of mitosis due to their interaction with achromatic spindle (microtubules and centrioles), the DNA and regulating proteins.

Removal of Estrogens from Water

Conventional treatment plants were not designed to remove or degrade emerging pollutants such as estrogens. As a consequence, the effluents from treatment plants contain significant fractions of these substances which are discharged into the environment and accumulate there. One of the first investigations about the removal of estrogens was performed by Ternes, Kreckel and Mueller (1999) with activated sludge from a treatment plant. These investigators found that estradiol was oxidized into estrone and then degraded, while ethinylestradiol persisted, and conjugated estradiol separated and was released in its simple form.

Other subsequent investigations have proposed processes for retaining, degrading or elimination estrogens. Treatments that have been used can be classified as physical, biological and advanced oxidation. Silva *et al*. (2012) summarized the processes investigated to-date for the removal of estrone, estradiol, estriol and ethinylestradiol in water, which are as follows.

1. Physical: adsorption (activated carbon, activated granular carbon, ionic exchange resins, chitin, chitosan, molecularly imprinted polymers, Mg-Al layered double hydroxide and carbon nanotubes) and membrane filtration (ultrafiltration, nanofiltration, inverse osmosis, direct contact membrane distillation and hollow fiber microfiltration).

2. Biological: aerobic (activated sludge, percolator filter, membrane bioreactor and fixed-bed reactor systems), nitrification, anaerobic, microalgae (*Selenastrum*, *Ankistrodesmu*, *Lemna*, *Anabaena*, *Chlorococcus*, *Spirulina*, *Chlorella*, *Scenedesmus* y *Anaebena*) and enzyme treatment systems (ligninolytic, laccase, radish peroxidase) and isolated microorganisms (*Fusarium proliferatum*).

3. Advanced oxidation processes: photolysis (UVC, UVB, visible UVA, solar, photosensitive), heterogeneous photocatalysis (titanium dioxide, zinc oxide, zinc sulfide, ferric oxide, silicium, tin oxide and cadmium sulfide, among others) , strong oxidants (ferrate, ozone, hypochlorous acid, chlorine dioxide, manganese oxide, iron-tetra-amido macrocyclic), combination of strong oxidants with ultraviolet radiation (UV-hydrogen peroxide, photo-Fenton, resin coated with Fenton reactive) and sonolysis (20-1000 kHz).

Conclusions and Recommendations

Studies about the effects of estrogens on humans have recognized them as a factor that increases the risk of breast and uterine cancer. Nevertheless, there is no legislation requiring that patients be warned that the therapeutic use of estrogens may present a risk factor for cancer. In addition, because of the use of hormone therapies, human and animal waste are the main source of estrogen in the environment.

With regard to the effects of estrogens on fauna, *in vitro* and *in vivo* evidence exists which indicates that effects such as feminization and dystrophies in sexual organs are produced, at certain concentrations and for particular species characteristics. On the other hand, investigators such as Caldwell, Mastrocco, Anderson, Lange and Sumpter (2012), and the pharmaceutical industry have contradicted this evidence, indicating that the experimental conditions created by the studies simulate concentrations that are very different than those found in the environment. This disagreement in the scientific community has limited regulations related to exposure to estrogens to protect aquatic life and humans.

Each of the treatments investigated to-date have advantages and disadvantages in terms of removal efficiency, scale and costs involved to adapt existing treatment plants. The use of advanced oxidation methods to remove estrogens from water is reported to have the most advantages. Nevertheless, it is important to continue these investigations using biomarkers to ensure that the byproducts of degradation are less estrogenic or that the estrogens become mineralized.

Statistical analyses are recommended of the production, sale and consumption of estrogens in regional environments in order to estimate and correlate the concentrations found in surface and groundwater. In addition, it is important to analyze the trends in regulating estrogens in surface water, groundwater and wastewater discharges. In Mexico, studies of estrogen concentrations in untreated and treated wastewater discharges are urgently needed and their potential effects on human health and ecosystems need to be identified. Lastly, the development of technologies to remove the emerging pollutants mentioned herein needs to be continued.

References

American Chemical Society (2014) *CAS Registry* [en línea]. Chemical Abstracts Service. Citado el 2 de junio de 2014. Recuperado de https://www.cas.org/.

Caldwell, D. J., Mastrocco, F., Anderson, P. D., Lange, R., & Sumpter, J. P. (2012). Predicted-No-Effect Concentrations for the Steroid Estrogens: Estrone, 17b-Estradiol, Estriol, and 17a-Ethinylestradiol. *Environmental Toxicology and Chemistry*, *31*(6), 1396-1406.

Cavalieri, E., Frenkel, K., Liehr, J. G., Rogan, E., & Roy, D. (2000). Chapter 4: Estrogens as Endogenous Genotoxic Agents-DNA Adducts and Mutations. *Journal of the National Cancer Institute Monographs*, *27*, 75-93.

Desbrow, C., Routledge, E. J., Brighty, G. C., Sumpter, J. P., & Waldock, M. (1998). Identification of Estrogenic Chemicals in STW Effluent. 1. Chemical Fractionation and *in vitro* Biological Screening. *Environmental Science & Technology*, *32*(11), 1549-1558.

Díaz-Torres, E., Gibson, R., González-Farías, F., Zarco-Arista, A. E., & Mazari-Hiriart, M. (2013). Endocrine Disruptors in the Xochimilco Wetland, Mexico City. *Water, Air, & Soil Pollution*, *224*(1586), 1586.

Dimogerontas, G., & Liapi, C. (2014). Endocrine Disruptors (Xenoestrogens): An Overview. In T. Eliades & G. Eliades (Eds.). *Plastics in Dentistry and Estrogenicity*. Berlin Heidelberg: Springer-Verlag.

EPA (2012). *CCL 3 List Chemical Contaminants* [en línea]. United States Environmental Protection Agency. Citado

el 2 de junio de 2014. Recuperado de http://water.epa.gov/scitech/drinkingwater/dws/ccl/ccl3.cfm.

EPA (2013). *Endocrine Disruptor Research* [en línea]. United States Environmental Protection Agency. Citado el 2 de junio de 2014. Recuperado de http://www.epa.gov/research/endocrinedisruption/faq.htm.

Gaitán, O. (2006). *Evaluación ecotoxicológica del estradiol y sus metabolitos primarios liberados al ambiente, a través de la actividad ganadera* (82 pp.). Tesis de doctorado. Pachuca, México: Universidad Autónoma del Estado de Hidalgo.

Gilbert, N. (November, 22, 2012). Drug-Pollution Law All Washed Up. *Nature*, *491*, 503-504.

Hammond, G. J. (1995). Potential Functions of Plasma Steroid-Binding Proteins. *Trends in Endocrinology & Metabolism*, *6*(9/10), 298-304.

Hileman, B. (January, 31, 1994). Environmental Estrogens Linked to Reproductive Abnormalities, Cancer. *Chemical & Engineering News*, *72*(5), 19-23.

Houtman, C. J., Legler, J., & Thomas, K. (2011). Effect-Directed Analysis of Endocrine Disruptors in Aquatic Ecosystems (pp. 237-265). In W. Brack (Ed.). *Effect-Directed Analysis of Complex Environmental Contamination*. Berlin Heidelberg: Springer-Verlag.

Jarošová, B., Bláha, L., Giesy, J. P., & Hilscherová, K. (2014). What Level of Estrogenic Activity Determined by *In Vitro* Assays in Municipal Waste Waters Can be Considered as Safe? *Environment International*, *64*, 98-109.

Li, C. I., Malone, K. E., Porter, P. L., Weiss, N. S., Tang, M. C., Cushing-Haugen, K. L., & Daling, J. R. (June, 25, 2003). Relationship between Long Durations and Different Regimens of Hormone Therapy and Risk of Breast Cancer. *Journal American Medical Association*, *289*(24), 3254-3263.

Matozzo, V., Gagne, F., Marin, M. G., Ricciardi, F., & Blaise, C. (2008). Vitellogenin as a Biomarker of Exposure to Estrogenic Compounds in Aquatic Invertebrates: A Review. *Environment International*, *34*, 531-545.

Muñoz, C. J. E. (2012). Contaminantes emergentes: a aspectos químicos microbiológicos y de salud (pp. 19-27). En G. Moeller & G. Buelna (Eds.). *Contaminantes emergentes: su importancia, retos y perspectivas sobre la medición, el tratamiento y la reglamentación*. Jiutepec, México: IMTA.

Nadal, A., Alonso-Magdalena, P., Soriano, S., Quesada, I., & Ropero, A. B. (2009). The Pancreatic Beta-Cell as a Target of Estrogens and Xenoestrogens: Implications for Blood Glucose Homeostasis and Diabetes. *Molecular and Cellular Endocrinology*, *304*(1-2), 63-68.

National Toxicology Program (2011). *Report on Carcinogens:* (499 pp.) (12th Edition). North Carolina, USA: U.S. Department of Health and Human Services Public Health Service.

Oetken, M., Bachmann, J., Schulte-Oehlmann, U., & Oehlmann, J. (2004). Evidence for Endocrine Disruption in Invertebrates. *International Review of Cytology*, *236*, 1-44.

Prat, N., Rieradevall, M., Barata, C., & Munné, A. (2013). The Combined Use of Metrics of Biological Quality and Biomarkers to Detect the Effects of Reclaimed Water on Macroinvertebrate Assemblages in the Lower Part of a Polluted Mediterranean River (Llobregat River, NE Spain). *Ecological Indicators*, *24*, 167-176.

Petrovic, M., Radjenovic, J., Postigo, C., Kuster, M., Farre, M., De Alda, M. L., & Barceló, D. (2008). Emerging Contaminants in Wastewaters: Sources and Occurrence (pp. 1-35). In O. Hutzinger, D. Barceló, & A. Kostianoy (Eds.). *The Handbook of Environmental Chemistry*. Berlin: Springer.

Pica, Y. (2012). Tipo y relevancia de las fuentes de compuestos emergentes y aspectos toxicológicos (pp. 29-47). En G. Moeller & G. Buelna (Eds.). *Contaminantes emergentes: su importancia, retos y perspectivas sobre la medición, el tratamiento y la reglamentación*. Jiutepec, México: IMTA.

PML (2013). *Diccionario de especialidades farmacéuticas 2013* [en línea]. Medicamentos PLM [citado el 2 de junio de 2014]. Recuperado de http://www.medicamentosplm.com.

PEV (2014). *Prontuario de Especialidades Veterinaria 2014* [en línea]. PLM México. Citado el 2 de junio de 2014. Recuperado de http://www.diccionarioveterinarioplm.com.

Routledge, E. J., Sheahan, D., Desbrow, C., Brighty, G. C., Waldock, M., & Sumpter, J. P. (1998). Identification of Estrogenic Chemicals in STW Effluent. 2 *In Vivo* Responses in Trout and Roach. *Environmental Science & Technology*, *32*, 1559-1565.

Riddiford, L. M., & Truman, J. W. (1978). Biochemistry of Insect Hormones and Insect Growth Regulators (pp. 307-357). In M. Rockstein (Ed.). *Biochemistry of Insect*. New York: Academic Press.

Silva, C. P., Otero, M., & Esteves, V. (2012). Processes for the Elimination of Estrogenic Steroid Hormones from Water: A Review. *Environmental Pollution*, *165*, 38-58.

Souza, M. S., Hallgren, P., Balseiro, E., & Hansson, L. (2013). Low Concentrations, Potential Ecological Consequences: Synthetic Estrogens Alter Life-History and Demographic Structures of Aquatic Invertebrates. *Environmental Pollution*, *178*, 237-243.

Ternes, T. A., Kreckel, P., & Mueller, J. (1999). Behavior and Occurrence of Estrogens in Municipal Sewage Treatment Plants - II. Aerobic Batch Experiments with Activated Sludge. *Science of the Total Environment*, *225*, 91-99.

Williams, E. S., & Brooks, B. W. (2012). Human Health Risk Assessment for Pharmaceuticals in the Environment: Existing Practice, Uncertainty, and Future Directions. In B. W. Brooks, & D. B. Huggett (Eds.). *Human Pharmaceuticals in the Environment: Current and Future Perspectives, Emerging Topics in Ecotoxicology* 4. New York: Springer.

Institutional Address of the Authors

M.C. Irwing M. Ramírez-Sánchez
Dr. Polioptro Martínez-Austria
Dr. Marco A. Quiroz-Alfaro
Dr. Erick R. Bandala

Universidad de Las Américas Puebla
Posgrado en Ciencias del Agua
Grupo de Investigación en Energía y Ambiente
Sta. Catarina Mártir, Cholula
72810 Puebla, México
Teléfono: +52 (222) 2292 652
irwing.ramirezsz@udlap.mx
marcoa.quiroz@udlap.mx
polioptro.martinez@udlap.mx
erick.bandala@udlap.mx

Estudio del flujo de agua en presas con sobre relajaciones sucesivas

• Norma Patricia López-Acosta* • José León González-Acosta •
Universidad Nacional Autónoma de México
*Autor de correspondencia

Resumen

López-Acosta, N. P., & González-Acosta, J. L. (septiembre-octubre, 2015). Estudio del flujo de agua en presas con sobre relajaciones sucesivas. *Tecnología y Ciencias del Agua*, *6*(5), 43-59.

Los denominados problemas de superficie libre son problemas de valores de frontera en los que una porción de la frontera, la superficie libre, no se conoce y debe determinarse como parte de la solución. Los procedimientos rigurosos y aproximados clásicos para el trazo de esta línea se limitan a medios homogéneos e isótropos con geometrías particulares. Actualmente es posible emplear métodos numéricos como los elementos finitos (MEF) para su determinación. Sin embargo, el MEF requiere la resolución de sistemas de ecuaciones lineales que involucran el almacenamiento y manejo de un gran número de matrices que incrementan el tiempo de cálculo. En este artículo se propone una alternativa para analizar problemas de superficie libre que se basa en la resolución numérica de ecuaciones de diferencias finitas mediante el método de sobre relajaciones sucesivas (SOR, Successive Overrelaxation). Se expone la implementación de dos técnicas basadas en el método SOR: la Solución de Baiocchi y el Método de la Presión Extendida, aplicando el proceso iterativo de Gauss-Seidel. Inicialmente se proporcionan las bases teóricas de estos métodos. De manera posterior, su aplicabilidad queda expuesta con el análisis del flujo no confinado en una presa homogénea y en otra heterogénea. Como parte de los resultados, se presentan las líneas de flujo superior obtenidas con cada técnica y las redes de flujo calculadas con el método SOR; asimismo, se explica cómo determinar el gradiente hidráulico y el gasto de infiltración a través del dominio de flujo mediante ecuaciones de diferencias finitas. Por último, se proporcionan comentarios concluyentes y recomendaciones de cómo aplicar y optimar el empleo de estas técnicas.

Palabras clave: superficie libre, flujo no confinado, Sobre Relajaciones Sucesivas (SOR), proceso iterativo de Gauss-Seidel, diferencias finitas, línea superior de flujo, Método de la Presión Extendida, método de Baiocchi, redes de flujo en presas.

Abstract

López-Acosta, N. P., & González-Acosta, J. L. (September-October, 2015). Study of Water Flow in Dams using Successive Over-Relaxation. Water Technology and Sciences *(in Spanish), 6(5), 43-59.*

Free surface problems represent boundary value problems in which a portion of the boundary, the free surface, is unknown and must be determined as part of the solution. Classical rigorous and approximate procedures used to draw this line are limited to homogeneous and isotropic media with specific geometries. Currently, this can be determined using numerical methods such as the finite element method (FEM). Nevertheless, FEM requires the storing and handling of a large number of matrices to solve linear equation systems, increasing calculation time. The present article proposes an alternative to analyze free surface problems based on the numerical solution of finite difference equations using the successive over-relaxation method (SOR). Two techniques are implemented with the SOR method— Baiocchi's Solution and the Extended Pressure Method with the iterative Gauss-Seidel process. First, the theoretical basis for these methods are provided. Then, their applicability is described according to an analysis of unconfined flow in a homogeneous and a heterogeneous dam. As part of the results, the upper flow lines obtained with each technique and the flow networks calculated with the SOR method are presented and the use of finite difference equations to determine the hydraulic gradient and flow rate through the flow domain is described. Lastly, conclusions and recommendations for applying and optimizing the use of these techniques are provided.

***Keywords**: Free surface, unconfined flow, Successive Over Relaxation (SOR), Gauss-Seidel's iterative process, finite differences, upper flow line, Extended Pressure method, Baiocchi's method, flow networks in dams.*

Recibido: 18/06/2014
Aceptado: 10/06/2015

Introducción

El método de relajación clásico es un proceso iterativo en el cual las soluciones para el flujo de agua a través de medios porosos pueden obtenerse conociendo simplemente la geometría del dominio y las condiciones de frontera hidráulicas (Allen, 1954; Finnemore y Perry, 1968). Este método puede resolver la ecuación de Laplace para un punto (nodo) relativo a sus puntos circundantes utilizando una ecuación algebraica de diferencia finita (Southwell, 1940). Para este procedimiento, se dibujan una malla cuadrada con dimensiones de $\Delta_x = \Delta_y$ en la zona de flujo si el medio es homogéneo e isótropo, y se traza una malla rectangular con dimensiones $\Delta_x \neq \Delta_y$ si el medio es anisótropo. Las intersecciones de los cuadrados o rectángulos constituyen los nodos de la malla. Para estos nodos, los valores aproximados de la caída hidráulica o potencial *h* (puntos donde h requiere calcularse) deben asignarse en relación con los valores conocidos de *h* en las fronteras de flujo. Estos valores usualmente corresponden a los niveles de agua superior e inferior o al nivel de agua aguas arriba (NAAR) y a los niveles de agua aguas abajo (NAAB) del problema en cuestión (lo que se conoce como *condiciones de frontera de Dirichlet*; Cheng y Cheng, 2005). Los valores asignados en los nodos son arbitrarios y pueden ser cero o el resultado de una estimación razonable. Sin embargo, aunque existen diversas técnicas que se pueden utilizar para asegurar que el valor del potencial impuesto sobre los nodos donde h no se conoce es lo más preciso posible (Young, 1950), es importante verificar la precisión de los datos asignados manualmente calculando el residuo en cada nodo. Por ejemplo, la diferencia entre el potencial hidráulico de los cuatro nodos circundantes se calcula con respecto al nodo central o interior, y así sucesivamente. Por lo tanto, el procedimiento de relajación implica el refinamiento sistemático de este residuo a través de la malla hasta que el residuo en todos los nodos de la malla de interés es cero o prácticamente cero. Este valor indica el cumplimiento de la ecuación de Laplace cuando se expresa como una diferencia finita y resulta en una solución para cierto problema de flujo de agua (Allen, 1954; Finnemore y Perry, 1968). El método de relajación clásico tiene varias desventajas. Por ejemplo, este método se vuelve largo y tedioso cuando se tratan de obtener soluciones aproximadas si el método no se ha programado utilizando una computadora. Además, este método no proporciona una solución general y debe aplicarse a un caso particular. Sin embargo, el método de relajación clásico puede adaptarse a diversas condiciones. Debido a la versatilidad que se demuestra para este método, se han hecho varias mejoras, incluyendo la optimación del tiempo de cálculo, tomando en cuenta las variaciones de los materiales en la región de flujo, y resolviendo problemas más complejos, como los de superficie libre (flujo no confinado).

El método de *Sobre Relajación Sucesiva* (SRS) (Young, 1950) es una modificación al método de relajación clásico. Este método es poderoso y puede usarse para obtener soluciones numéricas aproximadas para ecuaciones múltiples con soluciones analíticas desconocidas (Young, 1950). Una ventaja importante del método SRS es que resuelve automáticamente las variaciones en el potencial hidráulico para todos los nodos de malla que representan la región de flujo. El método SRS una el proceso iterativo de Gauss-Seidel, el cual utiliza ecuaciones de diferencias finitas cíclicas para resolver el problema de interés (Wang y Anderson, 1982). Aplicando este método, el proceso de solución se repite automáticamente para cada nodo hasta que se obtiene la tolerancia deseada o el error mínimo. Para problemas de flujo no confinado en los cuales se desconoce *a priori* la línea de flujo superior o la superficie libre, se han ideado métodos para modificar las ecuaciones de los nodos. Estos métodos pueden usarse para resolver problemas de superficie libre con las bases del método SRS, tales como la *solución de Baiocchi* (Baiocchi, 1971; Bruch, 1980) y el método de *presión extendida* (Brezis, Kinderlehrer y Stampacchia, 1978; Bardet y Tobina, 2002). La primera solución es útil para los medios homogéneos, y la segunda, para los medios homogéneos y heterogéneos.

Sin embargo, estos métodos no se han aplicado a casos prácticos.

Por lo general, los problemas de superficie libre representan un desafío en muchas áreas de mecánica de fluidos debido a que implican problemas de valores de frontera en los cuales una porción de la frontera se desconoce y debe determinarse como parte de la solución (Cryer, 1970). La presencia de la superficie libre o el manto freático hace más difícil los métodos de análisis. La parábola de Dupuit (Dupuit, 1863) y la parábola de Kozeny (Kozeny, 1931) son soluciones rigurosas para trazar la línea de flujo superior y solo son aplicables en medios homogéneos e isótropos con paredes verticales (Dupuit) o con filtros (Kozeny). Otros métodos de aproximación, tales como los métodos de *tangente* (Schaffernak, 1917; Iterson, 1916, 1917) y *seno* (Casagrande, 1932), permiten principalmente calcular el punto de descarga de la línea de flujo superior. En el presente, los métodos numéricos, tales como los del método de elemento finito (MEF) pueden emplearse para determinar el punto de descarga de la línea de flujo superior. Sin embargo, el MEF requiere resolver un sistema de ecuaciones lineales e implica almacenar y manejar matrices que incrementan el tiempo de cálculo.

Este artículo se enfoca en implementar el método SRS como una alternativa para analizar problemas de flujo de superficie libre o no confinado en medios homogéneos y heterogéneos. Primero, se proporciona el antecedente teórico del flujo de agua en suelos, especialmente en la solución a la ecuación de Laplace utilizando diferencias finitas. Luego, se obtienen las ecuaciones básicas del método SRS. Subsecuentemente, esta técnica se puede utilizar para evaluar problemas de flujo no confinado utilizando los métodos de Baiocchi y de presión extendida. La aplicabilidad de estas técnicas se demuestra analizando el flujo no confinado de agua a través de una presa de tierra homogénea y de una presa compuesta de diferentes materiales. Explicamos cómo determinar la línea de flujo superior y se usa su posición para resolver el problema de flujo considerando flujo confinado y modificando las condiciones de frontera y las ecuaciones fundamentales para determinar las líneas equipotenciales y de flujo. De tal modo, la línea de flujo superior se obtiene para cada técnica y los flujos netos se calculan con el método SRS. Además, se explica cómo calcular el gradiente hidráulico y el flujo de filtración o tasa de flujo a través del dominio del flujo utilizando ecuaciones de diferencias finitas. Por último, se presentan observaciones concluyentes y recomendaciones respecto a la aplicación del método SRS.

Base teórica de los flujos de agua en suelos

Ecuaciones de Laplace

El flujo laminar a través de medios porosos obedece la ley de Darcy y está gobernado por la siguiente ecuación:

$$v = -k\frac{dh}{dl} \tag{1}$$

donde:

v = velocidad de descarga.
h = presión total o caída hidráulica total.
k = permeabilidad del suelo.
l = distancia recorrida por una partícula de agua.

En un formato vectorial (Harr, 1962):

$$\vec{v} = -k\,grad(h) \tag{2}$$

Además, la presión total h se define por medio de la ley de Bernoulli como sigue (ignorando la carga de velocidad):

$$h = \left[(p/\rho g) + y\right] \tag{3}$$

donde:

p = presión hidrostática (o presión de poros).
ρ = densidad del agua.
g = aceleración debido a la gravedad.
y = presión de posición con respecto al nivel de referencia.

Debido a que las cantidades de flujo de entrada y salida en la dirección normal n a las

caras del elemento cúbico con dimensiones de *dx*, *dy* y *df* son las mismas (debido al *principio de continuidad de flujo*), se cumplen las siguientes ecuaciones:

$$\frac{\partial(nv_x)}{\partial x}dx\,dy\,dz+\frac{\partial(nv_y)}{\partial y}dx\,dy\,dz$$
$$+\frac{\partial(nv_z)}{\partial z}dx\,dy\,dz=0 \qquad (4)$$

Factorizando y removiendo términos, la *ecuación de continuidad* se obtienen en tres dimensiones como sigue:

$$\frac{\partial v_x}{\partial x}+\frac{\partial v_y}{\partial y}+\frac{\partial v_z}{\partial z}=0 \qquad (5)$$

Para resolver los problemas de flujo, es conveniente utilizar una *función de potencial de velocidad* ϕ más que la presión total *h*. La ϕ se describe de la manera siguiente:

$$\phi(x,y,z)=-kh \qquad (6)$$

Por lo tanto, la velocidad de descarga en cada una de las direcciones principales se convierte en:

$$v_x=\frac{\partial\phi}{\partial x};\quad v_y=\frac{\partial\phi}{\partial x};\quad v_y=\frac{\partial\phi}{\partial x} \qquad (7)$$

De tal manera, la *ecuación de Laplace* se obtiene sustituyendo la ecuación (7) en la ecuación (5):

$$\frac{\partial^2\phi}{\partial x^2}+\frac{\partial^2\phi}{\partial y^2}+\frac{\partial^2\phi}{\partial z^2}=0 \qquad (8)$$

Si el medio es homogéneo e isótropo y el flujo solo ocurre en dos dimensiones (*X* e *Y*, flujo bidimensional), entonces:

$$\frac{\partial^2\phi}{\partial x^2}+\frac{\partial^2\phi}{\partial y^2}=0 \qquad (9)$$

Solución aproximada de la ecuación de Laplace por medio de diferencias finitas

El concepto básico del método de diferencias finitas se basa en remplazar las derivadas parciales continuas de la ecuación que gobierna el flujo de agua con la tasa de variación de las variables *x* e *y* en pequeños incrementos finitos (Mahmud, 1996). De esta manera, las siguientes ecuaciones se obtienen cuando se aplica el desarrollo de la serie de Taylor a la función de potencial ϕ (Mitchell y Griffiths, 1980):

$$\phi_{i+1,j}=\phi_{i,j}+\frac{\partial\phi}{\partial x}\Delta x_1+\frac{1}{2!}\frac{\partial^2\phi}{\partial x^2}\Delta x_1^2 \qquad (10)$$

y:

$$\phi_{i-1,j}=\phi_{i,j}-\frac{\partial\phi}{\partial x}\Delta x_2+\frac{1}{2!}\frac{\partial^2\phi}{\partial x^2}\Delta x_2^2 \qquad (11)$$

donde:

Δx_1 = distancia en la dirección X_1 entre dos nodos.
Δx_2 = distancia en la dirección X_2 entre dos nodos.
i = fila en el cual se localiza el nodo de interés.
j = columna en la cual se localiza el nodo de interés.

La figura 1 muestra la representación de un nodo que es afectado por cuatro nodos

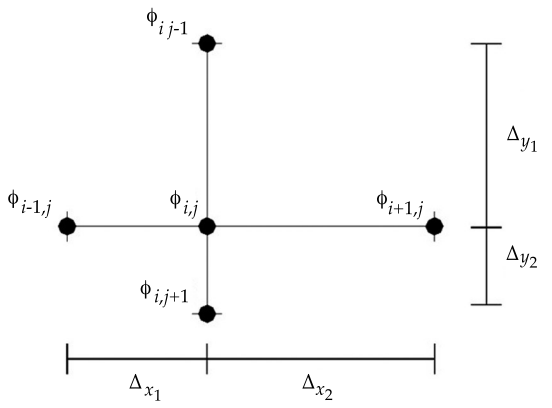

Figura 1. Arreglo de nodos en una región de flujo.

circundantes y puede usarse para observar las variables mencionadas previamente.

La expresión (10) es una aproximación a la solución de la ecuación de Laplace respecto a los nodos central y frontal ($\phi_{i+1,j}$). La ecuación (11) representa una aproximación a la solución de la ecuación de Laplace en relación con los nodos central y posterior($\phi_{i-1,j}$). Las ecuaciones para los nodos superior ($\phi_{i,j-1}$) e inferior ($\phi_{i,j+1}$) son análogos a las expresiones (10) y (11). A partir de las ecuaciones (10) y (11), y por medio de la aplicación de una serie de manipulaciones matemáticas, la solución de la función potencial $\phi_{i,j}$ está dado por:

$$\phi_{i,j} = \frac{\phi_{i,j+1} + \phi_{i,j-1} + \frac{\Delta x^2}{\Delta y^2}\left(\phi_{i+1,j} + \phi_{i-1,j}\right)}{2\left(1 + \frac{\Delta x^2}{\Delta y^2}\right)} \qquad (12)$$

Si $\lambda^2 = \frac{\Delta x^2}{\Delta y^2}$, entonces:

$$\phi_{i,j} = \frac{\phi_{i,j+1} + \phi_{i,j-1} + \lambda^2\left(\phi_{i+1,j} + \phi_{i-1,j}\right)}{2\left(1 + \lambda^2\right)} \qquad (13)$$

La ecuación 13 aproxima la solución de la ecuación de Laplace mediante el método de relajación clásico en términos de diferencias finitas. A partir de esta aproximación, se obtienen las soluciones de los nodos ubicados dentro de la región del flujo de interés. De igual modo, se determinan las expresiones para los nodos en otras ubicaciones (fronteras impermeables, esquinas, etc.,).

Bases de las ecuaciones básicas del método SRS

A partir de la ecuación (13), es posible aplicar una serie de operaciones algebraicas para obtener las ecuaciones básicas del método de sobre relajación sucesiva asumiendo lo siguiente (Young, 1950):

$$c = \phi_{i,j}^{m+1} - \phi_{i,j}^{m} \qquad (14)$$

donde:

c = residuo después de dos iteraciones de Gauss-Seidel en un nodo individual.
m = número de iteración.
$\phi_{i,j}^{m}$ = valor de la función potencial en el nodo i,j en la iteración m.
$\phi_{i,j}^{m+1}$ = valor de la función potencial en el nodo i,j, en la iteración m+1.

Resolviendo $\phi_{i,j}^{m+1}$ de (14), se obtiene la siguiente ecuación (Young, 1950):

$$\phi_{i,j}^{m+1} = \phi_{i,j}^{m} + \alpha c \qquad (15)$$

donde α es un *factor de relajación* que se añade a la ecuación. Para convergencia rápida, se recomienda que el factor de relajación esté dentro del intervalo $1 < \alpha < 2$ (Young, 1950). De hecho, el valor de α usa para denominar este método como sigue: *sobre relajación* si $1 < \alpha < 2$, y *sub relajación* si $0 < \alpha < 1$ (el proceso diverge). Además, si la ecuación (13) se sustituye en las ecuaciones (14) y (15), entonces (Wang y Anderson, 1982):

$$\phi_{i,j}^{m+1} = (1-\alpha)\phi_{i,j}^{m} + \alpha\frac{\phi_{i,j+1}^{m} + \phi_{i,j-1}^{m+1} + \lambda^2\left(\phi_{i+1,j}^{m} + \phi_{i-1,j}^{m+1}\right)}{2\left(1+\lambda^2\right)} \qquad (16)$$

La expresión (16) representa la solución de la ecuación de Laplace para un nodo central con respecto a los nodos adyacentes utilizando el método SRS. Las expresiones descritas con este método para evaluar la función potencial ϕ (Wang y Anderson, 1982) son aplicables a otras condiciones de flujo que se analizan en este artículo. Así, para un nodo ubicado en la frontera de una superficie horizontal impermeable, la solución a la ecuación de Laplace con el método SRS es:

$$\phi_{i,j}^{m+1} = (1-\alpha)\phi_{i,j}^{m+1} + \frac{\alpha}{2\left(1+\lambda^2\right)}\left[\left(\phi_{i+1,j}^{m} + \phi_{i-1,j}^{m+1}\right) + 2\lambda^2\phi_{i,j-1}^{m+1}\right] \qquad (17)$$

Para un nodo localizado en una frontera vertical impermeable, la solución es:

$$\phi_{i,j}^{m+1} = (1-\alpha)\phi_{i,j}^{m+1} + \frac{\alpha}{2(1+\lambda^2)}\left[\left(\phi_{i,j+1}^{m} + \phi_{i,j-1}^{m+1}\right) + 2\lambda^2\phi_{i+1,j}^{m+1}\right] \quad (18)$$

Para los nodos ubicados en los vértices o esquinas exteriores, la solución es:

$$\phi_{i,j} = (1-\alpha)\phi_{i,j}^{m} + \alpha\frac{\lambda^2\left(2\phi_{i,j-1}^{m+1} + \phi_{i,j+1}^{m}\right) + \left(2\phi_{i+1,j}^{m} + \phi_{i-1,j}^{m+1}\right)}{3(1+\lambda^2)} \quad (19)$$

Para los nodos ubicados en la zona de transición de dos materiales con permeabilidades diferentes, la solución es:

$$\phi_{i,j}^{m+1} = (1-\alpha)\phi_{i,j}^{m} + \frac{\alpha}{2}\left(\frac{(1+\gamma)\left(\frac{1}{2}\right)\left(\phi_{i,j+1}^{m+1} + \phi_{i,j-1}^{m+1}\right) + \gamma\phi_{i-1,j}^{m+1} + \phi_{i+1,j}^{m}}{1+\gamma}\right) \quad (20)$$

Para un nodo ubicado en la zona de transición de dos materiales y en una frontera inferior impermeable, la solución es:

$$\phi_{i,j}^{m+1} = (1-\alpha)\phi_{i,j}^{m} + \frac{\alpha}{2}\left(\frac{\gamma\left(\phi_{i-1,j}^{m+1} + \phi_{i,j-1}^{m+1}\right) + \phi_{i,j-1}^{m+1} + \phi_{i+1,j}^{m}}{1+\gamma}\right) \quad (21)$$

donde $\gamma = k_2/k_1$, k_1 es la permeabilidad del primer material y k_2 es la permeabilidad del segundo material.

Implementación del método SRS para problemas de flujo de agua no confinado

Si se determinan las zonas del dominio de flujo donde la presión del agua es cero para problemas de superficie libre o flujo no confinado, se asume que la línea de flujo superior se define en estos puntos (Cryer, 1970). La solución de Baiocchi (Baiocchi, 1971, Bruch, 1980) y el método de la presión extendida (Brezis *et al*., 1978; Bardet y Tobita, 2002) son dos variantes del método SRS que pueden usarse para determinar la posición de la línea de flujo superior en medios homogéneos o medios compuestos de materiales con diferentes valores de permeabilidad, respectivamente (como se explica adelante).

Soluciones a los problemas en medios homogéneos utilizando el método de Baiocchi (Baiocchi, 1971, Bruch, 1980)

En lugar de usar la función potencial de velocidad ϕ, el método de Baiocchi resuelve matemáticamente la ecuación de Laplace (en la zona de flujo y en sus fronteras) para flujo no confinado utilizando una nueva variable ω que depende de las características geométricas del problema (Bruch, 1980). La variable ω se expresa numéricamente con ecuaciones lineales de diferencias finitas para los nodos de la malla que discretizan la zona de flujo bajo estudio. Aplicando este método, es posible determinar la posición de la línea de flujo superior en un medio homogéneo ya que este genera valores de cero ($w = 0$) para los nodos con una presión total de agua de cero, esto significa que estos puntos están a la presión atmosférica. La forma de la expresión que describe ω depende de la ubicación de los nodos en la malla. Consecuentemente, las expresiones diferentes para obtener ω se describen en los siguientes párrafos (Bruch, 1980). Para nodos dentro de la región de flujo, ω se determina del modo siguiente:

$$w_{i,j}^{(m+1/2)} = \left(\frac{\Delta_x^2\Delta_y^2}{2\left(\Delta_x^2 + \Delta_y^2\right)}\right)\left[\frac{1}{\Delta_x^2}\left(w_{i-1,j}^{m+1} + w_{i-1,j}^{m} + \frac{1}{\Delta_y^2}\left(w_{i,j-1}^{m+1} + w_{i,j+1}^{m}\right) - 1\right)\right] \quad (22)$$

Así como:

$$w_{i,j}^{(m+1)} = \max\left\{0, w_{i,j}^{m} + \alpha\left(w_{i,j}^{(m+1/2)} - w_{i,j}^{m}\right)\right\} \quad (23)$$

donde α es el *factor de relajación*, max {…} es el valor absoluto máximo entre los dos valores de datos de la ecuación (23), y las variables restantes se definen en las secciones anteriores. Para los nodos ubicados en la frontera equipotencial aguas arriba, la variable w se define como:

$$w = \frac{1}{2}\left(L_1 - L\right)^2 \tag{24}$$

Para el nodo ubicado en la frontera equipotencial aguas abajo, w se calcula mediante:

$$w = \frac{1}{2}\left(L_2 - L\right)^2 \tag{25}$$

donde L_1 es la altura del nivel de agua aguas arriba (NAAR), L_2 es la altura del nivel de agua aguas abajo (NAAB), y L es la altura desde un punto de referencia (por ejemplo, el suelo del cimiento de la presa) para cada uno de los nodos de acuerdo con el caso de estudio.

Para nodos ubicados en la frontera de flujo inferior (base de la presa), la solución para w es:

$$w = \frac{L_1^2}{2} - \frac{L_1^2 - L_2^2}{2X_1}x \tag{26}$$

donde X_1 representa la longitud de la base de la presa en la dirección X, y x es la ubicación de cada nodo en la dirección X y 0 (origen) es el pie de la pendiente de la presa.

Soluciones a los problemas en medios heterogéneos utilizando el método de presión extendida (Brezis et al., 1978; Bardet y Tobita, 2002)

En este método, la presión hidrostática p se supone como la cantidad conocida en vez de la función potencial ϕ. Además, se utiliza el concepto de presión extendida (Brezis *et al*., 1978; Bardet y Tobita, 2002), el cual modifica la ley de Darcy del modo siguiente:

$$v' = -k \cdot \left[grad(p) + H_\varepsilon(p) grad(y) \right] \tag{27}$$

donde ε es la separación (Δy) entre dos nodos en la dirección Y. Además:

$$H_\varepsilon(p) = \begin{cases} 1 & if\ p \geq \varepsilon \\ p/\varepsilon & if\ p \leq \varepsilon \end{cases} \tag{28}$$

La solución de la ecuación (27) se determina similarmente para obtener la solución de la ecuación de Laplace utilizando el método SRS (ecuación 16) introduciendo el *factor de relajación* α. De nuevo, las expresiones que gobiernan el comportamiento en cada nodo dependen de sus ubicaciones en el dominio del flujo. De tal modo, las ecuaciones que definen p se describen más adelante (Bardet y Tobita, 2002). Para evaluar el comportamiento de los nodos ubicados dentro de la región de flujo, la presión hidrostática se define como:

$$\begin{aligned} p_{i,j}^{m+1} &= (1-\alpha)p_{i,j}^{m} \\ &+ \frac{1}{4}\alpha\left(p_{i,j+1}^{m} + p_{i,j-1}^{m+1} + p_{i+1,j}^{m} + p_{i-1,j}^{m+1} \right. \\ &\left. + \Delta_y \left[H_\varepsilon\left(\frac{p_{i,j}^{m} + p_{i,j-1}^{m+1}}{2} \right) - H_\varepsilon\left(\frac{p_{i,j}^{m} + p_{i,j+1}^{m}}{2} \right) \right] \right) \end{aligned} \tag{29}$$

Para los nodos ubicados en una frontera de flujo inferior permeable, la presión hidrostática se determina como sigue:

$$\begin{aligned} p_{i,j}^{m+1} &= (1-\alpha)p_{i,j}^{m} \\ &+ \alpha\left(\frac{1}{4}\left(2p_{i,j-1}^{m+1} + p_{i+1,j}^{m} + p_{i-1,j}^{m+1} \right) + \frac{\Delta_y}{2} \right) \end{aligned} \tag{30}$$

En contraste con el método de Baiocchi, el valor que se asigna a los nodos en las fronteras equipotenciales de la malla es igual a la presión hidrostática en relación con los niveles de agua aguas arriba o aguas abajo (NAAR o NAAB, respectivamente) para cada caso específico cuando se usa el método de presión extendida.

Para los nodos ubicados en la transición entre dos materiales con diferentes permeabilidades, las expresiones siguientes se usan para calcular la presión:

$$p_{i,j}^{m+1} = (1-\alpha)p_{i,j}^{m}$$
$$+\frac{1}{4}\alpha\left(2p_{i-1,j}^{m+1} + (1+\gamma)(p_{i,j-1}^{m+1} + p_{i,j+1}^{m}) + 2\gamma p_{i+1,j}^{m}\right.$$
$$\left.+\Delta_y\left[H_\varepsilon\left[\frac{p_{i,j}^{m}+p_{i,j-1}^{m+1}}{2}\right] - H_\varepsilon\left[\frac{p_{i,j}^{m}+p_{i,j+1}}{2}^{m}\right]\right]\right) \quad (31)$$

Para un nodo ubicado en la zona de transición y en la frontera inferior impermeable, la ecuación de aplicación es:

$$p_{i,j}^{m+1} = (1-\alpha)p_{i,j}^{m}$$
$$+\frac{1}{2}\gamma\left(\frac{p_{i-1,j}^{m+1} + (1+\gamma)p_{i,j-1}^{m+1} + \gamma p_{i+1,j}^{m}}{1+\gamma} + \Delta y H_\varepsilon\left[\frac{p_{i,j}^{m}+p_{i,j-1}^{m+1}}{2}\right]\right) \quad (32)$$

donde $\gamma = k_2/k_1$. Aquí, k_1 es la permeabilidad del primer material y k_2 es la permeabilidad del segundo material.

Aplicaciones prácticas

Las condiciones iniciales utilizando los métodos de Baiocchi y de la presión extendida

Una ventaja de trabajar con ecuaciones en los nodos de una malla es que estas pueden programarse sin mayores complicaciones utilizando hojas de cálculo sin más codificaciones o programaciones sofisticadas en otros tipos de software. Las ecuaciones de cada nodo se resuelven de manera independiente y numérica considerando solo los datos de los nodos adyacentes. En consecuencia, no es necesario (como en el método de elemento finito) estudiar el comportamiento de cada elemento, y luego con el ensamble resolver sistemas de ecuaciones lineales complejos cuando se evalúa el comportamiento global. Este proceso implica manejar y almacenar un gran número de matrices. En los

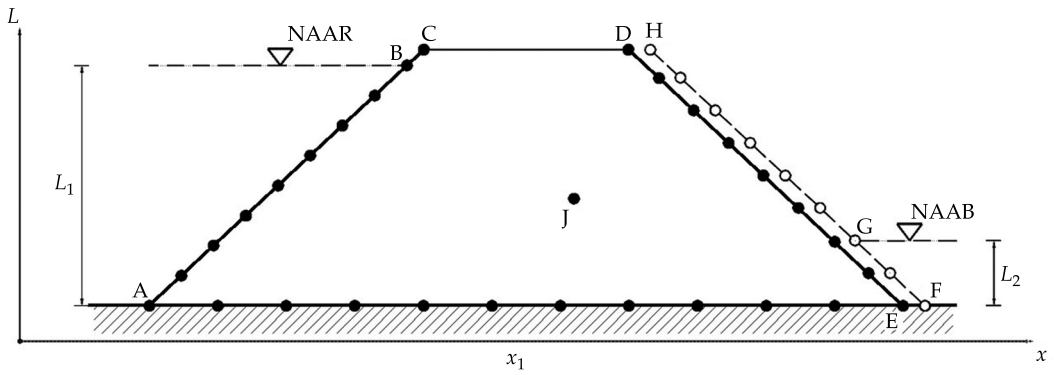

Figura 2. Aproximación de un problema de superficie libre (flujo no confinado) a través de la presa de tierra homogénea e isótropa.

Tabla 1. Parámetros de los métodos de Baiocchi y de presión extendida.

Frontera	Baiocchi	Presión extendida
AB	Ec. (24)	$p = L_1 - L$
AE	Ec. (26)	Ec. (30)
DE	Ecs. (22) y (23)	Ec. (29)
FG	Ec. (25)	$p = L_2 - L$
GH	$w = 0$	$p = 0$
J	Ecs. (22) y (23)	Ec. (29)

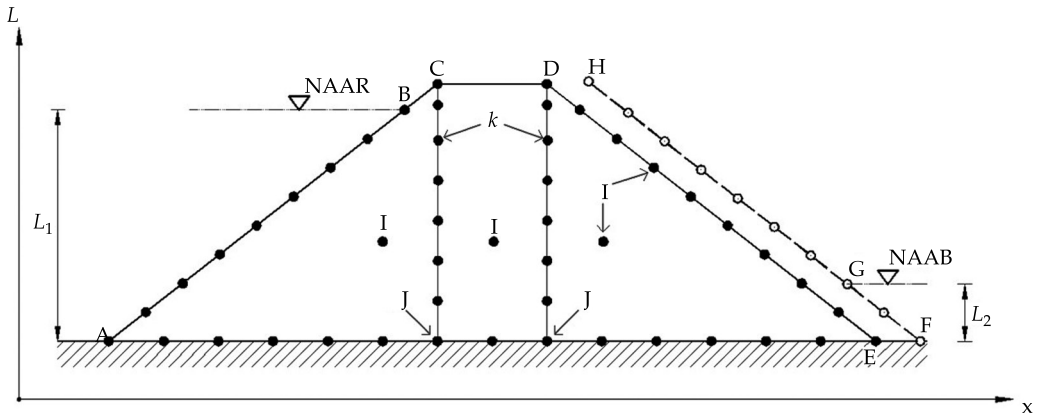

Figura 3. Aproximación de un problema de superficie libre (flujo no confinado) a través de una presa compuesta de materiales con diferentes permeabilidades.

Tabla 2. Condiciones de frontera y sus ecuaciones gobernantes.

Frontera	Presión Extendida	Frontera	Presión Extendida
AB	$p = L_1 - L$	GH	$p = 0$
AE	Ec. (30)	I	Ec. (29)
DE	Ec. (29)	J	Ec. (32)
FG	$p = L_2 - L$	K	Ec. (31)

siguientes párrafos, el uso de hojas de cálculo se ilustra mediante el uso de ecuaciones del método SRS para resolver dos problemas de superficie libre (flujo no confinado) en presas.

La figura 2 muestra un problema de flujo no confinado en una presa homogénea e isótropa. En la misma figura, se muestran las ubicaciones de algunos de los nodos y las fronteras con las ecuaciones o condiciones que gobiernan su comportamiento. Estos parámetros se listan en la tabla 1 para los métodos de Baiocchi y la presión extendida.

Similarmente, la figura 3 ejemplifica un problema de flujo en una presa que está construida de materiales con permeabilidades diferentes. Las condiciones de frontera y sus ecuaciones gobernantes para este caso cuando se aplican al método de presión extendida se proporcionan en la tabla 2.

Se recomienda que los nodos en la pendiente aguas abajo de la presa o la estructura de tierra (fronteras FGH, indicadas con círculos abiertos en la figuras 2 y 3, respectivamente) deben colocarse fuera de la zona de flujo (los *nodos fantasma*) (Wang y Anderson, 1982). Este proceso permite que la línea de flujo superior se desarrolle por completo dentro de la zona de flujo en vez de ser forzada a finalizar exactamente en el NAAB (nivel de agua aguas abajo). En otro caso, es posible que la superficie de descarga libre no esté bien definida.

En los problemas analizados de aquí en adelante, se supuso un *factor de relajación* de $\alpha = 1.7$, el cual es el valor recomendado para optimizar significativamente y reducir el tiempo de cálculo (Salmasi y Azamathulla, 2013). Además, los análisis se realizan en las siguientes etapas: 1) cálculo de la posición de la línea de flujo superior, 2) evaluación de la función potencial ϕ para trazar las línea equipotenciales, 3) estimación de los valores de la función de corriente ψ para trazar las líneas de flujo, 4) cálculo de los

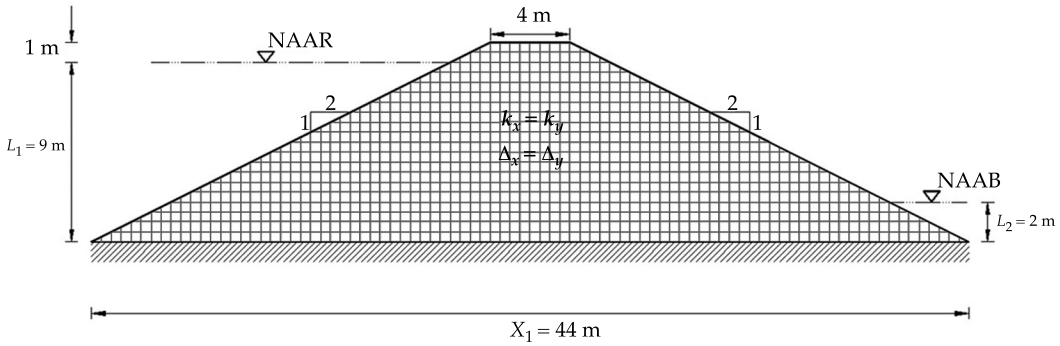

Figura 4. Características geométricas y malla utilizada para implementar el método SRS en una presa de tierra homogénea que se construyó sobre roca impermeable.

gradientes hidráulicos y 5) evaluación del flujo de filtración (como se describe más adelante).

Solución del problema de flujo para una presa homogénea

Se estudió el flujo de agua a través de una presa de tierra homogénea que se construyó en roca impermeable. La figura 4 muestra las características geométricas y la malla que se usó para implementar el método SRS, con un espaciamiento o distancia de nodo de $\Delta x = \Delta\gamma = 0.20$ m. La presa estudiada tiene pendientes 2:1 aguas arriba y aguas abajo con niveles de agua supuestos de NAAR = 9.0 m (aguas arriba) y NAAB = 2.0 m (aguas abajo).

Junto con una hoja de cálculo, la figura 5 presenta los resultados que se obtuvieron en la etapa 1) cuando se dedujo la posición de la línea de flujo superior. La hoja de cálculo se cortó a fin de apreciar los resultados en el pie de la presa y cerca de su cresta (en parte de la pendiente aguas arriba). Los valores en cada una de las celdas representan las soluciones que fueron obtenidas por medio de las ecuaciones de Baiocchi (figura 5a) y de presión extendida (figura 5b), las cuales se indican en la sección "las condiciones iniciales utilizando los métodos de Baiochhi y la presión extendida".

Una vez que se define la línea de flujo superior, las condiciones de frontera se modifican para continuar el proceso de cálculo. Primero, la función potencial ϕ se determina para trazar las líneas equipotenciales. Segundo, los valores de la función de corriente Ψ se obtienen trazando las líneas de flujo. De esta forma, en la etapa 2), los valores respectivos de la presión total h (ecuación (3)) se asignan en los nodos localizados en las fronteras de la infiltración de agua (aguas arriba), el área de descarga (aguas abajo) y en la línea de flujo superior para evaluar la función potencial ϕ. En cambio, los nodos de la frontera de flujo inferior (base impermeable de la presa) son gobernados por la ecuación (17). En la etapa 3 considerando una analogía de Ψ con ϕ, es posible usar las mismas ecuaciones para calcular la función de corriente ψ que se usó en el cálculo de la función potencial ϕ. Aquí, las condiciones de frontera se modifican otra vez de acuerdo con las siguiente situaciones: a) en la línea de flujo inferior (frontera impermeable), se asigna un valor de cero a todos los nodos ($\Psi_1 = 0$) y b) el valor asignado a la línea de flujo superior representa el flujo que pasa entre las líneas de flujo superior e inferior, lo cual corresponde al flujo de filtrado total a través de la presa ($\Psi_2 = q_{tot}$) (Bardet y Tobita, 2002; Bosch y Davis, 1997). La figura 6a exhibe la posición de la línea de flujo superior que se obtuvo utilizando las técnicas de Baiocchi y de presión extendida (basadas en el método SRS). Con fines de comparación, esta figura muestra también la posición de la línea

a) Valores de w calculados con la solución de Baiocchi

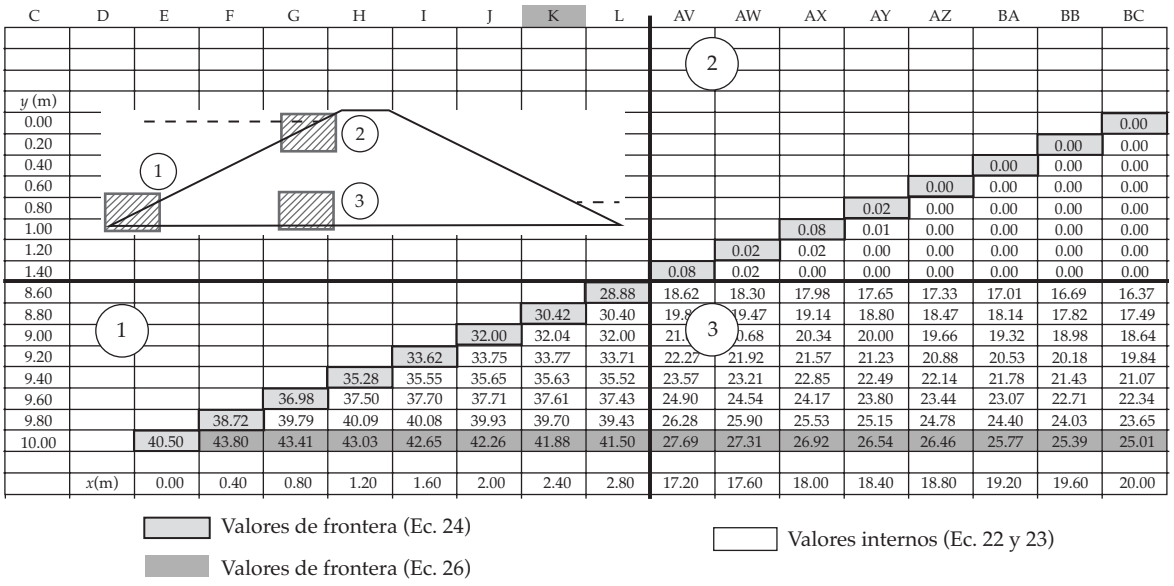

b) Valores de p calculados con el método de Presión Extendida

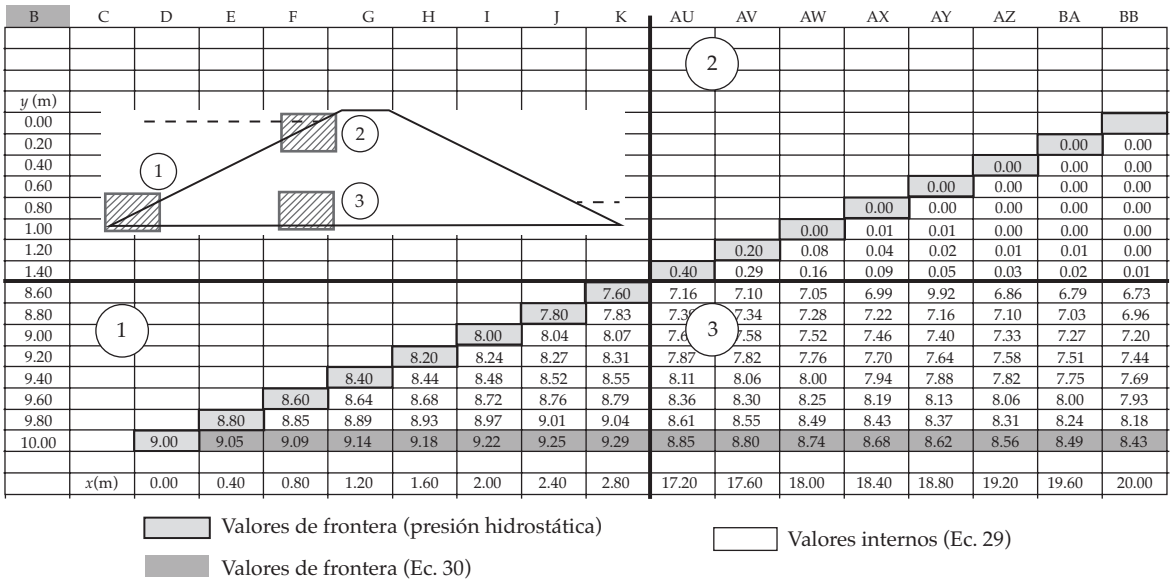

Figura 5. Valores de w y p que se calcularon en los nodos de fronteras y dentro de la zona de flujo (pendiente aguas arriba) aplicando: a) la solución de Baiocchi y b) el método de presión extendida.

de flujo superior que se calculó con la parábola de Kozeny (un método riguroso propuesto por Kozeny en 1931) y el método de elemento finito (un método numérico aproximado que se aplicó aquí mediante el algoritmo SEEP/W, Geo-Slope International Ltd., 2008).

Como se reveló en la figura 6a, las líneas de flujo superior calculadas con el procedimiento

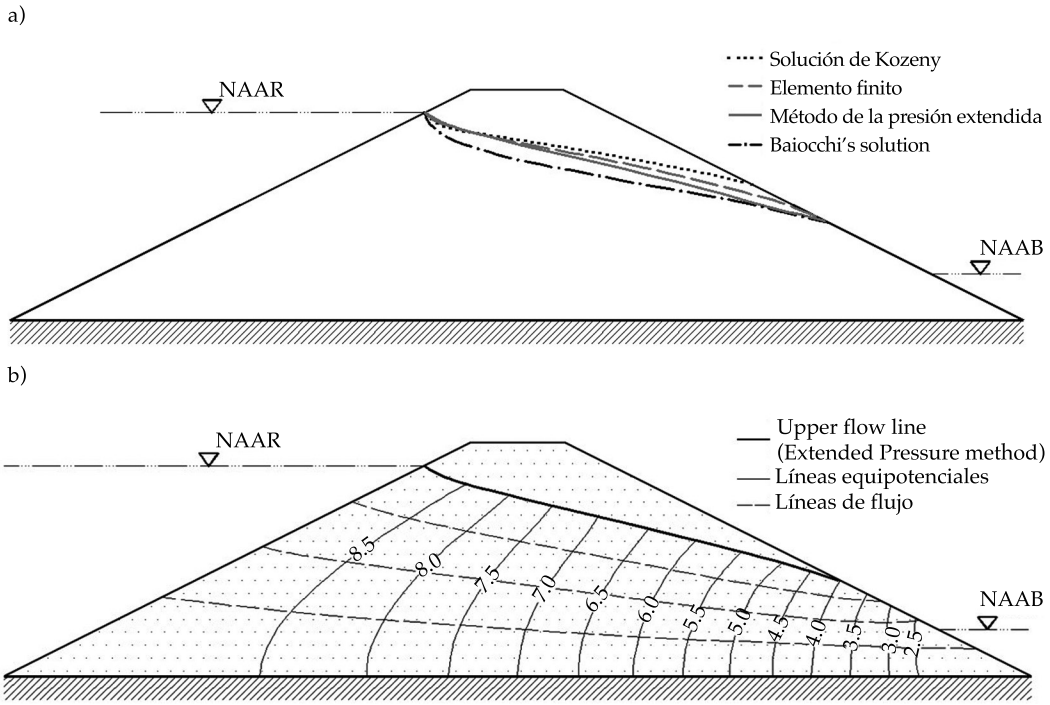

Figura 6. Estudio del flujo de agua a través de una presa de tierra homogénea e isótropa: a) comparación de las líneas de flujo superior obtenidas utilizando diferentes métodos y b) el flujo neto calculado numéricamente con el método de la presión extendida (basado en el SRS).

propuesto aquí utilizando el método SRS fueron similares a las determinadas por medio de otros métodos. En particular, la técnica de presión extendida corresponde a la solución que se obtuvo por medio del método de elemento finito. La figura 6b proporciona el flujo neto calculado numéricamente con base en el método SRS, el cual considera las posiciones de la línea de flujo superior que se obtuvieron con el método de presión extendida. Adicionalmente, la figura 6b confirma que el método SRS puede usarse para definir con exactitud el flujo neto.

Solución de problemas de flujo para una presa compuesta de materiales con permeabilidades diferentes

En este caso se estudió el flujo de agua a través de la presa compuesta por diferentes materiales. La figura 7 muestra las características geométricas y la malla que se usó para implementar el método SRS con un espaciamiento o distancia de nodos de $\Delta x = 0.20$ m y $\Delta\gamma = 0.10$ m, respectivamente. De igual manera, esta figura muestra un nivel de agua aguas arriba de NAAR = 9.0 m (1.0 debajo de la cresta de la presa) y pendientes aguas arriba y aguas abajo de 2:1 para la presa. El núcleo de la presa está compuesto de material de baja permeabilidad (k_2) relativa a los materiales de transición adyacente (k_1 y k_3). La razón entre las permeabilidades del material del núcleo y el material de transición aguas arriba es $k_2/k_1 = 0.1$, y la razón entre las permeabilidades del material del núcleo y el material de transición aguas abajo es $k_3/k_2 = 10$. En el pie de esta presa, se colocó un filtro de arena horizontal con alta permeabilidad y longitud de 10.0 m, el cual desahoga la presión de agua para evitar o mitigar problemas de erosión en esta parte de la presa.

Esta aplicación práctica se resuelve de manera similar a la aplicación previa del modo siguiente: etapa 1) deducción de la posición

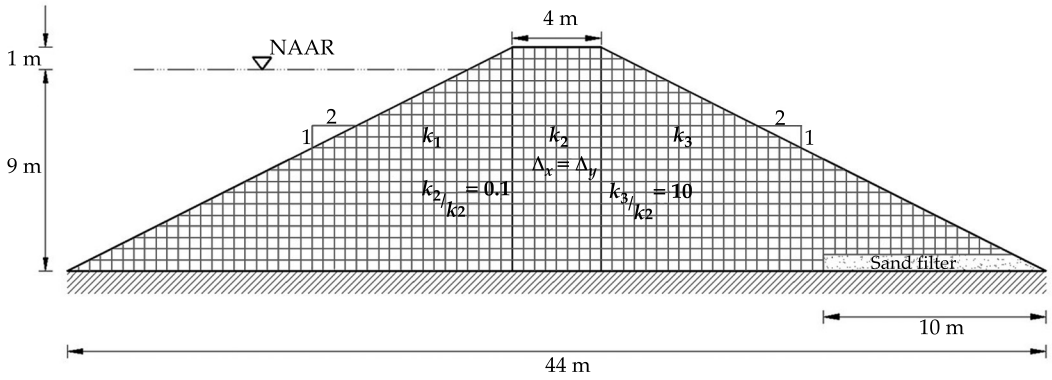

Figura 7. Características geométricas y malla utilizada para implementar el método SRS en una presa compuesta de diferentes materiales y un filtro de arena de alta permeabilidad en el pie de la pendiente aguas abajo.

de la línea de flujo superior con el método de la presión extendida, etapa 2) evaluación de la función potencial ϕ para trazar las líneas equipotenciales y etapa 3) cálculos de los valores de la función de cauce Ψ para trazar las líneas de flujo. Además, una vez que se obtuvieron las variaciones de la presión de agua en la presas, con el fin de completar la solución del problema de flujo se determinan los gradientes hidráulicos en la etapa 4) y el flujo de filtración se calcula en la etapa 5) como se indica más adelante. Para evaluar el gradiente hidráulico (magnitud resultante) dentro de la zona de flujo, puede aplicarse la siguiente expresión en términos de diferencias finitas (Budhu, 2000):

$$i(res)_{i,j} = \sqrt{\left(\frac{\left(\frac{1}{2}\right)\left(\phi_{i+1,j} - \phi_{i-1,j}\right)}{\Delta x}\right)^2 + \left(\frac{\left(\frac{1}{2}\right)\left(\phi_{i,j+1} - \phi_{i,j-1}\right)}{\Delta y}\right)^2} \quad (33)$$

donde i(res) es el valor del gradiente hidráulico (magnitud resultante) en cada nodo de la malla.

El cálculo de la tasa de flujo se determina trazando una línea vertical o plano a través de la región de flujo y utilizando los pares de nodos sobre esta línea que se ubican en dirección transversa al flujo. De tal modo, la tasa de flujo se obtiene de la siguiente ecuación (Budhu, 2000):

$$q_{tot} = \frac{k_x \Delta_y}{2\Delta_x}\left(\sum_{j=D}^{E}\left(\phi_{i-1,j} - \phi_{i+1,j}\right)\right) \quad (34)$$

donde:

q_{tot} = tasa de flujo total a través de la zona de flujo.
k_x = permeabilidad en la dirección X.
D = nodos ubicados en la línea inferior.
E = nodos ubicados en la línea superior.
Δx = distancia entre dos nodos en la dirección X.
Δy = distancia entre los dos nodos en la dirección Y.

La figura 8 muestra la hoja de cálculo que se usó para resolver el problema. Los valores de las celdas corresponden a la presión hidrostática (p) que se calculó para los nodos de la frontera impermeable, el filtro y el interior de la zona de flujo cuando se aplicó el método de la presión extendida (la hoja de cálculo se corta para mostrar una parte de los resultados).

La figura 9a muestra el flujo neto que se obtuvo numéricamente con el método SRS en la presa analizada. En este caso, la línea de flujo superior se calculó con la técnica de la presión extendida. Con fines de comparación, la figura 9b presenta la línea de flujo superior que se obtuvo utilizando el método de ele-

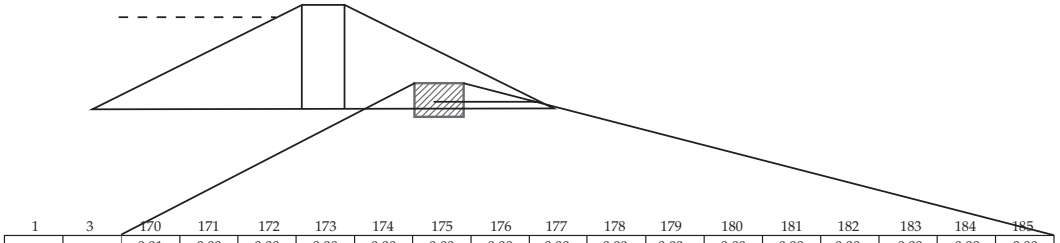

1	3	170	171	172	173	174	175	176	177	178	179	180	181	182	183	184	185
		0.01	0.00	0.00	0.00	0.00	0.00	0.00	0.00	0.00	0.00	0.00	0.00	0.00	0.00	0.00	0.00
y (m)		0.01	0.01	0.00	0.00	0.00	0.00	0.00	0.00	0.00	0.00	0.00	0.00	0.00	0.00	0.00	0.00
8.2		0.02	0.01	0.01	0.00	0.00	0.00	0.00	0.00	0.00	0.00	0.00	0.00	0.00	0.00	0.00	0.00
8.3		0.04	0.02	0.01	0.01	0.01	0.00	0.00	0.00	0.00	0.00	0.00	0.00	0.00	0.00	0.00	0.00
8.4		0.08	0.05	0.03	0.02	0.01	0.01	0.00	0.00	0.00	0.00	0.00	0.00	0.00	0.00	0.00	0.00
8.6		0.19	0.14	0.09	0.05	0.03	0.02	0.01	0.01	0.00	0.00	0.00	0.00	0.00	0.00	0.00	0.00
8.7		0.25	0.20	0.14	0.09	0.05	0.03	0.02	0.01	0.01	0.00	0.00	0.00	0.00	0.00	0.00	0.00
8.8		0.31	0.25	0.19	0.14	0.08	0.05	0.03	0.02	0.01	0.01	0.00	0.00	0.00	0.00	0.00	0.00
8.9		0.36	0.30	0.24	0.18	0.13	0.08	0.04	0.03	0.02	0.01	0.01	0.00	0.00	0.00	0.00	0.00
9		0.42	0.35	0.29	0.23	0.17	0.11	0.07	0.04	0.02	0.01	0.01	0.00	0.00	0.00	0.00	0.00
9.1		0.47	0.40	0.34	0.27	0.21	0.15	0.10	0.06	0.03	0.02	0.01	0.01	0.00	0.00	0.00	0.00
9.2		0.52	0.45	0.38	0.31	0.25	0.18	0.13	0.08	0.05	0.03	0.02	0.01	0.01	0.00	0.00	0.00
9.3		0.58	0.50	0.42	0.35	0.28	0.21	0.15	0.10	0.06	0.04	0.02	0.01	0.01	0.01	0.00	0.00
9.4		0.63	0.54	0.46	0.38	0.30	0.23	0.17	0.12	0.08	0.05	0.03	0.02	0.01	0.01	0.00	0.00
9.5		0.68	0.59	0.49	0.40	0.32	0.25	0.19	0.13	0.09	0.06	0.04	0.02	0.01	0.01	0.01	0.00
9.6		0.73	0.63	0.53	0.42	0.33	0.25	0.19	0.14	0.10	0.06	0.04	0.03	0.02	0.01	0.01	0.00
9.7		0.79	0.67	0.55	0.43	0.33	0.24	0.18	0.13	0.10	0.07	0.05	0.03	0.02	0.01	0.01	0.01
9.8		0.85	0.72	0.58	0.43	0.30	0.21	0.15	0.12	0.09	0.07	0.05	0.03	0.02	0.01	0.01	0.01
9.9		0.93	0.78	0.62	0.43	0.22	0.14	0.11	0.09	0.07	0.05	0.04	0.03	0.02	0.01	0.01	0.00
10		1.02	0.87	0.68	0.43	0.00	0.00	0.00	0.00	0.00	0.00	0.00	0.00	0.00	0.00	0.00	0.00
	x (m)	33.2	33.4	33.6	33.8	34	34.2	34.4	34.6	34.8	35	35.2	35.4	35.6	35.8	36	36.2

Valores de frontera (presión hidrostática de filtro)
Valores de frontera (Ec. 30)
Valores internos (Ec. 29)

Figura 8. Valores de la presión hidrostática (*p*) que se calcularon para los nodos de la frontera impermeable, en el filtro y dentro de la zona de flujo aplicando el método de la presión extendida.

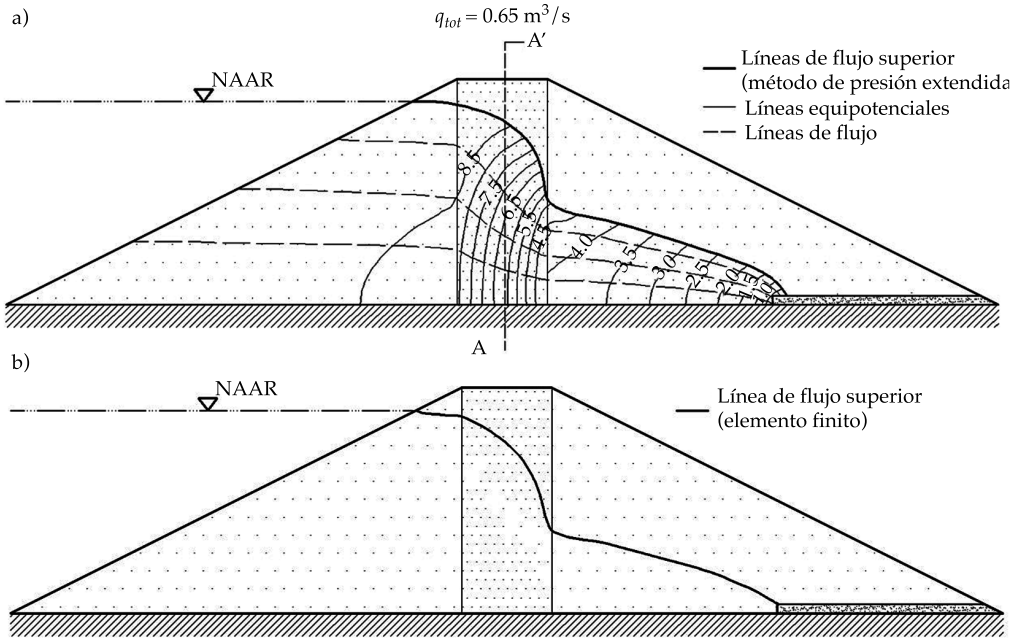

Figura 9. a) Flujo neto que se calculó con el método de SRS en una presa compuesta de diferentes materiales y un filtro horizontal en el pie de la pendiente aguas abajo y b) la línea de flujo superior obtenida por el método de elemento finito.

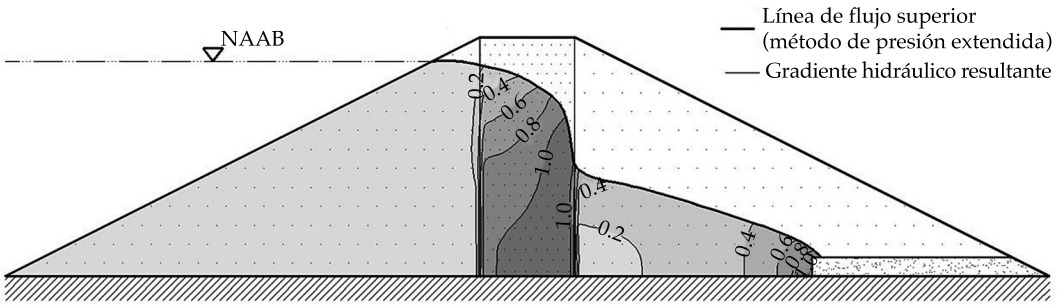

Figura 10. Valor de gradiente hidráulico resultante que se calculó mediante el método SRS.

mento finito a través del algoritmo SEEP/W (Geo-Slope International Ltd., 2008). Cuando se compararon los resultados obtenidos con SRS y MEF, se observaron similitudes. En la zona del material con permeabilidad menor, ocurre una pérdida mayor de carga hidráulica. Sin embargo, debido a la ley de continuidad para el flujo de estado estable, la tasa de flujo total que atraviesa las tres zonas de flujo es la misma $q_{tot} = 0.65$ m^3/s. Esta tasa de flujo se calculó en términos de diferencias finitas con la ecuación (34). De manera similar, la teoría clásica advierte (Cedergren, 1989) casos en los que el dominio del flujo consiste en dos o más porciones con diferentes permeabilidades (cada una consiste de un suelo homogéneo e isótropo), en el cual se distorsiona el flujo neto en las fronteras entre materiales contiguos (figuras 9a y 9b) de manera que la misma cantidad de flujo pasa por ambos lados de la frontera entre las dos líneas. Así, las figuras 9a y 9b señalan que la permeabilidad es menor para los canales de flujo más anchos y mayor para los canales de flujo más estrechos (Flores, 2000).

Finalmente, la figura 10 proporciona el gradiente hidráulico (magnitud resultante) en la zona de flujo que se calculó utilizando diferencias finitas con la ecuación (33).

Conclusiones

En este trabajo se propuso una alternativa para analizar problemas de superficie libre. Esta alternativa se estableció sobre la solución numérica de ecuaciones de diferencias finitas utilizando el método SRS (sobre relajación sucesiva). Se presentó la implementación de dos técnicas basada en el método SRS, incluyendo la solución de Baiocchi y el método de la presión extendida, el cual utiliza el proceso iterativo de Gauss-Seidel. Las ecuaciones del método SRS pueden habilitarse fácilmente utilizando hojas de cálculo para las soluciones de los diferentes tipos de problemas de flujo de complejidad variable (tal como los problemas de superficie libre) sin requerir programación sofisticada o software especializado. Utilizando el método SRS, las ecuaciones de cada nodo se resuelven de manera numérica independiente y automáticamente considerando los datos de los nodos adyacentes. De tal modo, no es necesario (como en otros métodos numéricos como el del MEF) estudiar el comportamiento de cada elemento y a partir de ahí resolver con el ensamble sistemas complejos de ecuaciones lineales con el fin de evaluar el comportamiento global, lo cual involucra el almacenamiento y manejo de un gran número de matrices que incrementa el tiempo de cálculo. La aplicabilidad del método fue expuesta mediante el análisis de flujo de agua no confinada a través de presas de tierra homogéneas y heterogéneas. Utilizando la técnica SRS, se calcularon las variaciones de la función potencial ϕ y la función de cauce Ψ para trazar numéricamente el flujo neto. Además, la magnitud resultante del gradiente hidráulico,

la tasa de flujo total y la posición de la línea de flujo superior se estimaron con las técnicas de Baiocchi y de presión extendida. A partir del análisis realizado, se mostró que el método de la presión extendida proporciona resultados con mejor aproximación que la solución de Baiocchi. En particular el método de la presión extendida proporciona resultados prácticamente iguales a aquellos calculados con el MEF. Una ventaja adicional que se observó en el método de la presión extendida es que no requiere de una discretización muy refinada del domino de flujo. En consecuencia, este método puede usarse para obtener buenos resultados incluso cuando es grande la separación entre los nodos de la malla (una red burda). Los resultados obtenidos demuestran que las técnicas implementadas en este artículo son simples y de fácil aplicación. Además, estas técnicas proporcionan resultados similares a los que se obtienen con los métodos numéricos populares actuales, tales como el método del elemento finito.

Reconocimientos

Los coautores agradecen al Programa de Becas (nivel postgrado) del *Instituto de Ingeniería de la Universidad Nacional Autónoma de México* (*UNAM*) por brindar apoyo durante la realización de este artículo y a los investigadores relacionados con el tema. Se espera que los trabajos desarrollados contribuyan de modo significativo con la comunidad científica de ingeniería geotécnica.

Referencias

Allen, N. de G. (1954). *Relaxation Methods in Engineering and Science* (257 pp.). New York: McGraw Hill.

Baiocchi, C. (1971). *Sur un problème a frontière libre traduisant le filtrage de liquides à travers des milieux poreux (On a Free Surface Problem Considering the Liquid Filtration through Porous Media)* (pp. 1215-1217). Paris: C.R. Academie des Sciences 273.

Bardet, J. P., & Tobita, T. (January, 2002). A Practical Method for Solving Free-Surface Seepage Problems. *Computers and Geotechnics*, *29*, 451-475.

Bosch, D. D., & Davis, F. M. (June, 1997). Methods for Calculating Flow from Observed or Simulated Hydraulic Head. *Advances in Engineering Software*, *28*, 267-272.

Brezis, H., Kinderlehrer, D., & Stampacchia, G. (1978). *Sur une nouvelle formulation du problème de l'écoulement à travers une digue (On a New Formulation of the Flow Problem through a Dam)*. Serie A. Paris: C. R. Academie des Sciences.

Bruch, J. C. (1980). A Survey of Free Boundary Value Problems in the Theory of Fluid Flow through Porous Media: Variation Inequality Approach - Part I. *Advances in Water Resources*, *3*, 65-80.

Budhu, M. (2000). *Soil Mechanics and Foundations* (616 pp.). New York: John Wiley & Sons Inc.

Casagrande, L. (1932). *Naeherungsmethoden zur Bestimmung von Art und Menge der Sickerung durch geschuettete Dämme (Approximate Methods to Determine the Seepage through Spillway Dams)*. Thesis. Vienna: Institute of Technology.

Cedergren, H. R. (1989) *Seepage, Drainage and Flow Nets*. New York: John Wiley & Sons.

Cheng, A., & Cheng, D. T. (2005). Heritage and Early History of the Boundary Element Method. *Engineering Analysis with Boundary Elements*, 29, 268-302.

Cryer, C. W. (July 1970). On the Approximate Solution of Free Boundary Problems Using Finite Differences. *Journal of the Association for Computing Machinery*, *17*, 397-411.

Dupuit, J. (1863). *Etudes théoriques et pratiques sur le mouvement des eaux dans les canaux découverts et à travers les terrains perméables (Theoretical and Practical Studies of the Movement of Water in Open Channels through Permeable Media)*. Paris: Dunond.

Finnemore, E. J., & Perry, B. (October, 1968). Seepage through an Earth Dam Computed by the Relaxation Technique. *Water Resources Research*, 4, 1059-1067.

Flores, R. (2000). *Flujo de agua a través de los suelos* (4a edición). *Avances en Hidráulica 4*. México, DF: Asociación Mexicana de Hidráulica, Instituto Mexicano de Tecnología del Agua.

Geo-Slope International, SEEP/W-2007 (2008). *Scientific Manual: Seepage Modeling with SEEP/W 2007. An Engineering Methodology* (3rd Ed.). Alberta, Canada: Geo-Slope International, Ldt, Calgary.

Harr, M. E. (1962). *Groundwater and Seepage* (313 pp.). New York: McGraw-Hill Inc.

Iterson, F. F. Th. Van. (1916, 1917). Eenige Theoretische Beschouwinger over Kwel (Some Theoretical Considerations about Seepage). *De Ingenieur*, *31*, 629-633.

Kozeny, J. (1931). Grundwasserbewegung bei freiem Spiegel, Fluss-und Kanalversickerung- Nasserkraft und Wasserwirtschaft (Groundwater Movement with Free Surface in Channels and Hydroelectric Energy by Seepage in Channels). *Wasserkraft und Wasserwirtschaft*, *3*, 28-31.

Mahmud, M. (December, 1996). Spreadsheet Solutions to Laplace´S Equations: Seepage and Flow Net. *Jurnal Teknologi*, *25*, 53-67.

Mitchell, A. R. & Griffiths, D. F. (1980). *The Finite Difference Method in Partial Differential Equations* (272 pp.). New York: John Wiley & Sons Ltd.

Salmasi, F., & Azamathulla, H. M. (September, 2013). Determination of Optimum Relaxation Coefficient Using Finite Difference Method for Groundwater Flow. *Arabian Journal of Geosciences*, *6*, 3409-3415.

Schaffernak, F. (1917). Uber die Standsicherheit durchlaessiger geschuetteter Dämme (Regarding the stability of permeable draining dams). *Allgemeine Bauzeitung*, *82*, S.73.

Southwell, R. V. (1940). *Relaxation Methods in Engineering Science*. Oxford: Oxford University Press.

Wang, H. F., & Anderson, M. P. (1982). *Introduction to Groundwater Modeling: Finite Difference and Finite Element Methods* (237 pp.). San Francisco: W. H. Freeman.

Young, D. (1950). *Iterative Methods for Solving Partial Difference Equations of Elliptic Type* (74 pp.). Ph. D. Dissertation. Cambridge: Harvard University.

Dirección institucional de los autores

Dra. Norma Patricia López-Acosta

Investigadora
Universidad Nacional Autónoma de México
Instituto de Ingeniería
Circuito Escolar, Ciudad Universitaria, Delegación Coyoacán
04510 México, D.F., México
Teléfono: +52 (55) 5623 3600, extensión 8555
nlopeza@iingen.unam.mx

M.I. José León González-Acosta

Ingeniero de Proyecto
Universidad Nacional Autónoma de México
Instituto de Ingeniería
Circuito Escolar, Ciudad Universitaria, Delegación Coyoacán
04510 México, D.F., México
Teléfono: +52 (55) 5623 3600, extensión 8555
lgonzalez.a87@gmail.com

Relationship between Dissolved Oxygen, Rainfall and Temperature: Zahuapan River, Tlaxcala, Mexico

• Hipólito Muñoz* • Saturnino Orozco • Andrea Vera • Juan Suárez •
• Edelmira García • Mercedes Neria • José Jiménez •
Universidad Autónoma de Tlaxcala, México
*Corresponding Author

Abstract

Muñoz, H., Orozco, S., Vera, A., Suárez, J., García, E., Neria, M., & Jiménez, J. (September-October, 2015). Relationship between Dissolved Oxygen, Rainfall and Temperature: Zahuapan River, Tlaxcala, Mexico. *Water Technology and Sciences* (in Spanish), 6(5), 61-76.

The concentration of dissolved oxygen (DO) in the Zahaupan River has decreased over the years due to pollution. The objective of the present work is to identify how DO is related to rainfall and temperature. Measurements of DO were taken at two points (MP1 and MP2) in the river. The Mann-Whitney test was used to compare concentrations at the measurement points and the measurements obtained during the dry and rainy seasons. A relationship was found between DO and the temperature of the river. DO was higher at MP1 (upstream) than at MP2 and significant differences were found between both. Before and during the rainy season, DO values had atypical trends while after the rainy period they were comparable to those reported by the literature. Significant relationships were found between variances and average DO and accumulated rainfall. DO values during the rainy season were higher than those during the dry period and significantly different. It is concluded that DO is related to temperature and that rainfall positively affects DO concentrations in the river.

Keywords: Dissolved oxygen, temperature, rainfall, Zahuapan River.

Resumen

Muñoz, H., Orozco, S., Vera, A., Suárez, J., García, E., Neria, M., & Jiménez, J. (septiembre-octubre, 2015). Relación entre oxígeno disuelto, precipitación pluvial y temperatura: río Zahuapan, Tlaxcala México. Tecnología y Ciencias del Agua, *6(5), 61-76.*

La concentración de oxígeno disuelto (OD) en el río Zahuapan ha disminuido a través de los años debido a la contaminación. El objetivo de este trabajo es conocer la relación del OD con la precipitación pluvial y temperatura. Se realizaron mediciones de OD en dos puntos (PM1 y PM2) del río. Se utilizó la prueba de Mann-Whitney para comparar las concentraciones entre los puntos de medición y entre las de la temporada de sequía con las de lluvia. Se encontró relación entre el OD y la temperatura de la corriente. El OD fue mayor en PM1 (corriente arriba), comparado con PM2 y entre ambos hubo diferencias significativas. Antes y en la temporada de lluvia, los valores de OD tuvieron tendencias atípicas; después de las lluvias, las tendencias fueron comparables con las reportadas en la literatura. Se obtuvieron relaciones significativas entre las varianzas y promedios del OD con la lluvia acumulada. Los valores de OD de la temporada de lluvias fueron mayores y significativamente diferentes comparadas con las de sequía. Se concluye que el OD está relacionado con la temperatura y que las precipitaciones pluviales afectaron de manera positiva la concentración de OD en el río.

Palabras clave: *oxígeno disuelto, temperatura, lluvias, río Zahuapan.*

Received: 20/08/2013
Accepted: 01/05/2015

Introduction

Human activities have affected rivers in many ways, for example, through deforestation, urbanization, agriculture, drainage canals, discharge of pollutants and control of flows (dams, dikes, etc.) (Bellos & Sawidis, 2005). The pollution of rivers from untreated wastewater is serious in developing economies. When discharged into water bodies, conventional, unconventional and emerging constituents of municipal wastewater (Metcalf & Eddy Inc.,

2003) decrease the concentration of dissolved oxygen (DO). Under natural conditions, the rivers should have a DO saturation of at least 80%, with daily cyclical variations. This should be the case even in pristine water bodies due to the rates of photosynthesis (Riđanović, Riđanović, Jurica, & Spasojević, 2010). Changes in DO concentrations over time are controlled by primary production, community respiration and aeration rates (Riley & Dodds, 2013). In turn, these factors are influenced by temperature (Wehmeyer & Wagner, 2011), depth of the river, turbidity (Shields & Knight, 2012), availability of light and autotrophic activity (Bernot & Wilson, 2012), hydrometric conditions (He, Chu, Ryan, Valeo, & Zaitlin, 2011), high levels of organic matter (Guzmán *et al*., 2011), turbulence and mixing volume (Mulholland, Houser, & Maloney, 2005), type of substrate or riverbed (Huggins & Anderson, 2005) and runoffs caused by rainfall (Graves, Wan, & Fike, 2004). With respect to rainfall, reports have suggested both a positive effect on DO (Barceló, López, Solís, Domínguez, & Gómez, 2012) as well as no apparent relationship between rainfall and DO (Wehmeyer & Wagner, 2011).

The concentration of DO in the Zahuapan River has been decreasing over the years. In the 1970s it was still possible to swim in this river (author's experience). A document published by Sedue (1985) reported a DO concentration in 1978 of 6 to 8 mgl^{-1}. In Mexico, legislation related to ecological water quality criteria (CE-CCA-001-89) sets the minimum limit at 5 mgl^{-1} for the protection of aquatic life in both fresh water and seawater (Sedue, 1989). With the widespread implementation of drainage service in the main population centers in Tlaxacala, in the 1980s untreated wastewater began to be discharged into the ravines and river. This had a negative effect on DO concentrations, as shown by data published the Tlaxcala State Government's General Department of Ecology (CGE, 1997), which obtained an average DO for 1997 of 3.03 mgl^{-1}. In the year 2007, the concentrations decreased further still, to an average value of 2.97 mgl^{-1} (Muñoz *et al*., 2012). While in the southern portion of the river the concentrations can remain equal to zero through the entire year, in 2012 the average DO concentration decreased even further, as shown by the data published in the webpage of the Tlaxcala State Water Commission (CEAT, 2012), which reported a value of 2.5 mgl^{-1}. DO is a key indicator of the quality of water in a river given that it affects nearly all of the chemical and biological processes in water bodies (Wenner, Sanger, Arendt, Holland, & Chen, 2004). Nevertheless, the only reports of DO concentrations from the Zahuapan River to-date have been based on instantaneous samples. Therefore, the objective of this work is to contribute information about variations in DO concentrations and the relationship between this variables with air temperature and rainfall.

Methodology

Description of the Study Area

The Zahuapan River is formed from runoff, springs and wastewater discharges generated in the sub-basin, named Zahuapan Sub-Basin Rh18Ai-R by the Institute of Statistics, Geography and Information (INEGI, 2010). This sub-basin is located in the upper Balsas River basin, in Hydrological Region 18. The Balsas River basin is composed of two large physiographic provinces — the Southern Sierra Madre and the Volcanic Belt— whose evolution over geological times produced a wide variety of orographic, climatic and hydrological characteristics. This led to the formation and development of soils with different properties, in a wide range of conditions that in turn have contributed to a rich diversity of

flora and fauna (Conagua, 2010). Zahuapan sub-basin RH18Ai-R is located in the Volcanic Belt. Its area measures 1631.6 km^2 (INEGI, 2010). The Zahuapan River begins in the northern portion of the sub-basin and runs towards the Tlaxacal and Puebla (Figure 1) state borders. The Atlangatepec Dam is the largest hydraulic work to interrupt the flow of the river. The river is approximately 98 km long from the headwaters to the confluence with the Atoyac River, running from north to south with a mean slope of 0.011. The width and depth of the river varies throughout its course. Mean annual precipitation is approximately 700 mm. The economic activity is primarily seasonal agriculture in the northern portion of the sub-basin and in the south a combination of agricultural (irrigation and seasonal) and industrial activities exists. The majority of the population is located in the south-central part of the sub-basin, with population densities over 1 000 inhabitants km^{-2} in some of the urban areas.

Compilation and Analysis of the Information

Sixteen daily DO measurements were taken at two points in the Zahuapan River (Figure 1). Point 1 (MP1) was located upstream from point 2 (MP2) at a distance of 1 968 meters. The measurement period began on February 16, 2012 and ended on January 29, 2013. The days measured during the dry and rainy seasons were selected such that the measurements included seven days of the week. The dry and rainy seasons were defined based on the bulletins issued by the National Water Commission (Conagua, Spanish acronym)

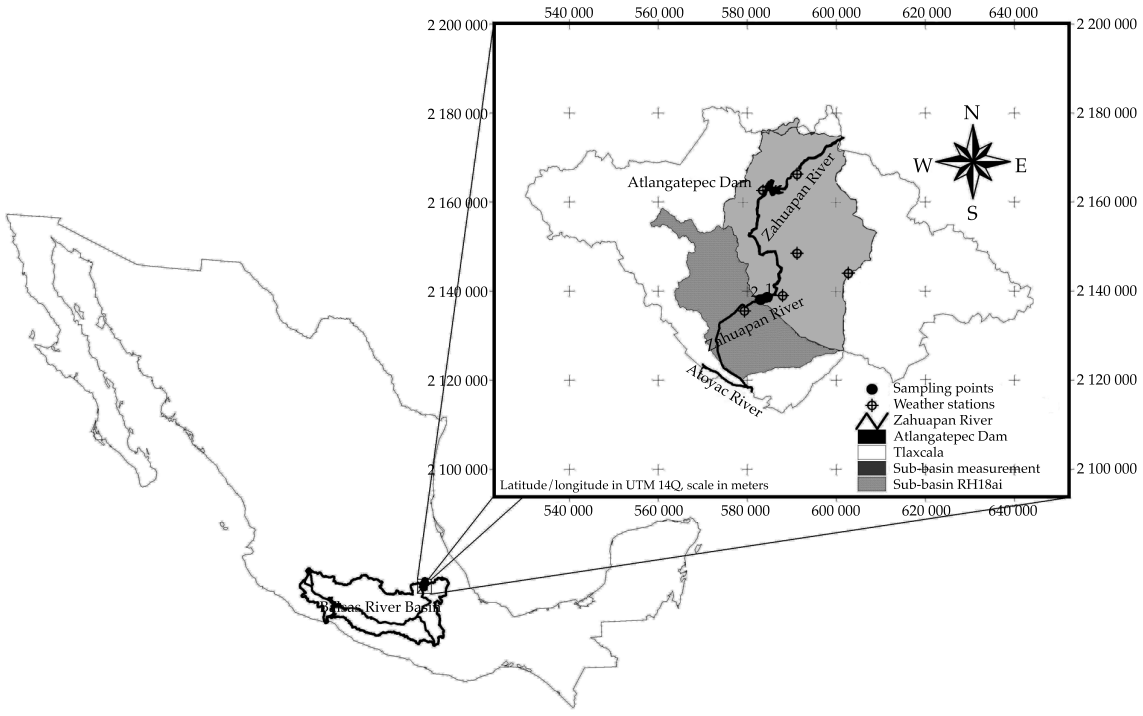

Figure 1. Study area in the Zahuapan River sub-basin, Tlaxcala, Mexico.

which indicate the beginning and end of the hurricane season (Conagua, 2012). The readings were performed at the edge of the river, which can be considered representative of the entire cross-section since the electrodes were installed in shallow areas (depth of 50 cm or less) where there was good mixing. DO concentrations, water temperature (*T*water) and atmospheric pressure were measured. New luminescent electrode technology by Hach® was used, obtained from the company Aquatec-Mexico S.A. de R.L., which was calibrated according to the manufacturer's specification. Measurements were recorded every 5 minutes. The electrodes remained submerged in the river's current for the duration of each day of measurements, which was 8 hours for the majority of measurements. The percentage of saturated DO (%DOsat) was calculated with the equation %DOsat = (DO/DOsat)*100, where DOsat is the DO at saturation, which was calculated according to Master (2008). The average, minimum, maximum, variance, Kurtosis and CCA percentile were calculated. The latter was used by this work as an indicator of the percentage of data under 5 mgl^{-1} of DO, which is the minimum limit established by the CE-CCA-001/89 for water bodies (Sedue, 1989). When the minimum value of the data was over 5 mgl^{-1}, then 0% of the data was less than this limit, or the CCA percentile is equal to zero, which implies that the DO concentration of the river met the ecological criterion during the measuring period. When the maximum value was less than 5 mgl^{-1}, then 100% of the data registered on that measuring day was less than this limit, or the CCA percentile equals 100. All the statistical analyses and graphs were generated with the *Statistica* program, version 8.0 (Statsoft, Inc.,2007). Correlation coefficients were used to identify the relationship of DO concentrations between points MP1 and MP2, between DO and *T*water, and between DO and precipitation (P) recorded at five weather stations (WS) and the weather observatory (WO). The correlations were performed using the average and variance of the DO for each measurement with the daily precipitation (Pdaily) and accumulated precipitation (Paccu). Correlation matrices of these variables were generated for 1 to 20 days prior to the day on which DO was measured. The precipitation data was provided by Conagua (Conagua, 2013). The significance of the *r* value was estimated with the Pearson test and the Mann-Whitney test was used to statistically compare DO concentrations between MP1 and MP2, and between DO during the rainy and the dry season.

Results

a) Current temperature -air temperature-DO

Table 1 shows the results from the basic statistics, which consist of the average, minimum, maximum, variance, Kurtosis and CCA percentile of the river temperature (*T*water) and DO. A minimum water temperature of 11.2°C and a maximum of 23.4°C were recorded, the former in winter and the latter in summer. The average temperatures of the water in the river at the two measuring points and the air temperature had the same trends (Figure 2), although the temperature at MP2 (*T*water2) was slightly higher (approximately 1°C) than at MP1 (*T*water1). The averages of the water temperatures were higher than those of the air temperature. The CE-CCA-001/89 (Sedue, 1989) Ecological Water Quality Criteria establishes a maximum temperature for the protection of aquatic life in water bodies equal to that of natural conditions +1.5 °C. The temperature at MP2 exceeded this limit on four occasions and at MP1 on two occasions. The temperature of the water was less than the air temperature on three days (two at MP1 and one day at MP2). The variance ranged from 0.69 to 13.54 at MP1 and between 0.40 and 10.34 at MP2. Negative Fischer's Kurtosis

Table 1. Basic statistics related to temperature and dissolved oxygen measured in the Zahaupan River (the shaded cells indicate rainy season, the others dry season).

Date		Water Temperature in the River						Dissolved Oxygen in the River					
		N	Average	Minimum	Maximum	Variance	Kurtosis	Average	Minimum	Maximum	Variance	Kurtosis	CCA percentile
Thurs Feb 16, 2012	MEASURING POINT 1	36	17.7	16.3	19.0	0.7	-1.3	2.83	2.60	3.09	0.02	-1.5	100
Fri March 16, 2012		47	19.4	16.1	22.4	3.8	-1.3	3.78	2.20	4.34	0.30	2.2	100
Tues April 3, 2012		60	17.5	13.0	21.8	7.8	-1 l .3	3.26	2.19	4.38	0.46	-1.3	100
Wed May 16, 2012		138	20.0	15.3	23.1	7.1	-1.1	3.11	1.04	4.20	0.96	-1.4	100
Sat June 16, 2012		99	17.7	16.3	19.8	1.8	-1.5	3.74	3.15	4.43	0.06	0.2	100
Thurs June 28, 2012		73	19.0	17.0	22.9	3.1	-1.1	5.77	5.24	6.42	0.10	-0.8	0
Fri July 20, 2012		97	18.4	15.7	21.3	2.5	-0.8	5.98	5.34	6.95	0.23	-0.9	0
Sun Ago 12, 2012		93	16.9	16.0	18.6	0.8	-1.1	6.66	6.13	7.06	0.08	-1.2	0
Mon Sept 10, 2012		97	19.6	16.0	22.5	4.1	-1.1	5.35	4.46	5.86	0.22	-1.2	29
Tues Oct 02, 2012		98	19.3	15.4	22.1	5.4	-1.3	5.40	4.51	5.90	0.17	-0.7	15
Wed Oct 10, 2012		98	16.6	13.4	19.5	3.8	-1.4	6.76	6.21	7.11	0.08	-1.0	0
Sat Oct 13, 2012		98	18.9	14.1	22.2	8.2	-1.3	6.22	5.38	6.92	0.26	-1.4	0
Sun Nov 18, 2012		95	18.0	12.3	22.2	13.5	-1.5	5.72	4.56	6.34	0.26	-0.1	13
Mon Nov 26, 2012		98	16.6	11.2	21.2	13.5	-1.6	7.43	4.75	8.48	1.46	-0.2	8
Mon Dec 17, 2012		65	14.7	11.3	19.8	8.9	-1.5	6.31	4.34	7.56	1.36	-1.3	22
Tues Jan 29, 2013		97	16.0	11.2	20.3	12.0	-1.6	5.80	3.50	6.81	1.34	-0.6	25
Thurs Feb 16, 2013	MEASURING POINT 2	24	18.4	17.2	19.4	0.4	-0.8	1.26	1.05	1.40	0.01	-1.2	100
Fri March 16, 2012		36	20.3	17.1	23.2	3.8	-1.2	4.15	3.64	4.40	0.06	-0.1	100
Tues April 03, 2012		44	18.6	14.1	22.5	7.1	-1.3	3.72	2.72	4.57	0.17	0.8	100
Wed. May 16, 2012		129	21.0	15.2	24.5	9.4	-1.0	2.86	0.00	4.35	2.17	-1.1	100
Sat June 16, 2012		86	17.8	16.2	20.1	2.1	-1.5	3.25	2.58	3.79	0.09	-0.2	100
Thurs June 28, 2012		66	19.5	17.0	23.4	4.2	-1.2	4.88	4.07	5.72	0.24	-1.0	63
Fri July 20, 2012		89	19.0	15.8	22.3	3.1	-0.7	5.35	4.38	6.53	0.40	-1.1	38
Sun Ago 12, 2012		95	17.5	16.1	19.2	1.2	-1.6	5.86	5.19	6.68	0.24	-1.3	0
Mon Sept 10, 2012		89	20.1	15.9	23.0	5.4	-1.3	4.66	2.47	5.61	1.05	-0.5	44
Tues Oct 02, 2012		87	19.3	15.5	22.1	5.6	-1.5	3.60	2.96	4.22	0.19	-1.6	100
Wed Oct 10, 2012		84	17.0	13.8	19.3	3.3	-1.4	6.07	5.29	6.52	0.13	-1.4	0
Sat Oct 13, 2012		91	18.8	14.0	22.4	8.5	-1.4	5.09	3.74	6.27	0.74	-1.6	46
Sun Nov 18, 2012		90	17.4	12.5	21.4	10.3	-1.5	3.31	1.71	4.44	0.71	-1.2	100
Mon Nov 26, 2012		91	16.2	11.3	20.4	10.3	-1.5	5.22	2.53	6.30	1.09	0.3	35
Mon Dec 17, 2012		57	14.4	11.2	18.6	6.0	-1.3	4.36	2.26	5.43	1.14	-1.0	58
Tues Jan 29, 2013		87	15.7	11.1	20.2	10.6	-1.5	3.20	1.52	4.18	0.84	-1.0	100

values were obtained for all measurements at the two points, which indicates a platykurtic distribution of the data, that is, the peaks are smaller than those of a normal distribution.

Table 2 shows the results from the Pearson correlation coefficients (r) between DO and Twater. Significant coefficients were obtained for all the measurements, indicating a good relationship between these variables. There was a high number of correlation coefficients (72%) with a negative sign. Those with a positive sign were obtained from measurements taken in March, June, November, December and January. The coefficients closest to 1 or

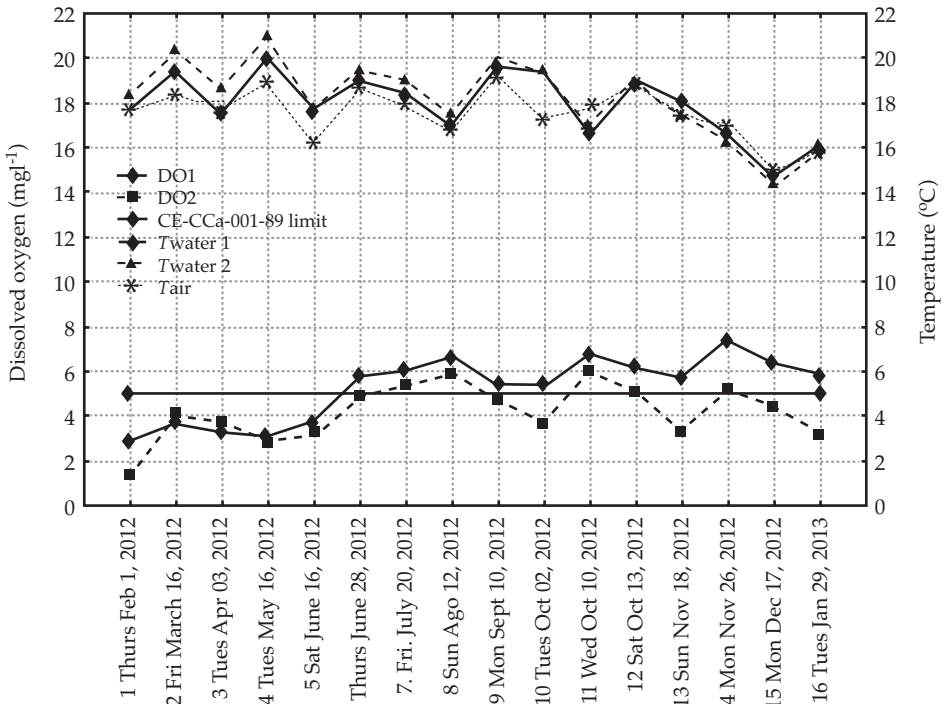

Figure 2. Dissolved oxygen (DO) concentrations, temperature of the Zahuapan River current (*T*water) and air temperature (*T*air), by measurement date..

Table 2. *r* values for water temperature-DO ratio in the Zahauapan River current, between measuring points DO1:DO2 and saturation percentage (the shaded cells indicated rainy season, the others dry season).

Date	Values of *r*			% saturation	
	***T*water:DO1**	***T*water: DO2**	**DO1:DO2**	**DOsat1**	**DOsat2**
1. Thurs Feb 16, 2012	-0.902*	-0.855*	0.769*	38.3	17.4
2. Fri March 16, 2012	-0.875*	0.777*	-0.506*	53.6	60.6
3. Tues Apr 03, 2012	-0.957*	-0.405*	0.299	43.9	52.0
4. Wed May 16, 2012	-0.695*	-0.422*	0.741*	44.5	41.9
5. Sat June 16, 2012	-0.366*	0.246*	-0.577*	51.1	44.6
6. Thurs June 28, 2012	-0.974*	-0.958*	0.980*	81.1	69.0
7. Fri. July 20, 2012	-0.940*	-0.960*	0.988*	82.7	74.8
8. Sun Aug 12, 2012	-0.980*	-0.970*	0.991*	89.1	79.4
9. Mon SEpt 10, 2012	-0.600*	-0.616*	0.944*	76.5	67.0
10. Tues Oct 02, 2012	-0.850*	-0.968*	0.837*	76.6	50.7
11. Wed Oct 10, 2012	-0.953*	-0.941*	0.970*	89.7	81.1
12. Sat Oct 13, 2012	-0.952*	-0.982*	0.986*	87.1	70.5
13. Sun Nov 18, 2012	0.363*	-0.223*	0.861*	79.0	44.5
14. Mon Nov 26, 2012	0.833*	0.518*	0.920*	100.1	69.4
15. Mon Dec 17, 2012	0.920*	0.800*	0.970*	81.2	55.4
16. Tues Jan 29, 2013	0.889*	0.581*	0.867*	77.3	42.1

* Significant at $p < 0.05$.

-1 were obtained for the ratio *T*water:DO1. These coefficients were observed to have seasonal variations. During the rainy season, the ratio of *T*water to DO had *r* values near -1.

b) Dissolved Oxygen

The average of the 16 measurements was 5.26 mgl^{-1} at MP1 (73.7% of the saturation DO (DOsat) value)and 4.18 mgl^{-1} at MP2 (59.1% of DOsat). The average DO concentration per measuring day was between 2.83 mgl^{-1} (38.3% DOsat) and 7.43 mgl^{-1} (110.2 % DOsat) at MP1, and between 1.26 mgl^{-1} (17.4 %DOsat) and 6.07 mgl^{-1} (81.2% DOsat) at MP2 (Table 1). The average concentrations at MP1 were higher than those at MP2, except for the measurements in March and April. The Mann-Whitney test found that the DO concentrations at MP1 were significantly different ($p<0.05$) than those at MP2. The differences in concentration between the two measuring points were between 2.6 and 0.15 mgl^{-1}.

The average concentrations at MP1 and MP2 were over the 5 mgl^{-1} limit for the minimum DO level in water bodies for the protection of aquatic water, as established by the CE-CCA-001/89 Ecological Water Quality Criteria (Sedue, 1989). The minimum values measured per day were between 1.04 $mgl\text{-}1^{-1}$ (16.1% DOsat) to 6.21 mgl^{-1} (84.6% DOsat) at MP1 and 0 mgl^{-1} (0% DOsat) to 5.29 mgl^{-1} (75.2% DOsat) at MP2. The maximum values measured per day were between 3.09 mgl^{-1} (39.8%% DOsat) to 8.48 mgl^{-1} (125.1% DOsat) at MP1 and 1.4 mgl^{-1} (18.9% DOsat) to 6.68 mgl^{-1} (87.4% DOsat) at MP2. The variance was between 0.02 and 1.46 mgl^{-1} at MP1 and between 0.01 and 1.14 mgl^{-1} at MP2. Negative Kurtosis coefficients were obtained on all except two of the days in which measurements were taken. A negative Kurtosis indicates a distribution that is flatter than the normal distribution. Table 1 shows CCA percentile values of 100 during the dry season (five at MP1 and eight at MP2).

At PM1, the average %DOsat had an increasing trend over the months (Table 2) from February 16 to November 26th. The DOsat percentages measured on March 16 and April 3 were higher at MP2.

c) Relationship of DO with hour of the day

Figure 3 shows DO concentration trends in relation to the hour of the day. Two types of trends can be seen. One was a decreasing trend in DO in the river for the 12 measurements taken between February 16 and October 13, 2012, with higher values in the morning when beginning the measurements and decreasing over the course of the day. Meanwhile, an increasing trend followed by a decreasing trend was observed in the DO concentrations in the river for the last four measurements taken after the rainy season, between November 18 and January 29, 2013. These concentrations were lower in the mornings, rose to their maximum value and then tended to decrease. In Figure 3, the measurements from June 28 to January 29 are seen to have exceeded the DO limit of 5 mgl^{-1} during different hours of the day. DO levels under this limit were recorded more times at PM2. In addition, the measurements taken at this measuring point on October 2, November 18 and January 29 were below the 5 mgl^{-1} limit.

At MP1, average DO concentrations of 3.34 mgl^{-1} (46% DOsat) were obtained during the dry season at the beginning of the year (February 16 to June 16), 6.02 mgl^{-1} (83.3% DOsat) during the rainy season (from June 28 to October 13) and 6.31 mgl^{-1} (84.4% DOsat) during the dry season after the rains (November 18 to January 13). At MP2, average DO concentrations of 3.05 mgl^{-1} were obtained during the dry season at the beginning of the year (43.3% DOsat), 5.07mgl^{-1} (70.4% DOsat) during the rainy season and 4.02 mgl^{-1} (52.8%

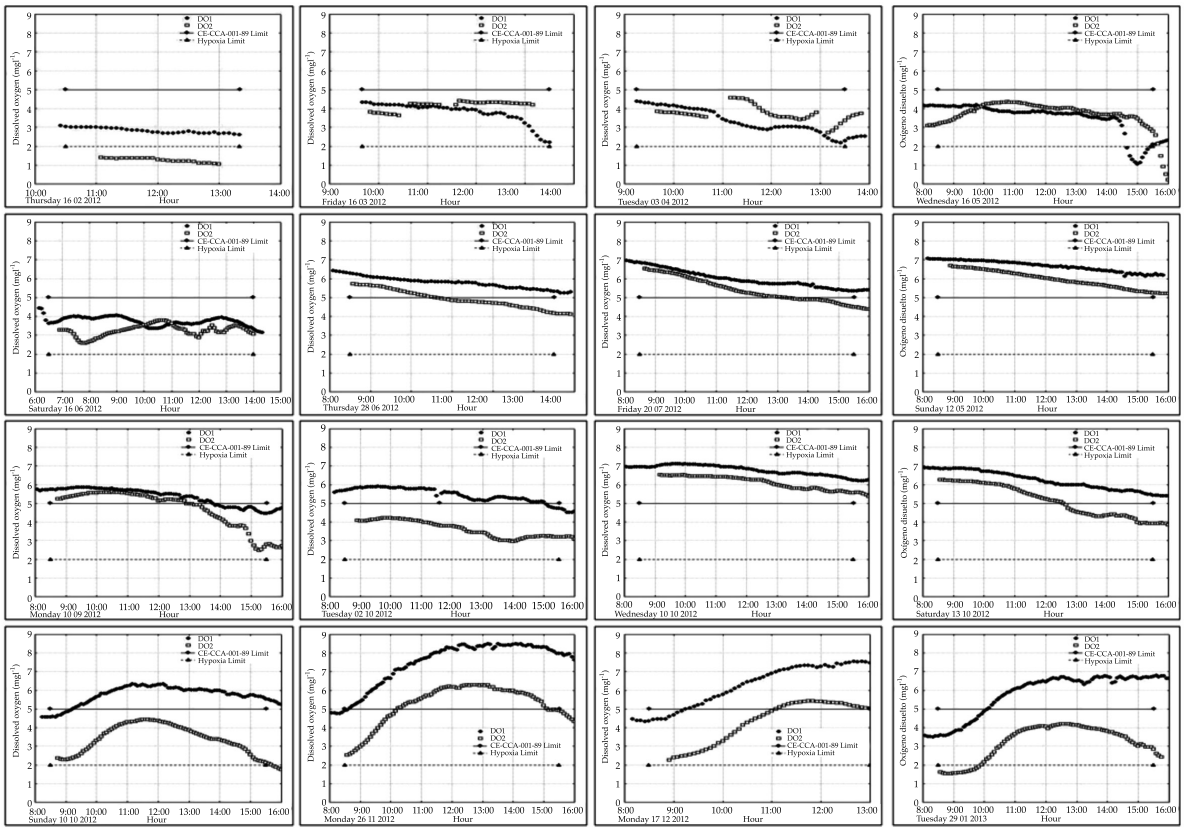

Figure 3. Trends in data for dissolved oxygen (DO) concentrations in the Zahuapan River, according to hour of the day.

DOsat) during the dry season at the end of the year. The concentrations registered every 5 minutes at MP1 were between 1.04 mgl^{-1} (16.1% DOsat) and 8.48 mgl^{-1} (125.1% DOsat). The measurements from November 26 to December 17 registered values over 100% DOsat (supersaturation), while the measurements on May 16th registered values under 28% DOsat (hypoxia) during 40 minutes. At PM2, the concentrations taken every 5 minutes were between 0 mgl^{-1} (0% DOsat) and 6.68 mgl^{-1} (87% DOsat). The measurements taken on February 16, May 16, November 18 and 26, December 17 and January 29 registered values under 28% (hypoxia).

The correlation coefficients between DO at PM1 versus DO at PM2 are shown in Table 2. Before the June 28th measurements, both the negative and positive coefficients were statistically significant, and only positive values were obtained after that date, even during the dry season at the end of the year.

d) Relation of DO to Precipitaiton (P)

The precipitation (P) registered at Conagua's weather observatory (WO) located 2 km from the measuring points was 981 mm in the year 2012 (Conagua, 2013). During the hurricane season which officially began on June 1st in the Atlantic Ocean and ended on November 30 (Conagua, 2012), 851 mm (87% of the annual total) was registered. Based on the precipitation records from the WO, 7 of the 16 measurements were taken during the rainy season between June 28 and October 13

and 9 were taken during the dry season at the beginning and the end of the year. During the rainiest months (June, July and August) 634 mm were registered (65% of the annual total). On June 16, 17, 18 and 19 tropical cyclone *Carlota* hit the coasts of Oaxaca and 49 mm were registered at the WO. Tropical cyclone *Ernesto* reached the Zahuapan River sub-basin on August 10. That day 26.5 mm were registered at the WO, while 58.7 mm was registered at the Tlaxco WS which is also located in the sub-basin, 30 km north of the sampling points. The WO did not register any significant rainfall on August 17 with respect to Hurricane *Helen* which was then a tropical storm, or on August 20 with respect to tropical wave 12. Although the hurricane season officially began on June 1st, continuous rains were registered as of the afternoon of June 16th. And while the hurricane season officially ended on November 30th, the last significant rainfall of the season in the sub-basin was registered on October 9th, which affected the DO measurements taken on October 10 and 11.

Figure 4 shows the correlation coefficient (r) values obtained for the relationship between P and DO. The coefficients that were significant ($p < 0.05$) and more consistent (highlighted in the figure) correspond to the relationship between the DO variances for MP1 and the Paccu registered at the five WS and the WO. A good correlation with average DO was also observed at the WO. No consistently significant correlation coefficients (shown in gray)were found between Pdaily and DO. At PM1, the correlation coefficients between Paccu and the DO variance remained significant as of 12 days of accumulated rainfall prior to measuring DO, and at PM2 the correlation between Paccu and average DO was significant as of 8 days.

Discussion

Unfortunately, the literature does not report data similar to those presented in this work

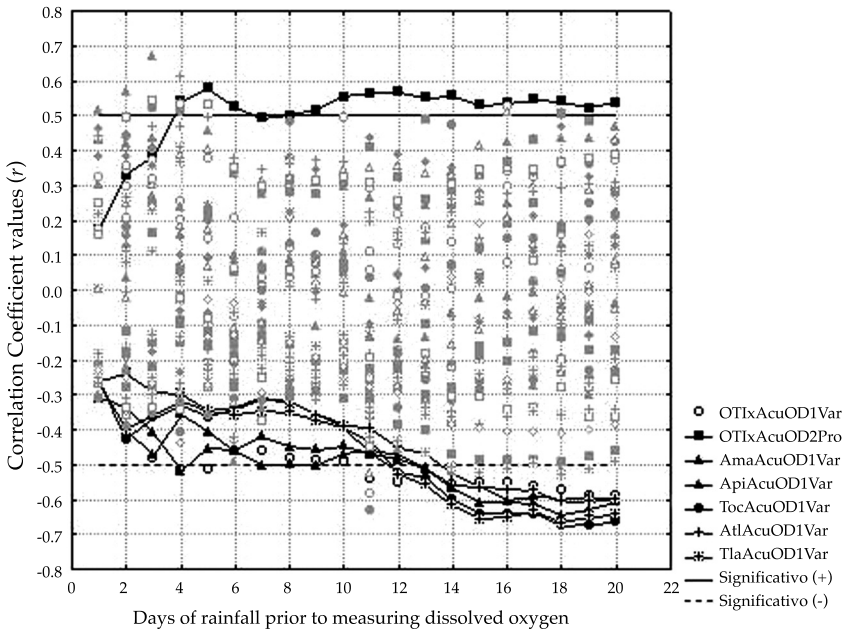

Figure 4. Correlation coefficients between dissolved oxygen (DO) concentrations and precipitation (P).

for Mexican rivers or with conditions similar to those of the Zahaupan River. Therefore, except for a few occasions this discussion will be based on information from rivers located in other countries.

a) Water Temperature-Air Temperature-DO

Average air temperatures were between 16.4°C (June 16) and 19.7 °C (September 10) during the hours when measurements were taken. It is important to mention that the lowest and highest water temperatures were not measured on the coldest and hottest days, which is similar to reports in the literature. The minimum water temperature of the river (11.2°C) was registered in winter and the maximum (23.4°C) in summer. According to the data from the 16 days during which measurements were taken, no seasonal variations in air or water temperatures were observed (Figure 2). At PM1 the average air temperatures were lower (0.05 to 1.74 °C) than the average water temperatures from March 16 to October 2, except for measurements taken on February 16 and April 3. Average air temperatures were also lower than river temperatures at PM2 (0.59 a 1.61 °C), with no exceptions. Huggins and Anderson (2005) also reported lower air temperatures than water temperatures in several rivers located in the grain belt in the United States. Later, from October 10 to January 29th, average air temperatures were higher than the average water temperatures (0.04 to 1.74 °C at point 1 and 0.57 to 2.42 °C at point 2). The decrease in water temperature from October to January could not have been caused by an increase in flow (Sand-Jensen & Pedersen, 2005) since the rainy season ended in mid-October, but it may have been caused by the desilting of the river on September 10, 2012. The ratios of air temperature to water temperature were 1.18 at MP1 and 1.02 at MP2, which fall in the interval reported for the Magdalena River located in Mexico City (Montes, Navarro, Domínguez, & Jiménez, 2013). The correlation coefficients between air and water temperature at the two measuring points were significant for 14 of 16 measurements, except those on June 16 and July 20.

Bayram, Önsoy, Numan and Akinci (2013) mention that when significant correlations between air and water temperature exist, the weather is the main factor that controls the water temperature. Although the water temperature was higher than the air temperature (from February to October) it did not exceed the ecological criteria established by CE-CCA-001/89 (Sedue, 1989). The average water temperature was lower at MP1 than at MP2 (between 0.05 and 1.18 °C) from February to September. Bayram *et al*. (2013) and Sand-Jensen and Pedersen (2005) reported a similar result. The difference in elevation of 11 meters between MP1 and MP2 may not have caused this temperature difference, as mentioned by Bayram *et al*. (2013) who found that a 61 meter difference in elevation caused temperature differences between two points in a river. Meanwhile, the water temperature was higher at MP1 than at MP2 (0.13 to 0.91 °C) from October to January. Shade from the canopy of the vegetation on a river's banks is known to affect the temperature of a river. Nevertheless, since the segment between the two measuring points was completely uncovered and exposed to solar radiation the difference in temperature between the two measuring points may be due to another factor, such as the desilting of the river.

The correlations between the average air temperatures and average DO concentrations per measuring day were not significant at MP1 or MP2. Although Wehmeyer and Wagner (2011) reported that dissolved oxygen concentrations in the Roanoke River (United States) decreased during hot months, the averages of the data did not show a seasonal variation in the dissolved oxygen concentra-

tions in the Zahuapan River. All of the water temperature and oxygen concentrations measurements taken every 5 minutes had significant positive and negative correlation coefficients (Table 2). The coefficients were positive for 75% of the measurements at MP1 (from February 16 to October 13) and for 69% at MP 2 (from February 16 to November 18, except for March 16 and June 16). Negative coefficients indicate a inversely proportional relationship between water temperature and dissolved oxygen (Riđanović *et al*., 2010), a relationship which has been commonly reported by the literature. In this work, negative correlation coefficients were obtained with the majority of samples taken from February 16 to October 13, which includes the dry season at the beginning of the year and the rainy season. Meanwhile, positive correlation coefficients indicate a directly proportional relationship between water temperature and dissolved oxygen. Positive correlation coefficients were obtained during the dry season at the end of the year (November 18 to January 29, 2013). A directly proportional relationship between water temperature and dissolved oxygen is not easy to explain. For the case of the Zahuapan River, solar radiation could have increased the water temperature, but it also increases photosynthesis, to a greater degree resulting in an increase in dissolved oxygen concentrations. In the study section of the Zahaupan River, a biofilm formed on the rocks in the riverbed after the rainy season which could have possibly caused more dissolved oxygen to be generated than consumed, thus it increased over the course of the day as the temperature rose. This provides a partial explanation, since daytime fluctuations in oxygen are rarely dependent simply on the intensity of solar light but rather on complex factors (Tafangenyasha, Marshall, & Dube, 2010). Nevertheless, studies are needed to measure oxygen production and consumption in the river in order to verify this.

b) Dissolved Oxygen

The average DO concentrations obtained from the measurements taken from February 2012 to January 2013 at the two points in the Zahuapan River were lower than those from the Amacuzac (García, Molina, Quiroz, Trujillo, & *Díaz*, 2011) and Apatlaco Rivers (López & Hansen, 2013), both located in the state of Morelos, but higher than those from the Lerma River located in the State of Mexico (Barceló *et al*., 2012) and the San Pedro River in the state of Aguascalientes (Guzmán *et al*., 2011), whose concentrations were predominantly under 1 mgl^{-1}. Given that the catchment areas of the Zahuapan River and these other rivers have the highest population densities in Mexico, they have been impacted by human activities in similar ways. The average was over 5 mgl^{-1} for 62.5% of the measurements taken at MP1 and for 31.2% at MP2. The CCA percentile provides more detail about the percentage of data over 5 mgl^{-1} (the ecological criteria established by CE-CCA-001/89) (Sedue, 1989), which indicates that 100% of the data was under this limit for 5 and 8 measurements taken at points 1 and 2 during the dry season. The CCA percentile was valuable since it provided information about the percentage of the set of data that was over 5 mgl^{-1} of DO.

The average DO concentrations were higher at MP1 than at MP2, except for those taken in March and April. A similar result was reported by He *et al*. (2011) for measurements taken in the Bow River (Canada). Nevertheless, when the ecosystem of the river is unaltered the DO concentration can be higher downstream, as reported by Riley and Dodds (2013) for the Kings Creek (United States), who found a higher concentration downstream in rivers located in scrub and gallery forests. For the case of the Zahuapan River, DO concentrations were higher downstream only between 10 a.m. and 11 a.m. during the dry season at the beginning of the year, which

is when there was vegetation and biofilm on the rocks in the riverbed and the banks. Algae increase their photosynthesis as sunlight increases, producing more oxygen (Bernot & Wilson, 2012; Riley & Dodds, 2013). The correlation coefficients (Table 2) between DO concentrations at MP1 and at MP2 indicate the existence of a relationship between the DO concentrations at the two measuring points. Positive coefficients were obtained except for the measurements on March 16 and June 16. Although Wehmeyer and Wagner (2011) did not quantify the relationship of DO concentrations between points upstream and downstream in the Roanoke River, in general a positive correlation in DO concentrations can be seen upstream and downstream in Figure 24 of their report. For the case of the Zahuapan River, which is strongly affected by anthropogenic activities, oxygen consumption from the degradation of organic matter and decreased photosynthetic activity may be factors that cause DO to decrease downstream. This suggests that this river functions as a canal, as could occur in the Zahuapan River due to the rainy season and desilting.

c) Relationship between DO and the Hour of the Day

Figure 3 shows that the dissolved oxygen concentrations in the Zahaupan River obtained during the measurement hours can be classified into two groups. The first group is composed of the measurements from February 16 to October 13 which includes the dry season at the beginning of the year (January to June 16) and the rainy season (June 16 to October). In this group, the highest concentrations were registered in the mornings and decreased over the course of the day. This result is different than reports by other authors who observed higher DO concentrations after noon and lower ones at midnight (Harrison, Matson, & Fendorf, 2005; Huggins & Anderson, 2005; Wilding, Brown, & Collier, 2012) or before sunrise (Klose, Cooper, Leydecker, & Kreitler, 2012). The increase in DO during the day is caused by the availability of light and autotrophic activity (Bernot & Wilson, 2012). Other authors have reported that DO increases at night as the temperature decreases (Riley & Doods, 2013) because oxygen is more soluble at lower temperatures. Unfortunately, given a lack of infrastructure the present study could not take measurements during 24 continuous hours, which would be needed to identify the behavior of DO concentrations at night.

The second group is composed of measurements from November 18 to January 29, which includes the dry season at the end of the year. In this group, DO concentrations in the Zahuapan River were lower in the morning, increased around noon and decreased in the afternoon. This behavior is comparable to reports by several authors (Harrison *et al*., 2005; Huggins & Anderson, 2005; Bernot & Wilson, 2012; Klose *et al*., 2012; Wilding *et al*., 2012; Riley & Doods, 2013). It is important to mention that these results show that the dissolved oxygen concentrations in the river can decrease at a particular time of day to values under the ecological criteria established by Mexican legislation. As observed in the measurements taken in February, March, April, May, November, December and January, when concentrations fell under 2 mgl^{-1}, classified as hypoxia, this reflects a complex response to diverse factors, such as diffuse sources of organic load (Shields & Knight, 2012).

d) Relationship between DO and Precipitaiton

The average DO during the rainy season was higher than during the dry season, with statistical differences ($p < 0.05$). This result shows that precipitation positively affects DO concentrations in the Zahuapan River, which

is not consistent with reports by several authors who indicate that runoff from rainfall increases turbidity and decreases DO due to transported sediments and organic matter (Graves *et al*., 2004; Abowei, 2010; Shields & Knight, 2012). Egborge (1971), cited by Abowei (2010), reported that DO is generally higher in the tropics during the rainy season. This could occur in the Zhaupan River, although it is not exactly located in a tropical region. The averages of the DO registered during the dry season at the beginning of the year were less than at the end of the year. This may be due to the removal of macrophytes or vascular plants from the desilting of the river in June and September. Vascular plants negatively affect oxygen concentrations by transferring organic carbon to the system, creating shade, trapping sediments, reducing turbulence and generating redox gradients, and they are habitats for autotrophic and heterotrophic organisms (Caraco, Cole, & Strayer, 2006). Kaenel, Buehrer and Uehlinger (2000) reported that cutting macrophytes temporarily increases daytime concentrations and decreases the variation in oxygen, which is consistent with the results obtain by the present work.

Wehmeyer and Wagner (2011) did not find a correlation between annual average precipitation and annual average DO. Likewise, the present work did not find a relationship between the averages of the DO concentrations for each measuring day and the total monthly precipitations registered at the station closest to the measuring points. Nevertheless, at MP2 a significant positive correlation ($p < 0.05$) was found on a daily scale between average DO and the Paccu registered at the WO. At MP1, significant ($p < 0.05$) and negative correlations were identified between DO and the Paccu registered at the five WS and the WO. This result is not comparable to the report by Chapman,Chapman, Crisman and Prenger (2000) who found a negative relationship between DO and P, while a positive relationship was found by the present work. The negative relationship between DO and the variances indicates that P decreased the variability in DO concentrations.

This analysis also showed that at MP2 Paccu better explained the DO averages as of day 8, and at MP1 it better explained the variances in DO as of day 12. The positive relationship between the average DO at MP2 and the Paccu registered at the WO indicates that correlations between DO and P were detected in the Zahuapan River when the measuring sites were closer to each other, as mentioned by Chapman *et al*. (2000) for small rivers. The significant negative correlations between DO variances and the Paccu registered at the five WS and the WO indicate that the variability in DO concentrations could be related to the P registered at stations near or far (for example, 30km) from the site at which DO was measured.

Conclusions

Water temperatures were higher than air temperatures before and during the rainy season, but did not exceed the limit established by Mexican norms. The relationship between air and water temperature was significant. Significant negative correlation coefficients between DO concentrations and water temperature were observed before and during the rainy season and positive coefficients after the rainy season. The negative relationship between these variables is comparable to reports in the literature, but a positive correlation has not been reported and therefore this type of study needs to be continued.

Average concentrations between MP1 and MP2 were significantly different. Before and during the rainy seasons, DO values had atypical trends during the hours when measurements were taken, while after the rainy seasons the trends were comparable to those reported by the literature.

Positive correlation coefficients were obtained between average DO and accumulated precipitation, and negative coefficients were found between the variances of DO and accumulated precipitation. The positive correlation coefficients indicate that precipitation increased the concentrations of DO and the negative coefficients indicate that rainfall reduced the variances of the DO concentrations. Nevertheless, these effects of rainfall on DO were observed 8 to 12 days after the beginning of a series of rainy days.

Acknowledgements

The authors thank Aquatec-México S.A. de R.L. for the electrodes used in this work.

References

Abowei, J. F. N. (2010). Salinity, Dissolved Oxygen, pH and Surface Water Temperature Conditions in Nkoro River, Niger Delta, Nigeria. *Advance Journal of Food Sciences Technology*, 2(1), 36-40.

Barceló, Q. I., López, G. E., Solís, C. H., Domínguez, M. E., & Gómez, S. S. (2012). Water Quality Assessment of Jose Antonio Alzate Dam, the Lerma River and its Tributaries in the State of Mexico, Mexico. *Journal of Environmental Protection, 3*, 878-888, doi:10.4236/jep.2012.328103.

Bayram, A., Önsoy, H., Numan, B. V., & Akinci, G. (2013). Influences of Urban Wastewaters on the Stream Water Quality: A Case Study from Gumushane Province, Turkey. *Environmental Monitoring and Assessment, 185*, 1285-1303, doi: 10.1007/s10661-012-2632-y.

Bellos, D., & Sawidis, T. (2005). Chemical Pollution Monitoring of the River Pinios (Thessalia-Greece). *Journal of Environmental Management*, *76*(4), 282-292, doi: 10.1016/j.jenvman.2005.01.027.

Bernot, M. J., & Wilson, K. P. (2012). Spatial and Temporal Variation of Dissolved Oxygen and Ecosystem Energetics in Devils Hole, Nevada. *Western North American Naturalist*, *72*(3), 265-275, doi: http://dx.doi.org/10.3398/064.072.0301.

Caraco, N. F., Cole, J. J., & Strayer, D. L. (2006). Top-Down Control from the Bottom: Regulation of Eutrophication in a Large River by Benthic Grazing. *Limnology and Oceanography*, *51*(1), part 2, 664-670, doi: http://dx.doi.org/10.1641/0006-3568(2006)056[0219:VPAEOO]2.0.CO;2.

CEAT (2012). *Documentos: monitoreo del río*. Comisión Estatal del Agua de Tlaxcala. Recuperado de http://www.ceat.gob.mx/?page_id=3605.

CGE (1997). *Diagnóstico preliminar de la contaminación del río Zahuapan, Tomo II*. Tlaxcala, México: Coordinación General de Ecología, Gobierno del Estado de Tlaxcala.

Chapman, L. J., Chapman, C. A., Crisman, T. L., & Prenger, J. (2000). Predictors of Seasonal Oxygen Levels in an Ugandan Swamp/River System: A 3-Year Profile. *Verhandlungen des Internationalen Verein Limnologie*, *27*, 3048-3053.

Conagua (2013). *Solicitud de información pública o de acceso a datos personales: número de folio 1610100040213*. Comisión Nacional del Agua. Recuperado de http://www.infomex.org.mx/gobiernofederal.

Conagua (2012). *Pronostican menos ciclones tropicales en temporada 2012*. Comisión Nacional del Agua. Recuperado de http://www.conagua.gob.mx/CONAGUA07/Avisos/Aviso%20009-12.pdf.

Conagua (2010). *Estadísticas del agua en la cuenca del río Balsas, 2010*. México, DF: Comisión Nacional del Agua, Secretaría del Medio Ambiente y Recursos Naturales.

García, R. J., Molina, A. F. I., Quiroz, C. H., Trujillo, J. P., & Díaz, V. M. (2011). Distribución y sistemática del fitoplancton a lo largo del río Amacuzac (Morelos, México). *Acta Universitaria, 21*(2), 11-23.

Graves, G. A., Wan, Y., & Fike, D. L. (2004). Water quality characteristics of storm water from major land uses in south Florida. *Journal of the American Water Resources Association*, *40*(6), 1405-1419.

Guzmán, C. G., Ramírez, E. M., Thalasso, L. F., Rodríguez, N. S., Guerrero, B. A. L., & Avelar, G. F. J. (2011). Evaluation of Pollutants in Water and Sediments of the San Pedro River in the State of Aguascalientes. *Universidad y Ciencia Trópico Húmedo*, *27*(1), 17-32.

Harrison, J. A., Matson, P. A., & Fendorf, S. E. (2005). Effects of a Diel Oxygen Cycle on Nitrogen Transformations and Greenhouse Gas Emissions in a Eutrophied Subtropical Stream. *Aquatic Sciences*, *67*(3), 308-315.

He, J., Chu, A., Ryan, M. C., Valeo, C., & Zaitlin, B. (2011). Abiotic Influences on Dissolved Oxygen in a Riverine Environment. *Ecological Engineering*, *37*(11), 1804-1814, doi:10.1016/j.ecoleng.2011.06.022.

Huggins, D. G., & Anderson, J. (2005). *Dissolved Oxygen Fluctuation Regimes in Streams of the Western Corn Belt*

Plains Ecoregion. Kansas Biological Survey. Central Plains Center for BioAssessment. Kansas: University of Kansas, prepared in Fulfillment of USEPA Award X7-99790401, Report No. 130.

INEGI (2010). *Documento técnico descriptivo de la red hidrológica escala 1:50000, edición: 2.0*. Instituto Nacional de Estadística Geografía e Informática. Recuperado de http://antares.inegi.org.mx/analisis/red_hidro.

Kaenel, B. R., Buehrer, H., & Uehlinger, U. (2000). Effects of Aquatic Plant Management on Stream Metabolism and Oxygen Balance in Streams. *Freshwater Biology*, *45*(1), 85-95.

Klose, K., Cooper, S. D., Leydecker, A. D., & Kreitler, J. (2012). Relationships among Catchment Land Use and Concentrations of Nutrients, Algae, and Dissolved Oxygen in a Southern California River. *Freshwater Science*, *31*(3), 908-927, doi: 10.1899/11-155.1.

López, L. E., & Hansen, A. M. (2013). *Determinación del estado de salud e indicadores biológicos para la evaluación de la recuperación del río Apatlaco. Informe final*. Conacyt-IPN-IMTA, julio 2013. Recuperado de http://repositorio.imta.mx:8080/cenca-repositorio/handle/123456789/954.

Master, G. M. (2008). *Introduction to Environmental Engineering and Science* (3rd Edition). Englewood Cliffs, USA: Prentice Hall.

Metcalf & Eddy Inc. (2003). *Wastewater Engineering: Treatment and Reuse* (4th Edition). New York: McGraw- Hill Higher Education.

Montes, R. T., Navarro, I., Domínguez, R., & Jiménez, B. (2013). Modificación de la capacidad de autodepuración del río Magdalena ante el cambio climático. *Tecnología y Ciencias del Agua*, *4*(5), 71-83.

Mulholland, P. J., Houser, J. N., & Maloney, K. O. (2005). Stream Diurnal Dissolved Oxygen Profiles as Indicators of In-Stream Metabolism and Disturbance Effects: Fort Benning as a Case Study. *Ecological Indicators*, *5*(3), 243-252, doi: 10.1016/j.ecolind.2005.03.004.

Muñoz, N. H., Suárez, S. J., Vera, R. A., Orozco, F. S., Batlle, S. J., Ortiz, Z. J. A., & Mendiola, A. J. (2012). Demanda bioquímica de oxígeno y población en la subcuenca del río Zahuapan, Tlaxcala, México. *Revista Internacional de Contaminación Ambiental*, *28*(1), 27-38.

Riđanović. L., Riđanović, S., Jurica, D., & Spasojević, P. (2010). *Evaluation of Water Temperature and Dissolved Oxygen Regimes in River Neretva* (pp. 1-10) Ohrid, Republic of Macedonia: BALWOIS 2010.

Riley, A. J., & Dodds, W. K. (2013). Whole-Stream Metabolism: Strategies for Measuring and Modeling Diel Trends of Dissolved Oxygen. *Freshwater Science*, *32*(1), 56-69, doi: 10.1899/12-058.1.

Sand-Jensen, K., & Pedersen, N. L. (2005). Differences in Temperature, Organic Carbon and Oxygen Consumption among Lowland Streams. *Freshwater Biology*, *50*(12), 1927-1937, doi: 10.1111/j.1365-2427.2005.01436.x.

Sedue (1985). P*royecto de ordenamiento ecológico de la cuenca alta del río* Balsas, con atención a la micro*rregión del río Zahuapan*. Contrato núm. 412-009-85. México, DF: Secretaría de Desarrollo Urbano y Ecología, Análisis y Soluciones, S.C.

Sedue (1989). CE-CCA-001/89. CE-CCA-001/89: Criterios Ecológicos de Calidad del Agua. *Diario Oficial de la Federación*. México, DF: Estados Unidos Mexicanos, Secretaría de Desarrollo Urbano y Ecología.

Shields, F. D. Jr., & Knight, S. S. (2012). Significance of Riverine Hypoxia for Fish: The Case of the Big Sunflower River, Mississippi. *Journal of the American Water Resources Association*, *48*(1), 170-186, doi: 10.1111/j.1752-1688.2011.00606.x.

Statsoft, Inc. (2007). Statistica (Data Analysis Software System), version 8.0. Recuperado de www.statsoft.com.

Tafangenyasha, C., Marshall, B. E., & Dube, L. T. (2010). The Diurnal Variation of the Physico-Chemical Parameters of a Lowland River Flow in a Semi-Arid Landscape with Human Interferences in Zimbabwe. *International Journal of Water Resources and Environmental Engineering*, *2*(6), 137-147.

Wehmeyer, L. L., & Wagner, C. R. (2011). *Relation between Flows and Dissolved Oxygen in the Roanoke River between Roanoke Rapids Dam and Jamesville, North Carolina, 2005-2009* (pp. 2011-5040). Reston, USA: U.S. Geological Survey.

Wenner, E., Sanger, D., Arendt, M., Holland, A. F., & Chen, Y. (2004). Variability in Dissolved Oxygen And Other Water-Quality Variables within the National Estuarine Research Reserve System. *Journal of Coastal Research, Special Issue 45*, 17-38, doi: http://dx.doi.org/10.2112/SI45-017.1.

Wilding, T. K., Brown, E., & Collier, K. J. (2012). Identifying Dissolved Oxygen Variability and Stress in Tidal Freshwater Streams of Northern New Zealand. *Environmental Monitoring and Assessment*, *184*(10), 6045-6060, doi: 10.1007/s10661-011-2402-2.

Institutional Address of the Authors

Dr. Hipólito Muñoz
Dr. Saturnino Orozco
M.C. Andrea Vera
Dr. Juan Suárez
Dr. José Jiménez

Universidad Autónoma de Tlaxcala
Facultad de Agrobiología
Benito Juárez núm. 3
90250 Tlaxco, Tlaxcala, México
Teléfono: +52 (241) 4961 589
hipolito78@hotmail.com
orosat80@hotmail.com
cambisol@hotmail.com
jsuarezs71@hotmail.com
josejilo@hotmail.com

Dra. Edelmira García

Universidad Autónoma de Tlaxcala
Centro de Investigación en Genética y Ambiente
Autopista Texmelucan-Tlaxcala km 10.2
90120 Ixtacuixtla, Tlaxcala, México
Teléfono: +52 (248) 4815 500
mirosgn@yahoo.com.mx.

Lic. Mercedes Neria

Calle Pedro Pérez Núm. 80
90660 Cuaxomulco, Tlaxcala, México
meneri_20@hotmail.com.

Monitoring Soil Moisture using a Wireless Sensor Network

• María Flores-Medina • Francisco Flores-García • Víctor Velasco-Martínez •
Instituto Tecnológico de la Laguna, México

• Guillermo González-Cervantes* •
Instituto Nacional de Investigaciones Forestales, Agrícolas y Pecuarias, México
*Corresponding Author

• Francisco Jurado-Zamarripa •
Instituto Tecnológico de la Laguna, México

Abstract

Flores-Medina, M., Flores-García, F., Velasco-Martínez, V., & González-Cervantes, G., & Jurado-Zamarripa, F. (September-October, 2015). Monitoring Soil Moisture using a Wireless Sensor Network. *Water Technology and Sciences* (in Spanish), 6(5), 77-90.

Water has become a scarce resource and is crucial to the production of food. Therefore, it is increasingly necessary to generate new methods to manage and conserve this vital resource. This article presents a system that helps to continuously monitor soil moisture using a new communications technology— Wireless Sensor Networks (WSN). This is an emerging technology that has been used in agriculture over recent years. Part of the system includes the design and development of three sensor nodes to monitor soil moisture. Sensors were selected and coupled to measure soil moisture using the principle of Frequency Domain Reflectometry. The calibration method is described, which is based on the volumetric method as a reference to obtain fit parameters for the WSN nodes. An interface was designed to display and store the WSN information and the information was linked to a Dropbox account for remote access. The study presents the installation of the WSN system under controlled test conditions as well as the validation of the stability and functioning of the system for monitoring soil moisture. Lastly, the importance of this new technology to aid the monitoring of soil moisture and other variables in the crop cycles is analyzed.

Keywords: Soil moisture, wireless sensor network, automated monitoring system.

Resumen

Flores-Medina, M., Flores-García, F., Velasco-Martínez, V., González-Cervantes, G., & Jurado-Zamarripa, F. (septiembre-octubre, 2015). Monitoreo de humedad en suelo a través de red inalámbrica de sensores. Tecnología y Ciencias del Agua, *6(5), 77-90.*

El agua se ha convertido en un recurso escaso y es primordial para la producción de alimentos. Por esto, la generación de nuevos métodos para la administración y cuidado del vital recurso es cada día más necesaria. En este artículo se presenta un sistema que facilita el monitoreo continuo de la humedad del suelo basado en una nueva tecnología de comunicación: Red Inalámbrica de Sensores (RIS), tecnología emergente que se ha estado utilizando en el ámbito agrícola en los últimos años. Como parte del sistema, se diseñan y desarrollan tres nodo sensores enfocados al monitoreo de humedad en suelo. Se seleccionaron y acoplaron sensores que miden la humedad del suelo con el principio de reflectometría en el Dominio de la Frecuencia (RDF); se describe el método de calibración con el método volumétrico como referencia para obtención de los parámetros de ajuste en los nodos sensores de la RIS. Se diseñó una interfaz para visualización y almacenamiento de la información de la RIS; la información fue enlazada a una cuenta Dropbox para accederla de forma remota. Se presenta después la instalación del sistema RIS en condiciones controladas como prueba y validación de la estabilidad y funcionamiento del sistema en el monitoreo de la humedad del suelo. Finalmente se analiza la importancia de la contribución de esta nueva tecnología, para facilitar el monitoreo de la humedad en suelo y otras variables en los ciclos de cultivo.

Palabras clave: *humedad de suelo, redes inalámbricas de sensores, sistema de monitoreo automático.*

Received: 12/12/2014
Accepted: 02/06/2015

Introduction

Water is indispensable to the adequate production of good quality food and the nutrients needed so that it can reach the tables in our homes (Muñoz-Arboleda, 2009).

The water problem in desert regions has increased along with water scarcity worldwide.

La Laguna is made up of the largest producer cities in the region. It is located in a semi-desert region which for years has faced problems with the supply of water for its residents and various industrial activities (Guzmán-Soria *et al*., 2006). Agriculture is the sector which consumes the most water (80%) in order to produce food (Pfister, Bayer, Koehler, & Hellweg, 2011) and is one of the largest sectors in the Comarca Lagunera. Therefore, alternatives have begun to be investigated to improve the productivity of water.

To achieve efficiency in the agricultural process and prevent wasting water, the hydric requirement of each crop needs to be identified. To this end, the behavior of water in the substrate needs to be evaluated to determine how often to irrigate and the amount of water that needs to be supplied to avoid overuse (Santos-Pereira, De-Juan-Valero, Picornell-Buendía, & Martín-Benito, 2010). Identifying and monitoring soil moisture in cropland is a key component in the analysis of the water balance of plants, since it helps to determine the moisture available to them, evaluate water loss from evaporation and drainage and analyze the type of substrate that is suitable given the water-soil-plant behavior and the climate conditions that are favorable to the crops being produced (Salcedo-Pérez *et al*., 2007).

Direct and indirect methods to measure soil moisture exist (Santos-Pereira *et al*., 2010). Direct methods are performed manually by specialists and require time, special facilities and equipment, and continually affect the agricultural area. Indirect methods take *in situ* measurements and include special devices that function based on different operating principles (Florentino, 2006). Although indirect methods are quicker and more accurate, they require placing equipment in the field (such as data loggers) to interpret, extract and store data, or creating special and expensive facilities for measuring instruments. Therefore, obtaining and monitoring variables can be difficult using either method, and recording and observing changes in soil moisture over the duration of agricultural cycles can be complicated.

Wireless sensor networks (WSN) is a technology that has been used in different areas (Luo, 2012). It consists of several electronic modules (sensor nodes), each coupled with different sensors. The sensor nodes are distributed throughout the general area to be monitored. Each sensor node takes point measurements of the variables, using the sensors that were incorporated, for later processing. The information in the sensor node is strategically transmitted over a wireless network to the other sensors in the WSN or directly to a coordinator node. The coordinator node is typically connected to a server where all the information from the WSN is recorded (Garcia, Bri, Sendra, & Lloret, 2010; Hema, Murugan, & Chitra, 2012; Kumar, Øvsthus, & Kristensen, 2014; Rawat, Singh, Chaouchi, & Bonnin, 2014).

WSN systems continuously monitor variables without the need to continually maintain the electronics. To create an unattended and reliable system, the WSN components should be designed and coupled according to the application needs. Renewable energy can be used to supply the sensor nodes, making the technology autonomous and sustainable (Seah, Eu, & Tan, 2009). Since data is transmitted through a wireless medium installation is simple and costs are more accessible. WSN facilitate access to information from an office without the need for field equipment. A WSN can be included in a control system in which sensor nodes perform actions such as opening irrigation control valves, turning on fans, extractors, climate control devices and sprinklers, etc. ¾to serve as wireless sensor and actuator networks (WSAN) (Aqeel-ur-Rehman *et al*., 2010; Matijevics & János, 2010).

WSN systems have been used to monitor agricultural and meteorological variables (Aqeel-ur-Rehman, Azafar-Abbasi, Islam, & Ahmed-Shaikh, 2014; Mathurkar & Chaud-

hari, 2013; Mercado *et al.*, 2012; Wang, Zhang, & Wang, 2006) in open fields (Escolar-Díaz, Carretero-Pérez, Calderón Mateos, Marinescu, & Bergua-Guerra, 2011; Gopalakrishna-Moorthy, Yaashuwanth, & Venkatesh, 2013; Hwang, Shin, & Yoe, 2010; Patil, Davande, & Mulani, 2014; Santhosh & K-Paulose, 2012; Yu, Pute, Han, & Zhang, 2013) as well as greenhouses (Chaudhary, Nayse, & Waghmare, 2011; Kasaei, Kasaei, & Kasaei, 2011). They have also been used to monitor various crops with small or large network structures (Ruiz-Garcia, Lunadei, Barreiro, & Robla, 2009).

Recent investigations have included applications of WSN-based systems to monitor soil moisture in order to manage and optimize water consumption for farming (Khan, Ali, Suryani, Ahmad, & Zakarya, 2013; Kotamäki *et al.*, 2009; Majone *et al.*, 2013; Zhang *et al.*, 2011). Figure 1 shows the structure and distribution of a WSN-based system to monitor soil moisture in agriculture.

The National Interdisciplinary Research Center for Water, Soil, Plants and the Atmosphere (CENID-RASPA, Spanish acronym), part of the National Research Institute for Forestry, Agriculture and Livestock (INIFAP, Spanish acronym), and the Laguna Technological Institute (ITL, Spanish acronym) collaborated to create new instruments based on WSN to monitor agricultural variables in real-time both in the field and in greenhouses.

This article presents the design of a preliminary prototype system using WSN for the continuous monitoring of soil moisture. It also presents the design of an interface to view and store data. The work describes the calibration process, the integration of moisture probes with the sensor nodes that make up the WSN and the validation of the operations of the system in a greenhouse.

Materials and Methods

The tests of the WSN to monitor soil moisture were performed in a greenhouse in the city of Torreon, Coahuila, Mexico (latitude 25º 35′ 31.7″ and longitude -103º 22′ 40″). A decorative plant (*Caladium bicolor*) is grown in this greenhouse, which was used by this investigation a case study.

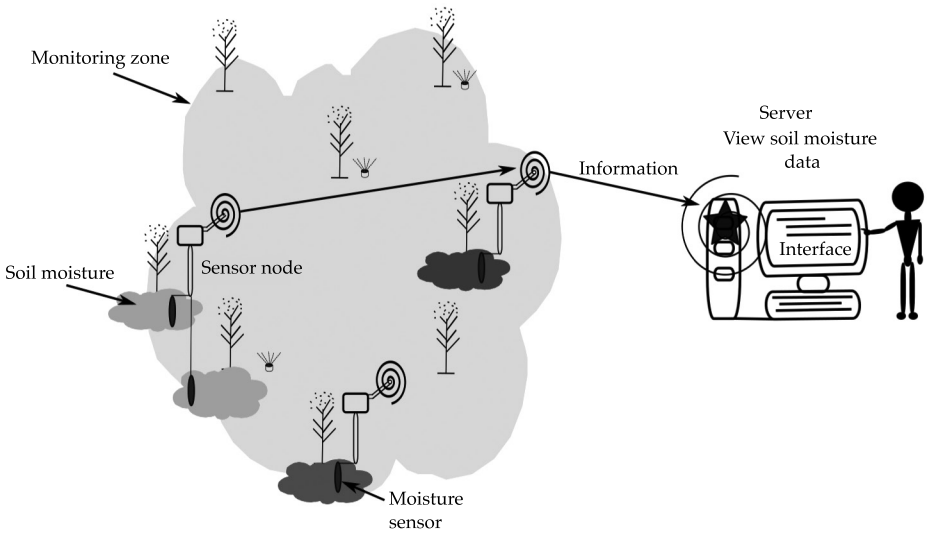

Figure 1. Conceptual model of a soil moisture monitoring system based on WSN.

Characteristics of the WSN

The system was composed of a coordinator node, a graphical user interface and three sensor node prototypes which were adapted with probes that measure soil moisture. The sensor nodes were built with Waspmote PRO Libelium WSN technology (Libelium, Zaragoza, Spain).

Sensor node 1 was adapted with two VH400 moisture probes (SH5 and SH6) to measure the moisture in the soil. An SHT11 sensor (THP1) was also included to measure air temperature, relative humidity and dew point. Sensor 2 was adapted with four VH400 moisture probes (SH1, SH2, SH3 and SH4) and sensor 3 with only one VH400 moisture probe (SH7).

The VH400 probe or sensor (Vegetronix, Riverton, United States) is high frequency, measures soil moisture with a linear response per section and has a range of 0 to 50 VWC. It is an indirect method which uses the Frequency Domain Reflectometry (FDR) principle (Vita-Serman, Schugurensky, Carrión, & Rodríguez, 2006). The probe uses the principle of radio frequency signals in which the signal reflected is proportional to the existing soil moisture (Capraro *et al*., 2008).

The SHT11 sensor (Sensirion, Stäfa, Switzerland) operates at temperature ranges between -40 and 123.8 ºC with an accuracy of ± 0.4 ºC and a relative humidity range between 0 and 100% with an accuracy of ± 3%. The dew point percentage is calculated based on these two variables according to the specifications on the sensor's data sheet. Both sensors are low-cost and present good accuracy in the operating range and low energy consumption.

Each node has a 7.2V solar panel (Libelium, Zaragoza, Spain) to utilize the solar radiation in the region in order to continuously recharge the 6 600 mAh lithium battery (Libelium, Zaragoza, Spain) which provides the power to the sensor nodes' electronics and the sensors.

Interface

The user interface was programmed as an add-on in the free *Lisboa* v. 1.8 *Quantum GIS (QGIS)* software platform (OSGeo, Beaverton, United States). It consists of a window with a row for each sensor node in the network, in which the information from the last data transmission received can be viewed. The data from previous events are stored in csv text files and the text files are stored by sensor node-date. Each file contains the data monitored by the sensor node over the course of an entire day. These data are linked to a Dropbox account (Dropbox, Inc., San Francisco, USA) so they can be viewed from other locations. Figure 2 shows the user interface.

The cycle of each sensor node consists of waking, performing and processing measurements, transmitting, waiting 1 minute for commands and sleeping 14 minutes to conserve energy. The interface can send configuration parameters during the waiting time of each sensor. Each sensor node transmits data related to the date, hour and the value in the agricultural sensors. Other technical data are also transmitted to monitor the correct functioning of the system, such as battery level. The interface has an "Add Layer" button that will later enable adding the vector layer corresponding to the data captured by the Quantum GIS (*QGIS*).

Calibration of Moisture Probes

Different known increments of water were added to 1 000 cm^3 of a vermicompost substrate. The substrate was first dried in a furnace at 105 °C for 24 hours. A reading was taken by each probe for each increment of water. The volumetric water content (VWC, in $cm^3 \cdot cm^{-3}\%$ or $\theta_v\%$) of the samples and the VWC read by the probes were calculated using the equations from the manufacturer. The average error when comparing the two VWC was obtained. These errors are presented in Table 1 in the results section.

Figure 2. Graphical Interface in QGIS.

Each probe was adjusted. Using the manufacturer's equations, the expected voltages corresponding to the VWC of each sample were calculated. The average error in the voltage of each probe was obtained and programmed into each probe as the offset. The VWC was recalculated with the manufacturer's equations using the calibration voltages. The 95% confidence intervals were then calculated for each one of the average errors using the different samples. The results are shown in Table 1.

Installation of the WSN

The greenhouse where the system was installed was tubular with a polyethylene lining and covered with a shade cloth. It measured 50 m long, 10 m wide and 6 m high. The inside of the greenhouse had a air cleaning system to decrease temperature and increase relative humidity. Two extractors at the front were continuously running to extract hot air. An extra fine nebulizer system was operating in the front half of the greenhouse to humidify the environment.

The sensor nodes were placed in three experimental sections in the greenhouse (Figure 3). Sensor node 1 was installed in a soil area of 18 m x 3 m, which had a mixed substrate containing several rows of plants. Each row was watered with a hose system. The SH5 probe was placed in one group of plants and the SH6 in another group. Sensor node 2 was installed in section 2 where a study was being performed in four groups of pots, each with a different type of substrate. Probes SH1, SH2, SH3 and SH4 were placed in one pot in each group. Sensor node 3 was put in a 3 m x 40 m wood pot containing a substrate which was

Table 1. Results from the calibration of probes.

Sensor	Average VWC error without adjusting (cm^3/cm^3 %)	*Offset* of voltage adjustment (V)	Average VWC error with adjustment (cm^3/cm^3 %)	Average VWC error 95% CI with adjustment (cm^3/cm^3%)
SH1	-27.5662	-0.7446	0.2771	±1.2458
SH2	-26.3693	-0.7018	-1.8720	±2.2766
SH3	-23.0769	-0.5789	-1.7680	± 2.1912
SH4	-10.6266	-0.3624	-0.3051	± 1.0500
SH5	-28.7696	-0.8347	-0.6428	±1.2339
SH6	-12.2114	-0.3689	-0.6849	±1.7369
SH7	-32.5981	-0.8607	-1.8494	± 2.6314

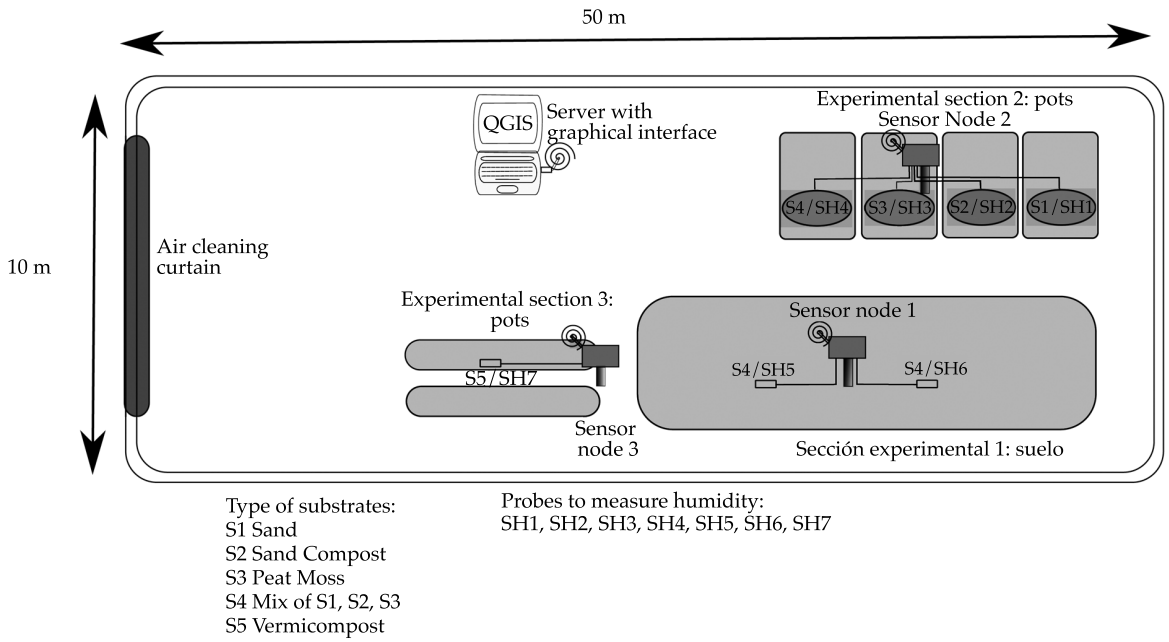

Figure 3. Layout of the greenhouse system for caladium.

different than the others. All the probes were installed on the surface of the substrate near the roots of the plant and far from the irrigation system's water outlet so as not to affect the readings.

The solar panels were placed in the top of each node at 23° from the vertical line, with a southern orientation to maximum the use of solar radiation. A Waspmote Libelium coordinator node (Libelium, Zaragoza, Spain), was connected to a computer a few meters from the experimental sections, where a *Lisboa* v. 1.8 *QGIS* and the user interface were installed.

Soil humidity in the different sections was monitored 24 hours per day with data events every 15 minutes for a period of 6 days. Sensor node 3 was added the second day of the experimental period.

Results

Figure 4 shows the physical installation of the sensor nodes (Figures 4a, 4b and 4c) and how the probes were installed on the surface of the substrate (Figure 4d).

Table 1 contains the average errors before and after the adjustments were made. It also shows the confidence intervals and the offset programmed for each probe.

Figure 5 shows the behavior of the probes with calibrations for each of the sensor nodes.

Figure 6 presents the continuous monitoring by the three sensor nodes during the test period.

Discussion

Probes

As can be seen when comparing the average errors shown in Table 1, the error decreased considerably with the adjustment of each of the probes. Probe SH7 had the highest errors, even after being adjusted. Figure 5c shows the saturation of probe SH7, which had a response under the 50% VWC guaranteed by the manufacturer, who also mentions that calibration is not needed (Vegetronix Inc., n.d.). Nevertheless, these results suggest the need for calibration since a different displacement error is shown for each probe. In addition, the error in probe SH7 (Table 1) indicates that a probe may not cover the 0 to 50% VWC range indicated by the manufacturer due to the displacement error. The probes should be calibrated according to the substrate in which they are going to be used. The data obtained from the calibration of each probe should be adjusted and programmed into the corresponding sensor node in order to increase the accuracy of the readings by the system. While the calibration process was performed in one substrate, it should be performed for each substrate.

When compared to other methods used to determine soil moisture, the VH400 probes were more sensitive to changes in moisture. This contributed to quicker and more reliable readings by the sensor nodes after calibrated adjustments, without the need to affect the area where soil moisture was measured. It also cost less than others that operate based on the same principle.

Monitoring

The WSN continuously monitored soil moisture in a stable manner throughout the test period, as seen in the graphs in Figure 6. The SH2 had a technical problem during this period and therefore readings from one of the groups in section 2 were lost. The behavior of surface moisture in each group was different because of the different characteristics of the substrates. A cyclical behavior was observed on the different days. The plants were watered in the morning, presenting the maximum moisture for the day. It then decreased during the hottest hours and the lowest moisture of the day occurred in the afternoon. It then began to increase and continued that trend through the night.

Interface

The user interface made it possible to observe the data at the moment in which they were transmitted (Figure 2). The stored data was used for analysis and graphed on an Excel 2007 spreadsheet (Microsoft Office, Redmond, USA). The graphical interface was designed with free *QGIS* software. A version is currently being developed to integrate work previously performed (Flores-Medina, Velasco-Martínez, Flores-García, & Cervantes-González, 2013) and validate it in the crop field. This will make it possible to view and analyze the information using GIS tools. The information will be stored in a *PostGIS* database (Boluwade & Ferdinand, 2011; Steiniger & Hay, 2009).

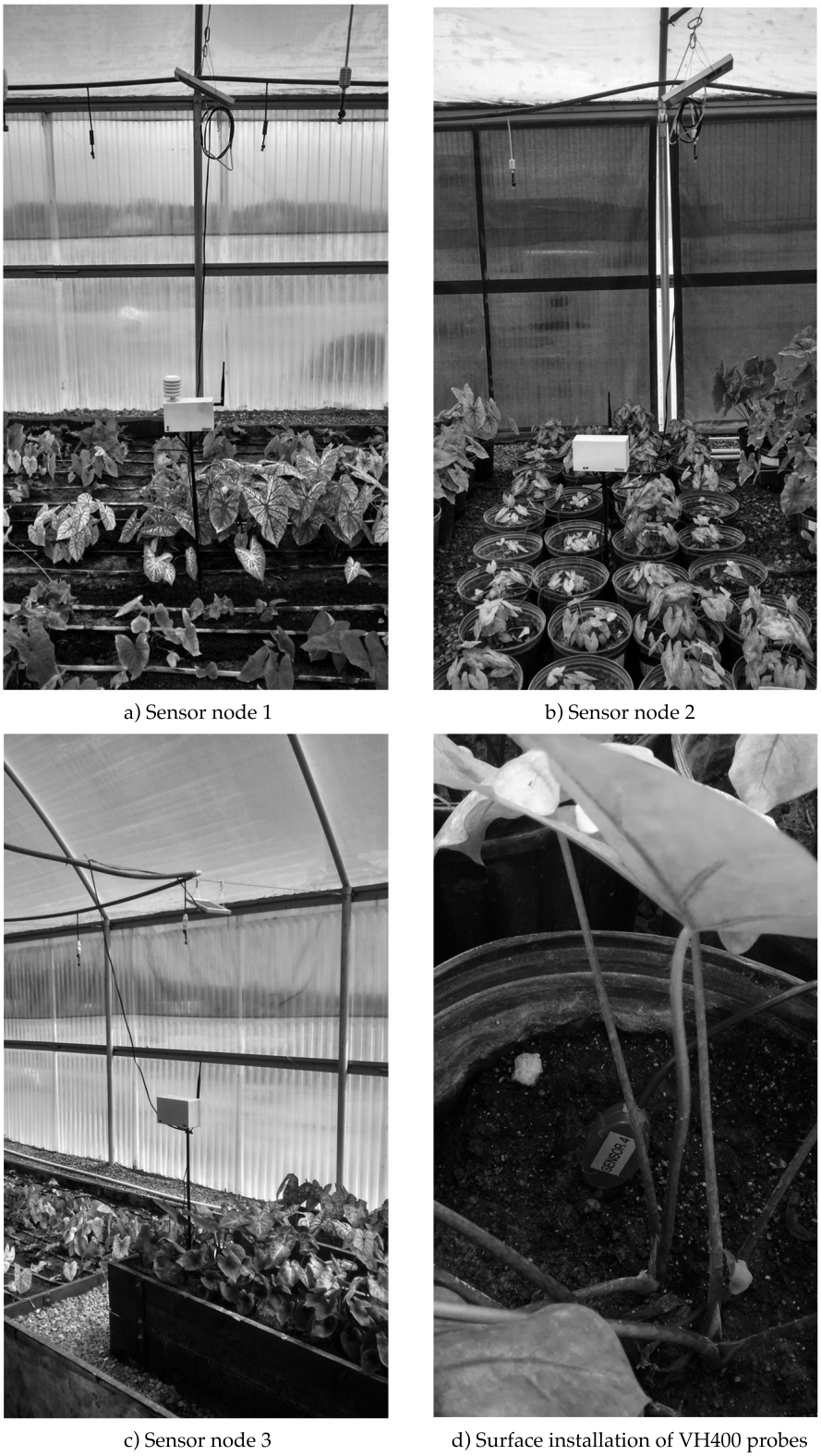

a) Sensor node 1

b) Sensor node 2

c) Sensor node 3

d) Surface installation of VH400 probes

Figure 4. Installation of greenhouse system for caladium.

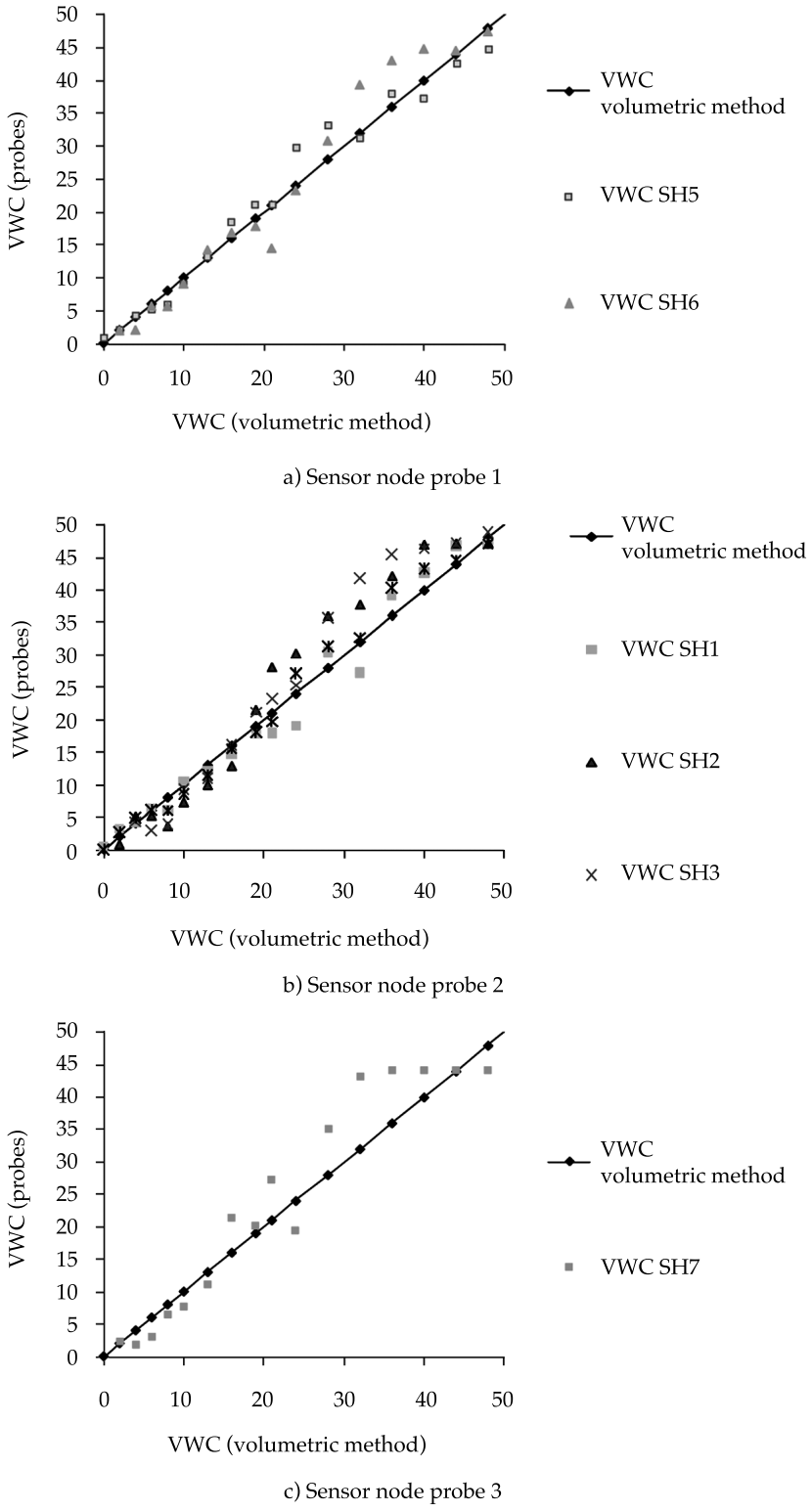

Figure 5. Response of probes with calibration.

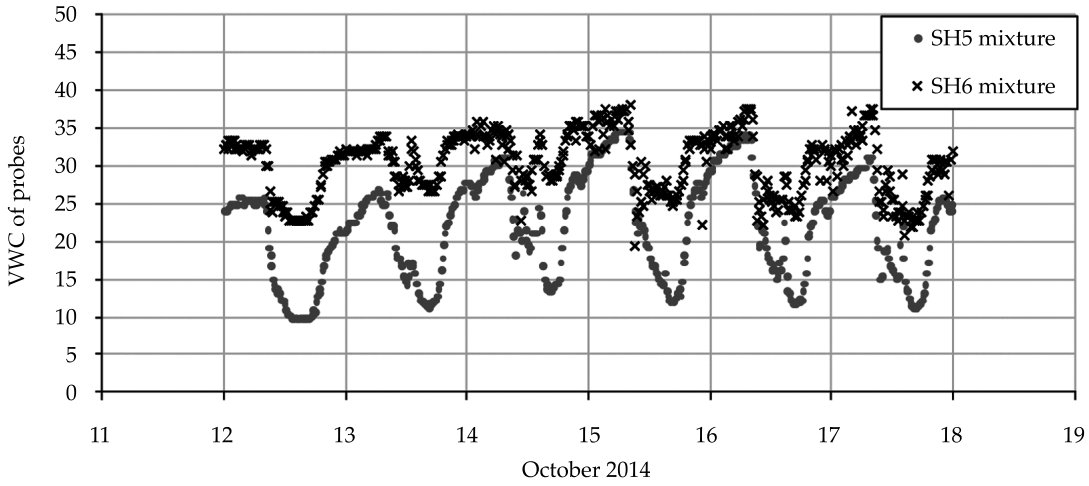

a) Sensor node 1

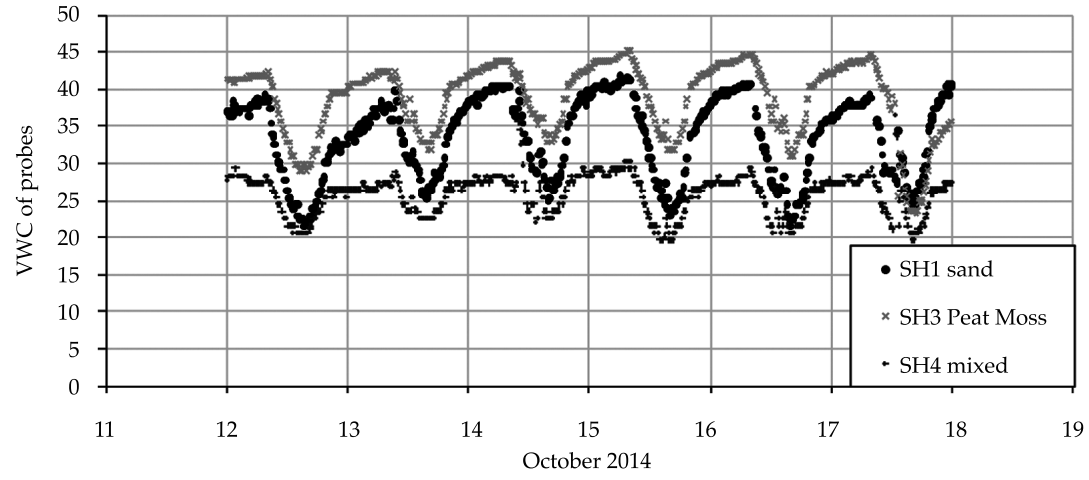

b) Sensor node 2

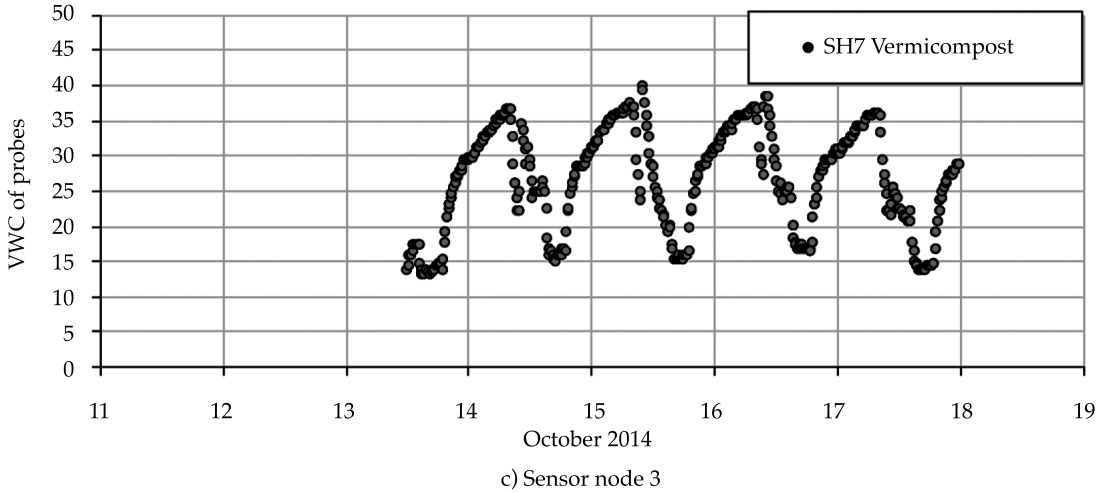

c) Sensor node 3

Figure 6. Continuous monitoring of the system.

System

Conserving non-renewable resources is increasingly of interest to scientific and technological fields. The present work focused on considering and learning about the implementation of new technologies that make it possible to improve prices, installation and time for agricultural production in La Laguna, in order to manage water and other resources. Several countries such as Spain (López-Fidalgo, 2010; Valdiviezo, 2009), the United States (Lea-Cox, Kantor, Anhalt, Ristvey, & Ross, 2007), Argentina (Mercado *et al*., 2012), India (Kar, De Sarkar, A., & Mukherjee, 2012) and others (Arai,2011; Ayday & Safak, 2009) have used WSN technologies to manage resources in agricultural fields. This technology has begun to be studied and implemented for agricultural applications in Mexico, for instance, at the University of Ensenada and the University of Colima (Aquino-Santos, González-Potes, Edwards-Block, & Virgen-Ortiz, 2011; Aquino- Santos, Villaseñor-González, Rangel-Licea, Álvarez-Cárdenas, & Edwards-Block, 2010; Cárdenas-Tamayo, Lugo-Ibarra, & García- Macías, 2010). Since Ensenada has a climate similar to that of the region of La Laguna (arid and hot), the WSN technology has shown good results, as was the case with these preliminary research steps. A system similar to the one studied herein is being tested in La Paz, Mexico (Gutiérrez, Villa-Medina, Nieto-Garibay, & Porta-Gándara, 2013). Unlike the system proposed herein, that investigation is focused on linking the data to a website.

Although the system designed by the present study focused on monitoring soil moisture, sensor nodes can be used with other sensors for other agricultural or climate variables of interest, such as sensor node 1 which has a SHT11 sensor for temperature and other variables, in addition to the VH400 moisture probe. Additional agricultural sensors can be installed in the same sensor node. It can operate not only in a greenhouse, which involves a short monitoring distance, but also in an open field with longer distances and different crops and agricultural conditions, as long as the sensors and the WSN communications parameters are calibrated. Nevertheless, it is important to remember that this instrument is intended to provide information to specialists in order to analyze events that occur in the field and provide elements for decision-making.

Conclusions

In the search for new technologies that contribute to the optimal use of water for crop production, the WSN system proposed was found to facilitate the monitoring of soil moisture and can be included in a new methodology to monitor and manage water in Comarca Lagunera. The methodology to calibrate the probes and obtain operating parameters made it possible to quickly obtain reliable soil moisture measurements. The design of an interface to view and store the information made the data available for analysis and as a history of events. The system provided data related to the volumetric water contents in real-time, continuously and in controlled conditions, and presented variations corresponding to the different types of soil. The system can be transferred to the field, with the calibration of the elements, to provide detailed and precise information with which to observe water supplies and losses during irrigation cycles. Soil moisture information monitored by WSN systems can be analyzed and used by experts to make decisions about the use and management of water for crops.

Acknowledgements

The authors thank the National Council for Science and Technology for its grants to conduct postgraduate studies, and the investigators at INIFAP for fostering the creation of Mexican technology and innovation. Thank you to the

owner of the greenhouse for facilitating the implementation of the system for these investigative purposes and to the entire work team which contributed to this preliminary research stage.

References

Aqeel-ur-Rehman, Azafar-Abbasi, A., Islam, N., & Ahmed-Shaikh, Z. (2014). A Review of Wireless Sensors and Networks' Applications in Agriculture. *Computer Standards & Interfaces*, *36*(2), 263-270, doi:10.1016/j.csi.2011.03.004.

Aqeel-ur-Rehman, Shaikh, Z. A., Yousuf, H., Nawaz, F., Kirmani, M., & Kiran, S. (2010). Crop Irrigation Control using Wireless Sensor and Actuator Network (WSAN). In *International Conference Information and Emerging Technologies (ICIET)* (pp. 1-5), doi:10.1109/ICIET.2010.5625669.

Aquino-Santos, R., González-Potes, A., Edwards-Block, A., & Virgen-Ortiz, R. A. (2011). Developing a New Wireless Sensor Network Platform and its Application in Precision Agriculture. *Sensors*, *11*(1), 1192-211, doi:10.3390/s110101192.

Aquino-Santos, R., Villaseñor-González, L. A., Rangel-Licea, V., Álvarez-Cárdenas, O., & Edwards-Block, A. (2010). Performance Analysis of Routing Strategies for Wireless Sensor Networks. *Rev. Fac. Ing. Univ. Antioquia*, *52*, 185-195.

Arai, K. (2011). Wireless Sensor Network for Tea Estate Monitoring in Complementally Usage with Satellite Imagery Data Based on Geographic Information System (GIS). *International Journal of Ubiquitous Computing (IJUC)*, *1*(2), 12-21.

Ayday, C., & Safak, S. (2009). Application of Wireless Sensor Networks with GIS on the Soil Moisture Distribution Mapping. In *Symposium GIS Ostrava 2009 - Seamless Geoinformation Technologies* (pp. 1-6). Ostrava, Czech Republic. Retrieved from http://gis.vsb.cz/GIS_Ostrava/GIS_Ova_2009/sbornik/Lists/Papers/040.pdf

Boluwade, A., & Ferdinand, A. (2011). The Design and Development of Spatial Database Management Systems (SDMS) for Hydrographic Studies using Coupled Open-Source GIS and Relational Database . Conceptual Design Logical Database design Physical Database Design Database Implementation. *The Pacific Journal of Science and Technology*, *12*(1), 286-291.

Capraro, F., Tosetti, S., Vita, F., Patiño, D., Schugurensky, C., & Fullana, R. (2008). Sistema de monitoreo continuo de la humedad en suelo para el control de riego en un olivar (Olea europaea L.) empleando LabVIEW (pp. 28-42). In *37º JAIIO*. Jornadas de Inf. Ind. - Agroinformática (JII 2008 Agroinfo), Santa Fe, Argentina.

Cárdenas-Tamayo, R. A., Lugo-Ibarra, M. G., & García-Macías, J. A. (2010). Better Crop Management with Decision Support Systems Based on Wireless Sensor Networks. In *7th International Conference on Electrical Engineering, Computing Science and Automatic Control (CCE 2010)* (pp. 412-417). Tuxtla Gutiérrez.

Chaudhary, D. D., Nayse, S. P., & Waghmare, L. M. (2011). Application of Wireless Sensor Network for Greenhouse Parameter Control in Precision Agriculture. *International Journal of Wireless & Mobile Networks (IJWMN)*, *3*(1), 140–149. doi:10.5121/ijwmn.2011.3113 140.

Escolar-Díaz, S., Carretero-Pérez, J., Calderón-Mateos, A., Marinescu, M.-C., & Bergua-Guerra, B. (2011). A Novel Methodology for the Monitoring of the Agricultural Production Process Based on Wireless Sensor Networks. *Computers and Electronics in Agriculture*, *76*(2), 252–265, doi:10.1016/j.compag.2011.02.004

Florentino, A. (2006). Métodos para medir el contenido de agua en el suelo. *Venesuelos*, *14*, 48-70.

Flores-Medina, M. de J., Velasco-Martínez, V. D., Flores-García, F. G., & Cervantes-González, G. (2013). Sistema de Monitoreo y Análisis Basado en una Red Inalámbrica de Sensores y SIG para el Campo Agrícola. In A. Espinoza, J. L. Meza, M. F. J. Cepeda, & G. D. Guerrero (Eds.), *5º Encuentro Regional de Investigadores y 4º Encuentro de Jóvenes Investigadores*. (pp. 491-500). Torreón Coahuila: Rucerhall. Retrieved from http://www.cieslag.org/.

Garcia, M., Bri, D., Sendra, S., & Lloret, J. (2010). Practical Deployments of Wireless Sensor Networks : A Survey. *International Journal on Advances in Networks and Services*, *3*(1 & 2), 170-185.

Gopalakrishna-Moorthy, K., Yaashuwanth, C., & Venkatesh, K. (2013). A Wireless Remote Monitoring of Agriculture Using Zigbee. *International Journal of Engineering and Innovative Technology (IJEIT)*, 2(8), 72-74.

Gutiérrez, J., Villa-Medina, J. F., Nieto-Garibay, A., & Porta-Gándara, M. Á. (2013). Automated Irrigation System Using a Wireless Sensor Network and GPRS Module. *Instrumentation and Measurement, IEEE*, *63*(1), 166-176, doi:10.1109/TIM.2013.2276487.

Guzmán-Soria, E., García-Salazar, A., Mora-Flores, S., Fortis-Hernández, M., Valdivia-Alcalá, R., & Portillo-Vázquez, M. (2006). La demanda de agua en la Comarca Lagunera, México. *Agrociencia*, *40*(6), 793-804.

Hema, L. K., Murugan, D., & Chitra, M. (2012). Wireless Sensor Networks ' Emergence And Growth- A Survey. *International Journal of Computational Engineering Research (IJCER)*, *2*, 217-224.

Hwang, J., Shin, C., & Yoe, H. (2010). A wireless sensor network-based ubiquitous paprika growth management system. *Sensors*, *10*(12), 11566-11589. doi:10.3390/s101211566.

Kar, S., De Sarkar, A., & Mukherjee, N. (2012). An Integrated Framework in Geographic Information System using

Wireless Sensor Network. *International Journal of Computer Applications*, *iRAFIT*(2), 13-18. doi:Issn: 09758887.

Kasaei, S. H., Kasaei, S. M., & Kasaei, S. A. (2011). Design and Development a Control and Monitoring System for Greenhouse Conditions Based-On Multi Agent System. *BRAIN. Broad Research in Artificial Intelligence and Neuroscience*, 2(4), 28-35.

Khan, R., Ali, I., Suryani, M. A., Ahmad, M., & Zakarya, M. (2013). Wireless Sensor Network Based Irrigation Management System for Container Grown Crops in Pakistan. *World Applied Sciences Journal*, *24*(8), 1111-1118, doi:10.5829/idosi.wasj.2013.24.08.1151.

Kotamäki, N., Thessler, S., Koskiaho, J., Hannukkala, A. O., Huitu, H., Huttula, T., … Järvenpää, M. (2009). Wireless In-Situ Sensor Network for Agriculture and Water Monitoring on a River Basin Scale in Southern Finland: Evaluation from a Data User's Perspective. *Sensors*, *9*(4), 2862-2883, doi:10.3390/s90402862.

Kumar, A. A., Øvsthus, K., & Kristensen, L. M. (2014). An Industrial Perspective on Wireless Sensor Networks - A Survey of Requirements, Protocols and Challenges. *Communications Surveys & Tutorials, IEEE*, *16*(3), 1391-1412, doi:10.1109/SURV.2014.012114.00058.

Lea-Cox, J. D., Kantor, G., Anhalt, J., Ristvey, A., & Ross, D. S. (2007). A Wireless Sensor Network for the Nursery and Greenhouse Industry. In *Proceedings of Southern Nursery Association Research Conference* (Vol. 52, pp. 454-458). TX, USA. Retrieved from http://sensornet.umd.edu/Publications/Lea-Cox *et al*., 2007 SNA 52_454-458.pdf.

López-Fidalgo, A. (2010). Redes de sensores sin cables para agricultura de precisión en regiones minifundistas (pp. 1-26). In *CONAMA10 Congreso Nacional del Medio Ambiente*, Galicia, España.

Luo, Z. (2012). Overview of Applications of Wireless Sensor Networks. *International Journal of Innovative Technology and Exploring Engineering (IJITEE)*, *1*(4), 4-6.

Majone, B., Viani, F., Filippi, E., Bellin, A., Massa, A., Toller, G., … Salucci, M. (2013). Wireless Sensor Network Deployment for Monitoring Soil Moisture Dynamics at the Field Scale. *Procedia Environmental Sciences*, *19*, 426-435, doi:10.1016/j.proenv.2013.06.049.

Mathurkar, S. S., & Chaudhari, D. S. (2013). A Review on Smart Sensors based Monitoring System for Agriculture. *International Journal of Innovative Technology and Exploring Engineering (IJITEE)*, 2(4), 76-78.

Matijevics, I., & János, S. (2010). Control of the Greenhouse's Microclimatic Condition Using Wireless Sensor Network. *IPSI Journal*, *6*(2), 35-38. Retrieved from http://www.internetjournals.net/journals/tir/2010/July/Paper 05.pdf.

Mercado, G., Borgo, R., Antivilo, F. G., Uriburu, G. O., Diedrichs, A., Tromer, S., … Pérez, S. (2012). Red de Sensores SIPIA (pp. 69-73). In *XIV Workshop de Investigadores en Ciencias de la Computación*, Posadas, Argentina.

Muñoz-Arboleda, F. (2009). Importancia del agua en la nutrición de los cultivos. *Cenicaña. Carta Trimestral*, *31*(3-4), 16-18.

Ortiz-Sanchez, A., Gonzales-Cervantes, G., Alvarez-Reynal, V., Potisek-Talavera, M., Chavez-Simentel, J., & Valenzuela-Nunez, L. (2013). *Inducción de crecimiento en raíz y tubérculo mediante la aplicacion de productos orgánicos y hormonales (estudio de caso* Caladium bicolor*).* In Agricultura Organica: Sexta Parte. (pp. 61–75). Torreón, México: Red Internacional de Agricultura Orgánica, SEP.

Patil, S. S., Davande, V. M., & Mulani, J. J. (2014). Smart Wireless Sensor Network for Monitoring an Agricultural Environment. *International Journal of Computer Sciencie and Information Technologies (IJCSIT)*, *5*(3), 3487-3490.

Pfister, S., Bayer, P., Koehler, A., & Hellweg, S. (2011). Projected Water Consumption in Future Global Agriculture: Scenarios and Related Impacts. *Science of the Total Environment*, *409*(20), 4206-4216, doi:10.1016/j.scitotenv.2011.07.019.

Rawat, P., Singh, K. D., Chaouchi, H., & Bonnin, J. M. (2014). Wireless Sensor Networks: A Survey on Recent Developments and Potential Synergies. *The Journal of Supercomputing*, *68*(1), 1-48, doi:10.1007/s11227-013-1021-9.

Ruiz-Garcia, L., Lunadei, L., Barreiro, P., & Robla, J. I. (2009). A Review of Wireless Sensor Technologies and Applications in Agriculture and Food Industry: State of the Art And Current Trends. *Sensors*, *9*(6), 4728-4750, doi:10.3390/s90604728.

Salcedo-Pérez, E., Galvis-Spinola, A., Hernández-Mendoza, T. M., Rodríguez-Macias, R., Zamora-Natera, F., Bugarin-Montoya, R., & Carrillo-González, R. (2007). La humedad aprovechable y su relación con la materia orgánica y superficie específica del suelo. *Terra Latinoamericana*, *25*(4), 419-425.

Santhosh, S., & K-Paulose, J. (2012). Development and Deployment of Wireless Sensor Network in Paddy Fields of Kuttanad. *International Journal of Engineering and Innovative Technology (IJEIT)*, *2*(1), 84-88. Retrieved from http://ijeit.com/vol 2/Issue 1/IJEIT1412201207_15.pdf.

Santos-Pereira, L., De-Juan-Valero, J. A., Picornell-Buendía, M. R., & Martín-Benito, J. M. (2010). *El riego y sus tecnologías*. Albacete: CREA-UCLM.

Seah, W. K. G., Eu, Z. A., & Tan, H.-P. (2009). Wireless Sensor Networks Powered by Ambient Energy Harvesting (WSN-HEAP) - Survey and Challenges. In *2009 1st International Conference on Wireless Communication, Vehicular Technology, Information Theory and Aerospace & Electronic Systems Technology* (pp. 1-5). Aalborg: Ieee. doi:10.1109/WIRELESSVITAE.2009.5172411.

Steiniger, S., & Hay, G. J. (2009). Free and Open Source Geographic Information Tools for Landscape Ecology. *Ecological Informatics*, *4*(4), 183-195, doi:10.1016/j.ecoinf.2009.07.004.

Valdiviezo, D. V. (2009). *Diseño de una Red de Sensores Inalámbrica para Agricultura de Precisión*. Pontificia Universidad Católica del Perú.

Vegetronix Inc. (n.d.). Retrieved from http://www.buscagro.com/detalles/Evaluacion-del-comportamiento-de-sensores-de-humedad-de-suelo-del-tipo--FDR--de-..._35922.html.

Vita-Serman, F., Schugurensky, C., Carrión, R., & Rodríguez, S. (2006). Evaluación del comportamiento de sensores de humedad de suelo del tipo (FDR) de desarrollo local, en relación al contenido de agua y a la textura de suelo (p. 6). In *III Jornadas de Actualización en Riego y Fertirriego*, Mendoza, Argentina.

Wang, N., Zhang, N., & Wang, M. (2006). Wireless Sensors in Agriculture and Food Industry - Recent Development and Future Perspective. *Computers and Electronics in Agriculture*, *50*(1), 1-14, doi:10.1016/j.compag.2005.09.003.

Yu, X., Pute, W., Han, W., & Zhang, Z. (2013). A Survey on Wireless Sensor Network Infrastructure for Agriculture. *Computer Standards & Interfaces*, *35*(1), 59-64, doi:10.1016/j.csi.2012.05.001.

Zhang, R., Guo, J., Zhang, L., Zhang, Y., Wang, L., & Wang, Q. (2011). A Calibration Method of Detecting Soil Water Content based on the Information-Sharing In Wireless Sensor Network. *Computers and Electronics in Agriculture*, *76*(2), 161-168, doi:10.1016/j.compag.2011.01.010.

Institutional Address of the Authors

M.C. María de Jesús Flores Medina

Instituto Tecnológico de la Laguna
División de Estudios de Posgrado e Investigación
Blvd. Revolución s/n esq. con Av. Cuauhtémoc
27000 Torreón, Coahuila, México
Teléfono: +52 (871) 7051 331, extensión 515
mary_rosch@hotmail.com

Dr. Francisco Flores-García

Instituto Tecnológico de la Laguna
División de Estudios de Posgrado e Investigación
Blvd. Revolución y Calzada Cuauhtémoc s/n
27000 Torreón, Coahuila, México
Teléfono: +52 (871) 7051 331, extensión 515
francisco.floresgarcia@gmail.com

M.C. Víctor Velasco-Martínez

Instituto Tecnológico de la Laguna
División de Estudios de Posgrado e Investigación
Blvd. Revolución y Calzada Cuauhtémoc s/n
27000 Torreón, Coahuila, México
Teléfono: +52 (871) 7051 331, extensión 515
yoalieh@gmail.com

Dr. Guillermo González Cervantes

Centro Nacional de Investigación Disciplinaria en
Relación Agua-Suelo-Planta-Atmósfera CENID-RASPA
INIFAP
Km 6.5 margen derecha, Canal Sacramento
35140 Gómez Palacio, Durango, México
Teléfono: +52 (871) 1590 105
gonzalez.guillermo@inifap.gob.mx

Dr. Francisco Jurado Zamarripa

Profesor Investigador
Instituto Tecnológico de la Laguna
División de Estudios de Posgrado e Investigación
Blvd. Revolución y Calzada Cuauhtémoc s/n
27000 Torreón, Coahuila, México
Teléfono: +52 (871) 7051 331, extensión 515
fjurado@itlalaguna.edu.mx

Hydro-Agricultural Infrastructure under Climate Change Scenarios

• Mauro Iñiguez • Waldo Ojeda-Bustamante* •
Instituto Mexicano de Tecnología del Agua
*Corresponding Author

• Carlos Díaz-Delgado •
Universidad Autónoma del Estado de México

Abstract

Iñiguez, M., Ojeda-Bustamante, W., & Díaz-Delgado, C. (September-October, 2015). Hydro-Agricultural Infrastructure under Climate Change Scenarios. *Water Technology and Sciences* (in Spanish), 6(5), 91-103.

Large irrigation systems consist of a complex series of infrastructure to supply irrigation services. The flow of water, or the system flow, running through this infrastructure is a hydraulic variable required to satisfy water demand for crops. The majority of general ocean-atmospheric circulation models indicate warmer and dryer environments in most of Mexico, with significant effects on evapotranspiration of crops, a basic agronomic variable for determining the capacity of hydro-agricultural infrastructure. The present work presents the development of a methodology to evaluate the integrated evapotranspiration of crops in large irrigation areas containing diversified crop patterns with different planting dates and agricultural cycles. This serves as a basis to analyze the resulting changes in infrastructure given projected climate change scenarios assuming two possible agricultural adaptation actions. The Santa Rosa Irrigation Users Association is analyzed as a case study, located in "Rio Fuerte" Irrigation District 075, Sinaloa, Mexico. The results indicate an increase of 5% in the design flow capacity of large irrigation areas for the climate change adaptation measures analyzed for the middle of the century with an A1B emissions scenario. Likewise, an increase of 5% in the design capacity will also occur for small irrigation areas with and without adaptation measures. In terms of the annual volume requirement given the same A1B emissions scenario and the adaptation measurements studied, there would be an increase of 8.5%. It is concluded that the methodology developed can be applied to any irrigation district in Mexico to analyze the impact of climate change on irrigation infrastructure.

Keywords: Evapotranspiration, sizing irrigation canals, water requirements, global warming.

Resumen

Iñiguez, M., Ojeda-Bustamante, W., & Díaz-Delgado, C. (septiembre-octubre, 2015). La infraestructura hidroagrícola ante escenarios del cambio climático. Tecnología y Ciencias del Agua, *6(5), 91-103.*

La infraestructura hidroagrícola en grandes sistemas de riego consta de una serie compleja de obras civiles para cumplir con el servicio de riego. Por esta infraestructura se conduce el flujo de agua o gasto del sistema, variable hidráulica necesaria para satisfacer la demanda hídrica de los cultivos. Las proyecciones climáticas de la mayoría de los modelos de circulación general océano-atmósfera indican ambientes más cálidos y secos en la mayor parte de México, con efectos significativos sobre la evapotranspiración de los cultivos, variable agronómica básica en la determinación de la capacidad de la infraestructura hidroagrícola. En este trabajo se presenta el desarrollo de una metodología para evaluar la evapotranspiración integrada de los cultivos, determinada para grandes áreas de riego, con un patrón diversificado de cultivos, con diferentes fechas de siembra y varios ciclos agrícolas, base para analizar los cambios consecuentes sobre la infraestructura en las condiciones proyectadas bajo escenarios de cambio climático y asumiendo dos acciones posibles de adaptación agrícola. Como caso de estudio se analiza la Asociación de Usuarios de Riego Santa Rosa, del Distrito de Riego 075, "Río Fuerte", Sinaloa, México. Los resultados obtenidos indican que para las medidas de adaptación al cambio climático analizadas para mediados de siglo y asumiendo el escenario de emisiones A1B, la capacidad de conducción del gasto de diseño de la infraestructura para grandes áreas de riego podría incrementarse en un 5%. De igual manera, para las pequeñas áreas de riego con o sin medidas de adaptación, el incremento en la capacidad de diseño será también de 5%. Respecto al volumen necesario anual, bajo el mismo escenario de emisiones A1B y de acuerdo con las medidas de adaptación estudiadas, habrá un aumento de 8.5%. Se concluye que la metodología desarrollada puede ser aplicable en cualquier distrito de riego de México para analizar el impacto del cambio climático en la infraestructura de riego.

***Palabras clave**: evapotranspiración, dimensionamiento de canales de riego, requerimientos hídricos, calentamiento global.*

Received: 24/05/2013
Accepted: 20/05/2015

Introduction

In Mexico, irrigation zones are key components in achieving national goals related to food security, job creation and increased incomes and standards of living for producers and residents in rural areas. The hydro-agricultural infrastructure in a region with large-scale irrigation is composed of a number of elements, the most important of which are: a) intake works in storage and diversion dams, b) distribution canal network and c) intakes in the distribution system (canal intakes and the grange intakes that supply agricultural parcels). This infrastructure is designed to meet the maximum water demand based on a presumed cultivation plan, all of which is characterized by the hydraulic variable called flow, or volumetric flow.

Water flows through the infrastructure according to the laws of fluid mechanics and, thus, depends on the hydraulic design of the main and distributary canals. It is established by dimensioning the cross-sections to join the structures in a network, such as inverted siphons, bridges, canals, tunnels, etcetera. Knowledge about the evapotranspiration of the crops in an irrigation region is crucial to the efficient use of resources and to determine the optimal dimensions of a canal network (Spare, Wang, & Hagan, 1980). The methods most commonly used to determine the capacity of a canal are those proposed by Clement (1979) and Clemmens (1987), both of which require the estimation of the evapotranspiration of the crops. The National Water Commission (Conagua, Spanish acronym) has its own method to estimate this agronomical variable which has been used to design canals in Mexico (SRH, 1973). In this procedure, flow is the most important variable for this type of study, in terms of engineering as well as economic feasibility. The country's hydraulic infrastructure is a crucial element in socio-economic stability since it contributes to increasing medium- and long-term agricultural productivity. That is why new technologies continually need to be adapted and adopted as science advances so that new plans can be developed and designs and methodologies adjusted as the technology changes or in light of new patterns in climatic variables that alter the behavior of the hydro-agricultural infrastructure. This will contribute to providing irrigation services in an equitable, timely and efficient manner.

To meet the food demands of a continuously growing population, it will be necessary to continue the historically increasing trend in production and, eventually, double this, as mentioned by Tubiello, Soussana and Howden (2007). Intensification and diversification are the two main trends in agriculture used to drive its development and reduce poverty (Dixon, Gulliver, & Gibbon, 2001). Nevertheless, since agriculture is very sensitivity to climate variability, changes in climate patterns will impact agricultural production systems and can limit development and sustainability in various vulnerable agricultural regions (Ojeda- Bustamante, Martínez, & Hernandez, 2008b).

The global scientific community currently recognizes climate change as an indisputable fact, with direct impacts on agricultural activities, potential effects on agricultural systems produced by increased spatial and temporal variability in temperature and precipitation (Ojeda-Bustamante, Sifuentes-Ibarra, Iñiguez, & Montero, 2011), and more frequent severe events (droughts, torrential rains, heat waves and cyclones) that place abiotic and biotic stress on agricultural systems, among other impacts.

In 2000, the IPCC defined a set of greenhouse gas emissions scenarios, known as SRES scenarios (IPCC, 2000). Four SRES emissions scenarios (A1, A2, B1 and B2) describe the possible ways in the which the global population, changes in land use, new technologies, energy resources and economic and political structures may evolve over the

coming decades (Anandhi, 2007). These future global influences are represented by two dimensions — one represents economic environmental concerns and the other global or regional development models. In addition, the A1 scenario has three scenario markers (A1b, A1F1 and A1T) while the others only have one scenario each. **Scenario A1** represents very rapid growth with increasing globalization, an increase in global wealth, with convergence among regions and reduced regional differences in per capita income. It also presumes materialistic consumption with rapid technological change and low population growth. There are three variations in this scenario corresponding to energy sources: balance across all energy sources (A1N), intensive use of fossil fuels (A1F1) and use of non-fossil fuels (A1T). **Scenario A2** is based on a differentiated world governed by the market with rapid population growth and an economic growth that is less rapid than A1. Underlying themes are trust and preservation of local identities. **Scenario B1** is based on global dematerialization and the introduction of clean technologies. The emphasis is on global solutions to attain economic, social and environmental sustainability. In **Scenario B2**, the population increases at a rate higher than in A1, with development driven by local efforts aimed at social, economic and environmental sustainability. It is important to mention that these emissions scenarios are based on suppositions about future driving forces such as demographic, socioeconomic and technological developments that may or may not occur.

Climate change projections include changes in the thermal and dynamic currents in the atmosphere caused by an increased accumulation in the atmosphere of gasses involved in the greenhouse effect, primarily from anthropogenic activities (Intergovernmental Panel on Climate Change, IPCC, 2007). Thus, projections by Coupled General Circulation Models (CGCM) corresponding to the six emissions scenarios indicate that temperature and carbon dioxide will increase significantly over the current century. CGCM provide the most reliable climate change projections and can be used for hydrological modeling (Park *et al*., 2009). With respect to Mexico, these models project a decrease in precipitation over most of the territory (Montero- Martínez, Lobato-Sánchez, Ojeda-Bustamante, Santana-Sepúlveda, & Prieto, 2013).

Climate change will impact the supply and demand of water used in agriculture (Yano, Aydin, & Haraguchi, 2007). A variety of studies about the impact of climate change on irrigation has been reported over recent years. The impact of changes in climate patterns on the variability of runoff projected for agricultural storage dams was reported by Park *et al*. (2009), who evaluated the operations of a dam reservoir under climate change based on supply, storage volume and agricultural demand on the distribution network (Parisa-Sadat, Bozorg-Haddad, Akbari-Alashti, & Mariño, 2015). Ojeda-Bustamante, Sifuentes- Ibarra, Íñiguez and Montero (2011) reported on the impact of climate change on the development and water requirements of crops without considering adaptation actions. They concluded that the water demand of crops would be reduced 13% during the autumn-winter (AW) cycle and 6% during the spring-summer (SS) cycle, while it would increase 7% for the perennial cycle by the end of the century. Several responses to address climate change have been suggested by Salinger, Sivakumar and Motha (2005), and Olesen *et al*. (2011), the most important of which are changes in crop patterns and in the planting season. Nevertheless, these actions need to be analyzed locally. For Mexico, Ojeda-Bustamante *et al*. (2011) recommend the use of long-cycle crops and a compacted planting season in coldest months. Daccache and Lamaddalena (2010) reported a 20 to 27% increase in the installation costs of irrigation systems to meet future irrigation demands.

With the intensification of environmental variables due to climate change, the use of historical climate information for the design and operations of hydro-agricultural systems may now be questionable (Ojeda *et al.*, 2008b). In terms of designing a hydro-agricultural network, more uncertainty can be expected given changing environmental conditions and crop behavior, as well as measures that producers may possibly implement to adapt to climate change. Therefore, the design of irrigation systems should take into account possible changes in future climate patterns, and given the lack of studies in Mexico it is important to quantify the impact on design variables for the dimensioning of irrigation infrastructure.

The present work is aimed at quantifying the impacts of climate change on hydro-agricultural infrastructure, with the argument of applying possible adaptation actions to crops to modify the irrigation plan for the study region by using long-cycle crops and a compacted planting period in the coldest months by the middle of the century, under emissions scenario A1B.

Materials and Methods

Study Area

The present analysis and modifications to the design and operations of hydro-agricultural infrastructure is based on a case study whose characteristics are typical of agricultural irrigation zones. The study area corresponds to the Santa Rosa irrigation module in Irrigation District 075 (ID-075, Figure 1), located in the Valle de Fuerte, in the northern portion of the state of Sinaloa, Mexico. It has a mean latitude of 25º 50´ and longitude of 109º 5´, with an average elevation of 20 masl.

The land is flat and its soil textures are predominantly clay-loam, with typical values of 50% for clay and 20% for sand, a low organic matter of under 1%, apparent density of 1.2 g cm^{-3} and a available volumetric moisture of 15%. The area is located in an arid region in the northern part of the state of Sinaloa. The rainy period is in September and October and is primarily caused by cyclones. The Santa Rosa Irrigation Module has a physical irrigable area of 34 316 hectares, a crop repetition factor of up to 27% in the spring-summer (SS) cycle during periods with a high availability of water. This size of this module is the largest in ID-075. The distribution of water in the module is scheduled based on the weekly demand and the allocation procedure (delivery-reception) is also based on a weekly irrigation schedule. The federal Conagua department is responsible for the operations of the headworks (storage dam). The Federation of Civil Irrigation Users Associations (ACUR, Spanish acronym), known as SRL is responsible for the main network and each ACUR, which operates an irrigation model, is responsible for the administration, operations and maintenance of the secondary network. According to the classification of distribution methods (Iñiguez, De León, Prado, & Rendón, 2007), the responsibility for the control is shared (user-Conagua). The irrigation frequency is scheduled by each ACUR. The flow delivered to each parcel is

Figure 1. Location of ID-075, state of Sinaloa, Mexico.

limited by the capacity of the grange intake (average capacity of 120 l s^{-1}) and the duration is scheduled by the user and the ACUR. Under these operating conditions, the irrigation model studied presents an overall annual operating efficiency of 51.4%, which reflects the water distribution method used in the ID-075. The users have a period during the week in which to request from ACUR the irrigation flow and duration, which ACUR provides within 72 hours of accepting the request for the irrigation service. The Santa Rosa module's distribution network is supplied by the lateral Emilio Grivel Canal, which begins at km 18+430 of the main Valle del Fuerte Canal. The module's canal network is hydraulically divided into 11 irrigation sections to provide the irrigation service.

The ID-075 has a culture of systematizing agricultural and hydrometric information, with a very complete database containing information from the Santa Rosa module from the past 13 agricultural years. This was generated using *Spriter* (Spanish, acronym), a real-time irrigation forecast system (Ojeda-Bustamante, González- Camacho, Sifuentes-Ibarra, Isidro, & Rendón- Pimentel, 2007).

Climatology of the Study Area

The historical climatology used corresponds to average monthly values for the period 1961 to 1990 from the Los Mochis weather station, located in the center of the irrigation district. This station has the meteorological variables needed to estimate reference evapotranspiration (ET_o), in mm day^{-1}. Since the area is semi-arid, precipitation was not considered by this work since the highest irrigation demand occurs during dry periods.

This work selected greenhouse gas emissions scenario SRES-A1B because it represents an intermediate scenario. A set of 23 coupled general circulation models (CGCM) was used according to the methodology and database by Montero-Martínez *et al*. (2013) to project precipitation and minimum and maximum temperatures. For projections for the middle of the century (2050), the monthly values for the period 2040 to 2060 were averaged to identify monthly anomalies in precipitation and temperature.

Cultivation Plan

The present analysis took into account the typical irrigation plan in the area which includes the crops with planting dates and areas. The main crops in ID-075 are corn, sorghum, beans, fruits, sugar cane, fodder crops (mainly alfalfa) and garden vegetables (tomato and potatoes). In the typical cultivation plan, 11.7% of the area is for perennial crops and 88.3% is for annual crops, of which 80% have an autumn-winter (AW) cycle and 20% are secondary crops during the spring-summer (SS) cycle.

The typical distribution of the established area and the corresponding harvest area for the four main crops in the autumn-winter (AW) cycle was obtained based on the agricultural information about the behavior of the cycles in ID-075's Santa Rosa module over the past 13 years (Conagua, 2014).

The planting period was considered to be early October to late December for corn, late September to mid November for beans, late September to late December for potatoes and early September to late December for tomatoes. The tomato crop did not have one period for the entire established area since this crop has an extended planting period and, therefore, the first harvests occurred when the planting period had not yet ended. For the case of beans, potatoes and corn, the planting ended before the first harvest and there was a period during which the established area of these crops was 100%. The distribution curves were generated for planting and harvesting for the spring-summer (SS) and perennial cycles as well as for the autumn-winter (AW) cycle.

To achieve the objective of the present work and quantify the impacts of climate change on hydro-agricultural infrastructure based on climate change scenarios, a new methodology was used to determine the agronomical variable, that is, the integrated evapotranspiration for large irrigation zones. This methodology is applied to large irrigation districts in Mexico for current conditions and for comparison periods with climate change scenarios. This variable is the basis for the alternative proposal to determine the volumetric flow needed at the beginning of the irrigation canal.

Estimation of Weighted Evapotranspiration ET_{zx} *in an Irrigation Region for Current Conditions*

The information needed to estimate ET includes the historical climatology and the irrigation plan for the area that indicates the crops proposed with dates, planting area and agricultural cycles.

To overcome this limitation the time period can be expressed in development units in terms of "physiological time" instead of chronological time, usually as thermal time. The concept of degree-day (°*D*) comes from this, defined for a specific period as the degrees accumulated over the cardinal temperature interval where the crop is developed. The concept of degree-day-development (°*D*) is one of the most commonly used tools to predict the phenology and development of crops (Ojeda-Bustamante, Sifuentes-Ibarra, & Unland, 2006), compared with other options such as days after planting or percentage of phenological development. Through the temperature, the concept °*D* indirectly integrates the calorific energy accumulated during the different phenological development stages of the crops. The daily estimation of °D requires knowledge about the daily mean air temperature (*Ta*) based on the following equations (Ojeda-Bustamante *et al*., 2006):

$$\begin{aligned} {}^{o}D &= T_a - T_{c\text{-min}}, \quad T_a \langle T_{c\text{-max}} \\ {}^{o}D &= T_{c\text{-max}} - T_{c\text{-min}}, \quad T_a \geq T_{c\text{-max}} \\ {}^{o}D &= 0, \quad T_a \leq T_{c\text{-min}} \end{aligned} \tag{1}$$

Where $T_{c\text{-min}}$ is the minimum air temperature and $T_{c\text{-max}}$ the maximum within which a crop develops, and varies for each crop depending on the study area. The crop coefficients can be expressed as a function of accumulated degree-days according to the equations proposed by Ojeda-Bustamante *et al*. (2006). The estimate of ET_{zr} is performed with four steps.

Step 1

Reference evapotranspiration is estimated and evapotranspiration (ET_c) is obtained for each crop and planting date (Allen, Pereira, Raes, & Smith, 2006; Ojeda-Bustamante, Hernandez, & Sánchez, 2008a). The concept of the accumulation of degree-day-development (°*D*) is used as an alternate criterion to express the number of days in the phenological cycle of the crops and thereby estimate the crop coefficient using the equations by Ojeda-Bustamante *et al.* (2006). In this case, an ET_c curve is identified for each one of the various planting dates that make up the planting period in the irrigation zone. Daily $ET_{c\text{-}i}$ values are obtained using equation (1) and the parameters of the crops are used to estimate the crop coefficient as a function of the °D. Evapotranspiration of a crop from the planting date (PD) to the harvest date (HS) is given by equation (2):

$$ET_{c-i} = \sum_{i=PD}^{HD} K_{c-i} ET_{o-i} \tag{2}$$

Where $K_{c\text{-}i}$ and $ET_{o\text{-}i}$ are the crop coefficient and reference evapotranspiration on day *i*, respectively. Equation (1) is repeated for each crop in each cycle (perennial, autumn-

winter (AW) and spring-summer (SS)). After determining daily and maximum daily $ET_{c\text{-}i}$, the daily established area and maximum daily and accumulated volumes are determined for each crop and planting date.

Step 2

A unique evapotranspiration curve is generated for each crop according to the different planting dates. The $ET_{c\text{-}i}$ curves of the crops are weighted based on the planted area per planting date (PD) and the weighted potential evapotranspiration of the crop (ET_{1c}) is obtained, which contains the daily $ET_{c\text{-}i}$ values of the crop for the planting dates in an agricultural cycle. The evapotranspiration of a crop (ET_{1c}) on a given day i is determined by the evapotranspiration contributions from a planting date j estimated for day i, weighted by the planted area according to $f_{c\text{-}j}$. This value is determined with equation (3):

$$ET_{1c-i} = \sum_{j=1}^{NP} f_{c-i,j}\, ET_{c-i,j} \qquad (3)$$

Where j defines the crop for the given planting date j; that is, a number of plantings (NP) are involved for the crop being analyzed; i is the day in the development period of the crop analyzed which covers the day of the first planting (FP) to the day of the last harvest (LH) for the NP of the crops. NP is the total number of plantings of the crop analyzed; $f_{c\text{-}i,j}$ is the weight factor for the planted area with respect to the total for the planting date j, given by equation (4):

$$f_{c-i,j} = \frac{S_{c-i,j}}{S_{t(1c)-i}} \qquad (4)$$

$S_{c\text{-}i,j}$ is the established area of the crop analyzed for planting date j. $S_{t(1c)\text{-}i}$ is the sum of the established areas of the crop analyzed for the different planting dates on day i, where $S_{t(1c)-i} = \sum_{j=1}^{NP} S_{c-i,j}$. After determining the daily $ET_{1c\text{-}1}$, and based on the calculations, the values of the daily established area are determined, with the respective volume.

Step 3

The evapotranspiration per agricultural cycle (SS, AW and perennial) is included, which is based on the area of each crop in the region's irrigation plan. For example, on day i, the integrated evapotranspiration of the crops in the autumn-winter (AW) cycle can be estimated with equation (5):

$$ET_{\text{cycle}-i} = \sum_{k=1}^{NC} f_{i,k} ET_{1C-i,k} \qquad (5)$$

Where $k = 1$ to n_k; NC is the number of crops to be grown in each cycle (AW, SS and perennial); i is defined for the day and k for the crop; $f_{i,k}$ is the weighting factor of the crop i for a given cycle, according to the equation:

$$f_{i,k} = \frac{S_{c-i,k}}{S_{t-i}} \qquad (6)$$

$S_{c\text{-}i}$ is the established area of the crop k on day i in the cycle analyzed; $S_{t\text{-}i}$ is the total area on day i, $S_{t-i} = \sum_{k=1}^{NC} S_{c-k}$. Finally, the value of the integrated evapotranspiration for the cycle analyzed is obtained. The established area and daily volume are determined with the value of $ET_{cycle\text{-}i}$.

Step 4

Lastly, an overall integrated daily curve of the cycles is obtained based on which the weighted evapotranspiration of an irrigation zone (ET_{zr}) is found. The value of ET_{zr} on a day i is the sum of the $ET_{cycle\text{-}i}$ of each cycle. If there are three agricultural cycles ($N_{ac} = 3$):

$$ET_{zr-i} = \sum_{r=1}^{N_{ac}=3} f_{zr-i,r} ET_{\text{cycles}-i,r} \quad (7)$$

Where N_{ac} is the number of cycles (AW, SS, perennial) to be analyzed in the present analysis on day *i*; $f_{rz-i,r}$ is the weighting factor for cycle *r* on day *i* according to the following equation:

$$f_{zr-i,r} = \frac{S_{i,r}}{S_{zr-i}} \quad (8)$$

S_{ir} is the established area in cycle *r* for day *i*; S_{zr-i} is the total established area in the agricultural year analyzed for day *i* $S_{zr-i} = \sum_{r=1}^{N_{ac}} S_{i,r}$. N_{ac} is the number of cycles in the agricultural year. At the end of this step a daily integrated ET_{zr-i} value is obtained for the evapotranspiration in an irrigation zone and the established area and daily volume are determined.

The maximum ET_{zr} value of the general integrated curve is taken as the value of the weighted evapotranspiration of the irrigation zone. The daily ET_{zr} is related to the established daily area and the daily volume required by the system.

Equation (9) shows the relationship between global efficiency and evapotranspiration, which are variables used to determine the volumetric flow needed at the beginning of the irrigation canal section:

$$Q_d = 115.74 \frac{(ET_{zr} * area)}{E_g} \quad (9)$$

Where Q_d is the design flow (1 s^{-1}); ET_{zr} is the weighted evapotranspiration (m day^{-1}), E_g is the global efficiency of the design; 115.74 is the transformation coefficient to 1 s^{-1} ha^{-1}, area in hectares. Since the areas are large, the irrigation service is assumed to operate 24 hours per day.

For the purpose of design and the conduction capacity of the canal, the conduction and application efficiency values reported by SRH (1973) were used. The global efficiency, η, for the design is determined by multiplying the conduction and application efficiencies, $\eta_{conduction}$ x $\eta_{application}$. As an example, a global efficiency of η = 49% has been reported for earthen canals. It is worth mentioning that the actual application efficiency varies depending on the technology applied and can potentially reach η = 90%. The application efficiency of a parcel reported by SRH (1973) is considered to be η = 70% for technified gravity irrigation.

Estimation of Weighted Evapotranspiration in an Irrigation Zone (ET_{zr})

For climate change scenarios, the recommendations by Ojeda- Bustamante *et al*. (2011) for Mexico were considered, that is, the use of long-cycle crops and a compacted planting period in the coldest months. The information needed to estimate *ET* includes: climatology for the middle of the century under scenario A1B; irrigation plan for the area with the same crops proposed but having a long cycle, with planting dates and compacted surfaces, with the same areas in the agricultural cycles. The procedure to estimate ET_{zr} is the same as for current conditions.

Because of the large number of calculations involved, algorithms to estimate the evapotranspiration of crops in an irrigation zone according to the proposed methodology were programmed in Java programming language. Given that precipitation in the irrigation districts in Mexico during the highest demand period is virtually null, this work assumes that evapotranspiration is equivalent to the irrigation requirements of the crops. For the case in which precipitation during the highest demand period is important, this should be subtracted from daily evapotranspiration.

Results and Discussion

Estimation of Weighted Evapotranspiration in an Irrigation Zone (ET_{zx}) for Current Conditions

Figure 2 shows the ET_c curve for the corn crop with planting date December 16, 2004 (planting number 8) in the autumn-winter (AW) cycle, resulting from the application of equation (1), the basis of the methodology. The maximum ET_c value is 6.2 mm day^{-1}. The established area for this planting date was considered to be 1 135.5 ha and the maximum volume demanded was 70 719.6 m³ día-1. These values are for Julian Day 113, corresponding to April 22, 2005.

Figure 3 shows an example of a unique ET_{c1} curve —hectares of the corn crop for the autumn-winter (AW) cycle. It includes the evapotranspiration corresponding to the different planting dates and weights them based on the planted area per planting date, as indicated by equation (2). The maximum volume required by corn in the autumn-winter (AW) cycle of the agricultural year in the Santa Rosa module in ID-075 are presented for Julian Day 99, corresponding to April 9, 2005. The maximum volume is 557 134.56 m³ day^{-1}, the ET_{c1} is 5.3 mm day^{-1} and the area is 10 383.36 hectares.

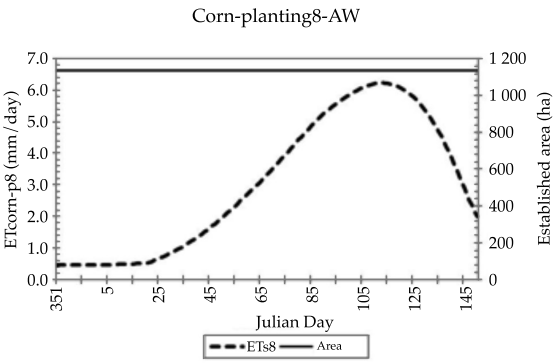

Figure 2. Relation of ET_c -hectares one planting.

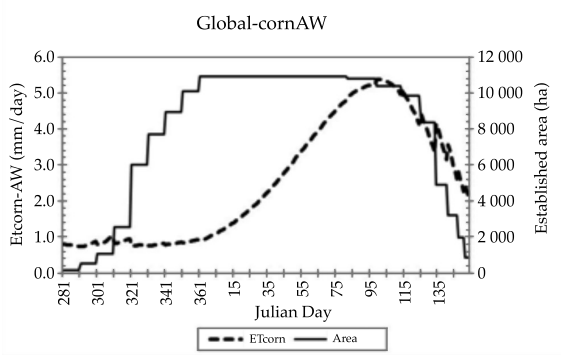

Figure 3. ET_{c1}-hectares (corn) curve.

For the next step in the methodology, evapotranspiration per agricultural cycle is integrated, taking into account the area per crop in the SS, AW and perennial cycle, as indicated by equation (4). Figure 4 (corresponding to step 3) shows the integrated $ET_{1c\text{-}i}$ curve for the AW cycle. The values that stand out in the AW cycle are the required volume for Julian Day 87, on March 28, 2005, with a maximum demand of 672 200.7 m³ day^{-1}; $ET_{1c\text{-}i}$ = 4.9 mm day^{-1} and area of 13 710.8 hectares.

The final stage of the proposal is to obtain the integrated general curve of the three cycles (SS, AW and perennial) for the study year

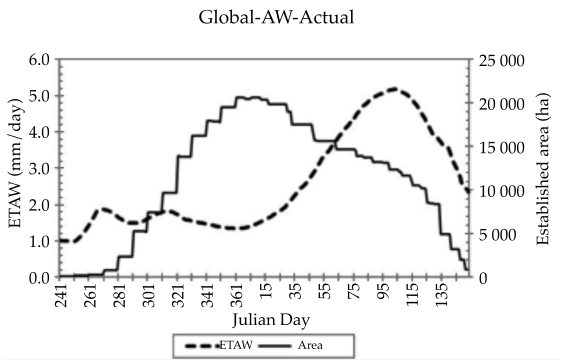

Figure 4. $ET_{ciclo\text{-}OI}$-hectares curve.

and find the weighted evapotranspiration in the irrigation zone (equations (7) and (8)). The peak value occurred on Julian Day 105, on April 15, 2005, day 231, with a maximum volume of 918 487.63 m³ day^{-1}; ET_{zr} = 4.08 mm day^{-1} and an area of 22 517.93 ha. The results for the entire year are shown in Figure 5.

The volumetric flow is determined with equation (9), the flow required of the network. Since the areas are large the irrigation service is assumed to operate 24 hours per day. The global efficiencies used correspond to those recommended by SRH (1973). Given the established area of 22 517.93 ha, global efficiency η = 0.49 and ET_{zr} = 4.08 mm day^{-1}, a volumetric flow of 21.70 m³ sec^{-1} was determined. When multiplying the established area per day and the ET_{zr} day, considering a global efficiency of 100%, the curve that integrates the daily volume required over the entire year is obtained. Figure 6 shows the volume required or demanded, with a maximum volume of 918 487.63 m³ day^{-1}.

Estimation of the Weighted Evapotranspiration in an Irrigation Zone (ET_{zx})

For a second option under conditions corresponding to climate change scenarios, the procedure to estimate *ET* is the same as for actual conditions. The proposal analyzed corresponds to an adaptation strategy that compacts the planting dates and uses long-cycle crops. It is defined with modifications of the zone's irrigation plan, which includes the crops proposed with dates, planted areas and agricultural cycles.

Only the result from Step 4 is shown, which represents the weighted estimations. The general integrated curve is obtained for the three cycles in the agricultural year (SS, AW and perennial) and the weighted evapotranspiration of an irrigation zone is found, as shown in Figure 7.

The final result in the proposal consisted of obtaining the weighted evapotranspiration in an irrigation zone. Equations (7) and (8) result in an ET_{zr} of 4.1 mm día^{-1} and an area of 23 419 ha. When multiplying from day to day the area by the ET_{zr}, and with a global efficiency of 100% (data from Figure 7), the curve that integrates the daily volume demanded over the year is obtained, which has a peak value on Julian Day 96 (June 6, 2051), with a maximum volume of 961 740.67 m³ día^{-1}. For the obtained area of 23 419 ha, global efficiency of η = 0.49 and ET_{zr} = 4.1 mm día^{-1}, a volumetric flow of 22.72 m³ sec^{-1} is obtained with equation (9).

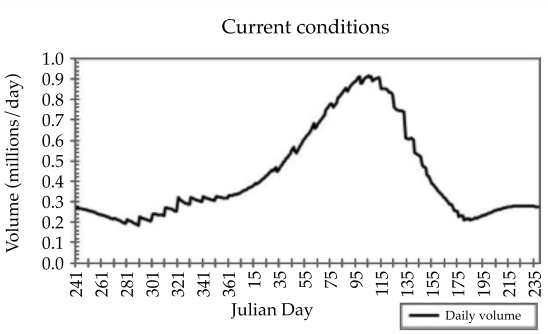

Figure 6. Volume demanded-day.

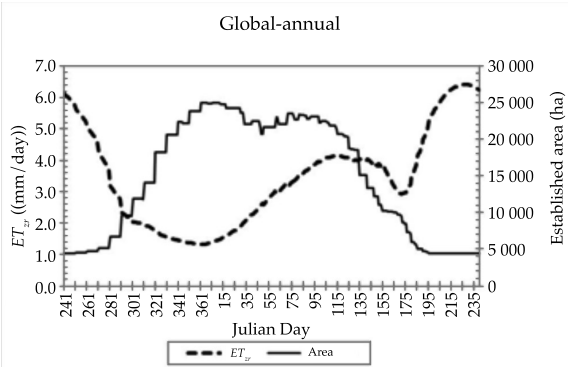

Figure 5. ET_{zr}- hectares curve.

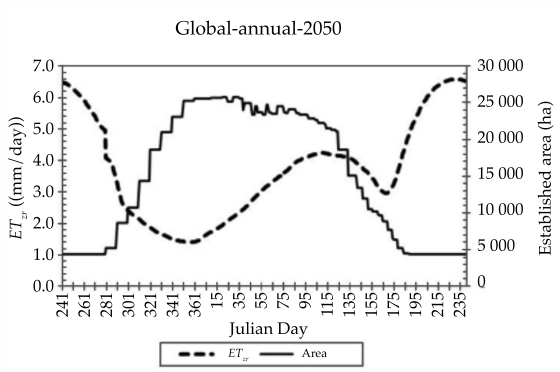

Figura 7. Figure 7. Variation in the ET_{zr} -daily area, for the year 2050.

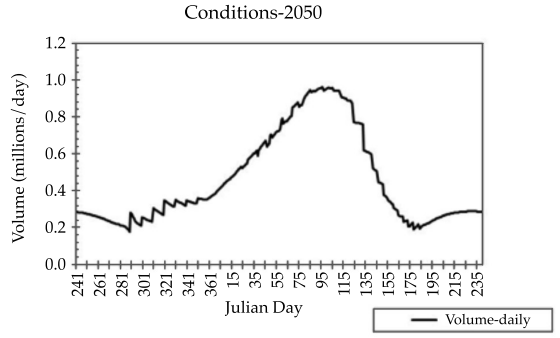

Figure 8. Volumes daily for the year 2050.

Conclusive Consequences

The results obtained for the actual conditions and future conditions under the climate change scenario in terms of the variation in percentages of maximum daily volumetric flow required indicate an increase of 5.08%. This represents an increased flow at the beginning of the network from 21.70 $m^3 sec^{-1}$ to 22.72 m^3 sec^{-1},that is, an increase of 1.03 m^3 sec^{-1} to be transported by the hydraulic infrastructure for the conditions presented. The total annual volume needed would increase 8.2% for the conditions in ID-074, Rio Fuerte, Sinaloa Mexico, from a volume of 154 544 085 m^3 to 167 117 884 m^3; that is, an additional volume of 12.58 million m^3 needed at the beginning of the agricultural cycle.

For the case of the sections at the end of the branches or the end of the irrigation network, the capacity of the canal is designed to supply the maximum volumetric flow required by small areas, according to SRH (1973). That is, for areas less than 1 000 ha (the maximum demand for the design capacity of the canal) a monocrop needs to be considered and its ET_{c-i} should be the highest in the irrigation plan. For the case study, perennial crops had the highest ET_{c-i} . Table 1 shows the results from the perennial crops in the irrigation plan based on the application of equation (2), for the current period and the climate change scenario for 2050.

It is important to note that no adaptations to climate change are recommended for perennial crops. In the case of alfalfa, because they are perennial, the percentage increase in ET_{c-i} is 5.03%, which used a reference to calculate flow and volume.

The irrigation zones are designed with historical information from the region related to crop patterns, historical climatology, maximum water requirements and the soil moisture regime. The results from this study indicate that the design dimension of the infrastructure could be increased in given changes in climate patterns and possible adaptation actions. Nevertheless, the above analysis was performed based on scenario A1B and without future modifications in the cultivation plan. The increase in the design capacity of canals may be different than that estimated by the present work depending on the emissions scenario used and the producers' future application of climate change adaptations not analyzed in this work (which were not the subject of the present study), such as conversion of crops, technification of parcel irrigation, resurfacing or enclosing canals, among others. Therefore, the possible consequences of climate change on the

Table 1. Results from perennial crops in irrigation district 075 for current conditions and for the year 2050.

Scenarios	Current				Scenario 2050				Difference 2050-2000
Crop	Julian Day	ET_{c-i} (mm/d)	Surface (Ha)	Volume (m^3/day)	Julian Day	ET_{c-i} (mm/d)	Surface (Ha)	Volume (m^3/day)	%
Alfalfa	144	6.707	500	33 535	156	7.064	500	35 320	1.053
Mango	149	6.405	300	19 215	156	6.435	300	19 305	1.005
Sugar Cane	226	6.585	1 000	65 850	231	6.779	1 000	67 790	1.029

demand of crops needs to be analyzed so that the conduction capacity of the current infrastructure will meet new irrigation requirements created by the response by agricultural producers and climate patterns.

Conclusions

As climate change intensifies, the use of historical climate information to design and operate irrigation systems may be questionable. Nevertheless, it is difficult to estimate the impact of climate change on agricultural systems because of the difficulties involved in predicting future climate scenarios and the future actions adopted by producers or promoted by governments. Based on the results, it is concluded that the design flow capacity of irrigation infrastructure should take into account three factors when designing hydro-agricultural infrastructure for climate change scenarios:

a) For the end of the canal branches or the end of networks, the capacity of the canal with and without adaptation conditions will be affected with only 5% of the flow conduction capacity.
b) To supply larger areas, the beginning of the section or the entire canal, with adaptation conditions, will be affected with 5% or more of the design flow capacity.
c) The annual volume used under the same cultivation plan with adaptation conditions will be affected with an increase of 8.5%.

References

Allen, G. R., Pereira, L., Raes, D., & Smith, M. (2006). *Estudio FAO Riego y drenaje 56. Evapotranspiración del cultivo: Guías para la determinación de los requerimientos de agua de los cultivos* (298 pp.). Serie cuadernos técnicos. Roma: FAO.

Anandhi, A. (2007). *Impact Assessment of Climate Change on Hydrometeorology of Indian River Basin for IPCC SRES Scenarios*. Ph.D. Dissertation. Bangalore, India: Indian Institute of Science.

Clement, R. (1979). *Computation of flow in Irrigation Systems Operating 'On Demand'*. Traducción al inglés del US Bureau of Reclamation. Le Tholonet: La Société du canal de Provence et d'Aménagement de la Region Provencale (December, 13, 1965).

Clemmens, A. J. (1987). *Delivery System Schedules and Required Capacities, Planning, Operation, Rehabilitation and Automation of Irrigation Water Delivery Systems*. Symposium Procedings, ASCE, New York.

Conagua (2014). *Estadística histórica de producción agrícola de los Distritos de Riego*. México, DF: Comisión Nacional de Agua, Gerencia de Distritos de Riego.

Daccache, A., & Lamaddalena, N. (2010). Climate Change Impacts on Pressurized Irrigation Systems. *Proceeding of the Institution of Civil Engineers-Engineering Sustainability, 163*, 97-105.

Dixon, J., Gulliver, A., & Gibbon, D. (2001). *Farming Systems and Poverty* (412 pp.) Rome/Washington, DC: FAO/World Bank.

Iñiguez, C. M., De León, M. B., Prado, H. J. V., & Rendón, P. L. Ingeniería Hidráulica en México, (2007). Análisis y comparación de tres métodos para determinar la capacidad de conducción de canales, aplicados en el distrito de riego La Begoña. *Ingeniería Hidráulica en México*, 22(2), 81-90.

IPCC (2000). *Emission Scenarios. A Special Report of Working Group III of the Intergovernmental Panel on Climate Change*. In N. Nakićenović & R. Swart (Eds.). Cambridge: Cambridge University Press. Recuperado de http://www.ipcc.ch/ipccreports/sres/emission.

IPCC (2007). *Cambio climático 2007: Informe de síntesis. Contribución de los grupos de trabajo I, II y III al Cuarto Informe de Evaluación del Grupo Intergubernamental de Expertos sobre el Cambio Climático* (104 pp.). Equipo de redacción principal: R. K. Pachauri, & A. Reisinger, directores de la publicación. Ginebra: Intergovernmental Panel on Climate Change.

Montero-Martínez, J. M., Lobato-Sánchez, R., Ojeda-Bustamante, W., Santana-Sepúlveda, J. S., & Prieto, R. (2013). Sistema de consulta de proyecciones regionalizadas de cambio climático para México. *Tecnología y Ciencias del Agua*, *4*(2),113-128.

Ojeda-Bustamante, W., Sifuentes-Ibarra, E., & Unland, H. (2006). Programación integral del riego en maíz. *Agrociencia*, *40*, 13-25.

Ojeda-Bustamante, W., González-Camacho, J. M., Sifuentes-Ibarra, E., Isidro, E., & Rendón-Pimentel, L. (2007). Using Spatial Information Systems to Improve Water Management in Mexico. *Agricultural Water Management*, *89*, 81-88

Ojeda-Bustamante, W., Hernández, L., & Sánchez, I. (2008a). *Requerimientos de riego de los cultivos. Manual para diseño de zonas de riego pequeñas* (pp. 1-49). Jiutepec, México: Instituto Mexicano de Tecnología del Agua.

Ojeda-Bustamante, W., Martínez, P., & Hernandez, L. (2008b). Repercusiones del cambio climático en la agricultura de riego. Capítulo 6 (pp. 73-83). En A. Aguilar & P. Martínez (Eds). *Efectos del cambio climático en los recursos hídricos de México*. Vol. II. Jiutepec, México: Instituto Mexicano de Tecnología del Agua.

Ojeda-Bustamante, W., Sifuentes-Ibarra, E., Íñiguez, M., & Montero, J. M. (2011). Impacto del cambio climático en el desarrollo y requerimientos hídricos de los cultivos. *Agrociencia*, *45*, 1-21.

Olesen, J. E., Trnka, M., Kersebaum, K. C., Skjelvag, A. O., Seguin, B., Peltonen-Sainio, P., Rossi, F., Kozyra, J., & Micale, F. (2011). Impacts and Adaptation of European Crop Production Systems to Climate Change. *Eur. J. Agron.*, *34*, 96-112.

Park, G. A., Ahn, S. R., Lee, Y. J., Shin, H. J., Park, M. J., & Kim, S. J. (2009). Assessment of Climate Change Impact on the Inflow and Outflow of Two Agricultural Reservoirs in Korea. *Transactions of the ASABE*, *52*(6), 1869-1883.

Parisa-Sadat, A., Bozorg-Haddad, O., Akbari-Alashti, H., & Mariño, M. A. (April, 2015). Determination of Irrigation Allocation Policy under Climate Change by Genetic Programming. *Journal of Irrigation and Drainage Engineering*, *141*(4), 04014059.

Salinger, M. J., Sivakumar, M. V. K., & Motha, R. (2005). Reducing Vulnerability of Agriculture and Forestry to Climate Variability and Change: Workshop Summary and Recommendations. *Climatic Change*, *70*, 341-362.

SRH (1973). *Proyecto de Zonas de Riego*. México, DF: Secretaría de Recursos Hidráulicos, Dirección de Proyectos de Grande Irrigación, Departamento de Canales.

Spare, D. P., Wang, J., & Hagan, E. (1980). Sizing Rice Irrigation Canals. *Transaction of the ASAE*, *23*(4), 914-918.

Tubiello, F. N., Soussana, J.-F., & Howden, S. M. (2007). Crop and Pasture Response to Climate Change. *Proc. Nat. Acad. Sci.*, *104*(50), 19686-19690.

Yano, T., Aydin, M., & Haraguchi, T. (2007). Impact of Climate Change on Irrigation Demand and Crop Growth in a Mediterranean Environment of Turkey. *Sensors-Basel*, *7*, 2297-2315.

Institutional Address of the Authors

Dr. Mauro Iñiguez
Dr. Waldo Ojeda-Bustamante

Instituto Mexicano de Tecnología del Agua
Paseo Cuauhnáhuac 8535, Colonia Progreso
62550 Jiutepec, Morelos, México
Teléfono: +52 (777) 3293 600
mic@tlaloc.imta.mx
wojeda@tlaloc.imta.mx,

Dr. Carlos Díaz-Delgado

Centro Interamericano de Recursos del agua (CIRA)
Facultad de Ingeniería
Universidad Autónoma del Estado de México
Cerro de Coatepec s/n, ciudad Universitaria
50130 Toluca, Estado de México, México
cdiazd@uaemex.mx

Xelaju River Basin at the beginning of the rainy seasons, Chiapas, Mexico.

Photo: Neptalí Ramírez Marcial.

Border Irrigation Design with the Saint-Venant and Green & Ampt Equations

• Heber Saucedo* •
Instituto Mexicano de Tecnología del Agua
*Corresponding Author

• Manuel Zavala •
Universidad Autónoma de Zacatecas

• Carlos Fuentes •
Instituto Mexicano de Tecnología del Agua

Abstract

Saucedo, H., Zavala, M., & Fuentes, C. (September-October, 2015). Border Irrigation Design with the Saint-Venant and Green & Ampt Equations. *Water Technology and Sciences* (in Spanish), 6(5), 105-114.

A design procedure for border irrigation is presented. The procedure is based on the use of Saint-Venant equations to describe water flow over the soil and the Green and Ampt equation to model water flow in the soil. The main advantage of the model presented is that its application requires very little computation time compared to a full hydrodynamic model using Saint- Venant equations to describe water flow over soil, internally coupled with the Richards equation to model water flow in the soil. The results obtained from applying the model to 10 types of different soils were used to generate operating design tables for border irrigation.

Keywords: Border irrigations, Saint-Venant equations, Green & Ampt equation, optimal flow.

Resumen

Saucedo, H., Zavala, M., & Fuentes, C. (septiembre-octubre, 2015). Diseño de riego por melgas empleando las ecuaciones de Saint-Venant, y Green y Ampt. Tecnología y Ciencias del Agua, *6(5), 105-114.*

Se presenta un método de diseño de riego por melgas basado en la aplicación de un modelo que emplea las ecuaciones de Saint-Venant para describir el flujo del agua sobre el suelo, y la ecuación de Green y Ampt para representar el flujo del agua en el suelo. La principal ventaja del modelo presentado es el poco tiempo de cómputo que requiere para su aplicación, en comparación con el necesario para ejecutar un modelo hidrodinámico completo reportado en la literatura, mismo que emplea las ecuaciones de Saint-Venant para el flujo del agua sobre el suelo, acopladas internamente con la ecuación de Richards, que permite modelar el flujo del agua en el suelo. Con base en los resultados obtenidos mediante la aplicación del modelo para diez tipos de suelo diferentes se han elaborado cuadros de diseño operativo del riego por melgas.

***Palabras clave**: riego por melgas, ecuaciones de Saint-Venant, ecuación de Green y Ampt, gasto óptimo.*

Received: 14/02/2015
Accepted: 11/05/2015

Introduction

The objective of designing border irrigation is to apply the most uniform application depth needed by a crop while maintaining a high application efficiency. The design of irrigation consists of determining the application flow rate and length of time needed to apply that flow at the head of the border to achieve the highest uniformity possible, that is, to determine the optimal flow rate given the border length and the hydrodynamics of the specific soil.

Rendón, Fuentes and Magaña (1997) reported that the optimal design flow rate is linearly proportional to the length of the border to be irrigated. The result is obtained using a model generated with equations by Lewis and Milne (1938) to describe the flow of water over the surface of soil, and Green and Ampt (1911) to describe the flow of water in soil. It is important to note that the use of the Lewis and Milne (1938) equations is the most simplified way to model the flow of water on a free surface in border irrigation.

The objective of the present study was to develop a model in which a precise method is used to model the flow of water on a free surface, and therefore based on Saint-Venant equations. Meanwhile, the Green and Ampt equation is used to describe the flow of water in the soil, which is a simple way to model this flow, maintaining the physical-mathematical bases in its representation.

Flow of Water Over the Soil Surface

The flow of water over a free surface is modeled with Saint-Venant equations which result from applying the laws of conservation of mass and momentum. In a border, the relationship between its width and the water depth permits using equations for runoff over an infinitely wide surface (Woolhiser, 1975). The continuity equation is written as:

$$\frac{\partial h}{\partial t}+\frac{\partial q}{\partial x}+\frac{\partial I}{\partial t}=0 \qquad (1)$$

The momentum equation is written in the form recommended by Saucedo, Fuentes and Zavala (2005):

$$\frac{1}{h}\frac{\partial q}{\partial t}+\frac{2q}{h^2}\frac{\partial q}{\partial x}+\left(g-\frac{q^2}{h^3}\right)\frac{\partial h}{\partial x}$$

$$+g(J-J_o)+\beta\frac{q}{h^2}\frac{\partial I}{\partial t}=0 \qquad (2)$$

where $q(x,t) = U(x,t)h(x,t)$ is the volumetric flow rate per unit width of the border [L^2T^{-1}]; x is the spatial coordinate in the main direction of the movement of water in the border [L]; t is time [T]; U is the mean velocity; h is the water depth [L]; J_o the topographic slope of the border [LL^{-1}]; J the friction slope [LL^{-1}]; $V_1 = \partial I/\partial t$ the infiltration flow [LL^{-1}], that is the volume of infiltrated water per unit of time, unit border width and unit border length; I is the infiltrated water depth [L]; g gravitational acceleration [LL^{-2}]; $\beta = U_{lx}/U$, where U_{lx} is the projection in the direction of the movement of the exit velocity of the water mass due to infiltration.

The relationship between the hydraulic variables q and h with the friction slope, called the law of hydraulic resistance, is adopted according to Fuentes, De León, Saucedo, Parlange and Antonino (2004), using a law of potential resistance:

$$q=k\nu\left(\frac{h^3gJ}{\nu^2}\right)^d \qquad (3)$$

where v is the kinematic viscosity coefficient of the water [L^2T^{-1}] and k is a dimensionless factor; d is a dimensionless parameter which ranges from $1/2 \le d \le 1$ according to the type of flow; the extreme values $d = 1/2$ and $d = 1$ correspond to Chezy and Poiseuille laminar flow regimes, respectively.

To establish the initial and boundary conditions for the Saint-Venant equations used to model border irrigation, a closed border is considered to prevent a loss of mass outside the irrigation area. For the advance stage, we have:

$$q(x,0)=0 \quad \text{and} \quad h(x,0)=0 \qquad (4)$$

$$q(0,t)=q_o, \quad q(x_f,t)=0 \quad \text{and} \quad h(x_f,t)=0 \qquad (5)$$

where $x_f(t)$ is the position of the water front during time t and q_o is the application flow

rate at the head of the border. For the storage stage:

$$q(0,t) = q_o, \qquad q(L,t) = 0 \tag{6}$$

where L is the length of the border and q_o is the flow rate applied at the head of the border. For the depletion phase:

$$q(0,t) = 0, \qquad q(L,t) = 0 \tag{7}$$

To close the system, the way in which the infiltrated water depth evolves over time needs to be known at every position on the border, that is, the law of infiltration.

Water Flow in the Soil

The Green and Ampt model (1911) is established based on the continuity equation and the Darcy Law, according to the following hypotheses: a) the initial moisture profile in a soil column is uniform, $\theta=\theta_o$; b) the water pressure on the soil surface is hydrostatic; $\psi = h \geq 0$, where h is the water depth; c) the wetting front is well defined, characterized by a negative pressure $\psi = -h_f < 0$ where h_f is the wetting front suction; and d) the region between the soil surface and the wetting front is completely saturated (piston flow), $\theta=\theta_s$ and $K = K_s$, where K_s is the hydraulic conductivity at saturation, that is, the value of the hydraulic conductivity of the Darcy Law corresponding to the volumetric water content at saturation. The resulting ordinary differential equation is:

$$V_I = \frac{dI}{dt} = K_s\left[1 + \frac{(h_f + h)\Delta\theta}{I}\right] \tag{8}$$

where $\Delta\theta=\theta_s - \theta_o$ is the storage capacity; I is the accumulated infiltrated volume per unit of soil surface, or infiltrated water depth.

Numerical Solution

To calculate the optimal volumetric flow, a numerical model developed by Saucedo, Zavala and Fuentes (2011) is used for the four stages in border irrigation. Figure 1 shows the layout of the calculation cells for the advance, wetting or ponding, depletion and recession stages. The discrete form of the continuity equation for the advance stage is written as:

$$\begin{aligned}
&\left[\omega q_\ell + (1-\omega)q_j\right]\delta t - (x_\ell - x_j)\begin{bmatrix}\omega(h_\ell + I_\ell)\\ +(1-\omega)(h_j + I_j)\end{bmatrix}\\
&-\left[\omega q_r + (1-\omega)q_m\right]\delta t + (x_r - x_m)\begin{bmatrix}\omega(h_r + I_r)\\ +(1-\omega)(h_m + I_m)\end{bmatrix}\\
&-\left[\phi h_\ell + (1-\phi)h_r + \phi I_\ell + (1-\phi)I_r\right](x_r - x_\ell)\\
&+\left[\phi h_j + (1-\phi)h_m + \phi I_j + (1-\phi)I_m\right](x_m - x_j) = 0
\end{aligned} \tag{9}$$

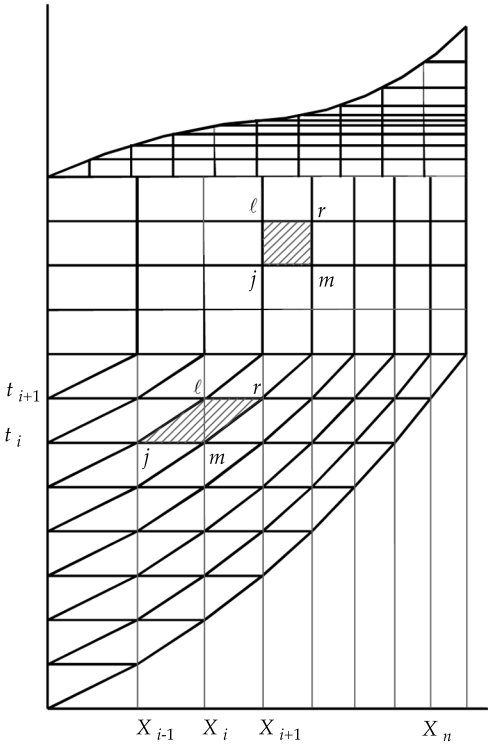

Figure 1. Layout of the calculation cells for the advance, wetting or ponding, depletion and recession phases.

For the wetting, depletion and recession stages:

$$\left[\omega q_\ell + (1-\omega) q_j\right]\delta t - \left[\omega q_r + (1-\omega) q_m\right]\delta t$$
$$-\left[\phi h_\ell + (1-\phi) h_r + \phi I_\ell + (1-\phi) I_r\right](x_r - x_l)$$
$$+\left[\phi h_j + (1-\phi) h_m + \phi I_j + (1-\phi) I_m\right](x_m - x_j) = 0 \quad (10)$$

The momentum equation has the same discrete form for all four irrigation stages:

$$2\bar{q}\bar{h}(q_r - q_\ell)\delta t + \left(g\bar{h}^3 - \bar{q}^2\right)(h_r - h_\ell)\delta t$$
$$+\bar{h}^2(x_r - x_\ell)\left[\omega q_r + (1-\omega) q_\ell - \omega q_m - (1-\omega) q_j\right] \quad (11)$$
$$+g\,\delta t\,\bar{h}^3(x_r - x_\ell)\left[\omega J_r + (1-\omega) J_\ell - J_o\right]$$
$$+\beta\,\delta t\,\bar{q}\bar{h}(x_r - x_\ell)\left[\omega I_r + (1-\omega) I_\ell - \omega I_m - (1-\omega) I_j\right] = 0$$

In equations (9) through (11), δt is the time step, ω and ϕ are weight factors in space and time and the other variables are defined according to Figure 1. The coefficients are calculated based on the values belonging to the previous time level: $\bar{q} = (1-\phi) q_m + \phi q_j$, $\bar{h} = (1-\phi) h_m + \phi h_j$ (Saucedo *et al.*, 2005). The small variables are introduced (Strelkoff & Katopodes, 1977): δh_r, δq_r, δh_ℓ and δq_ℓ, such that for the interior cells we have $h_\ell = h_j + \delta h_\ell$, $h_r = h_m + \delta h_r$, $q_\ell = q_j + \delta q_\ell$ y $q_r = q_m + \delta q_r$. These are substituted in the discrete continuity and momentum equations, and a system of algebraic equations is obtained whose solution enables advancing the values of the hydraulic variables over time. The detail of the inputs for the matrix system can be consulted in Saucedo *et al*. (2011).

The Green and Ampt equation (8) is numerically solved using a finite differential method. The procedure is well documented in the literature and can be consulted in Burden and Faires (1985), for example.

A constant time step of $\Delta t = 1.0$ s was used to couple the Saint-Venant and Green and Ampt equations. The discretization used to solve the complete Saint-Venant equations is based on those reported in the literature by Katopodes and Strelkoff (1977): $\Delta t_{min} = 5$ s; Akanbi and Katopodes (1988): $257 t_{max} = 1$ s; Playán, Walker and Merkley (1994) $257 t_{min} = 2.12$ s.

Advantages of the Simplified Model

The main advantage of the simplified model based on the use of the Saint-Venant and Green and Ampt equations is less computing time to obtain the results from the application of the model. For example, from an experiment reported by Fuentes (1992), the following data are presented: unit flow rate $q_o = 0.0032$ m³/s/m; topographic slope of $J_o = 0.002$ m/m; border length $L = 100$ m; parameters of the law of resistance from Fuentes *et al.*(2004) of $d = 1$ and $k = 1/54$; parameter of the momentum equation of $\beta = 2$; initial value of the volumetric water content $\theta_o = 0.2749$ cm³/ cm³. The parameters of the hydrodynamic characteristics, θ_s, θ_r, m and η, were determined based on the granulometric curve corresponding to loam soil from Montecillo. The methodology suggested by Fuentes (1992) results in $\theta_s = 0.4865$ cm³/ cm³, $\theta_r = 0.0$ cm³/ cm³, $m = 1258$, $n = 2.2878$ and $\eta = 11.0$. The values of the parameters $\psi_d = 32.75$ cm and $K_s = 1.84$ cm/h were obtained by applying an inverse procedure to describe data from an irrigation test performed with the experiment mentioned.

Using a desktop computer with an Intel ® Core™ i7-4770 CPU @ 3.40 GHz and 8.0 GB of ram, a computing time of 3 505 seconds (58.5 minutes, approximately) was needed to apply the complete hydrodynamic model based on the Saint-Venant and Richards equations to model the four stages of gravity irrigation (advance, wetting or ponding, depletion, recession) while only 23.6 seconds were needed for the simplified model based on the Saint-Venant and Green and Ampt equations; that

is, the simplified model used in the example analyzed herein was 150 times faster than the complete hydrodynamic model. Figure 2 shows the comparison of the results obtained during the simulation of the advance stage using both models for the case of the advance front and Figure 3 shows the evolution over time of the water depth and the infiltrated water depth at the head of the border. The results are very similar, in spite of the large difference in computing time needed to apply both models. It is important to clarify that the comparison was performed using loam soil. A greater difference in computing times is expected for soil textures with more clay.

Another advantage of the simplified model over the complete hydrodynamic model is that the information needed to apply it is generally easier and less expensive to obtain.

Design of Border Irrigation

Two methods can be used to design border irrigation (Rendón *et al.*, 1997): irrigation tests and physical-mathematical models. Irrigation tests consist of performing field experiments in which the experimental variables are irrigation flow rate, border length and type of soil. The results from the experiments indicate the unit flow rate and border length combinations for each type of soil that correspond to applying a specific application depth with a high degree of uniformity. The disadvantages of irrigation tests include the considerable amount of time required to execute them, their high cost and the large number of tests needed to determine the irrigation flow rate corresponding to the highest irrigation uniformity. Therefore, they are only recommended for calibrating design methods.

It is crucial to recognize at least three efficiencies related to irrigation processes: application, irrigation requirement and irrigation uniformity. Application efficiency (Ea) is defined as $Ea = Vr / Vp$, where Vr is the volume required to meet the water demands at the root zone of the crop [L^3] and Vp is the projected volume [L^3]; Vr is obtained with

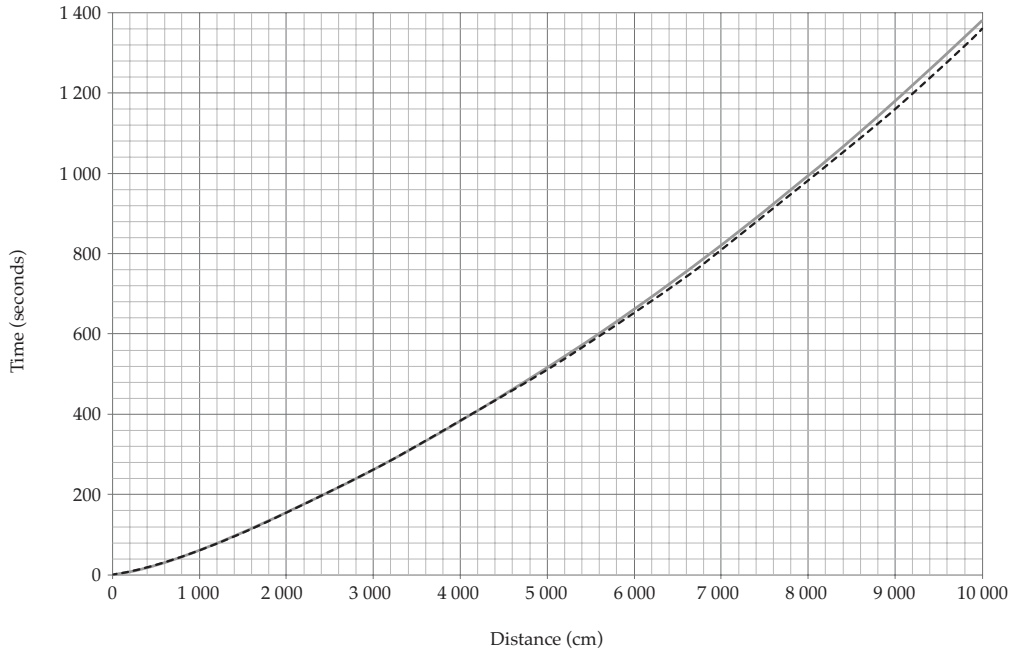

Figure 2. Advance fronts botained by applying the complete hydrodynamic model (solid line) and the simplified model (dotted line). Loam soil from Montecillo.

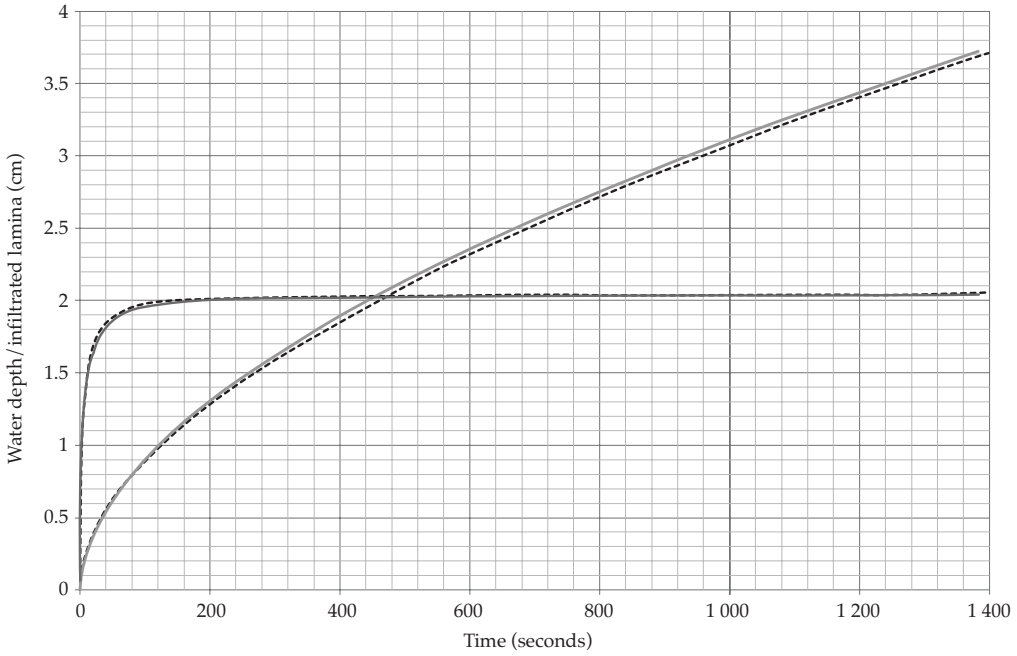

Figure 3. Evolution over time of the water depth and infiltrated lamina at the border head, obtained by applying the complete hydrodynamic model (solid line) and the simplified model (dotted line). Loam soil from Montecillo.

the expression $Vr = LnAr$, where Ln is the net application water depth [L] defined by the irrigation requirement of the crop, and Ar is the irrigation area considered [L^2]. The projected volume is calculated by $Vp = QpTr = LbAr$, where Qp is the projected flow rate [L^3T^{-1}], Tr is irrigation time [T] and Lb is the brute irrigation lamina. When dividing the numerator and denominator in equation (18) by Ar, we get $Ea = Ln/Lb$. The irrigation requirement efficiency (Er) is defined as $Er = Vd/Vr$, where Vd is the available volume [L^3]. This efficiency indicates the degree to which the water requirement by the crop is met.

The ideal situation with respect to uniformity occurs when all the plants receive the same amount of water, which is the same as applying a uniform lamina throughout the length of the border. To evaluate the uniformity of the distribution of the infiltrated water depth, the Christiansen uniformity coefficient (CUC) can be used:

$$CUC = 1 - \frac{\sum_{i=1}^{n} \left| I_i - \hat{I} \right|}{n\hat{I}} \qquad (12)$$

where I_i is the infiltrated water depth at point i [L], $\hat{I}$ is the mean infiltration depth [L] and n is the number of points considered to perform the calculation.

The numeral model developed to couple the Saint-Venant and Green and Ampt equations can be used to determine the flow rate that results in the highest uniformity efficiency, while maintaining high application and requirement efficiencies, that is, to determine the optimal irrigation flow rate.

The procedure that follows is used to calculate the optimal flow rate for different types of soil, differentiated by their hydrodynamic characterization. The value of the pressure at the wetting front (h_f) as well as the hydraulic conductivity at saturation (K_s) are determined based on the values provided by Rawls and

Brakensiek (1981) for soil texture. The volumetric water content at saturation has been assimilated by the total soil porosity (ϕ), which has been determined using the same procedure.

The volumetric water content needed to assign the initial condition $\theta = \theta_o$ in the Green and Ampt equation was determined by taking into account the available moisture for each type of soil, assuming that 50% is consumed prior to irrigation. The available moisture was determined by subtracting the volumetric water content corresponding to field capacity (FC) at the permanent wilting point (PWP). The values of FC and PWP for each type of soil were estimated in accordance with Rawls and Brakensiek (1981), associated with the texture triangle.

Table 1 shows the values of the parameters for the Green and Ampt equation for 10 soil types. With these values and the initial volumetric water content, the combination of border length and the optimal flow rate can be determined for each soil, for a particular application depth.

The uniformity coefficient varies depending on the irrigation flow rate. Figure 4 shows this situation for three different soil types. The inflexion points in each curve represent the optimal flow rate for a border length of 100 m and an application depth of 10 cm for each type of soil specified in the figure.

The optimal irrigation flow rate for different border lengths is determined. Figure 5 graphically represents this calculation for loam soil with three different application depths. A mostly linear relationship can be seen between the optimal irrigation flow rate and the length of the border. The proportionality constant corresponding to these variables can be expressed as the application flow rate per unit area, that is, per unit width and per unit length. The result is shown in Table 2 for three typical application water depths measuring 8, 10 and 12 cm. This table can be used to design border irrigation.

Conclusions

A method to design border irrigation was developed by applying a model based on the use of the Saint-Venant equations for flow of water over soil, and the Green and Ampt equation for the infiltration of water in the soil. The main advantage of the model presented is the short computing time needed for its application as compared to the complete hydrodynamic model reported in the literature which uses SaintVenant equations for water flow over soil, internally coupled

Table 1. Mean parameters for the Green and Ampt (1911) infiltration equation used to design gravity irrigation.

Soil	θ_o (cm³/cm³)	θ_s (cm³/cm³)	h_f (cm)	K_s (cm/h)
Sandy loam	0.16	0.46	12	2.9
Loam	0.20	0.46	25	1.5
Silty loam	0.17	0.55	30	1.0
Silt	0.14	0.50	35	0.8
Sandy clay loam	0.18	0.42	12	2.0
Clay loam	0.25	0.48	38	0.4
Silty clay loam	0.26	0.49	60	0.15
Sandy clay	0.25	0.42	25	0.5
Silty Clay	0.32	0.48	100	0.05
Clay	0.36	0.49	100	0.05

with the Richards equation to model water flow in the soil.

References

Akanbi, A., & Katopodes, N. (1988). *Model for Flow Propagation on Initially Dry Land*. *Journal of Hydraulic Engineering*, *114*(7), 689-706.

Burden, R. L., & Faires, J. D. (1985). *Análisis numérico* (721 pp.). México, DF: Grupo Editorial Iberoamérica.

Fuentes, C., De León, B., Saucedo, H., Parlange, J. Y., & Antonino, A. (2004). El sistema de ecuaciones de Saint-Venant y Richards del riego por gravedad: 1. La ley potencial de resistencia hidráulica. *Ingeniería Hidráulica en México*, *18*(2), 121-131.

Fuentes, C (1992). A*pproche fractale des transferts hydriques dans les sols non saturès* (267 pp.). Tesis de doctorado. Grenoble: Universidad Joseph Fourier.

Green, W. H., & Ampt, G. A. (1911). Studies in Soil Physics, I: The Flow of Air and Water Through Soils. J. *Agric. Sci.*, *4*, 1-24.

Katopodes, N., & Strelkoff, T. (1977). Hydrodinamics of Border Irrigation, Complete Model. *Journal of the Irrigation and Drainage Division*, *IR3*, 309-324.13188.

Lewis, M. R., & Milne, W. E. (1938). Analysis of Border Irrigation. *Transactions of the ASAE*, *19*, 267-272.

Playán, E., Walker, W. R., & Merkley, G. P. (1994). Two-Dimensional Simulation of Basin Irrigation. I. Theory. *Journal of Irrigation and Drainage Engineering*, *120*(5), 837-856.

Rawls, W. J., & Brakensiek, D. L. (1981). Estimating Soil Water Retention from Soil Properties. *Amer. Soc. Civ. Eng.*, *108*(IR2), 167-171.

Rendón, L., Fuentes, C., & Magaña, G. (1997). Diseño del riego por gravedad (pp. I-75 a I-87). En *Manual para diseño de zonas de riego pequeñas*. Jiutepec, México: Instituto Mexicano de Tecnología del Agua.

Richards, L. A. (1931). Capillary Conduction of Liquids through Porous Mediums. *Physics*, *1*, 318-333.

Saucedo, H., Fuentes, C., & Zavala, M. (abril-junio, 2005). El sistema de ecuaciones de Saint-Venant y Richards del riego por gravedad: 2. Acoplamiento numérico para la fase de avance en el riego por melgas. *Ingeniería Hidráulica en México*, *20*(2), 109-119.

Saucedo, H., Zavala, M., & Fuentes, C. (abril-junio, 2011). Modelo hidrodinámico completo para riego por melgas. *Tecnología y Ciencias del Agua*, antes *Ingeniería Hidráulica en México*, *2*(2), 23-38.

Strelkoff, T., & Katopodes, N. (1977). Border-Irrigation Hydraulics with Zero Inertia. *Journal of the Irrigation and Drainage Division*, *IR3*, 325-342, 13189.

Woolhiser, D. A. (1975). Simulation of Unsteady Overland Flow (pp. 485-508). In K. Mahmood & V. Yevjevich (Eds.). *Unsteady Flow in Open Channels*. Vol II. Fort Collins, USA: Water Resources Publications.

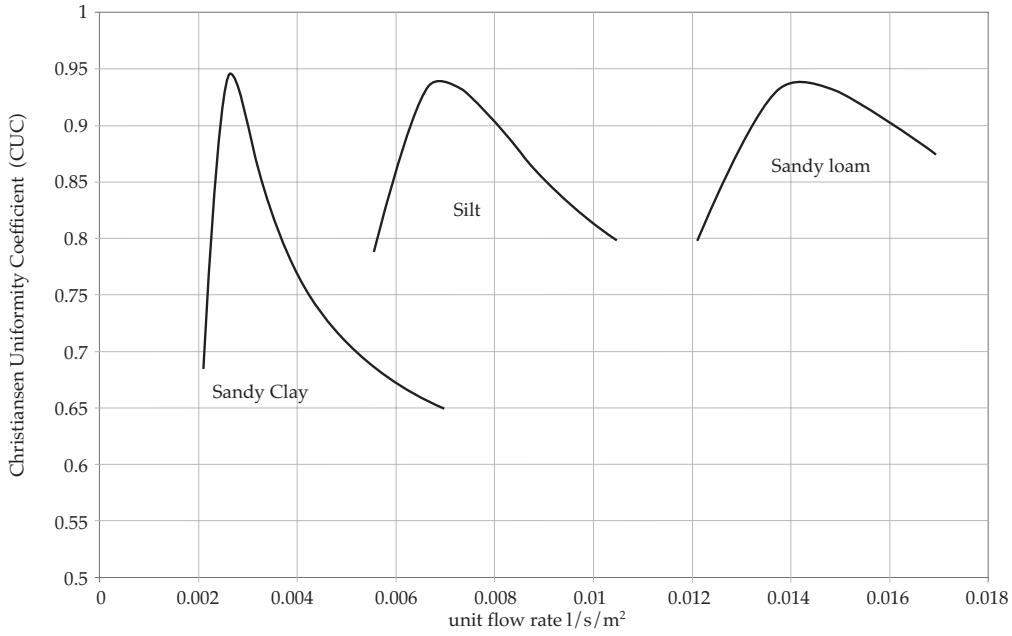

Figure 4. Variations in uniformity efficiency based on irrigation flow rate for three types of soil. Irrigation depth of 10 cm.

Table 2. Border Irrigation Design Table: flow rate in l/s/m² for the optimal irrigation application depth. Friction factor κ = 1/54, topographic slope J_o = 0.002. Saint-Venant and Green and Ampt equations.

Soil	Irrigation depth of 8 cm			Irrigation depth ofe 10 cm			Irrigation depth of 12 cm		
	Qopt	TR	CUC	Qopt	TR	CUC	Qopt	TR	CUC
	l/s/m²	hours	-	l/s/m²	hours	-	l/s/m²	hours	-
Sandy loam	0.01565	1.6	0.921	0.01425	2.2	0.938	0.01330	2.8	0.951
Loam	0.00965	2.6	0.922	0.00875	3.5	0.939	0.00810	4.5	0.952
Silty loam	0.01040	2.4	0.922	0.00890	3.4	0.936	0.00800	4.5	0.949
Silt	0.00810	3.1	0.924	0.00700	4.3	0.937	0.00620	5.9	0.950
Sandy clay loam	0.01740	1.5	0.923	0.01515	2.0	0.938	0.01360	2.7	0.951
Clay loam	0.00330	7.5	0.927	0.00285	10.6	0.941	0.00270	13.4	0.952
Silty clay loam	0.00175	13.7	0.924	0.00145	20.9	0.940	0.00130	27.9	0.953
Sandy clay	0.00290	8.5	0.929	0.00265	11.4	0.945	0.00245	14.7	0.959
Silty Clay	0.00060	40.6	0.888	0.00051	59.0	0.901	0.00046	77.5	0.911
Clay	0.00053	46.5	0.888	0.00045	67.3	0.901	0.00040	90.3	0.911

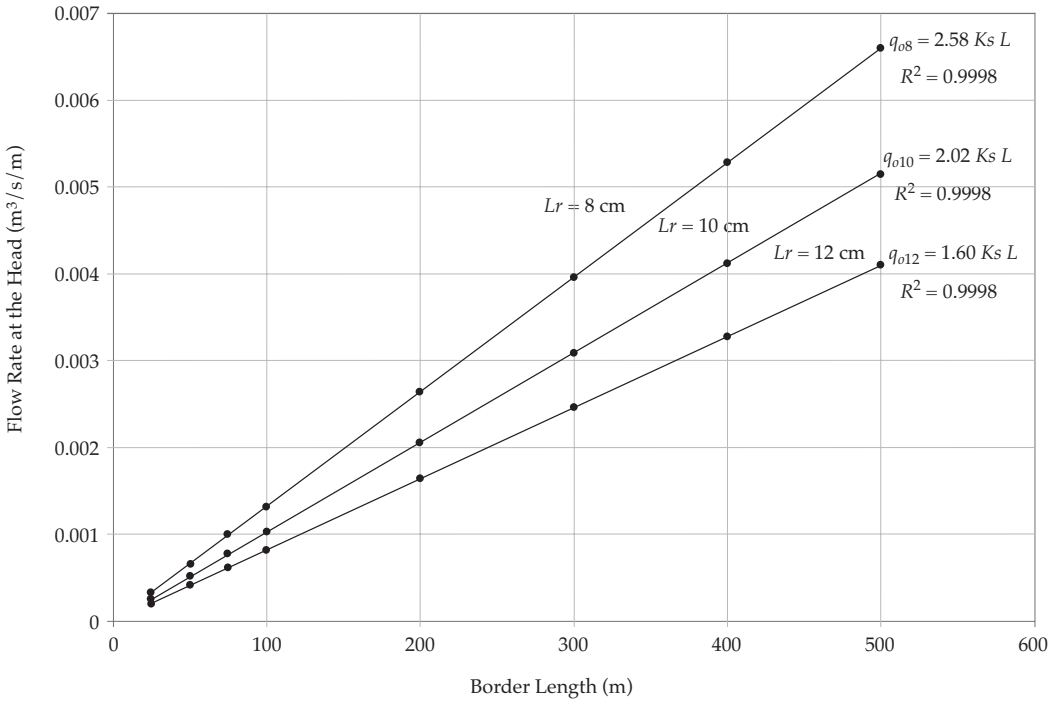

Figure 5. Relationship between border length and optimal flow rate supply for loam soil with three application depths: 8, 10 and 12 cm; K_s in cm/s.

Institutional Address of the Authors

Dr. Heber Saucedo
Dr. Carlos Fuentes

Instituto Mexicano de Tecnología del Agua
Paseo Cuauhnáhuac 8532, Colonia Progreso
62550 Jiutepec, Morelos, México
Teléfono: +52 (777) 3293 600
hsaucedo@tlaloc.imta.mx
cfuentes@tlaloc.imta.mx

Dr. Manuel Zavala

Universidad Autónoma de Zacatecas
Av. Ramón López Velarde # 801, Colonia Centro
98000 Zacatecas, Zacatecas, México
Teléfono: +52 (492) 9239 407
mzavala73@yahoo.com

Technical Note

Hydric Dispersion of Arsenic in the San Antonio-El Triunfo Mining District, Baja California Sur, Mexico

• Berenice Hernández-Cruz* • Faustino de Luna-Cruz • José A. Sánchez-Cruz • • Francisco Martín Romero •
Universidad Nacional Autónoma de México
*Corresponding Author

Abstract

Hernández-Cruz, B., De Luna-Cruz, F., Sánchez-Cruz, J. A., & Romero, F. M. (September-October, 2015). Hydric Dispersion of Arsenic in the San Antonio-El Triunfo Mining District, Baja California Sur, Mexico. *Water Technology and Sciences* (in Spanish), 6(5), 115-124.

The granulometric characteristics of the San Antonio-El Triunfo mining district, Baja California Sur, Mexico were studied in order to determine the relationship between the distribution of arsenic (As) and the size of particles containing As that are transported by runoff. The characteristics of rainfall at five weather stations were analyzed. Effective rainfall was obtained and used to simulate runoff. The simulation resulted in the determination of runoff velocity in m3/s, a value related to the Hjulstrom diagram, to identify the size of particles that were transported or deposited. The results show velocities over 3.0 m/s which transported particles between 0.001 and 100 mm, and velocities under 2.0 m/s which did not transport particles. Materials are deposited from this alternation between velocities. Deposits of materials over 2.0 mm in diameter are associated with high concentrations of As (500 – 1 000 mg/kg) measured in the study area, which were interpolated with a geographic information system. Given the configuration of the distribution of As in surface soil, it can be concluded that water is the primary cause of the movement of As. In addition, diameters of 2.0 mm contain the highest amount of As. Although few studies have performed a physical characterization such as the one herein, their scientific contributions are crucial, especially for environmental issues. By combining the physical characterization with geochemical data and remediation studies, a comprehensive perspective can be obtained for the management of sites affected by mining waste.

Keywords: Distribution of Arsenic, dispersion of Arsenic, runoff speeds, sizes of particles, riverbed.

Resumen

Hernández-Cruz, B., De Luna-Cruz, F., Sánchez-Cruz, J. A., & Romero, F. M. (septiembre-octubre, 2015). Dispersión hídrica de arsénico en el distrito minero de San Antonio-El Triunfo, Baja California Sur, México. Tecnología y Ciencias del Agua, *6(5), 115-124.*

Se efectuó un estudio de las características granulométricas en el distrito minero de San Antonio-El Triunfo, Baja California Sur, México, con el fin de relacionar la distribución del arsénico (As) y el tamaño de partículas que contienen As y son movilizadas por escurrimiento. Las características de la precipitación se analizan mediante cinco estaciones meteorológicas. Se obtiene la lámina de lluvia efectiva, que se utiliza para la simulación del escurrimiento. El resultado de la simulación es la velocidad del escurrimiento en m^3/s, este valor se relaciona con el diagrama de Hjulström, para conocer el tamaño de partículas que se transportan o sedimentan. Los resultados muestran la existencia de velocidades superiores a 3.0 m/s, que movilizan partículas de 0.001 hasta 100 mm, y velocidades inferiores a 2.0 m/s que no movilizan partículas. Dicha alternancia entre las velocidades va depositando los materiales. Los depósitos de materiales mayores a 2.0 mm de diámetro se asocian con altas concentraciones de As (500-1 000 mg/kg), medidas en el área de estudio e interpoladas con un sistema de información geográfica. Dada la configuración que se tiene de la distribución del As en suelos superficiales, se puede concluir que el agente hídrico es el principal responsable del movimiento de As y que son las partículas de diámetro de 2.0 mm las que concentran la mayor cantidad de As. Los estudios de caracterización física, como el presente trabajo, son poco frecuentes; sin embargo, su aporte científico es fundamental, principalmente en temas ambientales. Conjuntar la caracterización física con los datos geoquímicos y los estudios de remediación permite tener una visión integral en la gestión de sitios impactados con residuos mineros.

Palabras clave: *distribución y dispersión de arsénico, velocidad de escurrimiento, tamaño de partícula, cauce principal.*

Received: 16/07/2014
Accepted: 28/05/2015

Introduction

The high concentrations of arsenic (As) found in the hydrographic basin where the San Antonio-El Triunfo mining district is located, in Baja California Sur, Mexico, are primarily associated with mining activity that has been conducted for over two centuries, and which is currently being reactivated with the exploration of metallic ores such as gold a silver (Carrillo & Drever, 1997; COREMI, 1999; SGM, 2014).

This mining district is located 45 km southeast of the city of La Paz. Its geographic coordinates are between 23° 55′ north, 110° 02′ west and 23° 49′ north 110° 00′ west (Figure 1).

Mining activity began with the presence of several companies between 1878 and 1911, and has created the majority of the areas that contain mining wastes. A total of 3.6 tons of gold, 700 tons of silver and 2 500 tons of lead were extracted between 1784 and 1983. The generation of an estimated 800 000 tons of mining waste has been associated with these extractions (Carrillo & Drever, 1997). These wastes are characterized as disaggregated material that easily erodes and is transported by surface water and deposited at other sites.

The hydrography of the site is characterized by intermittent water flows and dry riverbeds. Geomorphologically, these dry channels are wide with heterogeneous surface substrates and do not present spatial or temporal patterns (Suárez, Vidal, Navarro, Gómez, & López, 2010). Precipitaiton is sporadic, typically short and intense, and primarily caused by tropical depressions, storms and hurricanes (Marmolejo, Sánchez, Romero, Sánchez, & Magallanes, 2011).

While the As values in the deposits in rivers are reported to be relatively low (under 0.8 mg/kg), factors such as precipitation, drainage and mining activity, along with climatological and geological components can increase As concentrations in the ecosystems (Cullen & Reimer, 1989). Rivers located in mining areas or regions with metallic mineralizations can contain sediments with As concentrations of around 200 to 400 mg/kg (Appleton, Williams, Orbea, & Carrasco, 2001).

Furthermore, As values from 8 890 to 505 000 mg/kg have been registered in the Hondo-Gaillinas-El Carrizal stream located in the basin next to the study area (Marmolejo *et al.*, 2011).

Particles with high As concentrations found in some mining wastes (such as in the present work) can be leached and dragged by runoff to lower portions of the basin.

Therefore, it is important to identify the dynamics of the pollutant and its relationship with particles transported by flows, supposing that a heterogeneous transport of the material would be associated with heterogeneous As concentrations, and would be found

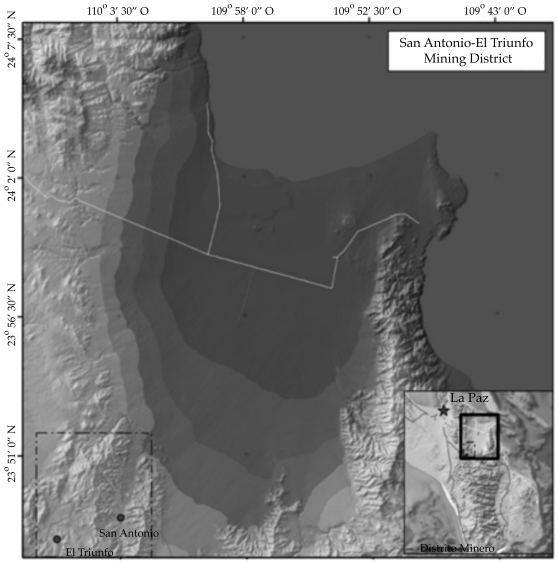

Figure 1. Location of the San Antonio-El Triunfo mining district. The highest elevations are between 700 and 800 meters. The dotted rectangle shows the approximate area in which the mining wastes are located. The map on the bottom right shows a rectangle with a solid line indicating the area of the San Juan de Los Planes basin.

not only in fine particles but in particles of any size, as typically occurs.

Materials and Methods

Construction of Precipitaiton Values

Daily precipitation records were used from the computerized weather database (CLICOM, Spanish acronym) of the National Weather Service. The CLICOM records from the area represent an area of 756 km^2 (Figure 2).

Hietograms were generated to identify the temporal distribution of rainfall. Three steps were used to create these hietograms. First, a set of daily rainfall depths was obtained. Second, an order number was assigned to each rainfall depth according to its magnitude. Third, the rainfall depths of the hietograms were arranged according to the order defined by the maximum rainfall series identified.

Simulation of Precipitations

The "Flubidi" model by the Engineering Institute of the Mexican National Autonomous University (UNAM) was used for the behavior of surface runoff, considering the nature of the hietograms that were generated, which take into account the spatial and temporal variation of rainfall. This model has been used by technical reports by the National Water Commission (Conagua, Spanish acronym) and by master's theses from the hydraulics area of the UNAM.

The model operates with concentrated parameters for small basins (under 1 000 km^2). The simulation is performed with Saint-Venant equations for shallow water, representing surface flow (Fuentes, Domínguez, & Franco, 1981). A rectangular finite volumes method was also used, with an uncentered mesh and first-order finite differences.

In addition, the model is based on the principle of the conservation of mass in two

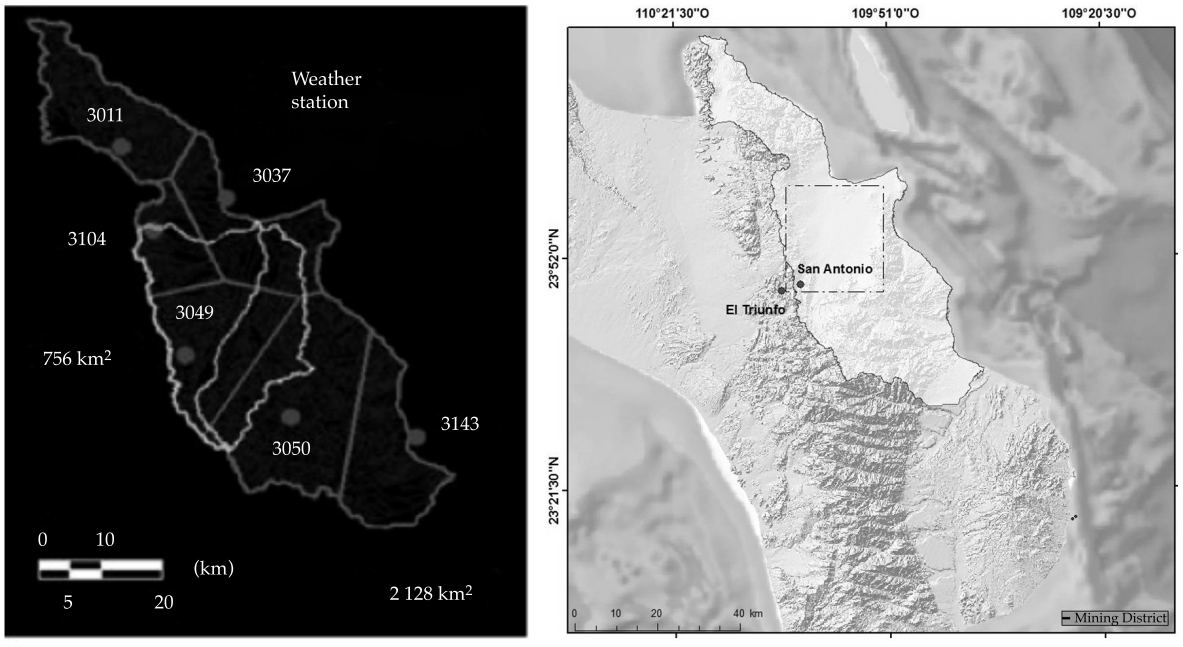

Figure 2. Location of the hydrological basin in the which the mining district is located, and the area of the sub-basin corresponding to the CLICOM records (white line) used to generate the hietograms.

dimensions (time and area) to obtain the velocity of surface flow. Lastly, the effective rainfall volume entering the basin is calculated with continuity and impulse equations (Fuentes, De Luna, Sánchez, & Lorenzo, 2012).

Construction of the Distribution of the As Plume

The As values in soil and surface sediments previously reported by technical reports about the study area were used (Environmental Biochemistry Group, School of Chemistry, Geology Institute, 2012). In particular, data from northern and northeast San Antonio have a uniform spacing that covers an approximate area of 63 km^2.

The sampling campaign performed by the workgroup was systematic and a large number of samples was obtained. The samples can therefore be considered to be representative of the area. A random sampling was also performed in the field to corroborate the As concentrations and the two results were consistent.

The As data obtained was interpolated using the Kriging method (with IDRISI Taiga software) to generate a map of the surface distribution of As in the study area.

The distribution of the As plume obtained was overlaid with the drainage network to view the relationship between the dispersion of As and the water.

Relation of Precipitaiton Values and Particle Sizes

Runoff velocities are related to the behavior of the different sizes of the particles that can be deposited, transported or eroded, depending on the flow velocity. The Hjulstrom diagram is used to identify the threshold of each particle size in relation to the flow velocity (Figure 3) (Boggs, 2006).

A map was created to represent the velocities obtained by mathematical simulation models. Information from the Hjulstrom diagram was used as a reference to identify the sites where the particles were deposited, according to particle sizes. With the information obtained it is possible to establish whether the deposit of a particular particle size contributes to an increase in As concentrations.

Results and Discussion

The calculation of accumulated precipitation indicated a main rainfall trend of very intense rainfalls lasting less than 24 hours (Figure 4). Figure 4 shows two graphs, one with all of the return periods separated according to different shades of gray and another with a detailed representation of the day with the most accumulated rainfall (day 3).

The data registered a maximum rainfall intensity of 92.7 mm/h. This result represents 64.3% of the 24-h rainfall, in which 88.8% of the rainfall over 24 hours occurred roughly eight hours after the event began and 100% (144.16 mm) had accumulated over 20 hours (Figure 5).

The result from the simulation of flows indicates a relationship between rainfall and runoff. The velocity of flow is shown in m/s (Figure 6). Figure 6 presents a map with seven control points which distinguish between the upper, middle and lower parts of the basin. The maximum runoff velocity was found in the middle basin (number 7 and 8) and the slowest velocities in the lower basin (numbers 12, 14 and 15).

According to the Hjulstrom diagram, the velocities are sufficient to erode consolidated material containing particles with diameters of 0.001 to 10 mm, and transport unconsolidated material ranging from fine particles up to the size of gravel and blocks (10-200 mm).

The materials were heterogeneous throughout the 12 kilometers of the river, with granulometries corresponding to gravel and blocks between 2.00 and 100 mm in diameter.

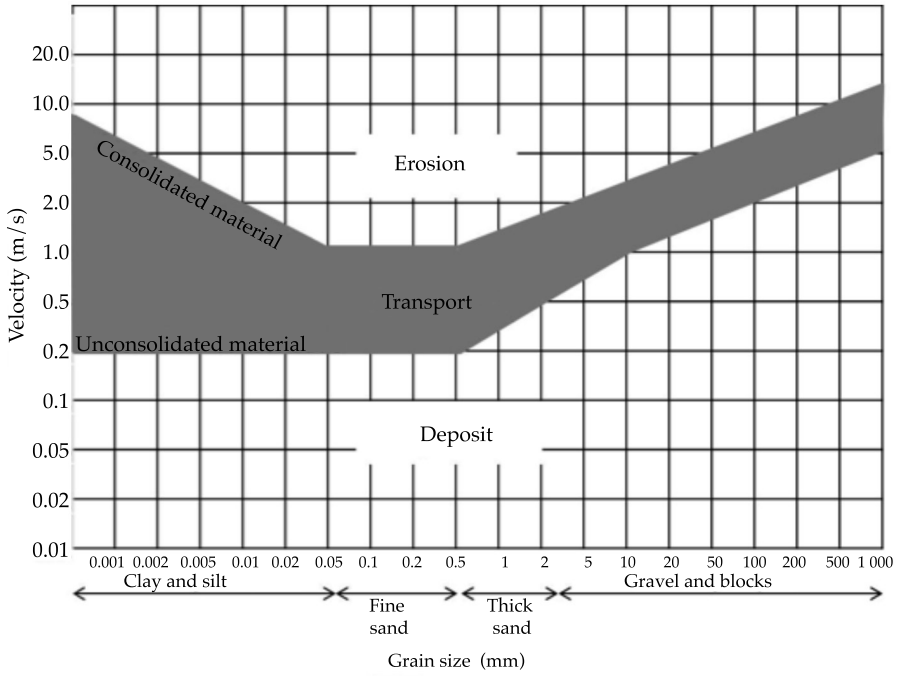

Figure 3. Hjulstrom experimental diagram. The gray line shows the boundary between erosion and deposit of particles. The top edge of the gray line is the transport threshold for consolidated particles, the bottom edge is the threshold for unconsolidated particles (Boggs, 2006).

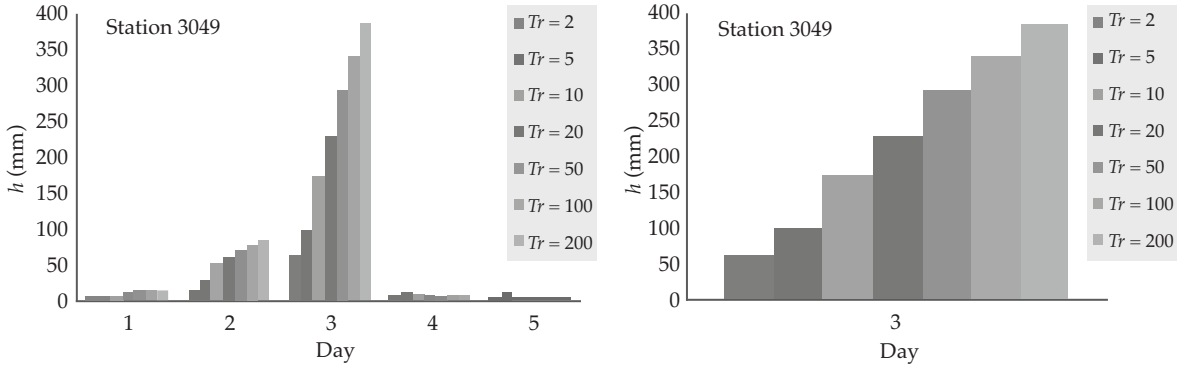

Figure 4. Accumulated rainfall depth. Graph A presents the results from weather station 3049. The horizontal axis is the number of days and the vertical is the rainfall depth in millimeters. Graph B shows the data for the day with the maximum accumulated rainfall.

The mining wastes were located in the upper basin, represented by numbers 4 and 2 on the map in Figure 6, and had varying granulometries. The particles from the main channel showed a trend from thick sands (0.5 – 2.0 mm) to gravel and blocks (2.0- > 1 000m). The velocities in this area were over 2.5 m/s (Figure 6).

If the velocities in the San Antonio stream were under 2.5 m/s, the thick granulometries

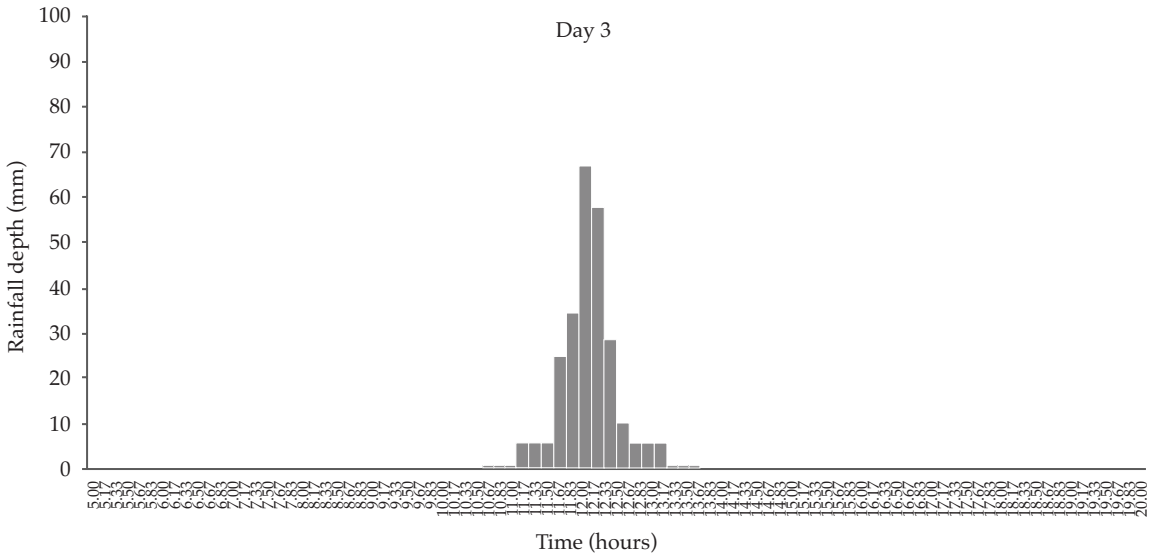

Figure 5. Distribution of 24-hour rainfall in 10-minute intervals. The maximum rainfall flow rate occurred 12 hours after rainfall began, the maximum rainfall depth was 70 mm..

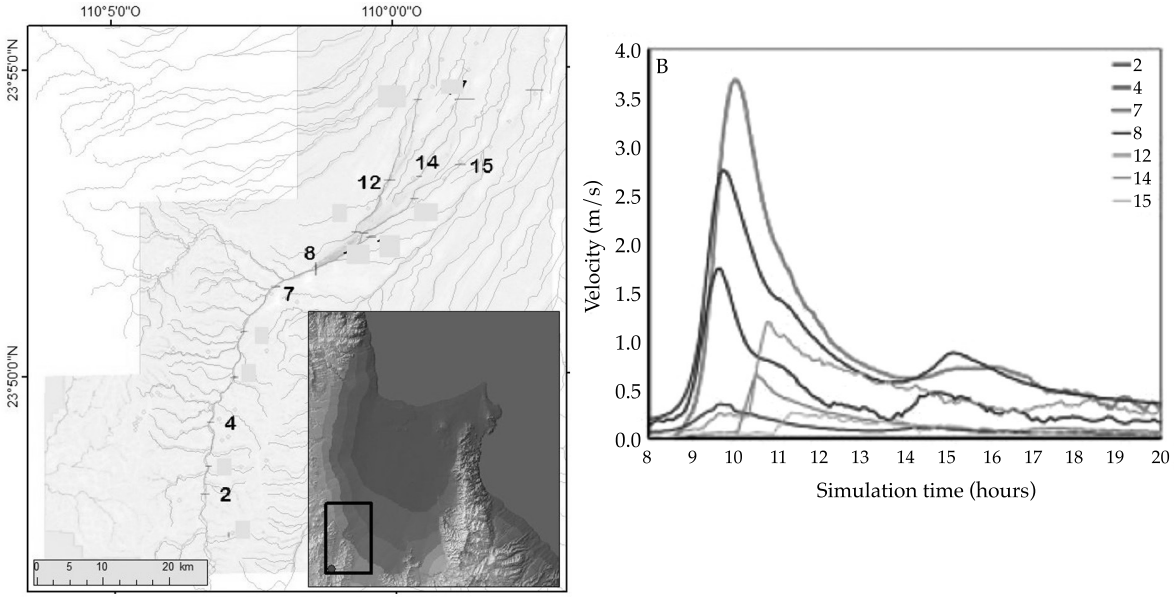

Figure 6. Results from the simulation of runoff: a) map representing the control points graphed in Figure b and their location in the basin (black rectangle on the map); b) flow velocity trends. The vertical axis indicates the rainfall depth in mm and the horizontal represents the rainfall simulation time.

containing high As concentrations could not be transported to the middle basin, and therefore the possibility that thick particles could be responsible for transporting As to lower portions of the basin would be discarded.

When velocities are under 2.5 m/s, as seen in number 8 on the graph in Figure 6, some particle sizes begin to be deposited (Figure 7). Figure 7 shows the heterogeneity of the material present, given a change in the flow velocity.

The middle portion of the basin (defined by numbers 8-11 on the map in Figure 6) presents more heterogeneous particles with deposits of material of all sizes, although blocks and gravel remain on the banks of the river in the vegetation and the fine materials collect in the channel (Figure 8).

Lastly, when the flow velocity is between 0.3 and 1.0 m/s (number 12, 14 and 15 in the graph in Figure 6) the particles become more homogeneous. And although thick materials are still found at some of the points, they are scarce when vegetation is in the area and tend to disappear in the entire lower portion of the basin, where fine materials are predominant in the river as well as on its banks (Figure 9).

As concentrations between 300 and 1 000 mg/kg are found in the northeast, associated with the deposit of particles over 100 mm, since the velocity continues to be sufficient to transport fine particles and deposit gravel and blocks (Figure 10). Velocities from 3.0 to 5.0 m/s were found throughout the course of the Higuerillas stream (located in the west, Figure 10), until reaching the San Antonio stream where they converge.

Since this velocity can transport thick particles throughout the entire length of the stream the As values were low. The case is different for the San Antonio stream, where velocities alternated between 2.0 to 3.0 m/s and over 3.0 m/s. This alternation also is reflected in the As concentrations, which increase or decrease as the thick materials are deposited in the channel (Figure 11).

Conclusions

The data from the hietograms clearly show a trend of intense rainfall with short duration. These characteristics contribute to runoff in terms of the water's infiltration capacity, and therefore particles can be transported when rainfall occurs.

Flow velocities over 2.5 m/s drag particles containing As and transport the pollutant to the lower portion of the basin. When the

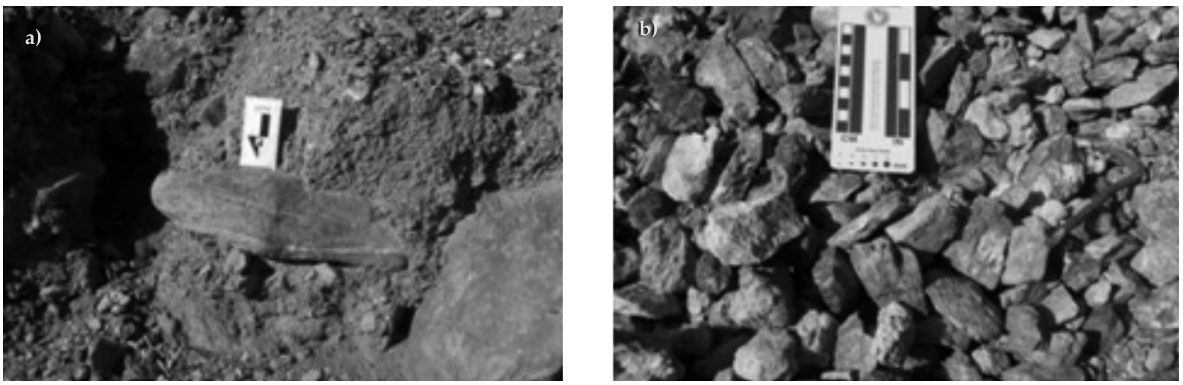

Figure 7. Granulometries in the upper basin: a)consolidated material in mining wastes; b) unconsolidated material on the surface.

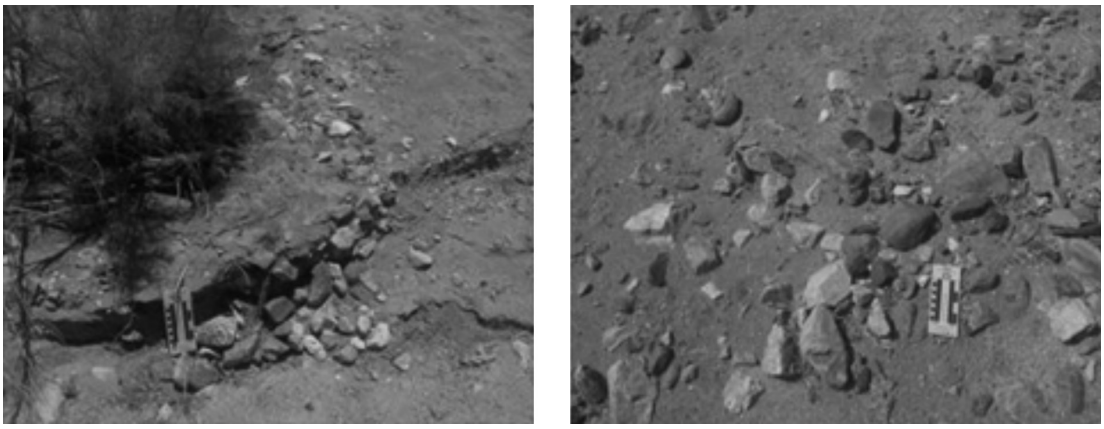

Figure 8. Middle basin. The particles that are the size of blocks are angular, indicating little transport of the material. The fine material is found in the channel and between the thick particles located on the banks.

Figure 9. Lower portion of the basin. The sediments are predominantly fine, the soil on the walls of the channel is more developed and vegetation cover is scarce.

velocity is under 2.5 m/s, As concentrations over 114 mg/kg (registered as the natural value) do not exist.

Particles larger than gravel and blocks (≥ 100 mm) are associated with an increase in As, with an increase or presence of As where they are located. Since the velocities generated cannot move particles of this size they are not deposited downstream. In the stream near the town of Texcalama, the initial velocities cannot transport particles over 100 mm and therefore the distribution plume does not increase downstream.

With regard to the lower basin, As values were low (114 mg/kg) because the runoff velocities were not high enough to erode and transport particles the size of gravel which are moved from the upper part of the basin where the mining wastes were located. This represents an advantage for the population and for the ecosystem in general, given that high As concentrations were only found in

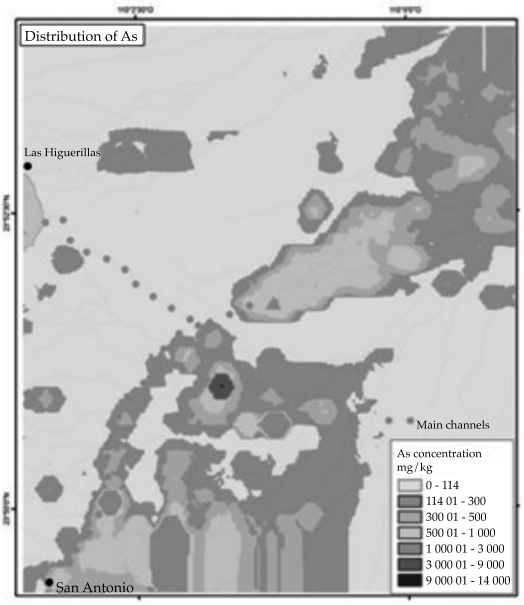

Figure 10. Hydrographic map. The gray points show the two channels of the main arroyos. The channel near the town of Las Higuerillas is north of San Antonio. The different shades of gray correspond to As concentrations.

the San Antonio channel and some of its secondary channels.

Agradecimientos
Acknowledgements

The authors thank the project "Environmental study of arsenic in the San Antonio-El Triunfo mining district"; the company Minera Pitalla, S.A de C.V. for providing the arsenic database and its support during the fieldwork; special thank you to engineer Rodrigo Hernández Ordoñez and Dr. Carles Canet Miquel for their helpful commentaries regarding the manuscript.

References

Appleton, J., Williams, T., & Orbea, H. (2001). Fluvial Contamination Associated Artisanal Gold Mining in the Ponce Enriquez, Portovelo-Zamura and Nambija Areas, Ecuador. *Water, Air and Soil Pollution*, *131*(1-4), 19-39.

Boggs, S. (2006). *Principles of Sedimentology and Stratigraphy.* Upper Saddle River USA: Pearson Prentice Hall.

Carrillo, A., & Drever, I. (1997). Environmental Assessment of the Potential for Arsenic Leaching into Groundwater from Mine Wastes in Baja California Sur, Mexico. *Geofísica Internacional*, *37*(1), 1-8

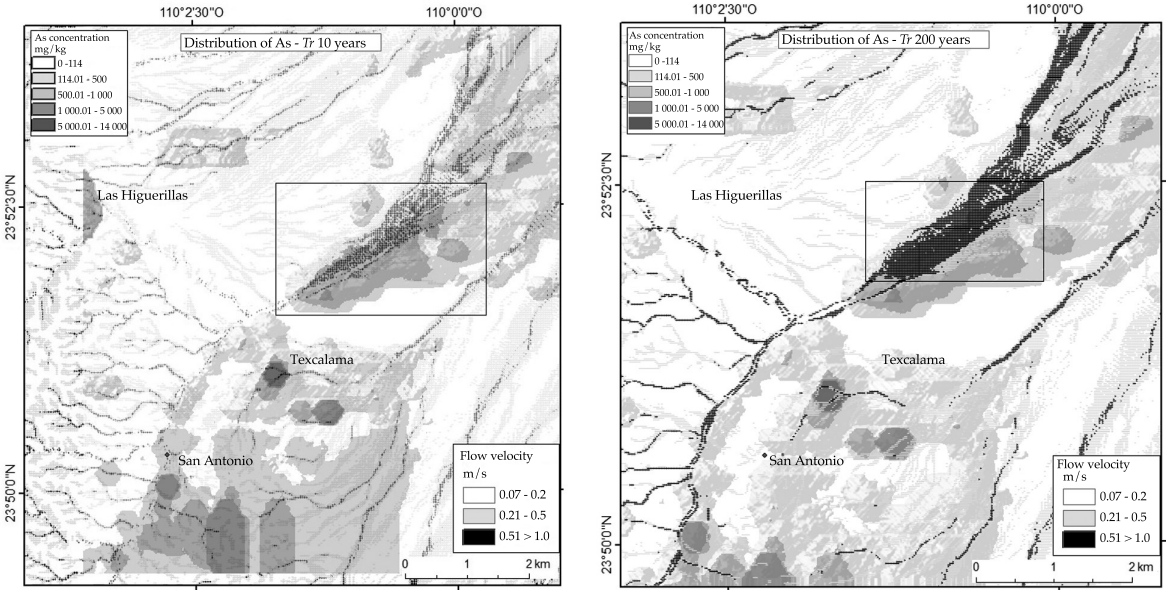

Figure 11. Relation of As concentration and the runoff velocity with two return periods (10 and 200 years). The point with the highest As concentration can be seen in the rectangle, where the flow is between 0.5 and 1.0 m/s, which cannot transport As downstream.

COREMI. (1999). *Monografía geológico minera del estado de Baja California Sur.* México, DF: Consejo de Recursos Minerales, Secretaría de Comercio y Fomento Industrial.

Cullen, W., & Reimer, K. (1989). Arsenic Speciation in the Environment. *Chem. Rev.*, *89*(4), 713-764.

Fuentes, O., De Luna, F., Sánchez, J., & Lorenzo, H. (2012). Obtención de hietogramas correspondientes a diferentes periodos de retorno. *Memorias del XXV Congreso Latinoamericano de Hidráulica.* San José, Costa Rica: Asociación Internacional de Ingeniería e Investigaciones Hidro-Ambientales (IAHR), 102-115.

Fuentes, O., Dominguez, R., & Franco, V. (1981). Relación entre Precipitación y Escurrimiento (pp. 1-66). En *Manual de Diseño de Obras Civiles, Sección Hidrotecnia.* México, DF: Comisión Federal de Electricidad.

Grupo de Biogeoquímica Ambiental, Facultad de Química, & Instituto de Geología (2012). *Estudio ambiental de arsénico en el distrito minero de San Antonio- El Triunfo.* México, DF: Universidad Nacional Autónoma de México.

Marmolejo, J., Sánchez, M., Romero, J., Sánchez, A., & Magallanes, V. (2011). Migration of As, Hg and Zn in Arroyo Sediments from Semiarid Coastal System Influenced by the Abandonded Gold Mining District at El Triunfo, Baja California Sur, Mexico. *Environ. Monit.*, *13*(8), 2182-2189.

SGM (2014). *Listado de proyectos mineros. Dirección General de Desarrollo Minero.* México, DF: Servicio Geológico Mexicano, Centro de documentación de la Dirección General de Desarrollo Minero, Secretaría de Economía.

Suárez, M., Vidal, M., Navarro, I., Gómez, R., & López, F. (2010). Los arroyos de Baja California Sur (México): caracterización ambiental y aplicación de un índice de estado de alteración. *(IAR), Rev C. & G.*, *24*(1-2), 63-77.

Institutional Address of the Authors

Dra. Berenice Hernández-Cruz

Facultad de Filosofía y Letras
Universidad Nacional Autónoma de México
Ciudad Universitaria, Avenida Universidad 3000,
Delegación Coyoacán
04510 México D.F., México
bere@geofisica.unam.mx

M.I. Faustino de Luna-Cruz

Instituto de Ingeniería
Universidad Nacional Autónoma de México
Ciudad Universitaria, Avenida Universidad 3000,
Delegación Coyoacán
04510 México D.F., México
Teléfono: +52 (55) 5623 3600 ext. 14
flunaC@iingen.unam.mx

M.I. José Alberto Sánchez-Cruz

Instituto de Ingeniería
Universidad Nacional Autónoma de México
Ciudad Universitaria, Avenida Universidad 3000,
Delegación Coyoacán
04510 México D.F., México
Teléfono: +52 (55) 5623 3600 ext.
JSanchezC@iingen.unam.mx

Dr. Francisco Martín Romero

Instituto de Geología
Universidad Nacional Autónoma de México
Delegación Coyoacán
04510 México D.F., México
Teléfono: +52 (55) 5622 4284 ext.129
fmrch@geologia.unam.mx

Technical Note

Application of Environmental Isotopes to Determine the Biodegradation of Organic Compounds

• Luis E. Lesser-Carrillo* •
Instituto Tecnológico y de Estudios Superiores de Monterrey
*Corresponding Author

Abstract

Lesser-Carrillo, L. E. (September-October, 2015). Application of Environmental Isotopes to Determine the Biodegradation of Organic Compounds. *Water Technology and Sciences* (in Spanish), 6(5), 125-131.

Microcosm experiments were conducted to determine the fractionation of stable carbon isotopes during naphthalene biodegradation. The experiments were developed under aerobic and anaerobic conditions (sulfate-amended, nitrate-amended and unamended) and with sterile controls. The liquid phase was analyzed to determine the carbon concentration and stable carbon isotopes of the naphthalene. The aerobic microcosms showed that naphthalene aerobically biodegraded in less than 60 hours. The $d^{13}C$ increased from -25.5 to -25.1‰ (enrichment of 0.4 ± 0.08‰) in only one sample, in which 95% of naphthalene was biodegraded. After 288 days, the anaerobic microcosms showed a naphthalene consumption of 30, 50 and 60% on average for the unamended, NO_3^- amended and $SO_4^=$ amended microcosms, respectively, relative to sterile controls. Under denitrifying conditions, $d^{13}C$ increased from -25.2 to -23.9‰ (enrichment of 1.3 ± 0.3‰) after a 95% biodegradation of naphthalene. The unamended microcosms demonstrated a slight enrichment (0.7 ± 0.3‰) of d13C from -25.2 to -24.5‰ after a biodegradation of 65% (after 288 days). For microcosms with $SO_4^=$ reduction conditions, no significant changes were detected in the $d^{13}C$ of naphthalene during biodegradation.

Keywords: Naphthalene, isotope, fractionation, biodegradation, aerobic, anaerobic.

Resumen

Lesser-Carrillo, L. E. (septiembre-octubre, 2015). Aplicación de isótopos ambientales en la determinación de la biodegradación de compuestos orgánicos. Tecnología y Ciencias del Agua, *6(5), 125-131.*

Se realizaron experimentos de microcosmos para determinar el fraccionamiento de los isótopos estables de carbono durante la biodegradación de naftaleno. Los microcosmos se realizaron bajo condiciones aeróbicas, anaeróbicas (con adiciones de sulfatos, con adiciones de nitratos y sin adiciones) y controles estériles. Se analizó la fase líquida para determinar la concentración e isótopos estables de carbono de naftaleno. Los microcosmos aeróbicos muestran que el naftaleno se degradó aeróbicamente en menos de 60 horas. El $d^{13}C$ se incrementó de -25.5 a -25.1‰ (enriquecimiento de 0.4 ± 0.08‰) en una sola muestra, en la que 95% del naftaleno había sido biodegradado. Los microcosmos anaeróbicos muestran que después de 288 días, los microcosmos sin adiciones, con adición de NO_3^- y con adición de $SO_4^=$ habían consumido, respectivamente, 30, 50 y 60% de naftaleno en promedio, comparados con los microcosmos de control. Bajo condiciones desnitrificantes, el $d^{13}C$ de naftaleno aumentó de -25.2 a -23.9‰ (enriquecimiento de 1.3 ± 0.3‰) después de una biodegradación de 95% del naftaleno. Para los microcosmos sin adiciones se detectó un ligero enriquecimiento en $d^{13}C$ de naftaleno de -25.2 a -24.5‰ (enriquecimiento de 0.7±0.3‰) después de una biodegradación de un 65% (después de 288 días). Para los microcosmos en condiciones reductoras de $SO_4^=$ no se percibieron cambios significativos en el $d^{13}C$ de naftaleno durante su biodegradación.

***Palabras clave**: naftaleno, fraccionamiento, isótopo, biodegradación, aeróbica, anaeróbica.*

Received: 04/05/2012
Accepted: 18/05/2015

Introduction

Pollution of aquifers caused by hydrocarbons has been widely documented (Fetter, 1993; Iturbe & Silva, 1989, Lesser-Carrillo, 2006). Naphthalene is a polynuclear aromatic hydrocarbon (PAH) produced primarily by refining petroleum. It is particularly found in tar and is a groundwater pollutant commonly found in facilities that preserve wood (Environment Canada, 1993; USEPA, 1992). It has been shown to be aerobically biodegradable (Ehrlich, Goerlitz, Godsy, & Hult, 1982; Heitkamp & Cerniglia, 1989) under anoxic (Agarry & Owabor, 2011; Maillacheruvu & Pathan, 2009; Kleemann & Meckenstock, 2011), iron reduction (Blum *et al*., 2009), denitrifying (Mihelcic & Luthy, 1998; Al-Bashir, Cseh, Leduc, & Samson, 1990) and sulfate reduction conditions (Thierrin, Davis, & Barber, 1995; Rockne & Strand, 1998).

Carbon has two stable isotopes (^{13}C and ^{12}C) and one radioactive isotope (^{14}C) (T1/2 = 5 730 years). The natural abundance of ^{13}C is 1.11% (Clark & Fritz, 1997). Due to kinetic processes, microorganisms can break ^{12}C-^{12}C bonds more than ^{12}C-^{13}C bonds during the biodegradation of organic compounds (Van de Velde, Marley, Studer, & Wagner, 1995). Therefore, the ratio of $^{13}C/^{12}C$ of the compound that is being broken down could increase during the biodegradation process. Several studies have shown a change in the isotope ratios of stable carbon during the biodegradation of chlorinated solvents (Hunkeler, Aravena, & Butler, 1999; Bloom, Aravena, Hunkeler, Edwards, & Frape, 2000; Sherwood-Lollar *et al*., 1999). BTEX compounds produce very small isotopic fractionation of carbon during its biodegradation (Sherwood-Lollar *et al*., 1999; Stehmeier *et al*., 1999; Ahad, Sherwood-Lollar, Edwards, Slater, & Sleep, 2000), as well as MTBE (Lesser *et al*., 2008). In a field study by Richnow, Annweiler, Michaelis and Meckenstock (2003) very low isotopic fractionation of naphthalene was found.

To study this phenomenon in the laboratory, the biodegradation of naphthalene in microorganisms can be reproduced, and the $^{13}C/^{12}C$ ratio of the naphthalene would be expected to increase as the biodegradation of the compound progresses. The objective of this study was to perform laboratory tests to determine the fractionation of stable carbon isotopes during the aerobic and anaerobic biodegradation of naphthalene.

Methods

Microcosm Experiments

Microcosm experiments were performed under aerobic and anaerobic conditions and with sterile controls. The anaerobic microcosms were created with sulfate amendments, nitrate amendments and without amendments. The purpose of the amendments was to promote the anaerobic biodegradation of naphthalene by adding electron acceptors that may have been exhausted in the sediments and water used. All the experiments were performed in triplicate. The microcosms were created in 60 ml glass vials. Each microcosm was filled with 20 g of sediments from an aquifer polluted with naphthalene, and approximately 55 ml of groundwater without allowing air into the vials. The anaerobic microcosms were prepared in an anaerobic chamber. A total of 144 microcosms were created.

The microcosms were sacrificed periodically in triplicate and the liquid phase was analyzed to determine the concentration of organic compounds and, when applicable, dissolved oxygen, nitrates or sulfates. For the analysis of stable carbon isotopes, the water samples were taken from the microcosms in 4.8 ml glass vials with a Teflon cap and without allowing air spaces. These samples were conserved with 1 μl of sodium azide per ml of sample and stored at 4°C until performing the analysis.

Laboratory Analysis

The concentrations of the organic and inorganic compounds from the water samples and the stable carbon isotopes were analyzed by the Organic Geochemistry Laboratory as well as the Environmental Isotope Lab at the University of Waterloo, Canada.

Results and Discussion

Aerobic Microcosms

In the aerobic microcosms, naphthalene degraded aerobically in less than 60 hours. These results agree with previous studies of the aerobic biodegradation of naphthalene (Ehrlich *et al*., 1982; Heitkamp & Cerniglia, 1989). The data obtained from these experiments demonstrate significant differences in the amount of naphthalene consumed by each microcosm (50 to 95%) after 48 hours.

Taking into account the results from the biodegradation naphthalene, 13 samples were analyzed for $d^{13}C$ from the microcosms. The results show a slight enrichment of $d^{13}C$ during aerobic biodegradation, increasing from -25.5 to -25.1‰ (enrichment of 0.4 ± 0.08‰) in just one sample in which 95% of the naphthalene biodegraded. The data clearly demonstrate that this enrichment is only apparent after the majority of the naphthalene has degraded (Figure 1).

Other investigators, such as O'Malley, Abrajano Jr. and Hellou (1994) also have observed very small isotopic enrichment in naphthalene in the final stages of its aerobic biodegradation. To compare this with other compounds, Stehmeier *et al*. (1999) found an isotopic enrichment of 1.1 ‰ during the aerobic biodegradation of benzene and Sherwood-Lollar *et al*. (1999) did not find any significant fractionation in toluene during its aerobic biodegradation.

This isotopic fractionation may or may not be sufficient to demonstrate the biodegradation of naphthalene in field situations, where many other processes contribute to decreasing the concentration of pollutants, such as advection, dispersion and adsorption.

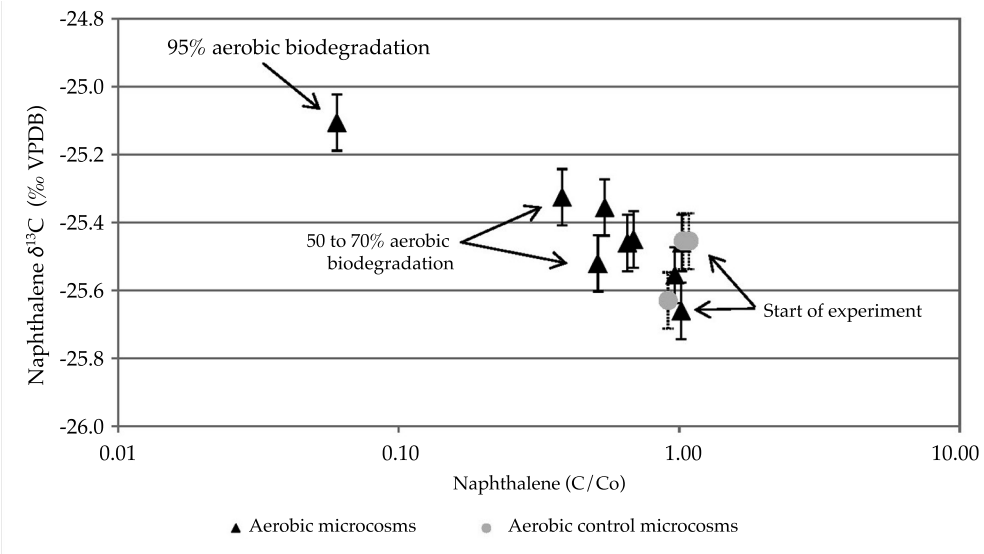

Figure 1. Naphthalene d13C during aerobic biodegradation in microcosms. The concentration of naphthalene is normalized and the error bars represent the analytical error.

Anaerobic Microcosms

These experiments were also performed in triplicate. The results show an average naphthalene consumption after 288 days of 30, 50 and 60% in relation to the control microcosms with the unamended, NO_3^- amended and $SO_4^=$ amended microcosms, respectively. Nearly all the naphthalene was consumed in four of the microcosms. The naphthalene in the sterile controls decreased only slightly over the same time period and, therefore, the majority of the decrease in naphthalene concentrations in the active microcosms is attributable to biodegradation.

The biodegradation rates were calculated by subtracting the loss in mass in the sterile controls. Apparent zero-order biodegradation rates (λ_0), of 0.26, 0.77 and 0.58 years^{-1} were obtained with microcosms without amendments, with NO_3^- amendments and with $SO_4^=$ amendments, respectively, and first-order biodegradation rates (λ_1) were 0.51, 1.50 and 2.23 years^{-1} for microcosms without amendments, with NO_3^- amendments and with $SO_4^=$ amendments, respectively. These rates are considerably lower than those obtained with aerobic degradation. Blum *et al*. (2009) obtained a λ_0 of 1.39 years^{-1}, similar to that reported by this study, while Agarry and Owabor (2011) reported a λ_0 of 5 to 31 years^{-1}.

NO_3^- and $SO_4^=$ concentrations were also analyzed with anaerobic microcosms to monitor their activity as electron receptors. The results indicate that a decrease in the naphthalene concentration in the $SO_4^=$ amended microcosms is correlated with a decrease in the concentration of $SO_4^=$ (data not shown). This demonstrates that the biodegradation of naphthalene was produced in a sulfate-reducing medium. Likewise, the decrease in the concentration of naphthalene in microcosms with NO_3^- amendment also is correlated with a decrease in the NO_3^- concentration (data not shown), demonstrating that the biodegradation of naphthalene is also produced under denitrifying conditions.

Taking into account the results from the biodegradation of naphthalene, 20 samples were analyzed for $d^{13}C$ in the microcosms. The results indicate that, under denitrifying conditions, $d^{13}C$ from naphthalene increased -25.2 to -23.9‰ (enrichment of 1.3 ± 0.3‰) after 95% biodegradation of naphthalene (Figure 2). This fractionation indicates that this effect may not be easily observed under denitrifying field conditions.

For microcosms without amendments, a slight enrichment in $d^{13}C$ from naphthalene of -25.2 to -24.5‰ was observed (enrichment of 0.7±0.3‰) after 65% biodegradation. This experiment did not demonstrate significant changes in $d^{13}C$ during biodegradation and no significant differences in $d^{13}C$ were observed among the microcosms.

Richnow *et al*. (2003) found an isotopic fractionation in naphthalene of 1.2 ‰ with an anaerobic aquifer. Meanwhile, Kelley, Coffin and Mueller (1998) analyzed the $d^{13}C$ from various PAHs (including naphthalene) in an aquifer with anaerobic conditions, and a very slight enrichment in $d^{13}C$ can be seen in their field data, although they do not consider it significant possibly because of the uncertainty in such low enrichment. The results from this study are consistent with those reported by Kelley *et al*. (1998).

Conclusions

In aerobic microcosms, naphthalene aerobically degraded in less than 60 hours. The biodegradation rates calculated were λ_1= 2.4 d^{-1}and λ_1 = 0.72 d^{-1}. The $d^{13}C$ increased from -25.5 to -25.1‰ (enrichment of 0.4 ± 0.08‰) in only one sample, in which 95% of the naphthalene had biodegraded. This result was statistically different than the other three samples with less biodegradation. The enrichment factor (*e*) for the aerobic biodegradation was -0.16, according to Rayleigh's distillation.

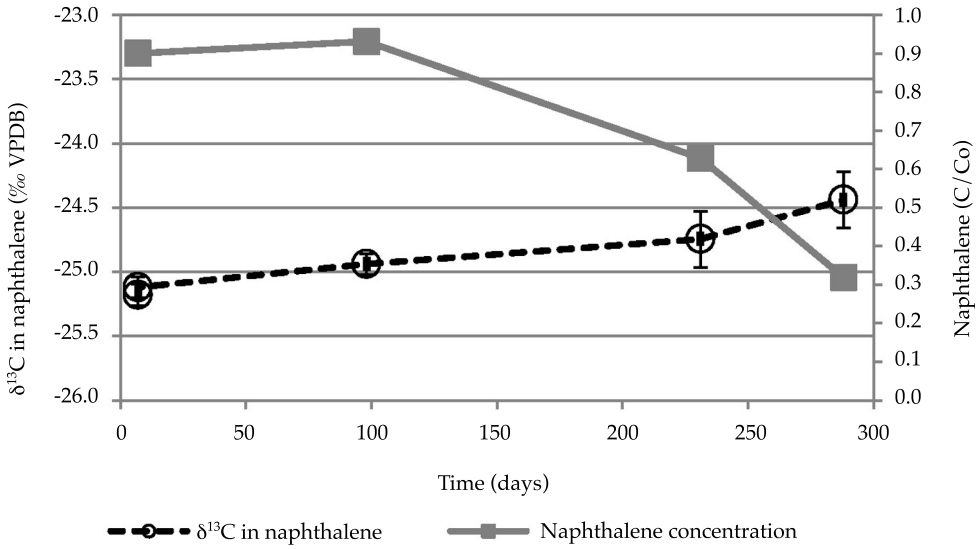

Figure 2. $\delta^{13}C$ in naphthalene during anaerobic biodegradation in microcosms with denitrifying conditions (NO_3- amendement). The concentration of naphthalene is normalized and the error bars represent the analytical error.

With anaerobic microcosms, average consumptions of 30, 50 and 60% of naphthalene were obtained in relation to the controls after 288 days in microcosms without amendment and with NO_3^- and $SO_4^=$ amendments, respectively. The biodegradation rates calculated for λ_0 were 0.26, .077 and .058 $years^{-1}$ for microcosms without amendments and with NO_3^- and $SO_4^=$ amendments, respectively. For the same cases, λ_1 was 0.51, 1.50 and 2.2 $years^{-1}$.

Under denitrifying conditions, $d^{13}C$ from naphthalene increased -25.2 to -23.9‰ (enrichment of 1.3 ± 0.3‰) after 95% of naphthalene had biodegraded, while *e* was -0.3. For sterile controls, the $d^{13}C$ values were statistically the same. For microcosms without amendments, a slight enrichment in $d^{13}C$ was detected, from -25.2 to -24.5‰ (enrichment.7 ± 0.3‰) after 65% biodegradation (after 288 days), with an *e* of -0.62.

For microcosms with $SO_4^=$ reducing conditions, no significant changes in $d^{13}C$ were observed during biodegradation and no statistical differences in $d^{13}C$ were observed with any of the microcosms.

Although the isotopic enrichment observed during the aerobic and anaerobic biodegradation of naphthalene was small, it was statistically significant. Nevertheless, this enrichment may not be sufficient to demonstrate the biodegradation of naphthalene in field conditions where many other processes (advection, dispersion and adsorption) also contribute to decreasing the concentration of this pollutant.

Acknowledgements

The author would like to extend his deepest gratitude to Jim Barker, PhD and Ramon Aravena, PhD., from the University of Waterloo, Canada, for their support in performing these experiments. The isotopic analyses were conducted at the Environmental Isotope Lab at the University of Waterloo.

References

Agarry, S. E., & Owabor, C. N. (2011). Anaerobic Bioremediation of Marine Sediment Artificially Contaminated with Anthracene and Naphthalene. *Environmental Technology*, *13*(12), 1375-1381.

Ahad, J. M. E., Sherwood-Lollar, B., Edwards, E. A., Slater, G. F., & Sleep, B. E. (2000). Carbon Isotope Fractionation during Anaerobic Biodegradation of Toluene: Implications for Intrinsic Bioremediation. *Environmental Science and Technology*, *34*(5), 892-896.

Al-Bashir, B., Cseh, T., Leduc, R., & Samson, R. (1990). Effect of Soil/Contaminant Interactions on the Biodegradation of Naphthalene in Flooded Soil under Denitrifying Conditions. *Applied Microbiology and Biotechnology*, *34*, 414-419.

Bloom, Y., Aravena, R., Hunkeler, D., Edwards, E., & Frape, S. K. (2000). Carbon Isotope Fractionation during Microbial Dechlorination of Trichloroetene, Cis-1,2-Dichloroethene, And Vinyl Chloride: Implications for Assessment of Natural Attenuation. *Environmental Science and Technology*, *34*(13), 2768-2772.

Blum, P., Hunkeler, D., Weede, M., Beyer, C., Grathwohl, P., & Morasch, B. (2009). Quantification of Biodegradation for O-Xylene and Naphthalene Using First Order Decay Models, Michaelis-Menten Kinetics and Stable Carbon Isotopes. *Journal of Contaminant Hydrology*, *105*, 118-130.

Clark, I., & Fritz, P. (1997). *Environmental Isotopes in Hydrogeology* (328 pp.). Boca Ratón, USA: Lewis Publishers.

Ehrlich, G. G., Goerlitz, D. F., Godsy, E. M., & Hult, M. F. (1982). Degradation of Phenolic Contaminants in Ground Water by Anaerobic Bacteria: St. Louis Park, Minnesota. *Ground Water*, *20*(6), 703-710.

Environment Canada (1993). Creosote-Impregnated Waste Materials. Priority Substance List Assessment Report (23 pp.). Environment Canada. (https://www.ec.gc.ca/toxiques-toxics/Default.asp?lang=En&n=5018787E-1)

Fetter, C. W. (1993). *Contaminant Hydrogeology* (458 pp.). New York: MacMillan Publishing Company.

Heitkamp, M. A., & Cerniglia, C. E. (1989). Polycyclic Aromatic Hydrocarbon Degradation by a Mycobacterium Sp. In a Microcosm Containing Sediment and Water from a Pristine Ecosystem. *Applied and Environmental Microbiology*, *55*(8), 1968-1973.

Hunkeler, D., Aravena, R., & Butler, B. J. (1999). Monitoring Microbial Dechlorination of Tetrachloroethene (PCE) in Groundwater Using Compound-Specific Stable Carbon Isotope Ratios: Microcosm and Field Studies. *Environmental Science and Technology*, *33*(16), 2733-2738.

Iturbe, R., & Silva, A. (1989). Revisión bibliográfica sobre contaminación de suelos y acuíferos. *Ingeniería Hidráulica en México* (ahora *Tecnología y Ciencias del Agua*), *4*(3), 51-56.

Kelley, C. A., Coffin, R. B., & Mueller, J. G. (1998). Stable Isotope Analyses – An Innovative Technique to Monitor Biodegradation of Petroleum Hydrocarbons. *Geotechnical News*, *16*(2), 20-24.

Kleemann, R., & Meckenstock, R. U. (2011). Anaerobic Naphthalene Degradation by Gram-Positive, Iron-Reducing Bacteria. *FEMS Microbial Ecology*, *78*, 488-496.

Lesser-Carrillo, L. E. (2006). Situación actual del MTBE (metal terbutil éter) en sistemas acuíferos. *Ingeniería Hidráulica en México* (ahora *Tecnología y Ciencias del Agua)*, *21*(2), 117-123.

Lesser, L. E., Johnson, P. C., Aravena, R., Spinnler, G., Bruce, C., & Salanitro, J. (2008). An Evaluation of Compound-Specific Isotope Analyses for Assessing the Biodegradation of MTBE at Port Hueneme, CA., *Environmental Science & Technology*, *42*(17), 6637-6643.

Maillacheruvu, K. Y., & Pathan, I. A. (2009). Biodegradation of Naphthalene, Phenanthrene and Pyrene under Anaerobic Conditions. *Journal of Environmental Science and Health Part A.*, *44*(13), 1315-1326.

Mihelcic, J. R., & Luthy, R. G. (1998). Microbial Degradation of Acenaphthene and Naphthalene under Denitrification Conditions in Soil-Water Systems. *Applied and Environmental Microbiology*, *54*(5), 1188-1198.

O'Malley, V. P., Abrajano Jr., T. A., & Hellou, J. (1994). Determination of the $^{13}C/^{12}C$ Ratios of Individual PAH from Environmental Samples: Can PAH Sources be Apportioned? *Organic Geochemistry*, *21*(6-7), 809-822.

Richnow, H. H., Annweiler, E., Michaelis, W., & Meckenstock, R. U. (2003). Microbial In Situ Degradation of Aromatic Hydrocarbons in a Contaminated Aquifer Monitored by Carbon Isotope Fractionation. *Journal of Contaminant Hydrology*, *65*, pp. 101-120.

Rockne, K. J., & Strand, S. E. (1998). Biodegradation of Bicyclic and Polycyclic Aromatic Hydrocarbons in Anaerobic Enrichments. *Environmental Science and Technology*, *32*(24), 3962-3967.

Sherwood-Lollar, B., Slater, G. F., Ahad, J., Sleep, B., Spivack, J., Brenan, M., & Mackenzie, P. (1999). Contrasting Carbon Isotope Fractionation during Biodegradation of Trichloroethylene and Toluene: Implications for Intrinsic Bioremediation. *Organic Geochemistry*, *30*, 813-820.

Stehmeier, L. G., Francis, M., Jack, T. R., Diegor, E., Winsor, L., & Abrajano Jr., T. A. (1999). Field and In Vitro Evidence for In-Situ Bioremediation using Compound-Specific $^{13}C/^{12}C$ Ratio Monitoring. *Organic Geochemistry*, *30*, 821-833.

Thierrin, J., Davis, G. B., & Barber, C. (1995). A Ground-Water Tracer Test with Deuterated Compounds for Monitoring In Situ Biodegradation and Retardation of Aromatic Hydrocarbons. *Ground Water*, *33*(3), 469-475.

USEPA (1992). *Contaminants and Remedial Options at Wood Preserving Sites* (pp. 152). Washington, DC: Office of Research and Development, EPA/600/R-92/182.

Van De Velde, K. D., Marley, M. C., Studer, J., & Wagner, D. M. (1995). Stable Carbon Isotope Analysis to Verify Bioremediation and Bioattenuation (pp. 241-257). In R.E. Hinchee, G. S. Douglas, & S. K. Ong (Eds.). *Monitoring and Verification of Remediation*. Columbus, USA: Battelle Press.

Institutional address of the author

Dr. Luis E. Lesser-Carrillo

Director de la Carrera de Ingeniería Civil
Departamento de Ingeniería Civil
División de Ingeniería y Arquitectura
Instituto Tecnológico y de Estudios Superiores de
Monterrey, Campus Querétaro
Av. Epigmenio González 500, Fraccionamiento San Pablo
76000, Querétaro, Querétaro, México
Teléfono: +52 (442) 2383 100, extensión 3512
lelesserc@itesm.mx

Sunrise over the Aguilereño tank in the Aguanaval River in Viesca, Coahuila, Mexico.

Photo: Francisco Valdés Perezgasga
(2015 National Award for Nature Conservation).

Discussion

Technical notes and technical articles are open to discussion according to the following guidelines:

- The discussion will be written in the third person.
- The writer of the discussion shall use the term "commentator" when referring to oneself and the term "author" when referring to the one responsible for the technical note or article.
- The discussion shall be sent within 12 months of the last day of the quarter in which the a technical article or note was published.
- The length of the discussion may be extended by written request from the commentator.
- The discussion is to be presented according to the Guide for Collaborators published in this journal (omitting data referring to the length and abstract). In addition, the bibliographical citation of the technical notes or articles to which the discussion refers shall be included.
- The maximum length of the discussion is 4 journal pages (approximately 10 cuartillas, including figures and tables).
- The figures and tables presented by the commentator shall be progressively marked with Roman numbers and when citing those generated by the author the original numeration should be respected.
- The editors will suppress data that does not pertain to the subject of the discussion.
- The discussion will be rejected if it contains topics addressed by other sources, promotes personal interests, is carelessly prepared, raises controversy involving already established facts, is purely speculative or falls outside the purpose of the journal.
- The discussion will be published along with commentaries from the author or authors to which it refers.
- The discussion will be directed by the editor in chief.

Site of Puente de Dios, municipality of Tamasopo, San Luis Potosi, in the Tamapon River Basin, Mexico.

Photo: Juan Alberto Velázquez.

Guide for Collaborators

The journal ***Water Technology and Sciences*** invites specialists to collaborate with original, unpublished technical articles or notes **related to water, resulting from investigations and provide original contributions**, based on the disciplines of hydrology, hydraulics, water management, water and energy, water quality, and physical, biological and chemical sciences as well as political and social sciences, among other disciplines, according to the guidelines stated below.

PREPARATION OF THE ARTICLE

FORMAT

Font: Palatino throughout the entire document (body of text, tables and figures).

Font Size: Use 8, 9, 10 and 20 points, according to the following table:

8 points (Palatino)	9 points (Palatino)
• Tables. • Figures. • Acknowledgements.	• Name of authors. • Institution of authors. • Abstract. • *Abstract* and *keywords*. • Institutional address of the authors.
10 points (Palatino)	**20 points capital letters (Palatino)**
• Body of the text. • Title of the work in Spanish.	• Title of the work in English.

Line Spacing: double-spaced.

Page Numbers: all pages shall be numbered.

Length

Technical article: **30 pages** (numbered), including figures and tables.

Technical note: **10 pages** (numbered), including figures and tables.

CONTENS

Title

The article shall present significant contributions to scientific and technological knowledge pertaining to the specialty. It shall be based on finished works or those that have completed a development cycle. It shall show results from a series of experiences over 1 year or more of investigations and be supported by an adequate bibliographical review. **The basic structure of the text shall contain an introduction, the development and the conclusions**. The classic layout is preferable: abstract, introduction, methodology, results, discussion, conclusion and references.

Title

The title, **written in Spanish and English**, shall be informative and not exceed 12 words.

Abstract

The abstract, **written in Spanish and English**, shall be concise and provide a broad overview of the investigation (objective, method, results and conclusions) without exceeding 250 words.

Key Words

Eight words or key phrases (maximum) shall be provided **in Spanish and English** that facilitate the identification of the information.

Footnotes

Not admitted. The information is to be incorporated into the text.

Acknowledgements

To be included after the text and before the references.

Tables

- One page for each table.
- A list of all the tables cited shall be presented after the references.

Figures

- One page for each figure.
- All the names of the figures shall be included after the tables.
- They should be high-resolution (300 dpi).

Note: When the article is approved by the publication, the author shall send each figure in JPG format with high-resolution (300 dpi).

References

- The entire bibliography must be referenced in the main body of the text.
- In the case of addressing scientific and technological topics that are common domain, works that denote the knowledge of the authors about the state-of-art shall be cited.
- Avoid self-citations to the extent possible
- APA format shall be used as a basis.

Some examples of references in APA format are:

Complete Books

Last name, A. A. (Year). Title of work. city published: Publisher.
Last name, A. A. (Year). Title of work. Consulted at http://www.xxxxx
Last name, A. A. (Year). Title of work. doi:xxxxx
Last name, A. A. (Ed.). (year).City published: Publisher.

Book Chapters

Last Name, A. A., & Last Name, B. B. (Year).. Title of chapter or entry. In A. Last Name, B. Last Name & C. Last Name (Eds.), Title of book (pp. xxx-xxx). Place: Publisher.
Last Name, A. A., & Last Name, B. B. (Year).. Title of chapter or entry. In A. Last Name, B. Last Name & C. Last Name (Eds.), Title of book (pp. xxx-xxx). Consulted at http://www.xxxxxxx

Newspaper Article or Note Consulted Online

Last Name, A. A., & Last Name, B. B. (Year). Title of article. Title of publication, issue (number), pp. Consulted at http://www.xxxxxxx

That is: Last Name, A. A., & Last Name, B. B. (Year). Title of article. Title of publication, 1(2), 5-17, pp. Consulted at http://www.xxxxxxx

Printed Newspaper Article or Note

Last Name, A. A., & Last Name, B. B. (Year). Article Title. Title of publication, 8(1), 73-82.

Newspaper Article Publication with DOI

Last Name, A. A., & Last Name, B. B. (Year). Article Title. Title of publication, 8(1), 73-82, doi:xxxxxx

Conferences or Symposiums

Collaborator, A. A., Collaborator, B. B., Collaborator, C. C., & Collaborator, D. D. (Month, year). Title of collaboration. In E. E. President (Presidency), Title of symposium. Symposium held at the conference by Name of Organization, Place.

Language

Spanish or English

Separation of numbers and use of decimal points

In *Tecnología and Ciencias del Agua*, the separation between thousands is denoted with a blank space. A decimal point is used to separate whole numbers from fractions. In this regard, refer to Diccionario panhispánico de dudas, edited by the Real Academia Espyearla and the Asociación de Academias de la Lengua Espyearla, in 2005, with respect to numeric expressions: "**the Anglo-Saxon use of the period is accepted, normal in some Hispano-American countries…: π = 3.1416.".**

Delivery of Article

Send the article in *Word* with the name of the authors and institutional address to **revista.tyca@gmail.com**, with copy to Elizabeth Peña Montiel, elipena@tlaloc.imta.mx.

General Information

The review process will begin once the material is received, during which time the manuscript could be rejected. If the text is suitable for review, having fulfilled the Editorial Policy and the Editorial Committee having determined so, it will proceed to the review stage.

Depending on the review process, the text may be accepted without changes, with minor changes, with extensive changes or rejected.

Once a work is published, the main author has the right to two journals and ten offprints free of charge.

In there are any questions, please write to Helena Rivas López, hrivas@tlaloc.imta.mx or Elizabeth Peña Montiel, elipena@tlaloc.imta.mx

Citations within the body of the text

Type of citation	First appearance in text	Subsequent appearances	Format in parenthesis, first citation in text	Format in parenthesis, subsequent citing in text
Work by one author	Last name (Year)	Last name (Year)	(Last name, year)	(Last name, year)
Work by two authors	Last name and Last name (Year)	Last name and Last name (Year)	(Last name & Last name, Year)	(Last name & Last name, Year)
Work by three authors	Last name, Last name and Last name (Year)	Last name *et al*. (Year)	(Last name, Last name, & Last name, year)	(Last name of first author *et al*., year)
Work by four authors	Last name, Last name, Last name and Last name (Year)	Last name *et al*. (Year)	(Last name, Last name, Last name, & Last name, year)	(Last name of first author *et al*., year)
Work by five authors	Last name, Last name, Last name, Last name and Last name (Year)	Last name *et al*. (Year)	(Last name, Last name, Last name, Last name, & Last name, year)	(Last name of first author *et al*., 2008)
Work by six or more authors	Last name of first author *et al*. (Year)	Last name of first author *et al*. (Year)	(Last name of first author *et al*., Year)	(Last name of first author *et al*., year)
Groups (easily identified with abbreviations) such as authors	Complete name of institution (Acronym, year)	Acronym (Year)	(Complete name of institution [acronym], year)	(Institution, year)
Groups (without abbreviations) such as authors	Complete name of institution (year)	Complete name of institution (year)	(Complete name of institution, year)	

Editorial Policy

Mission

Disseminate scientific and technical knowledge and advances related to water through the publication of previously unpublished articles and technical notes that provide original contributions.

Our Principles

- Impartiality
- Objectivity
- Honesty

Our Values

- Knowledge
- Experience
- Thematic expertise

Contents

Interdisciplinary, composed of previously unpublished articles and technical notes related to water, that result from research and provide original scientific and technological contributions or innovations, developed based on the fields of knowledge of diverse disciplines.

Topics Covered

Interdisciplinary, related to water, with priority topics in the following knowledge areas:

- Water and energy
- Water quality
- Physical, biological and chemical sciences
- Hydro-agricultural sciences
- Political and social sciences
- Scientific and technological development and innovation
- Water management
- Hydrology
- Hydraulics

Type of Contributions

Technical article: scientific document that addresses and communicates, for the first time, results from a successful investigation or innovation, whose contributions provide and increase current knowledge about the topic of water.

Technical note: text that addresses advances in the field of hydraulic engineering and professional practices in the field of water, while not necessarily making an original contribution in every case it must be a previously unpublished work.

Some of the articles submitted to the review process can result in being published as notes and vice versa. This will occur through a proposal and process of mutual agreement between the authors and the editor responsible for the topic. The article and the note have nearly the same structure (abstract, introduction, methodology, results, discussion, conclusion, references).

Review Process

The journal is governed by a rigorous review process which establishes that each article be analyzed separately by three reviewers who recommend its acceptance, acceptance with minor changes, acceptance with extensive changes, rejection or acceptance as a technical note with the required changes.

At least one of three reviewers will be sought from a foreign institution.

The reviewers may not belong to the same institution as the authors proposing the article for publication.

When the decisions are opposing or inconsistent, the involvement of other reviewers or the members of the Editorial Committee may be requested.

On occasion, the approval of an article will be decided by two reviewers in addition to the opinion of the editor of the corresponding topic or, the editor in chief.

A rejected article will not be accepted for a new review process.

The review process will be performed in such a way that neither the authors nor the reviewers know the names of the other party.

The review process is performed by high-level specialists and experts who are national and internationally renowned in their professional fields and have the ability to reliably evaluate, in a timely manner, the quality as well as the originality of contributions, in addition to the degree of scientific and technological innovation in the topic under which it is submitted for possible publication.

This participation is considered a professional contribution and will be performed as a courtesy.

The reviews have a "Guide for the Reviewer" provided by the journal's Editorial Department.

Final Ruling

The ruling resulting from the review process is not subject to appeal.

Authors

Works are published from authors of any nationality who present their contributions in Spanish; nevertheless, we all accept works in Spanish or English.

Responsibility of the Authors

Submitting a proposal for the publication of an article commits the author not to simultaneously submit it for consideration by other publications. In the event an article has been submitted to another media for eventual publication, the author agrees to do so with the knowledge of the Editorial Department, which will suspend the review process and inform the Editorial Committee of the decision by the authors.

Collaborators whose articles have been accepted will formally cede the copyright to ***Tecnología y Ciencias del Agua***.

The authors are responsible for the contents of the articles.

The author is responsible for the quality of the Spanish used. If the writing is deficient the work will be rejected. ***Water Technology and Sciences*** will only be responsible for the editorial management.

The author commits to making the changes indicated by the editor of the topic in the time frame establish by the editor. In the event these indications are not met, the article will be removed from the review process and be classified as rejected.

The author shall be attentive to resolving the questions and proposals presented by the editors and the editorial coordinator.

Each author shall approve the final printed proofs of their texts.

It is suggested that authors consult the "Guide for Collaborators."

Readers

Academics, investigators, specialists and professionals interested in the analysis, investigation and search for knowledge and solutions to problems related to water.

Reception of Articles

The reception of articles and notes is ongoing.

Time period

Bimonthly, appearing in the second month of the period.

Subscription and Distribution

The journal is distributed through paid and courtesy subscriptions.

Open Access

Water Technology and Sciences, previously ***Hydraulic Engineering in Mexico***, provides a digital version of all the material published since 1985.

Special editions and issues

Water Technology and Sciences will publish special numbers independently or in collaboration with other journals, professional associations or editorial houses with renowned prestige and related to water resources.

In addition, it will publish articles by invitation, acknowledging the professional advances of prominent investigators.

In both cases, the quality of the technical continents and scientific contributions will be reviewed.

Water Technology and Sciences is registered in the following national and international indices and abstracts:

• Thomson Reuters Science Citation Index® (ISI) • Expanded Thomson Reuters Research Alert® (ISI) • Índice de revistas mexicanas de investigación científica y tecnológica del Consejo Nacional de Ciencia y Tecnología (Conacyt) (2013-2018) • Sistema de Información Científica Redalyc (Red de Revistas Científicas de América Latina y El Caribe, España y Portugal), Universidad Autónoma del Estado de México • EBSCO (Fuente Académica Premier NISC; Geosystems, como Marine, Oceanographic and Freshwater Resources) • ProQuest (Cambridge Scientific Abstracts) • Elsevier (Fluid Abstracts: Process Engineering; Fluid Abstracts: Civil Engineering) • CAB Abstracts, CAB International • Latindex (Sistema Regional de Información en Línea para Revistas Científicas de América Latina, el Caribe, España y Portugal), Universidad Nacional Autónoma de México • Periódica (Índice de Revistas Latinoamericanas en Ciencias), Universidad Nacional Autónoma de México • Catálogo Hela (Hemeroteca Latinoamericana), Universidad Nacional Autónoma de México • Actualidad Iberoamericana, CIT-III, Instituto Iberoamericano de Información en Ciencia y Tecnología.

Other Sources

The journal can also be found archived in Google scholar.